Cranfield UNIVERSITY

CRANFIELD UNIVERSITY

ABBA A. IBRAHIM

INTELLIGENT MULTIPHASE FLOW MEASUREMENT

SCHOOL OF ENGINEERING

PhD THESIS

CRANFIELD UNIVERSITY

School of Engineering
Department of Process and Systems Engineering

PhD THESIS

Academic Year 2007 – 2008

ABBA A. IBRAHIM

Intelligent Multiphase Flow Measurement

Supervisor: Dr. H. Yeung

April 2009

This thesis is submitted in partial fulfilment of the requirements for the Degree of Doctor of Philosophy

ABSTRACT

The oil and gas industry's goal of developing high performing multiphase flow metering systems capable of reducing costs in the exploitation of marginal oil and gas reserves, especially in remote environments, cannot be over emphasised.

Development of a cost-effective multiphase flow meter to determine the individual phase flow rates of oil, water and gas was experimentally investigated by means of low cost, simple and non-intrusive commercially available sensors. Features from absolute pressure, differential pressure (axial), gamma densitometer, conductivity and capacitance meters, in combination with pattern recognition techniques were used to detect shifts in flow conditions, such as flow structure, pressure and salinity changes and measured multiphase flow parameters simultaneously without the need for preconditioning or prior knowledge of either phase.

The experiments were carried out at the National Engineering Laboratory (NEL) Multiphase facility. Data was sampled at 250 Hz across a wide spectrum of flow conditions. Fluids used were nitrogen gas, oil (Forties and Beryl crude oil – D80, 33° API gravity) and water (salinity levels of 50 and 100 g/l $MgSO_4$). The sensor spool piece was horizontally mounted on a 4-inch (102mm) pipe, and the database was obtained from two different locations on the flow loop.

The ability to learn from 'experience' is a feature of neural networks. The use of neural networks allows re-calibration of the measuring system on line through a retraining process when new information becomes available. Some benefits and capabilities of intelligent multiphase flow systems include:

- Reduction in the physical size of installations.
- Sensor fusion by merging the operating envelopes of different sensors employed provided even better results.
- Monitoring of flow conditions, not just flow rate but also composition of components.
- Using conventional sensors within the system will present the industry with a much lower cost multiphase meter, and better reliability.

ACKNOWLEDGEMENTS

I would like to thank my supervisor, Dr. Hoi Yeung for his guidance, and continued support throughout the various stages of this research work, especially the understanding and patience extended to me during the prolonged write up stage.

Many thanks to the staff and members of the Department of Process and Systems Engineering at Cranfield University, notably Professor Mike Sanderson, Janet Dare, Linda Whitfield, Samantha Skears and many others too numerous to mention, and fellow students of the School of Engineering. The valuable criticisms of Mr. Andrew Jamieson and Dr. Yi Cao have no doubt been a great source of encouragement to produce this report and the author is eternally grateful.

My thanks to Dr. Wai Lam Loh, Patricia Hone (NEL) for their various contributions in the laboratory for the experiments/data acquisition both in Glasgow and Cranfield.

My sincere gratitude to the Petroleum Technology Development Fund of Nigeria that has availed me the sponsorship to broaden my knowledge in this very challenging albeit interesting field of study.

Finally, I would like to express my sincere appreciation to my parents, family members and in-laws for the support and encouragement. A special thanks to my wife (Fatimah) for her patience and perseverance. I am deeply indebted; words alone can never express my profound appreciation. THANK YOU.

DEDICATION

This work is dedicated to my late father (Muhammadu Ibrahim)
and grandfather (Mahmoud Armiya'u)

May their souls rest in Aljannat Firdaus

LIST OF CONTENTS

LIST OF FIGURES

LIST OF TABLES

NOTATION

Symbol	Denotes	Units
a_f	Film region holdup	-
a_{fe}	Local holdup at end of film region	-
$a_o\, a_{os}$	Oil component fractions (multiphase flow)	-
a_s	Slug holdup	-
$a_w\, a_{ws}$	Water component fractions (multiphase flow)	-
A_g	Cross-sectional area occupied by gas	m^2
A_l	Cross-sectional area occupied by liquid	m^2
A_o	Cross-sectional area occupied by oil	m^2
A_p	Pipe cross-sectional area	m^2
A_w	Cross-sectional area occupied by water	m^2
b	Neuron bias	-
B_o	Bond number	-
B_s	Bandwidth	Hz
C	Distribution parameter (unaerated slug body)	-
Ce	Measured capacitance	F
Cm	Multiphase fluid mixture capacitance	F
C_{os}	Distribution parameter (aerated slug body)	-
Cp	Electrode-pipe wall capacitance	F
C_v	Critical wave velocity	ms^{-1}
C_w	Wave velocity	ms^{-1}
C_{wl}	Real component of wave velocity	ms^{-1}
iC_{wl}	Imaginary component of wave velocity	ms^{-1}
d	Euclidean distance or bubble diameter	m

D	Pipe diameter	m
D_g D_l	Gas / Liquid phase hydraulic diameter	m
e_n	Residual error of linear prediction	-
E	Photon energy	eV
E_d	Objective function for neural network error minimisation	-
E_q	Average quantisation error	-
E_r	Neural network output associated relative error	%
E_R	Residual error of linear prediction coefficients	-
E_t	Topographic error	-
E_T	Total signal energy	S^{-2}
E_W	Sum of squares of network weights	-
f	Neural network activation function	-
f_i	Interfacial friction factor	-
f_s	Sampling frequency	Hz
F	Modified objective function or input vector scale factor	-
F_c	Signal pseudo-frequency	-
F_r	Slug Froude number (unaerated slug body)	-
F_{rl}	Slug Froude number (aerated slug body)	-
g	Acceleration due to gravity	ms^{-2}
G	Conductivity, gain factor or mass flux	$S.m^{-1}$, - , $kg/s.m^2$
G_g	Gas mass flow rate	kgs^{-1}
G_o	Oil mass flow rate	kgs^{-1}
G_t	Total mass flow rate	kgs^{-1}
G_w	Water mass flow rate	kgs^{-1}
h	Number of hidden nodes	-

h_l	Height of liquid	m
h_{lf}	Height of liquid film	m
H	Hessian matrix, Time average liquid holdup	-
H_{max}	Maximum liquid holdup	-
H_s	Average liquid holdup in slug body	-
I	Current or measured gamma radiation intensity	V, s^{-1}
I_0	Initial gamma radiation intensity	s^{-1}
I_g	Gamma radiation intensity of gas filled conduit	s^{-1}
I_l	Gamma radiation intensity of liquid filled conduit	s^{-1}
I_o	Gamma radiation intensity of oil filled conduit	s^{-1}
I_w	Gamma radiation intensity of water filled conduit	s^{-1}
l_f	Length of film	m
l_s	Slug length	m
l_u	Total length of slug unit	m
L	Length, distance between sensors	m
m	Gradient	-
m_c	Best matching unit vector	-
n	Number of layers in neural network	-
N	Total number of points in a sampled record	-
p	Neural Network input	-
P	Pressure	bar
$P_{(x)}$	Probability Density Function	-
$q_{gf} q_{gt}$	Gas pickup / gas shedding flux velocities	ms^{-1}
$q_{lf} q_{lt}$	Liquid pickup / liquid shedding flux velocities	ms^{-1}
q_m	Mass Flow rate	kgs^{-1}

Q_g	Gas volumetric flow rate	m^3s^{-1}
Q_l	Liquid volumetric flow rate	m^3s^{-1}
Q_o	Oil volumetric flow rate	m^3s^{-1}
Q_t	Total volumetric flow rate	m^3s^{-1}
Q_w	Water volumetric flow rate	m^3s^{-1}
R	Covariance coefficient or input vector range	-
Re	Effective resistance, Reynolds number	Ω, -
R_m	Multiphase fluid mixture resistance	Ω
R_{xx}	Autocorrelation function	-
R_{xy}	Cross-correlation function	-
S_i	Interfacial width	m
S	Slip ratio or generic signal	-
S_1	Salinity 1 (50g/l $MgS0_4$ Solution)	g/l
S_2	Salinity 2 (100g/l $MgS0_4$ Solution)	g/l
t	Time or neural network target output	s, -
t_u	Time for the passage of a slug unit	s
T	Temperature	°C
u	Topographic error constant	-
u_b	Gas bubble velocity	ms^{-1}
V_{drift}	Drift velocity	ms^{-1}
V_{FRN}	Net gas volumetric entrainment rate	m^3s^{-1}
V_{FLT}	Liquid shedding rate	m^3s^{-1}
V_g	Gas phase velocity	ms^{-1}
V_l	Liquid phase velocity	ms^{-1}
V_o	Oil phase velocity	ms^{-1}

V_{sg}	Superficial gas velocity	ms^{-1}
V_{sl}	Superficial liquid velocity	ms^{-1}
V_{slip}	Slip velocity	ms^{-1}
V_w	Water phase velocity	ms^{-1}
V_t	Translation velocity	ms^{-1}
W	Neural network weight	-
$\bar{x}$	Mean	-
x_l	Liquid pick up rate	m^3s^{-1}
$x(t)$	Sample time history	-
x	Distance parallel to flow axis (upstream direction)	m
X	Lockhart-Martinelli number	-
y	Distance normal to flow axis, Neural network output	m, -
Z	Atomic number	-
Z_e	Electrical impedance	Ω
α	Control parameter in Bayesian regularisation	-
α_g	Gas volume fraction	-
α_l	Liquid volume fraction	-
α_s	Low void fraction peak	-
β	Angle of inclination, Water volume fraction or control parameter in Bayesian regularization	rad
γ	Oil volume fraction; linear attenuation coefficient; or number of effective parameters	-
γ_g	Gas linear attenuation coefficient	m^{-1}
γ_l	Liquid linear attenuation coefficient	m^{-1}
γ_o	Oil linear attenuation coefficient	m^{-1}
γ_w	Water linear attenuation coefficient	m^{-1}
δ	Outer layer error	-

$\delta(x)$	Boundary layer development profile	m
Δ	Sampling period	s
ΔP_{film}	Total film zone pressure drop	bar
ΔP_{slug}	Total slug body pressure drop	bar
ΔP_f	Slug body frictional pressure drop	bar
ΔP_m	Slug body mixing zone pressure drop	bar
ΔP_r	Slug body rear pressure drop	bar
ϕ	Phase inversion point (multiphase flow)	-
θ	Angle subtended by liquid film	rad
λ	Insitu water fraction (multiphase flow)	-
$\mu_g \mu_l$	Gas phase / liquid phase viscosities	Nm^{-2}
$\mu_o \mu_w$	Oil / water component viscosities	Nm^{-2}
v	Slug frequency	Hz
ρ_g	Gas density	kgm^{-3}
ρ_l	Liquid density	kgm^{-3}
ρ_m	Mixture density	kgm^{-3}
ρo	Oil density	kgm^{-3}
ρ_w	Water density	kgm^{-3}
τ	Average residence time	s
ω	Wave growth rate	m^3s^{-1}
Ω	Non dimensional slug frequency	-

Subscripts

g	gas
l	liquid
o	oil
d	Pipe diameter
w	water
m	mixture
f	film region

Acronyms

ACF	Autocorrelation function
A/D	Analogue/Digital
AFM	Abbon flow master
AMMS	Accuflow multiphase metering system
AP	Absolute Pressure
API	American Petroleum Institute
AV	Average value
BMU	Best matching unit
BPNN	Back propagation neural network
CCM	Compact cyclone meter
CK	Coefficient of kurtosis
CS	Coefficient of skewness
CV	Coefficient of variance
DP	Differential pressure
DTI	Department of trade and industry
DWT	Discrete wavelet transforms
ESMER	Expert system for multiphase metering
FFD	Fluidic flow diverter
FFT	Fast fourier transform
GOR	Gas oil ratio
GOSP	Gas oil separation plant
GVF	Gas volume fraction
KSOFM	Kohonen self-organising feature map
LDA	Linear discriminate analysis

LGR	Liquid to-gas ratio
LM	Levenberg-marquardt
LPC	Linear prediction coefficient
LSF	Line spectral frequency
MLP	Multi-layer perceptron
MPFM	Multiphase flow meter
NEL	National engineering laboratory
NMS	National measurement system
PCA	Principal component analysis
PDF	Probability density function
PR	Pattern recognition
PSD	Power spectral density
REMMS	Red eye multiphase metering system
RMS	Root mean square
SCG	Scaled conjugate gradient
SD	Standard deviation
SFFT	Short-time fourier transform
SG	Specific gravity
SSE	Sum of square errors
VI	Virtual instrument
VMS	Virtual metering system
WC	Water cut
WLR	Water liquid ratio
ZMUV	Zero-mean and unit variance

CHAPTER 1

INTRODUCTION

1.1 Background

In upstream oil and gas production operations, multiphase flow measurements i.e. knowledge of individual fluid (oil/gas/water) flow rates of each producing well is required for effective reservoir management, field development, operational control, flow assurance and production allocation, Department of Trade and Industry (DTI), (2003). The industry needs reliable and accurate multiphase meters as they can have an enormous impact on cost savings.

The conventional approach offshore often involves using test separation equipment mounted on fixed or floating platforms. This requires separation of the fluids into single-phase oil, gas and water from where the flow rates can be measured using proven meters such as turbine, positive displacement meters and orifice plates. This cumbersome and expensive approach is not acceptable for many future developments such as unmanned satellite platforms and seabed well completions. Instead, novel metering techniques, employing a variety of technologies have been developed, which eliminate the need for the deployment of three-phase separators. These multiphase flow meters (MPFMs) offer substantial economic and operating advantages over their phase separating predecessors. However, it is widely recognised that no single measurement technique has proved to be effective over the complete range for all multiphase metering requirements.

Despite the advances, industrial deployment of this technology remains expensive for meters that offer acceptable performance. Industry experts have forecasted that MPFMs will become feasible on an installation per well basis when their capital costs fall to around $40,000 – 60,000 U.S. Today this cost is in the range of $100,000 – 500,000 U.S. (varying with onshore/offshore, topside/subsea, physical dimensions and quantity ordered). Installation of these MPFMs can cost up to 25% of the hardware cost, and associated operating costs are estimated at between $20,000 and $40,000 U.S. annually, Scheers et al (2002).

Deployment of multiphase flow meters remains very low, as this technology is a nascent sector within the oil and gas industry. It has been suggested that with the current market climate, a modest target for the oil industry would be to have MPFMs installed on 1% of the world's wells by 2010, Jamieson (1998).

Thus, there is a clear need for further development of multiphase flow meters within the oil and gas industry.

Realising the need for reliable and accurate multiphase meters, the oil & gas industry and government bodies, have supported the development and demonstration of multiphase metering technology, which is seen as critical for the future economic development of many offshore reserves.

A recommendation from a previous survey project undertaken by Cranfield University in the 1996-1999 Flow Programme, funded by the then DTI (now DBERR - Department for Business, Enterprise and Regulatory Reform) NMS (National Measurement System) programme, is the creation of a sensor database for multiphase flow. Availability of the database will encourage the development of innovative signal analysis techniques which is the key to the development of cost effective multiphase meters. In conjunction with NEL, Cranfield University designed and assembled a sensor spool piece. The response data from the sensor spool piece were collected over a wide range of oil, water and gas flowrates in NEL's Multiphase Flow Loop in East Kilbride, Glasgow. Data were collected under two different salinities of 50 and 100 g/l $MgSO_4$. To ensure that the techniques developed are installation independent, the spool piece was placed at two different locations on the flow loop, where the flow regime induced by the pipe arrangement and location were expected to be different, Yeung et al (2002).

ESMER exploits advanced signal processing techniques to determine the individual phase flow rates of a multiphase flow mixture. The ESMER system comprises two modular sub-spools: the pressure spool and the impedance spool. The pressure spool contains a differential device (orifice/Venturi/V-cone) equipped with differential pressure and absolute pressure gauges and a temperature sensor. The impedance spool comprises a capacitance sensor for oil external applications, a conductance sensor for

water external applications, or both for full water cut range applications. The spools are installed in a horizontal orientation.

ESMER is a pattern recognition based meter that establishes the non-linear relationships between an array of sensor measurements and the individual phase flow rates by a combination of pattern recognition and neural network training as shown in **Figure 1.1.** Toral, et al (1998).

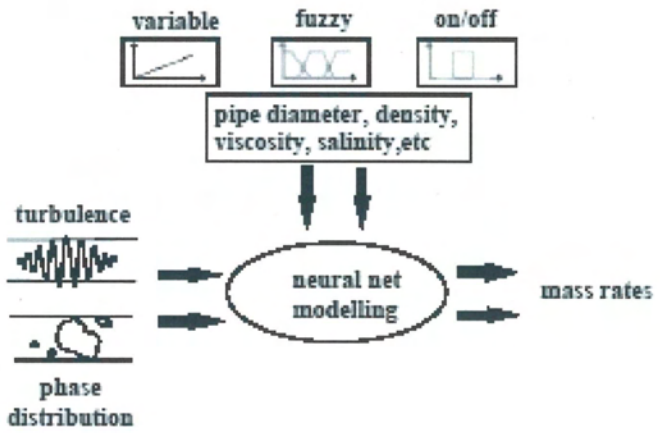

Figure 1.1 – ESMER Concept Model (Toral et al, 1998)

In 2002, ESMER was field tested by Sarawak Shell Berhad in Malaysia over a 20-month period, Cai, et al (2004). In a series of well tests, the meter's measurements were compared against those obtained from a conventional test separator. Good repeatability and trending of the meter against different production rates and flow patterns were reported and it was claimed that ESMER measurements matched the separator measurements to within ±10% for wells which were inside the operating envelope. However, it was noted that the accuracy of the meter deteriorated in well tests located at the boundary of the MPFM's operating envelope and with the passage of time.

1.2 Thesis Objectives

Owing to the increasing importance in the oil & gas industry for an accurate and cost effective solutions for multiphase flow measurement and the inherent technical limitations of the existing technology, this research work was conceived to evaluate the feasibility of using simple sensors and advanced signal analysis techniques for measuring three-phase (oil-water-gas) flow. This was as a follow up to the DTI sponsored Cranfield/NEL NMS project, Yeung et al (2002), as well as extending previous works carried out by numerous researchers, who have validated various methods and instrumentation in conjunction with advanced signal processing techniques for evaluating multiphase flow (mainly two-phase) in horizontal pipes. This research work aimed at evaluating new techniques of pattern recognition (PR) methodologies as well as applying those techniques for the first time to three-phase (oil, water & gas) slug flow in horizontal pipes at different salinity levels and different locations on the flow loop.

The work is focused on slug flow as this is the main flow regime encountered in upstream operations, and it should be reasonably straightforward to extend the use of the system to other flow regimes.

The main objectives of the research work are summarised as follows:

- To review the literature describing components of the multiphase metering systems, and the application of pattern recognition techniques in multiphase flow measurements.

- To experimentally collect the response from a range of simple sensors when subjected to three-phase (oil/water/gas) flow conditions, with operating conditions covering a wide range of gas and liquid superficial velocities, in a 4 inch (102mm) horizontal pipe, under two different salinities of 50 and 100 g/l $MgSO_4$, at two different locations on the flow loop.

- To analyse features from the sensor signals' characteristics in relation to key multiphase flow parameters.

- To apply an appropriate pattern recognition model (Neural Network) for the identification of individual phase flow rates and water-cut.

- To assess the performance of the system, for a range of multiphase flows, and the effectiveness of the neural network on the different pipe locations as well as the different salinity levels.

1.3 Layout of the Thesis

The thesis is divided into seven chapters. An overview of the contents (chapters 2-7) is presented below:

Chapter 2 Reviews multiphase flow measurement, concepts (direct/inferential methods), techniques and flow patterns. A review of commercial multiphase meters is also presented in this chapter. Other literature reviews undertaken are: neural network/applications, signal analysis and feature extraction, salinity effects in MPFM.

Chapter 3 Describes the experimental set up and sensor spool piece. The fluid properties and separation techniques are discussed. Technical description of the data acquisition system and sampling frequency are also presented. The flow diagram indicating the two locations of the sensor spool, experiments carried out, and typical sensor response is described.

Chapter 4 The Application of Neural Networks in Multiphase flow is presented. The response of each feature to individual superficial phase velocities is evaluated Features having individual phase velocity identification capabilities are proposed for determination of flow. Results of investigations of the effectiveness of feature dimensionality reduction and sensor fusion are presented. The performance of the Pattern Recognition (PR) system at test location 2 is evaluated in this chapter.

Chapter 5 The effect of salinity on phase flow rate is investigated. Salinity change, flow rate prediction at 50 g/l MgSO4 and 100 g/l MgSO4 is identified. Salinity based sensor discrimination, importance and points of retraining are evaluated.

Chapter 6 Discussion of research findings is presented, including performance, and effects of changes in the system (salinity, location). Also included are research applications and suggestions to improve performance.

Chapter 7 The main conclusions drawn from the research work are summarised and recommendations for future work presented.

CHAPTER 2

LITERATURE REVIEW

This chapter presents an overview of the basic concepts and principles of the multiphase flow phenomenon and its measurements. A review of the current state of multiphase flow measurement is presented looking at the various concepts and techniques employed in commercially available meters. The application of neural network and signal analysis techniques are also reviewed.

2.1 Multiphase Flow Measurement

The requirement for reliable and yet cost-effective multiphase meters has become increasingly important. Multiphase meters are especially needed in cases when several operators share the use of production and transportation facilities in the exploitation of marginal oil and gas reserves from different locations.

The simultaneous flow of oil, water and gas (multiphase) in a pipeline is a complex phenomenon, making it difficult to understand, predict and model. Well established single-phase flow characteristics, including boundary layer, velocity profile and turbulence, are rendered ineffective in describing their nature, Sanderson (2001).

A multiphase flow regime, observed under specific set of flow conditions, depends on a number of factors, including flow line geometry (size and shape), orientation (horizontal, inclined or vertical), and flow direction in vertical or inclined flows (up or down). Further complicating the matter is the physical distribution of the phases in the pipe and component transport properties (density, viscosity and surface tension). In a gas-liquid mixture, if there is no heat transfer between the phases, the mass flow rates (velocities) will increase progressively as the lower density and viscosity of the gas phase causes it to flow at a higher velocity relative to the liquid phase – a physical characteristic known as slippage.

When multiphase (oil, water & gas) flow simultaneously in pipes, the flow regime, pressure and velocity fields are strongly connected. Perhaps the most distinguishing aspect of multiphase flow is the variation in the physical distribution of the phases in

the pipe, a characteristic known as the flow regime. Under multiphase flow conditions in pipes, the flow regime that exists depends on the relative magnitude of the forces that act on the fluid. Gravity, buoyancy, turbulence, inertia, shear and surface tension forces vary significantly with flow rates, pipe diameter, inclination angle, and fluid properties of the phases. Multiphase phase flow regimes may therefore be viewed as a consequence of the interaction between these forces. To give an indication of the complexity and interaction between the forces mentioned above during multiphase flow in pipes, a further review of flow pattern is given in section **2.2**.

Figure 2.1 shows the operating envelopes of multiphase meters. It is an approach commonly used in other disciplines for displaying properties of three component mixtures.

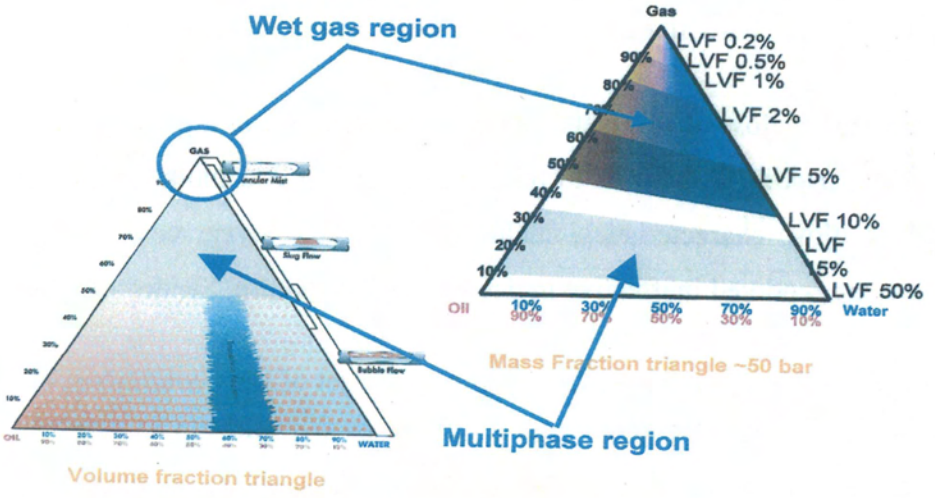

Figure 2.1 Multiphase Composition Triangle, Jamieson (1998).

The vertices of the triangle represent single-phase gas, oil and water, while the sides represent two-phase mixtures and any point within the triangle represents a unique three-phase mixture. The transition region indicates where the liquid fraction changes from water-in-oil to oil-in-water. The ranges of common multiphase flow regimes, which are affected by temperature, pressure, viscosity and flowline orientation, are indicated at the side of the triangle.

2.1.1 Concept/Operating Principles of Multiphase Measurements

The fundamental function of a multiphase flow meter in the oil & gas industry is to supply the user with information on the mass flow rate of oil, water and gas components in a flow. In an ideal situation, a flow meter should simply make direct measurements of each of these three quantities. Unfortunately, direct mass flow meters for multiphase flows do not yet exist. The approach of MPFMs to the challenge of multiphase flow measurement may be classified in the following categories:

- Phase Separation
- In-line Multiphase Flow Meters
- Combination of Inline and Partial Separation

As direct mass flow rate measurement in multiphase flow is yet to be achieved, the above mentioned approach uses inferential methods instead, Thorn and Hammer, (1997). The multiphase flow metering systems are dependent on primary variables:

- Phase Fractions
- Phase Velocities
- Phase Density

and to some extent secondary variables such as:

- Flow Regime
- Phase Viscosity
- Phase Salinity

Evaluation of the primary variables is a prerequisite in applying the inferential method for multiphase flow measurement. Determination of the secondary variables is not strictly required, but could facilitate more accurate measurements if they are taken into consideration. The flow regime parameter may be considered a primary variable if a flow regime dependent sensing technique is used in the determination of the core primary variables.

The inferential method requires the resolution of the instantaneous velocity, cross-sectional fraction, and density of each component in order to be able to calculate the individual flow rates and the total mixture flow rate as shown in **Figure 2.2**.

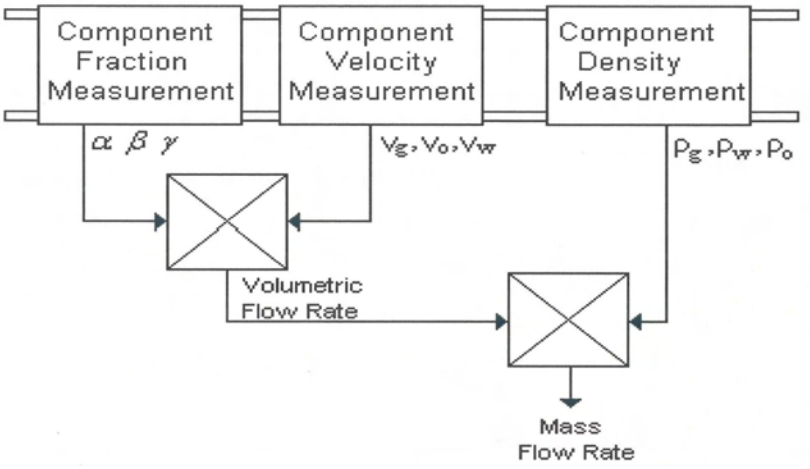

Figure 2.2 – Inferential Method of MPFM, Thorn and Hammer (1997)

Density data for all three components is readily available from other parts of the production process or can be estimated using PVT diagrams. Thus, the problem is to measure the component velocities and two of the three component volume fractions, usually the gas phase fraction and the liquid phase water fraction, in order to calculate the total mass flow.

$$G_t = \alpha V_g \rho_g + \beta V_w \rho_w + [1-(\alpha+\beta)] V_o \rho_o \tag{2.1}$$

where it is assumed:

$$\alpha + \beta + \gamma = 1 \tag{2.2}$$

It is common practice to simplify the problem by assuming that the liquid phase velocity parameters are equal, reducing the number of unknown variables to five. Homogenisation of the multiphase mixture may be employed to reduce the velocity parameters to a single uniform mixture velocity, Hewitt (1989).

Current state of the art multiphase flow meters employ a variety of technologies to determine the multiphase component volume fractions and velocities. These methods are detailed in subsequent sections along with an overview of some important computational techniques that could have a significant role in the future development of multiphase flow meters. A comprehensive review was undertaken by Sanderson (2001).

2.1.2 Measurement Techniques

In the three classes i.e. phase separation, inline & combination of inline/partial separation, different measurement techniques and strategies can be used to obtain

phase fraction and phase velocity information. Some typical examples of these techniques are shown in Table 2.1, State of the Art Multiphase Flow Metering, American Petroleum Institute (API), (2004).

Table 2.1 Measurement Techniques and Devices in MPFM, API 2566, (2004)

Composition Methods	**Velocity Methods**
Capacitance	Venturi
Conductivity/Inductance	Positive Displacement Device
Microwave/Infrared	Coriolis Device
Dual Venturi	Cross Correlation Techniques
Single/Multiple Gamma Ray Absorption	Acoustic Attenuation

2.1.2.1 Phase Volume Fraction Measurement

2.1.2.1.1 Electrical Impedance (Capacitance and Conductance) Methods

The basic principle of the impedance method of component fraction measurement is shown in **Figure 2.3**. If the electrical impedance (Z_e) is measured across two electrodes, between which an oil-water-gas mixture is flowing, then the measured resistance (R_e) and capacitance (C_e) will be given by:

$$R_e = \frac{1+\omega^2 R^2 (C_m + C_p)^2}{\omega^2 R_m C_p^2} \tag{2.3}$$

$$C_e = \frac{\left[1+\omega^2 R_m^2 C_m (C_m + C_p)\right] C_p}{1+\omega^2 R_m^2 (C_m + C_p)^2} \tag{2.4}$$

The resistance (R_m) and capacitance (C_m) of the mixture flowing through the pipe depends on the permittivity and conductivity of the oil, water and gas components, the void fraction and water fraction of the flow, and the flow regime. The resistance and capacitance measured across the electrodes will in turn depend upon R_m, C_m, and the excitation frequency ω of the detection electronics, geometry and materials of the sensor. For a particular sensor geometry (and hence fixed C_p) and flow regime, the measured impedance will be a direct function of the flow's component ratio.

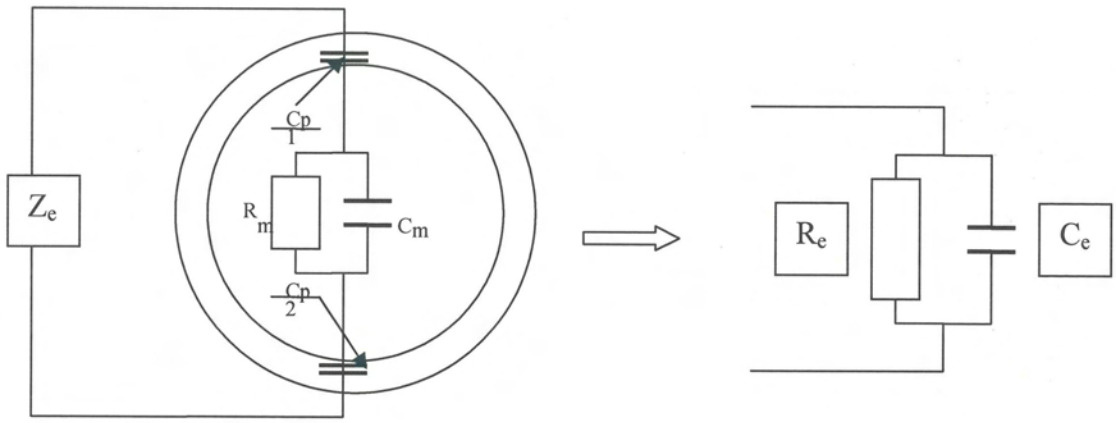

Figure 2.3 Capacitance method of component fraction measurement

Capacitance measurement is one of the most widely used techniques in the measurement of void fraction. The technique is based on the different dielectric constants of liquid, gas and pipe material. The meter generally consists of a couple of electrodes, a transducer and an indicator. The electrodes can be installed inwall of the pipe without obstructing the flow or outwall of the pipe. However, capacitance composition measurement technologies can only be used in a continuous oil or gas continuous flow regime because in the presence of continuous water phases, the capacitance will "short circuit".

When the liquid phase water cut is above 60-70%, capacitance measurements must be replaced by conductivity measurements as the fluid transforms from oil to water continuous. Typically, the conductivity will be measured by injecting a controlled electrical current into the flow and measuring the voltage drop between the electrodes along an insulated section of the pipe as shown in **Figure 2.4**.

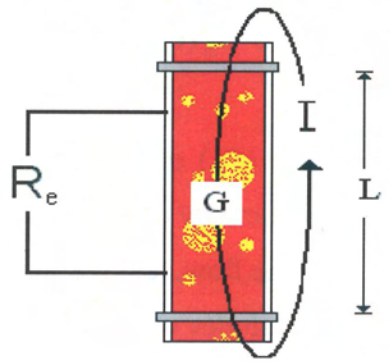

Figure 2.4 – Conductance Method for Component Fraction Measurement

Electrical current can be injected using contact electrodes or non-contact electrodes (inductive mode). Applying Ohm's law, the effective resistance (R_e) offered by the multiphase flow can be determined by dividing the measured voltage drop by the current injected (I). Since the distance between the electrodes is also known (L), this resistance measurement can be expressed in terms of conductivity (G). Electrical impedance methods have two limitations that have to be considered: flow regime dependence and measurement discontinuity over the full component fraction range. Switching between capacitance and conductivity measurements is used to overcome the latter although measurement difficulties can occur around the inversion point if the fluid oscillates between oil and water continuous.

Furthermore, to remove the uncertainty obtained in electrical impendence owing to its flow regime bias, two techniques are commonly exploited:

- Homogenisation of the multiphase mixture prior to measurement.
- Modification of electrode design to reduce bias.

Several modified electrode designs have been reported such as helical, Abouelwafa and Kendall (1979), and rotating fields, Merilo et al (1977). These sensor designs ameliorate the metering performance within identified flow regimes. Nevertheless, impedance sensors are still not suitable for use in applications where the flow regime is unknown or unstable.

2.1.2.1.2 Gamma Radiation Attenuation

Gamma radiation attenuation techniques can be used to resolve two-component mixture phase fractions using a single-energy gamma source or three-component mixtures using a dual-energy gamma source, Abouelwafa and Kendall (1980).

A collimated gamma ray beam is directed at the pipe with a sensor placed diametrically opposite the source on the other side of the pipe as shown in **Figure 2.5**.

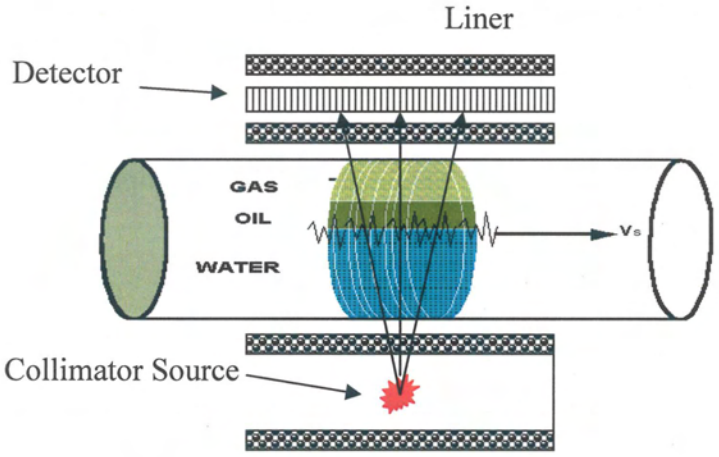

Figure 2.5 – Gamma Attenuation Measurement

The intensity of the gamma beam decays approximately exponentially as it passes through matter flowing in through the pipe measurement section. A gamma ray beam will be attenuated to different degrees by materials according to their density: a more dense material will attenuate the electromagnetic radiation to a greater extent than a less dense material. If the gamma source employed has two distinct energy levels, this can be exploited to determine the volumetric fractions of oil, water and gas in a three-phase mixture as the atomic attenuation coefficients depend not only on the density of a material but also on the energy of the gamma beam itself.

2.1.2.1.3 Microwave Sensor

Microwave sensors are used to distinguish between water and oil in the liquid phase of a multiphase flow. Water and oil have distinctly different dielectric constants and conductivities and it is this difference that allows a microwave sensor to determine the water content of a water-oil mixture.

Table 2.2 – Typical Properties of Gas, Oil and Water Components

Property	Oil	Gas	Water
Density Kg/m^3	10	840	998
Dielectric Constant (Dimensionless)	0	2	75
Conductivity μScm^{-1}	1	10^{-6}	10

There are three different microwave sensor operation principles, Nyfors and Vainikainen (1989).

- **Transmission sensor and measurement on a single frequency:**

A probe is used to transmit microwave radiation through the multiphase medium to a receiving probe. Caution must be exercised to prevent reflections in the pipe/sensor and a guided wave sensor may be deployed to prevent against this. The microwave-receiving sensor may be configured to output the attenuation of or the phase change in the transmitted microwave radiation.

- **Transmission sensor and measurement on a varying frequency:**

Owing to the large attenuation of water continuous liquid phases on high frequency microwaves, it may be beneficial to employ a varying frequency method where the frequency of microwave radiation transmitted is a function of the dielectric properties of the fluid. This can be implemented by monitoring the change of phase such that the meter can determine the frequency where the phase change is constant.

- **Resonator sensor:**

The meter measures the dielectric properties of the mixture using the resonant cavity method. A resonant cavity comprises a metal structure which confines an electric field, causing it to reflect back and forth within the cavity. By matching one of the dimensions of the cavity to the wavelength of the electromagnetic radiation, a standing wave is produced. When this cavity is filled with a specific fluid, the resonant frequency of the cavity will shift in direct proportion to the dielectric constant of the fluid present. As a result, by measuring the resonant

frequency and peak width, the dielectric properties of fluid can be determined. The system can be calibrated to give the water cut.

In practice, microwave sensors use a combination of techniques, using the resonating cavity principle for oil continuous flows and the varying transmission frequency for in water continuous. A microwave sensor would be used in tandem with either electrical impendence or gamma attenuation technique to obtain the gas volume fraction of the multiphase flow.

2.1.2.2.1 Phase Velocity Measurement

2.1.2.2.2 Positive displacement meter

The meter is based on a mechanism to segregate the multiphase flow into small incremental packages (partial separation type), such that in their transit through the device, the phases are temporarily confined without relative slip. By measuring the densities in packages, the mass flow rate of the multiphase fluid is obtained by multiplying the package volume flow rate by the density. Volumetric flow rates are obtained by a pulse generating and detection system monitoring rotor revolutions. The mass flow rates of individual phase liquids can be measured from sample properties such as oil density, gas density and water-cut. Representative liquid samples are taken from the meter's central chamber. Field tests of the meter showed up to 10% and 20% measurement error for volumetric and mass flow rates respectively, Tuss et al (1996). The main disadvantage of the meter is its intrusive nature. Also, mechanical parts of the meter, which require continuous maintenance, may fail under severe flow conditions.

2.1.2.2.3 Differential Pressure Measurements

In instances where a multiphase flow is sufficiently mixed, differential pressure-based flow measurement techniques such as Venturi and orifice sections can be utilised to determine the flow velocity and also measure the mixture flow rate, Olsen (1993). The pressure drop measured across these sections can be expressed as a function of the fluid flow rate and vice versa. The Venturi and orifice meter operating principles are well-established and well-understood single-phase flow measurement methods. Full descriptions of their technical designs are detailed in ISO 5167:2003.

Figure 2.6 illustrates the geometry of the Venturi and orifice inserts and their characteristic flow profiles. In the Venturi section, the reduction in the flow area results in increased fluid velocity and, consequently, reduced fluid pressure. The small angle of the downstream cone facilitates large pressure recovery by minimising frictional losses. In contrast, the abrupt reduction in flow diameter in the orifice plate results in the creation of regions of fluid recirculation and the downstream pressure recovery is hindered by the disturbed flow pattern induced by the restriction.

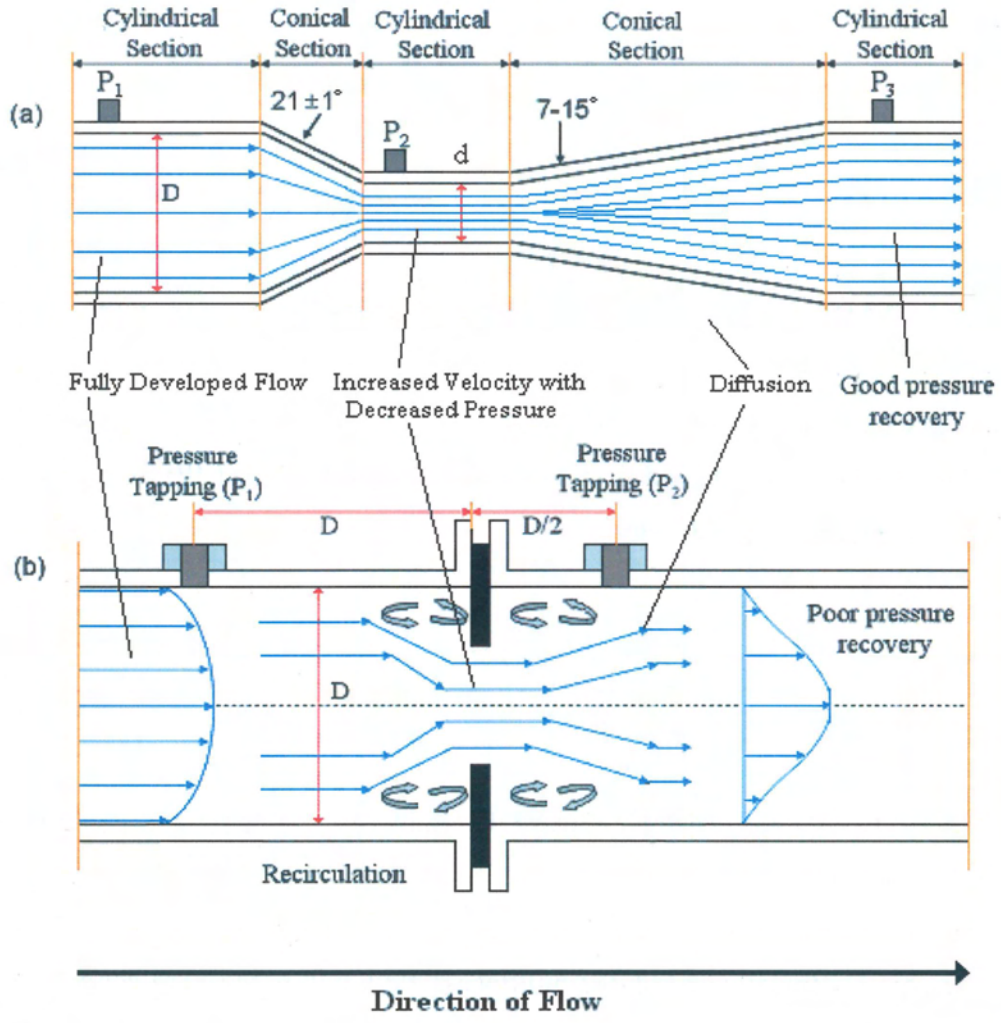

Figure 2.6 – Differential Pressure Measurement Systems (a) Venturi, (b) Orifice
Taken from Blaney (2008)

The use of orifice plates tends to be restricted to wet gas measurements owing to their poor pressure recovery properties. The gas phase flow rate can be determined from the two-phase mixture pressure drop through the application of either the Murdoch (1962) or Chisholm (1967) correlation.

Murdoch:
$$Q_g = \frac{Q}{1+1.26X} \tag{2.5}$$

Chisholm:
$$Q_g = \frac{Q}{\sqrt{1+CX+CX^2}} \tag{2.6}$$

where, Q denotes the wet gas flow rate derived from the orifice plate pressure drop and C is the Chisholm constant and X is the Lockhart-Martinelli parameter:

$$C = \left(\frac{\rho_l}{\rho_g}\right)^{0.25} + \left(\frac{\rho_g}{\rho}\right)^{0.25} \qquad (X<1) \tag{2.7}$$

$$X = \frac{Q_l}{Q_g}.\sqrt{\frac{\rho_l}{\rho_g}} \tag{2.8}$$

In order to determine the flow rate of the homogeneous gas-liquid mixture using a Venturi, an experimentally determined corrected differential pressure formula must be applied, such as that proposed by Hammer and Nordvedt (1991): i.e. the volumetric liquid flow rate can be obtained from a measured pressure drop (ΔP) for a known gas volume fraction and liquid density.

$$Q_l = \sqrt{\frac{(1-\alpha)\Delta P}{\rho_l}} \tag{2.9}$$

The Venturi method has many advantages including low cost, good pressure recovery, familiarity, and simple operation. Furthermore, high accuracy velocity measurements (relative error <1%) can be obtained as long as the multiphase flow mixture maintains homogeneity. On the other hand, the multiphase flow will require pre-conditioning in order to induce a state of homogeneity. In addition, the differential pressure lines of the Venturi meter require regular purging and scale formation can yield excessively high pressure drops.

2.1.2.2.4 Cross-Correlation

The cross-correlation method is a common technique, used for velocity measurement of multiphase flows, Beck and Plaskowski (1987). The principle of this technique is

shown in Figures 2.7 a-c. An upstream and a downstream sensor are mounted a distance L apart, producing the flow signals x(t) and y(t) respectively. The cross-correlation function is given by:

$$R_{xy}(\tau) = \frac{1}{T}\int_0^T x(t)y(t-\tau)dt \tag{2.10}$$

where $R_{xy}(\tau)$ is the value of the cross-correlation function when the upstream signal y(t) has been delayed by a time τ. T is the duration of the sensor data.

The transit time of the flow between the two sensors is found by the time lag τ^* at which the cross correlation function is a maximum. The velocity of the flow V can be found from:

$$V = \frac{L}{\tau^*} \tag{2.11}$$

The accuracy of this method depends on the validity of the relationship used to connect the velocity inferred from the correlation function's peak position to the mean velocity of the flow. Some general procedures for obtaining good cross-correlation accuracy are outlined in Beck and Plaskowski (1987).

1. B_s (sensor bandwidth) should be very large to enhance the flow noise turbulence (cross-correlation of white noise leads to a perfectly narrow correlation peak).
2. L (sensor separation) should be minimised to reduce the possibility of flow evolution between sensors. However, this separation should not be reduced too much to avoid relative spacing uncertainty ($\Delta x/x$), signal quantisation errors, and signal crosstalk errors.

Also Ong and Beck (1975), suggested the optimum sensor separation for homogeneous flow, was of the order of 3 to 4 pipe diameter.

There are a number of disadvantages with the cross-correlation method, including,

- Dedicated computer hardware is usually required, to evaluate the discrete form of the equation on continuous basis.
- The measurement errors will occur if the phases are travelling at different velocities.

To overcome this problem, a simultaneous measurement for more than one phase velocity must be achieved. And this measurement can be achieved, through a careful sensor design, e.g. capacitance, Olsvik et al (1995).

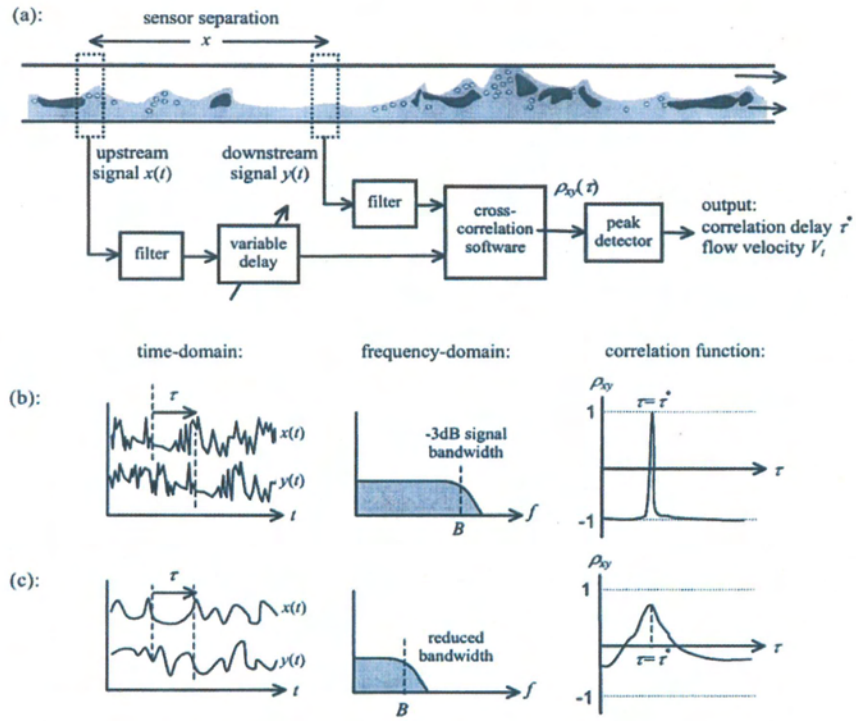

Figures .2.7 a-c – Cross- Correlation Principles Taken from Stewart (2002)

Figure 2.7 shows cross-correlation velocity measurement: (a) system components; (b) the ideal sensor output and the normalised function ρ_{xy}; (c) the actual sensor output and function ρ_{xy}, due to spatial filtering and flow evolution effects Stewart (2002).

2.1.2.2.5 Coriolis mass flow meters

The main components of a coriolis meter are; a U-shaped pipe and a T-shaped leaf string with a magnetic detector. When fluid passes through the meter, the momentum change causes an angular deflection of the tube proportional to the mass flow rate, which is sensed by a magnetic detector. The meter depends upon the detection of vibration amplitude, it is not suitable for use at high void fraction where mechanical vibration caused by slugs can introduce significant errors.

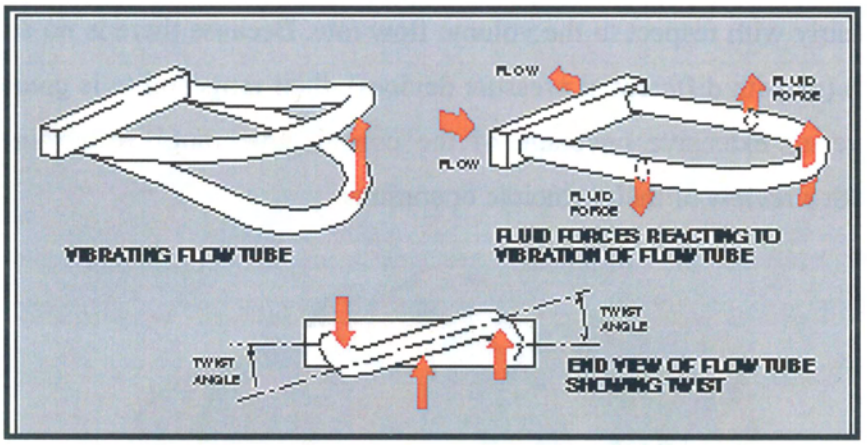

Figure 2.8 – Coriolis Flow Meter, taken from Meinold (1984)

Although Coriolis meters are traditionally used for liquid flow measurements, most manufacturers now offer them for gas applications. The meters are calibrated with water and the calibration is used for gas flow as well. Due to their ability to directly measure the mass flow rate, there is a particular interest to evaluate Coriolis performance in wet gas flow conditions. The results reported by Wood (2002) indicate that the Coriolis meter showed a clear pressure dependency in dry gas conditions, with the error becoming increasingly negative with increasing pressure. The meter also exhibited even greater errors in wet gas flow conditions. At all liquid fractions tested, the meter under-predicted the reference gas mass flow rate with measurement errors reaching as high as 50% in higher liquid loading.

The above results showed that the Coriolis meter under-predicted the actual gas density in both dry and wet conditions, leading to the meter under-estimating the gas mass flow rate. According to previous research work on general two-phase flow, Wood (2002), the meter can function up to 10% gas entrainment provided the two-phase gas-liquid flow remains homogenised within the small vibrating tubes of the Coriolis meter.

2.1.4.2.5 Turbine flow meters

Turbine flow meters (Figure 2.9) measure the volumetric flow of the flowing fluid (liquid or gas). The unit consists of a multiple-bladed rotor, housed in a non-magnetic body mounted with a pipe, perpendicular to the liquid flow. The rotor spins as the fluid passes through the blades. The rotational speed is a direct function of flow rate and can be sensed by magnetic pick-up, photoelectric cell, or gears. These instruments

operate linearly with respect to the volume flow rate. Because there is no square-root relationship (as with differential pressure devices), their rangeability is greater. Baker (1998) gave an extensive coverage of the considerable range of turbine designs together with a review of their principle operations.

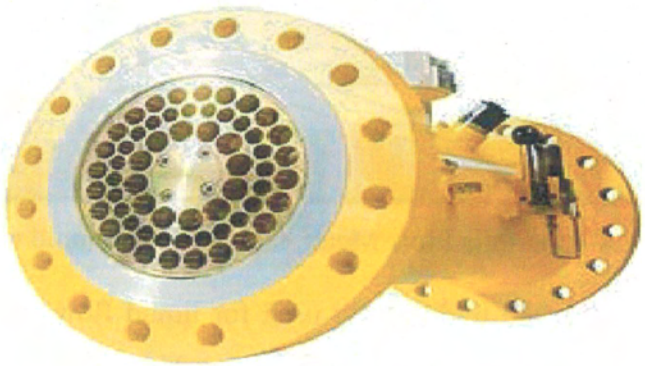

Figure 2.9 – Turbine Flow Meter, taken from Stewart (2002)

Stewart (2002), described a series of wet gas tests on a 6-inch Instromet gas turbine meter at the NEL (as part of the DTI sponsored project). The presence of even small quantities of liquid produced a significant effect on turbine meter readings at Reynolds numbers below 5 x 10^6. At higher Reynolds numbers the liquid appeared to have little effect on the meter. The author concluded that additional testing, preferably on more than one model of turbine meter would be required to provide a better examination of turbine meters in wet gas conditions.

2.1.4.2.6 Vortex Flow Meters

Vortex meters make use of a natural phenomenon that occurs when liquid flows around a bluff object. Eddies or vortices are shed alternately downstream of the object. The frequency of the vortex shedding is directly proportional to the velocity of the liquid flowing through the meter, Figure 2.10. The three major components of the flow meter are a bluff body strut-mounted across the flow meter bore, a sensor to detect the presence of the vortex and to generate an electrical impulse, and a signal amplification and conditioning transmitter whose output is proportional to the flow rate. Sanderson (1998), gave a review of vortex shedding flow meters.

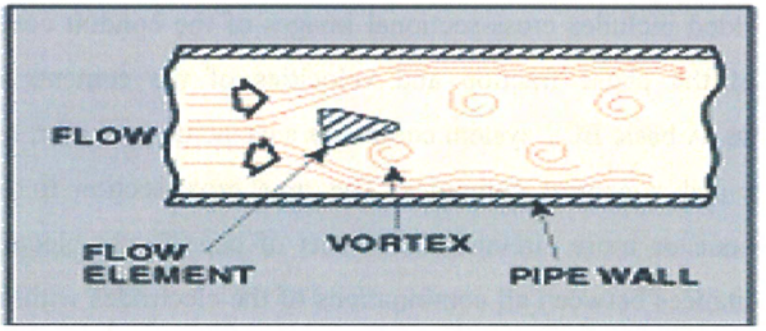

Figure 2.10 – Vortex Flow Meter, Sanderson (1998)

Vortex meters are normally used for processed natural gas and steam flow. A typical quoted accuracy in these applications for an uncalibrated meter is of the order of ± 1.5% of reading and ± 1.25% for calibrated flows, Sanderson (1998).

A 4-inch Fisher-Rosemount vortex meter was tested by the NEL in a horizontal orientation in wet gas at 15, 30 and 60 barg, Stewart (2002). The results showed that the meter over-estimated the reference gas flow rates with a relative error ranging from 0 to 30%, which was dependent on liquid volume fraction and gas velocity. These results indicated that if vortex meters are used for unprocessed natural gas, large measurement errors can be expected as the presence liquid causes the meter to over-estimate the actual gas flow rates.

2.1.2.3 Artificial Neural Networks

Application of neural networks (ANNs) is nascent to multiphase flow measurement. A neural network is a data processing paradigm that was inspired by the way the biological nervous system processes data. The real strength in the application of neural networks to multiphase flow measurement problems lies in their ability to represent both linear and non-linear relationships and their capability to learn these relationships directly from the data being modelled, Brown (2002). A more detailed discussion of ANNs, and other pattern recognition methods, as applied to multiphase flow measurement, is given in section **2.5.**

2.1.2.4 Tomography Systems

Electrical capacitance tomography (ECT) is a non-intrusive technique for obtaining distribution data of the contents of closed conduits by measurement of the variations in the dielectric properties of the fluid inside the conduit, Ismail et al (2005). Typical

information yielded includes cross-sectional images of the conduit contents and the measurement of the phase fraction and velocities of the contents of pipes for multiphase flows. A basic ECT system comprises a capacitance sensor, a capacitance-measuring unit and a control computer. The pipe cross-section to be imaged is surrounded by one or more circumferential sets of capacitance electrodes and the electrical capacitances between all combinations of the electrodes within each set are recorded. These data can then be used to build an image of the pipe contents enclosed by the sensors, based on variations in the permittivity of the material inside the measurement area.

2.2 Flow Pattern

Multiphase flows can distribute themselves in an infinite number of ways. Flow regimes are classifications that have been developed to describe, in general terms, the multiphase flow geometry. The flow regime adopted by a multiphase flow is dictated by a number of parameters including operating conditions, fluid properties, flow rates, pipe geometry, and pipe orientation.

Although many flow regime classifications exist, they can all be broadly classified into dispersed flow, separated flow, intermittent flow or a combination of these.

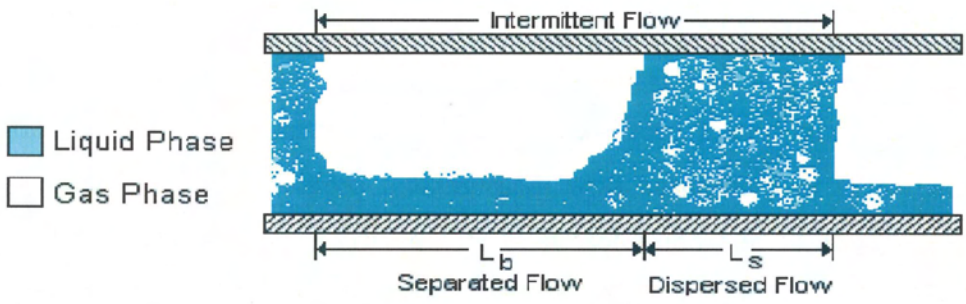

Figure 2.11 Classes of Multiphase Flow Regime, Blaney (2008)

A dispersed flow regime (L_b=0) is defined by a uniform phase distribution across both the radial and axial directions. The separated flow regimes (L_s=0) are distinguished by the fact that they comprise a non-continuous phase distribution in the radial direction but a continuous phase in the axial direction. The final group of multiphase flow regimes is the intermittent flow, which tend to display localised unsteady behaviour

due to a non-continuous phase in the axial direction. Liquid-liquid interactions in a multiphase system usually exhibit less significant influence, when compared to the gas-liquid interactions, on the flow regime. In such cases, the liquid-liquid portion can be modelled as a dispersed flow although it should be noted that the liquid mixture properties can be highly dependent on the volumetric ratio of the two components present.

Researchers have reported a number of experimental-based methods to rationalise flow regime identification. Data from sensors have been analysed using techniques such as template matching, Darwich et al (1989), statistical analysis of signal responses, Stapelberg and Mewes (1990), fractal analysis, Franca et al (1991), and neural networks, Wu et al (2001). While these techniques enable general classification of flows operating within particular regimes, describing the boundaries between flow regimes remains somewhat subjective as these are sensitive transitional areas rather than clear-cut boundaries. Accordingly, multiphase flows that lie close to regime boundaries still cannot be definitively established. Flow regimes maps are graphical charts that are used to predict the different types of flow patterns that will occur for a particular system. Baker (1954), was among the first to publish horizontal flow regime maps that enabled the flow pattern to be predicted upon knowing the mass velocities of the liquid and gas phases and the fluid properties. Other researchers, Nicklin et al (1962), Hewitt (1978), Spedding and Nguyen (1980), Spedding and Spence (1994), have all studied flow patterns, employing their own modified parameters to describe the gas and liquid flows. Mandhane et al (1974), published a set of multiphase flow maps that were able to predict the flow regime present in a pipe, based on the superficial phase velocity parameters. Taitel et al (1980), exploited superficial phase velocities to produce a model describing the flow regime transitions in vertical flow. Following its publication, the Taitel-Dukler map was found to define the transition between different flow regimes more accurately than other models. Flow regime maps plotted using the superficial phase velocity parameters are widely used in the oil and gas industry owing to their comparative simplicity.

A few detailed studies of oil, water and gas systems have been undertaken. These have reported the existence of similar flow regimes to those witnessed in standard two-phase flow systems but with particular emphasis being placed on identification of

the dispersed and continuous components in the liquid phase, Acikgoz et al (1992), Oddie et al (2003). However, certain key discrepancies have been reported between two- and three-phase flow patterns. At low flow velocities, the liquid density difference may be sufficient to induce separation of the oil and water phases. In vertical flow this can result in the production of alternating oil and water slugs while in the liquid phase substantial slip between the liquid phases has been reported, Brill and Arirachakan (1992). Furthermore, at low gas flow rates, near vertical multiphase flows have been shown to have significant differences when compared to flows contained in a purely vertical pipe, Spedding et al (2000).

2.2.1 Vertical Pipe Flow Regimes

Multiphase flow is fairly common in oil well pipelines despite the fact that the well pressure at the bottom can exceed the bubble point of the oil. The pressure drop experienced by the oil as it is transported from the seabed to the surface can result in gas liberation from the liquid oil phase. The flow regimes witnessed in vertical risers are usually fully developed and essentially axial-symmetrical. Generally, the multiphase flow features presented vary with well age, with older wells exhibiting a larger gas vapour fraction. Figure 2.12 illustrates a generic multiphase flow map, based on gas and liquid superficial velocities, for a vertically upward multiphase flow in a vertically orientated pipeline, Dykesteen et al (2005).

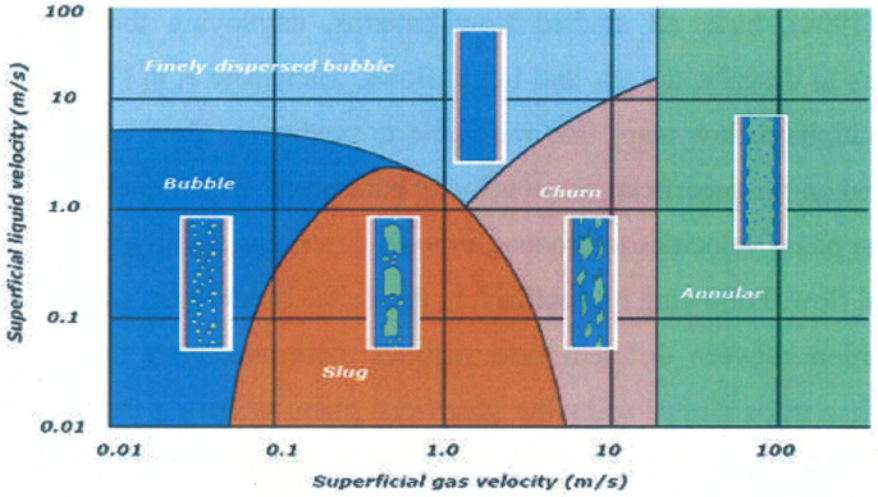

Figure 2.12 Multiphase Flow Regime Map for Vertical Flow, From Handbook of Multiphase flow Metering, Dykesteen et al (2005).

The vertical flow regimes are commonly categorised into four main classifications:

Bubble (including finely dispersed bubble): At low gas flow rates, a continuous liquid phase is formed with the gas phase producing discrete bubbles within the continuum. The gas bubbles may coalesce to form larger bubbles or slugs.

Slug: Increased gas flow rates increase bubble coalescence until the bubble diameter eventually approaches that of the pipe diameter. The resulting flow alternates between high-liquid and high-gas composition.

Churn: Somewhat similar to slug flow, but more chaotic in nature owing to the larger gas flow rates. The slug bubbles have become distorted to form longer, narrow structures and the flow adopts a random oscillatory nature. The liquid flow occurs mainly at the pipe wall but a significant proportion is vigorously mixed with the gaseous core.

Annular: At very high gas flow rates, the liquid phase is forced to flow up the pipe wall as a liquid film while the gas flows in the centre. The interface between the phases is typically wavy. The wavy interface enables liquid entrainment in the gaseous core. When the quantity of entrained liquid becomes significant, the flow is described as having an annular mist regime.

2.2.2 Horizontal Pipe Flow Regimes

As with vertical flow, flow regime transitions in horizontal pipes are functions of parameters such as pipe diameter, interfacial tension, and phase densities. However, the flow patterns exhibited in horizontal regimes are not axially symmetrical and a pipe length equivalent to at least 100 pipe diameters is required to establish fully developed flow.

Multiphase flow maps based on superficial phase velocities are also readily available for horizontal flows as shown in **Figure 2.13**, Dykesteen et al (2005). However, a multiphase map like this will only supply valid flow regime predictions for a specific pipe, pressure and fluid system. The flow regimes observed for horizontal flows will tend to be more complex than their vertical counterparts due to gravity induced asymmetries. The heavier phase will be inclined to accumulate at the bottom of the pipe.

Horizontal flow regimes are commonly categorised into six main classifications:
Bubble: The gas phase exists as discrete bubbles within a liquid continuum. The gas bubbles will tend to flow in the upper section of the pipe. However, with larger gas flow rates, a uniform bubble distribution across the pipe cross-sectional area may be witnessed.

Plug: Reducing the liquid flow rate will enable the gas bubbles to coalesce into larger bubbles or plugs which will occupy the upper section of the conduit.

Stratified: Further reductions to both the gas and liquid flow rates will result in phase stratification whereby the two phases flow separately with a relatively smooth interface. The liquid phase will occupy the lower section of the pipe due to gravity.

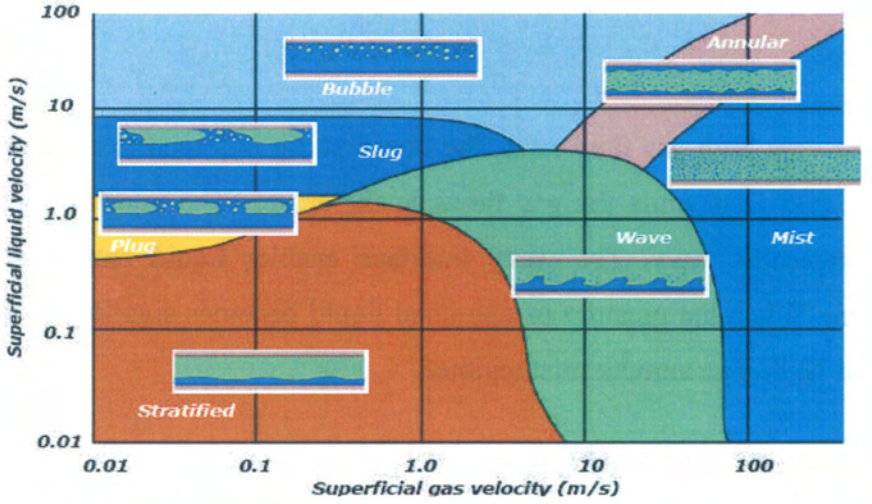

Figure 2.13 – Multiphase Flow Regime Map for Horizontal Flow, From Handbook of Multiphase flow Metering, Dykesteen et al (2005).

Wave: Increasing the gas flow rate of a stratified system will produce a less stable phase interface as a result of the increased turbulence. The interface between the liquid and gas phases will be irregular and wavy in nature although good separation between phases will be maintained.

Slug: Increasing the liquid flow will produce waves of a much larger magnitude until the liquid is increased to such a point where the wave occupies the whole of the pipe cross-section. This facilitates the propagation of a high velocity fluid slug down the pipe.

Annular/Mist: At very high gas flow rates, the liquid phase is forced to flow up.

2.2.3 Flow Regime Identification Methods

Several flow pattern recognition techniques have previously been employed for multiphase flow measurement and analysis. The most prominent work in this field documented in published literature is the pioneering research work by Imperial College researchers in developing the ESMER multiphase measurement system. Darwich (1989), proposed that time-varying characteristics of multiphase flow are reproducible and this fact could be exploited to determine the inherent hydrodynamic and sensor behaviour in different flow regimes and thereby infer the individual phase flow rates of a multiphase flow.

Signal analysis techniques such as PDF, which is a complete probabilistic description of the instantaneous values of the sensor signals data, yields the probability density function. It describes the probability that at a given time the signal will have the value within some defined range.

Statistical analysis of sensor signals for multiphase flow allows the time average cross sectional void fraction and the void probability density function (PDF) to be inferred. The slug flow is associated with a twin peaked PDF, where the low void fraction peak is pertinent to slug passage, and the high void fraction peak is associated with the stratified phase regions. Goudinakis (2004), investigated the feasibility of using an MLP neural network for flow regime identification in a horizontal pipeline. Stratified smooth, stratified wavy, bubble and slug flow regime classifications were identified using raw time-series.

2.3 Commercial Multiphase Flow Meters (MPFMs)

There are a number of commercial multiphase meters available in the market that have been deployed in the field. These meters employ a diverse range of measurement principles and solutions. Certain types of meter perform better in certain applications than others. Thus, a detailed comparison and selection process is needed to determine the MPFM best suited to a particular application. A review of current commercially available multiphase meters was undertaken as part of this research work. The information presented was compiled from published papers, sales documentation, third party test reports, and the author's enquiries to the vendors. However, access to

details of research undertaken pertaining to the development of the measurement technologies was limited owing to its commercial sensitivity. **(Appendix A)**

2.3.1 Phase Separation MPFMs

A methodology to measure high gas volume fraction, multiphase streams has been to utilise existing operational technology for part of the stream, which can handle low GLR and divert the remainder of the gas through a gas measurement leg of the system. Existing MPFMs that use this approach include those of Abbon Flow Master (AFM) 300C, Accuflow AMMS, Agar MPFM, Jiskoot-Starcut, Kvaerner-CCM, Megra, and WellComp.

2.3.2 In-Line Multiphase Flow Meters

These are further subdivided into two categories: those that utilise static mixers and those that do not have static mixers in their set up.

2.3.2.1 MPFMs with Static Mixers

The principal suppliers of operational multiphase meters, utilising this technology include: Jiskoot-Mixmeter, Schlumberger-Framo, TEA-Lyra and ISA-Multistream, Falcone et al (2002).

2.3.2.2 MPFMs without Static Mixers

The commercially available MPFMs that do not require flow conditioning (i.e. neither inline mixer nor separation) prior to metering include Schlumberger-VX, Roxar-Fluenter, Roxar-MFI, Kvaerner-DUET, FlowSys and ESMER.

Table 2.3 Commercial Multiphase Flow Meters

Concept	Metering System	System Designation
Phase Separators	Vortex, Ultrasonic, Coriolis	Accuflow AMMS
	FFD, Venturi, Microwave	Agar MPFM
	Dual Energy Gamma, X-Corr	Kvaerner-CCM
	Coriolis, Vortex, Infrared	REMMS
Inline with Static Mixers	FFD, Acoustic Detection	Abbon FM 300I
	Dual Energy Gamma, Cross-Correlation	Jiskoot-Mixmeter
	Dual Energy Gamma, Venturi	Schlumberger-Framo
	Venturi, Orifice, Impedence, Gamma.	TEA-Lyra
	Coriolis, Microwave	CCM meter
Inline without Static Mixers	Acoustic Detection	Abbon FM 300C
	Dual Energy Gamma, Venturi	Schlumberger-VX
	Capacitance, Conductance, X-Corr, Gamma	Roxar-Fluenta
	Dual Gamma, X-Corr	Kvaerner-DUET
	Capacitance, Conductance, Venturi	FlowSys
	Orifice,Venturi,V-cone, Impedence (Cap. & Cond.)	ESMER
Combination of Inline and Partial Separation	Venturi, Dual Energy Gamma	Haimo
	Venturi, Nozzle, Orifice, Impedence, Gamma	TEA LYRA

2.4 Pattern Recognition Techniques in Multiphase Flow Measurement

Fluid flow measurement accuracy is often limited by our understanding of the fundamental laws governing flow processes and is further exacerbated by the complex nature of multiphase flow, which does not fully lend itself to conventional fluid modelling techniques. The responses from instruments do however inherently contain all the information they have gathered about the process.

The following sections present an introduction to various signal processing and pattern recognition techniques relevant to the current research work, that relates to previous studies.

Pattern recognition aims to classify data (patterns) based on either a prior knowledge or on statistical information extracted from the patterns. The patterns to be classified are usually groups of measurements or observations, defining points in an appropriate multidimensional space. A complete pattern recognition system consists of three major steps: 1) a sensor that gathers the observations to be classified or described; 2) a feature extraction mechanism that computes numeric or symbolic information from the observations; and 3) a classification or description scheme that does the actual job of classifying or describing observations relying on the extracted features. Thus, a pattern recognition model has to be able to map the relationship between input features and the target outputs.

There are several pattern recognition techniques available to implement the mapping process including: artificial neural networks; statistical models; fuzzy logic; and expert systems. Although these models are distinguishable from each other, there is a certain amount of overlap between them: artificial neural networks can be thought of as an extension of conventional statistical pattern recognition techniques and fuzzy logic employs similar types of logical rules that can be found in expert systems.

2.4.1 Signal Processing

Signal processing involves the design, analysis and implementation of systems that extract information of interest from existing data signals. The continued progress of digital technology and information theory has stimulated the development of

sophisticated signal processing techniques that are exploited in many different fields, including speech recognition, audio signal processing, digital communications and analysis and control of industrial processes.

Most sensor outputs comprise a continuously varying analogue voltage waveform. In order to use the signal in further mathematical signal processing techniques on a computer system, it must first be digitised with an analogue-to-digital converter. Analogue signals are digitised employing a technique known as sampling. Sampling is executed in two stages: discretisation and quantisation. In discretisation, the space of a signal is partitioned into a series of equivalence classes. The quantisation process then allocates approximated representative signal values to each of the partitions from a set of finite values.

The Nyquist-Shannon sampling theorem is a fundamental theorem in the field of information theory which stipulates the constraints for accurately constructing a signal from a sampled version of itself. It states that the sampling frequency f_s must be strictly greater than twice the signal's bandwidth B_s, i.e. the difference between the maximum and minimum frequencies of its sinusoidal components, Jackson (1991).

$$f_s > 2B_s \tag{2.12}$$

Failure to satisfy the criterion set out in the Nyquist-Shannon theorem results in overlapping frequencies, whereby frequencies above half the sampling rate will appear as frequencies below half the sampling rate. This phenomenon is known as aliasing as the high frequencies are said to be "under an alias".

A classical example of aliasing can be seen when filming rotating objects, such as wheels and aeroplane propellers. The film 'sample' is at a fixed rate, while a wheel can rotate at different speeds. As the wheel exceeds the Nyquist frequency it appears to rotate backwards.

2.4.2 Feature Extraction

Given a digital representation of the signal, various parametric representations can be derived. In applications with time-varying signals, in order to exploit all the available

data, it may be possible to use all the sampled data points in the pattern recognition analysis. However, this may not be practical with systems that have long measurement times and/or high sampling frequencies where the number of data points is too large to be efficiently manipulated by a pattern recognition system. In these instances, a set of features that are capable of describing the signal's characteristics may be employed.

Selection of an appropriate feature set to represent raw data signals is crucial if feature extraction is to be employed successfully. Effective feature selection can be difficult as it necessitates the selection of a feature set that will distinguish between different data class volumes, and there are an infinite number of features and feature combinations from which to select. If too many features are included in the feature set, there is a tendency for the pattern recognition model to become over-complex and this will result in a reduced generalisation capability. In practice, a pattern recognition or data visualisation analysis will be conducted on the training data, using the selected feature set, in order to analyse its effectiveness.

The features employed to represent a signal can come from a variety of information domains, e.g. time, frequency, cepstrum or wavelet. The most effective domain depends on the problem being modelled. The goal of feature extraction is to reduce a large complex signal into a small number of manageable parameters that conserve the key features of the original signal.

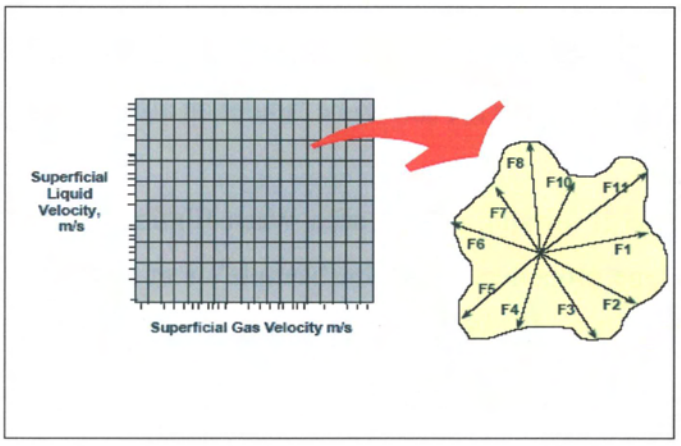

Figure 2.14 – Feature Vector in Multidimensional Space, Darwich et al (1989)

2.4.2.1 Moments of Amplitude Distributions

2.4.2.1.1 *PDF*

The Probability Density Function defines the probability that a sampled signal will assume a particular value within some range at any instant time. The probability density function, $P(x)$ can be defined as follows:

$$P(x) = \lim_{\Delta x \to 0} \frac{prob[x < x(t) < x + \Delta x]}{\Delta x} \tag{2.13}$$

$$P(x) = \lim_{\Delta x \to 0} \frac{1}{\Delta x} \left(\lim_{T \to \infty} \frac{T_x}{T} \right) \tag{2.14}$$

where $P(x)$ represents the PDF of sample time history record $x(t)$, T_x is the total time during which the signal will assume a value between x and Δx.

However, distribution of a signal is not a unique property and no information about signal structure or spectrum is given. Instead a set of properties known as moments of distribution function is obtained to describe the signal.

2.4.2.1.2 Mean

The mean (x), is the arithmetic average value of the data points, and it estimates the value around which a central clustering occurs. The first moment, known as the mean value, is given by:

$$\bar{x} = \frac{\sum_{i=1}^{N} x_i}{N} \tag{2.15}$$

where x is the amplitude value of the i^{th} point and N is the number of points in the sampled record.

2.4.2.1.3 Standard Deviation

The standard deviation is the root mean square of the amplitude deviations from the arithmetic mean and is a measure of the dispersion of the data. The standard deviation, SD, is defined as:

$$SD = \sqrt{\frac{\sum_{i=1}^{N}(x_i - \bar{x})^2}{N-1}} \tag{2.16}$$

2.4.2.1.4 Coefficient of Variance

The coefficient of variance measures the scatter in the data distribution in relative terms by dividing the standard deviation by the mean of the data. The coefficient of variance, CV, is expressed as:

$$CV = \frac{SD}{\bar{x}} \tag{2.17}$$

2.4.2.1.5 Coefficient of Skewness

The third moment, which is the measure of symmetry of distribution around its mean value, is known as skewness. A positive coefficient corresponds to a distribution with a greater number of large values for the parameter than would be expected for a Gaussian distribution. Conversely, a negative value for the coefficient implies a higher occurrence of smaller values. For a Gaussian distribution, the coefficient of skewness is zero. The coefficient of skewness is given as:

$$CS = \frac{\sum_{i=1}^{N}(x_i - \bar{x})^3}{(N-1)SD^3} \tag{2.18}$$

2.4.2.1.6 Coefficient of Kurtosis

Kurtosis, which is the measure of peakedness of a distribution, is the fourth moment of probability density function. A positive coefficient corresponds to a distribution with a greater extent of 'peakedness' than a normal distribution. On the other hand, a negative value for the coefficient implies a lesser degree of 'peakedness'. For a

Gaussian distribution, the coefficient of kurtosis is zero. Mathematically, the coefficient of kurtosis (CK) can be expressed as:

$$CK = \left(\frac{\sum_{i=1}^{N} (x_i - \bar{x})^4}{(N-1)SD^4} \right) - 3 \tag{2.19}$$

It should be noted that both the skewness and the kurtosis of a distribution are non-dimensional moments, unlike the mean and the standard deviation which have the same dimensions as the measured parameter.

2.4.2.1.7 Signal Energy

The signals' total energy is not related to the probability density function but is another useful amplitude feature that can be extracted from the signal time-series. In several applications, the signals being examined are directly related to physical quantities capturing energy in a physical system. The total energy in a discrete-time signal $x(n)$ over a time interval $n_1 \leq n \leq N$ is defined as:

$$E_T = \frac{\sum_{n=n_1}^{N} (x_n)^2}{N} \tag{2.20}$$

2.4.2.2 Linear Prediction Coefficients (LPCs)

Linear prediction modelling is one of the common speech coding techniques; it exploits the redundancies of a speech signal by modelling the speech signal as a linear filter, excited by a signal called the excitation signal. The excitation signal is also called the residual signal. Speech coders process a particular group of samples, called a frame or waveform. The speech encoders find the filter coefficients and the excitation signal for each frame. The filter coefficients are derived in such a way that the energy at the output of the filter for that frame/waveform is minimised. In physical terms, LP coefficients contain unique information on the spectral content of the waveform, which is generated by a physical process (speeches, multiphase flow, etc) and capture the variations in energy and spectral characteristics in a short time

interval. Since LP coefficients provide a simple and effective method of representing different signals in terms of small number of parameters, they can be used not only as a way of data compression but also as a supply for different statistical features for different signal conditions, Makhoul (1975).

The linear prediction is modelled in the time-domain by minimising the sum of the squared differences (over a finite time interval) between the actual signal samples and the linearly predicted ones resulting in a residual error. In doing so, a set of unique predictor coefficients, which are the weighting coefficients used in the linear combinations are determined.

The present signal sample $x(n)$ is modelled as a linear combination of the past outputs and the present and past inputs. This relationship is expressed in **Equation (2.21)**:

$$x(n) = \sum_{k=1}^{p} a_k x(n-k) + G\sum_{l=0}^{q} b_l u(n-l) \tag{2.21}$$

Where $b_0 = 1$, G is a gain factor, a_k and b_l are the filter coefficients of an unknown input u_n. The variable p denotes the number of past output samples being considered by the model, which is also representative of the order of the linear prediction function. By applying a z-transform, the transfer function of the system can thus be expressed:

$$H(z) = \frac{X(z)}{U(z)} = G\frac{1+\sum_{l=1}^{q} b_l z^{-1}}{1-\sum_{k=1}^{p} a_k z^{-k}} \tag{2.22}$$

where, $X(z)$ denotes the z-transform of $x(n)$, $U(z)$ is the z-transform of $u(n)$ and $H(z)$ is the transfer function of the system, which is the general pole-zero model.

Two special cases exist for the general pole-zero models. Firstly, when $b_l = 0$, for $1 \leq l \leq p$, $H(z)$ reduces to an all pole model known as the autoregressive model. The other special case occurs when $a_k = 0$, for $1 \leq k \leq p$, $H(z)$ transforms to an all-zero or moving average model.

The autoregressive model is commonly employed due to its comparative simplicity and computational efficiency. The autoregressive model only requires a set of linear equations to be solved. The residual error $e(n)$ is a by-product of the linear prediction technique and is the difference between the actual signal and the predicted signal. Accordingly, the following relationship holds:

$$e(n) = x(n) - \sum_{k=1}^{p} a_k x(n-k) \tag{2.23}$$

A simple test to obtain the optimal linear predictor order p is to check the variation of the residual error with the predictor order, which will almost be flat for $p > p_o$, where p_o is the optimal linear predictor order.

Autocorrelation and covariance are two widely used methods employed in the estimation of LPCs, Golub and Loan (1989). Both these methods select the short-term filter coefficients in such a way as to minimise the residual error using the least-squares technique. The autocorrelation method involves the generation of a Toeplitz matrix, a matrix in which all the elements along a given diagonal are equal, which guarantees the stability of the filter. This permits the application of the Levinson-Durbin recursion algorithm to solve the set of linear equations produced by the least-squares procedure.

Correlation is a measurement of the average dependency between two random signals. The correlation between pairs of a single signal's samples is known as autocorrelation (AC). The autocorrelation function, R_{xx} of a signal yields an average measurement of its time domain properties.

$$R_{xx}(\tau) = \lim_{T\to\infty} \frac{1}{2T} \int_{-T}^{T} x(t)x(t+\tau)dt \tag{2.24}$$

The difference between auto-correlation and cross-correlation is that while auto-correlation is applied to a signal with its shifted version, the cross-correlation is applied to two different signals. The cross-correlation function is a time averaged measure of shared signal properties, therefore it is suitable for signals comparison. The cross-correlation function relating two – $x(t)$ and $y(t)$ – is defined as:

$$R_{xy}(\tau) = \lim_{T\to\infty} \frac{1}{2T} \int_{-T}^{T} x(t)y(t+\tau)dt \tag{2.25}$$

where R_{xy} is a cross-correlation function and τ is a time shift or lag imposed upon one of the signals. The cross-correlation function has many important applications including measurement of time delays, and detection and recovery of signals noise.

2.4.2.3 Line Spectral Frequencies (LSFs)

LPCs have a multitude of other representations: Line Spectral Frequencies (LSFs), Reflection Coefficients (RCs), Log Area Ratio (LAR), Arcsine of Reflection Coefficients (ASRCs), etc. These parameters all have a direct relationship with the LPCs and will preserve all information contained within the LPCs.

Publications have reported that LSFs are computationally efficient and have good quantisation and interpolation properties, facilitating improved system approximation. Compared to other transmission parameters, the line spectral frequencies have been found to encode speech spectral data much more efficiently, Deller et al (1993). This enhanced efficiency is attributed to the close relationship between the LSFs and the formant frequencies. Furthermore, the line spectral frequencies naturally lend themselves to frame-to-frame interpolation, with smooth spectral changes, owing to their frequency domain interpolation.

The linear prediction analysis filter can be expressed in terms of LPCs, a_k, using the following equation:

$$A(z) = 1 - \sum_{k=1}^{p} a_k z^{-k} \tag{2.26}$$

where p is the order of the function $A(z)$. The path $(p+1)^{th}$ order symmetric and antisymmetric polynomials $P(z)$ and $Q(z)$ can be obtained from $A(z)$:

$$P(z) = A(z) + z^{-(p+1)} A(z^{-1}) \tag{2.27}$$

$$Q(z) = A(z) - z^{-(p+1)} A(z^{-1}) \tag{2.28}$$

The roots of the two polynomials lie on a unit circle and they form the LSFs. Kabal and Ramachandran (1986), published an algorithm that enables the LSFs to be extracted from the LPCs using the Chebyshev polynomial root finding method.

2.4.2.4 Data Pre-Processing

There are number of feature pre-processing techniques available in the literature. One method is to normalise the input features to the pattern classifier so that they fall in the range of [-1, 1]. Another normalisation technique is to equalise the magnitude and variation of each feature by applying zero mean and unit-variance normalisation to the feature vectors. Here the data values are centred (i.e. subtract the mean values from the data values in order to obtain centred anomalies) and then divided by their standard deviations to obtain a normalised data having zero mean and unit variance.

In certain situations, further feature pruning may be necessary, where the extracted and normalised features require dimensionality reduction. The process of selecting and extracting features from high dimensional data that can be used to discriminate the underlying classes, or identify the target from non-targets is referred to as dimensionality reduction. The motivation behind performing a dimensionality reduction is usually to remove the redundant information present in the data and reduce the computational complexity.

There are many different dimensionality reduction techniques, which may be broadly classified into two categories. In the first case, the relevant features are selected from the raw data in their original domain based on some discriminatory criterion. From a classification perspective, the objective of this criterion is to select those features that have a higher discriminatory capability of the system. The feature contour map superimposed on two-dimensional system variables used to guide the feature selection process is an example of this category.

In the second case, the features are transformed into a new feature domain, where they can be arranged in order of their importance, which is application-specific. The transformation techniques include Linear Discriminate Analysis (LDA), Webb (1999), Discrete Wavelet Transforms (DWT), Mallat (1989), and Principal Component Analysis (PCA), Jackson (1991). Amongst these, the PCA is commonly used in a wide range of applications, including document analysis, data mining, content-based image retrieval, face recognition, speech analysis and spectral remote sensing.

PCA is used to reduce a high dimensional vector to a low dimensional vector by exploiting the correlation existing in the data. PCA uncorrelates the resulting components, and the lower-order components are discarded.

PCA involves generating a new set of variables, called principal components. The first step in PCA is to calculate the data covariance matrix $\sum$:

$$\Sigma = \sum_{p=1}^{P} (x^p - \mu)(x^p - \mu)^T \tag{2.29}$$

Where P is the number of vectors in the data set and μ is the mean vector for the data set. The eigenvectors and eigenvalues of Σ are then calculated and ordered according to their variance. The eigenvectors corresponding to the largest eigenvalues are retained, and the input feature vectors are subsequently projected onto these eigenvectors to give the components (Principal Components) of the transformed vectors in the dimensional space. An orthogonal basis is extracted from the original feature vectors, which comprise the input space; hence all the principal components are orthogonal to each other. By having the vectors with the greatest information content (variability) ranked first, it is possible to decide when there is no benefit in extracting more vectors.

2.4.3 Pattern Recognition Models

Once a set of features has been selected, the next problem to be solved is to find a mapping from the components selected to the desired targets. The exact form of this mapping is to be determined from a data set of labelled examples. The procedure for constructing such a mapping is facilitated by the use of a particular pattern recognition model, which is the discussion of the next subsections. Many techniques are currently in use for solving pattern recognition problems. The best known of these are:

- Artificial Neural Networks (ANNs)
- Statistical Models
- Fuzzy Logic
- Expert Systems

2.4.3.1 Artificial Neural Networks

An artificial neural network (or neural network) is a mathematical computing paradigm that is based on the operation of a biological neural system: functions are executed collectively and in parallel by nodes, instead of there being a specific delineation of sub-tasks to which various nodes are assigned. The advent of neural networks facilitated the development of advanced pattern recognition systems with non-linear decision boundaries, through the implementation of simple training algorithms, to model complex multivariate relationships.

A neural network system will learn to classify inputs through a training process in which the network is presented with a series of inputs and target outputs. Based on this training data, the neural network will generate a map between the inputs and outputs. Subsequent input data will then be processed using the relationship derived using the training process to produce corresponding output variable values.

There are many classes and sub-classes of neural networks that are widely used in engineering applications. These have been described extensively in published literature, e.g. Lippmann (1987), Bishop (1995a), Hagan et al (1996). The most widely used neural network classes and subclasses are summarised in **Table 2.4.**

Three major learning paradigms can be applied in neural network modelling:

- Supervised learning
- Unsupervised learning
- Reinforcement learning

Pattern recognition and regression problems employ a supervised learning paradigm whereby a set of example inputs and targets is presented to the network and the aim of the learning process is to determine a function that describes the relationship between the variables. In unsupervised learning, the network training is entirely data driven and no target results for the input data vectors are provided. The Back-Propagation Neural Network (BPNN) is the core supervised learning technique employed in feed-forward neural networks. In the research work undertaken, the application of BPNN was examined.

Table 2.4 Neural Network Classes and Subclasses

NEURAL NETWORK CLASS	SUB – CLASS
Feed Forward	Multilayer Perceptron
	Radial Basis Functions
	Kohonen Self-Organising Feature Map (KSOFM)
Recurrent	Simple Recurrent Network
	Hopfield Network
Stochastic	Boltzmann Machine
Modular	Committee of Machines
	Associative Neural Networks

2.4.2.1.1 Multi Layer Perceptrons (MLP)

All types of neural network stem from the description by McCulloch and Pitts (1943), of a processing model comprising a building block known as a neuron and a networked interconnection. Rosenblatt (1958) expanded on this concept to investigate the computation of the eye and developed the first type of neural network which was known as a perceptron. However, Minsky and Papert (1969) showed that a single-layer perceptron neural network was limited to modelling linearly separable patterns and was unable to describe exclusive disjunction (XOR) functions and conjectured (incorrectly) that the same would be true of multilayer perceptrons. Grossberg (1973) later demonstrated that multilayer perceptron models could indeed resolve XOR problems.

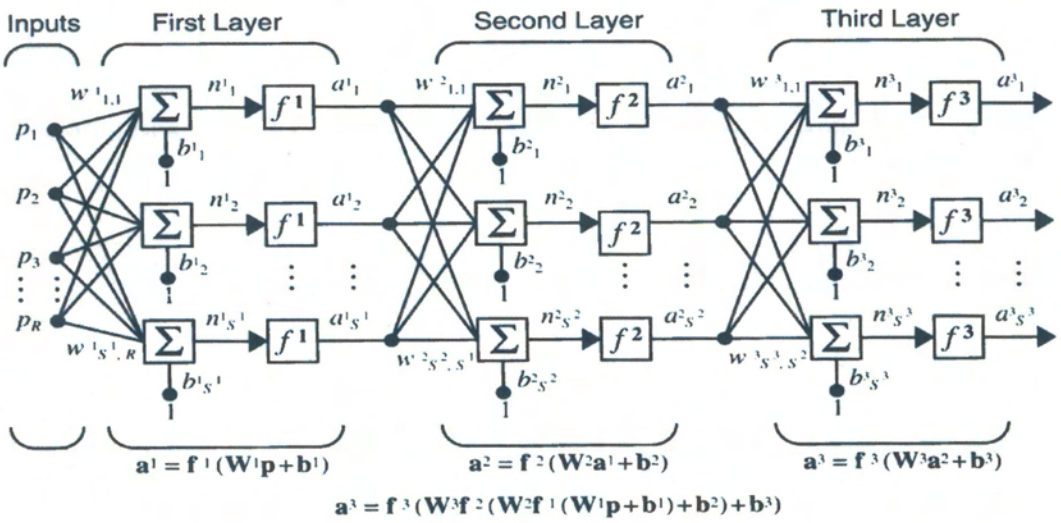

Figure 2.15 – Multi Layer Perceptron, taken from MATLAB

As shown in **Figure 2.15**, every input variable is represented by an input node, which is connected to all nodes in the hidden layers. Through training, these connections are assigned with independent weighting factors. The input to each node is multiplied by its associated weighting factor and then summed with the product of each of the other input nodes and their respective weighting factors. An activation threshold is then subtracted from this sum, and the result is processed by a non-linear transform function within the node.

It was shown in the 1960s that a single layer of perceptron could not learn how to compute the parity of a binary input pattern, Tarassenko (1998). It was then recognised that having several perceptrons operating in parallel could solve the problem. The output of one perceptron would become the input to another perceptron, i.e. by adding a second layer to the network and creating a multi layer perceptron.

Each input (p_i) is connected to all nodes in the first hidden layer. If successive hidden layers are employed, all outputs from the preceding layer are input to each node in the successive layer. For all nodes in the MLP, the inputs are summed (s), and after having been multiplied by their respective weights (w), a bias (b) is added to this total. The resulting value is used as the input to an activation function (f). Hence, the first hidden layer output ($y_{1,h}$) from each processing node in the MLP system with (I) inputs can be expressed by:

$$y_{1,h} = f^1\left(\sum_{i=1}^{I}(w^1{}_{i,h}\,p_i + b_{i,h})\right) \tag{2.30}$$

Accordingly, the outputs ($y_{0,j}$) from a two layer system (n=2) can be determined from the expression:

$$y_{0,j} = f^2\left(\sum_{h=1}^{H}\left(w^2{}_{h,j}\left(f^1\left(\sum_{i=1}^{I}(w^1{}_{i,h}\,p_i + b_{i,h})\right)\right) + b_{2,j}\right)\right) \tag{2.31}$$

Defining the network architecture is a key stage in neural network analysis. In most applications, the number of input and output neurons is fixed; thus, the problem of network architecture specification is reduced to the selection of layer function types, the number of hidden layers and the number of neurons therein.

It has been demonstrated that a two layer MLP with sigmoid non-linearity can approximate any function with arbitrary accuracy, Hornik et al (1989). Consequently, the only remaining parameter to be defined is the number of nodes to deploy in the hidden layer. There are no rules for the selection of the number of hidden nodes but, generally, the more complex the function one is attempting to model, the greater the number of hidden nodes required.

However, specifying the number of hidden nodes is a delicate balancing act: if too many nodes are used the network training data will simply be memorised and the system will exhibit poor generalisation; nevertheless, too few hidden nodes will result in a system with insufficient parameters to model the underlying function and severe underfitting will be experienced, Doan and Liong (2004).

2.4.3.1.2 MLP Neural Network Training Techniques

The purpose of MLP training algorithms is the iterative adjustment of the network weights and biases in order to minimise the network performance function. All training algorithms use the derivative of the performance function to determine the weight values that will minimise the performance function. Several different types of algorithm have been reported and exploited, **Table 2.5**:

Table 2.5 MLP Neural Network Training Techniques

Acronym	Algorithm	Optimisation Approach
GDM	Gradient Descent with Momentum	Modified Back-propagation
GDX	Variable Learning Rate	Modified Back-propagation
RP	Resilient Back-propagation	Modified Back-propagation
SCG	Scaled Conjugate Gradient	Numerical Optimisation Technique
CGB	Conjugate Gradient with Powell/Beale Restarts	Numerical Optimisation Technique
CGF	Fletcher-Powell Conjugate Gradient	Numerical Optimisation Technique
CGP	Polak-Ribiere Conjugate Gradient	Numerical Optimisation Technique
OSS	One-Step Secant	Numerical Optimisation Technique
LM	Levenberg-Marquardt	Numerical Optimisation Technique
BFGS	Quasi-Newton	Numerical Optimisation Technique

2.4.3.1.3 Back-propagation

Back-propagation (BP) is the core supervised learning technique employed in feed-forward neural networks. The errors propagate backwards from the output nodes to the inner nodes. The error for an output variable is calculated as the difference between the network outputs.

The basic characteristics of BP are the ability to form a mapping between sets of inputs and outputs by using activations extracted from input patterns, and the ability to generalise a situation since it learns how to respond to activations as the network is trained with different examples. The activation of each neuron in hidden and output layers are calculated from the sigmoid transfer (activation) function, **Figure 2.16**, Lippman (1987).

$$x_j^{'} = f\left(\sum_{i=0}^{N-1} w_{ij} x_i - \theta\right) \qquad 0 \le \mathrm{j} \le \mathrm{N_1} - 1 \qquad (2.32)$$

where;

$x_j^{'}$ is the output of the j^{th} node of hidden layer

x_i is the input value in i^{th} node of input layer

w_{ij} is the weight from input to hidden layer

N is number of nodes in input layer

$\mathrm{N_1}$ is number of nodes in hidden layer

θ is threshold value which is fixed for each neuron

f(ω) is sigmoid transfer function which is

$$f(\omega) = \frac{1}{1+e^{-\omega}} \tag{2.33}$$

Similarly, activations in output layer neurons are calculated by using the activation of neurons in the hidden layer. The weights are adjusted after each trial using the total mean square error between actual and calculated output values until the weights converge. This criterion is known as the Generalised Delta Rule.

The main disadvantage of BP is the requirement of a long training time. The design of the network structure is also important for obtaining high performance. Optimisation of structure and reduction of training time are other research areas of back-propagation neural networks.

One of the most important configuration parameters of the back-propagation network is the selection of the right number of hidden layers. Two hidden layers for computation were suggested Lippman (1987) for any decision boundary.

The other important parameter in structure design is the selection of the number of neurons in hidden layer(s). If the number of neurons is too small, the convergence of weights becomes difficult during training. However, keeping the number of neurons at a minimum reduces the training time.

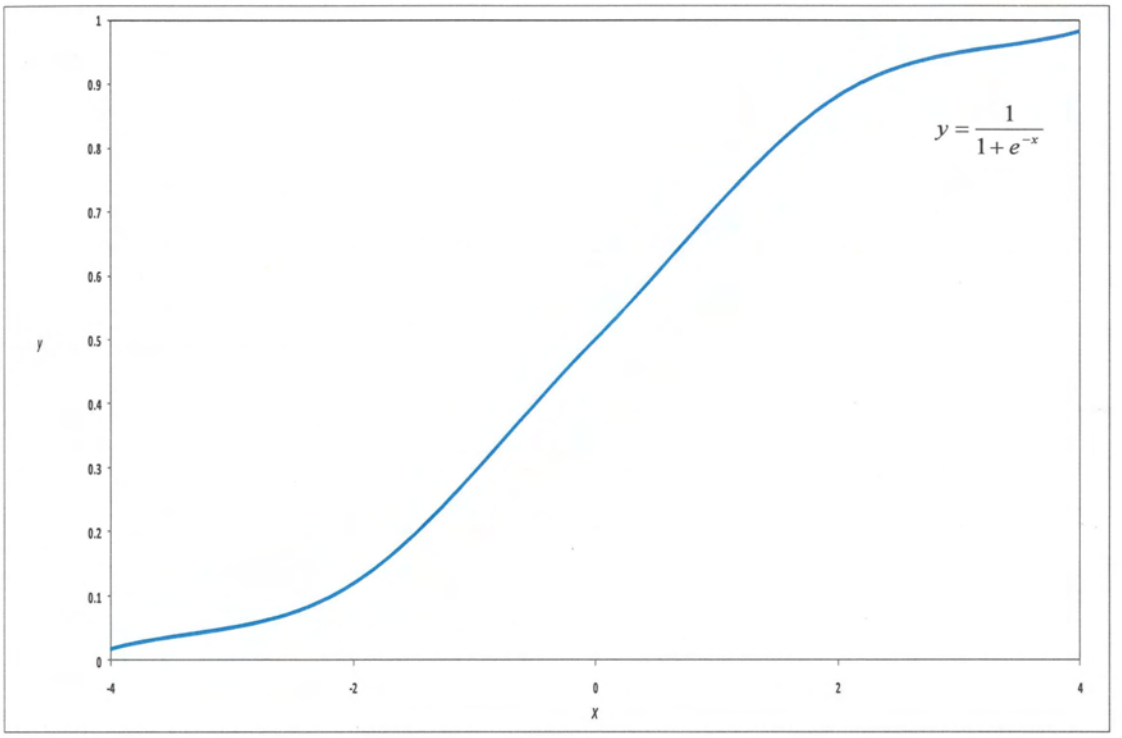

Figure 2.16 – The sigmoid transfer function of back-propagation neural network

The Generalised Delta Rule of BP always results in the mean square error decreasing if infinitesimal changes are made to the weights. However, this may take up too much time in training the network. The "learning rate" and "momentum term" are two parameters, which can reduce training time. A large "learning rate" speeds up training but causes oscillations in mean square error. Beginning with a large "learning rate" and then decreasing it when oscillations in error start is the best method of application of the "learning rate". The weights with "learning rate" are adjusted.

$$w_{ij}(t+1) = w_{ij}(t) + \eta \delta_j x_i^{'} \tag{2.34}$$

where, η is "learning rate" and δ_j is an error term for neuron j which is given by

$$\delta_j = y_j(1-y_j)(o_j - y_j) \tag{2.35}$$

if neuron j belongs to output layer and

$$\delta_j = x_j^{'}(1-x_j^{'})\sum_k \delta_k w_{jk} \tag{2.36}$$

if neuron $_j$ belongs to hidden layer. In above equations

o_j is desired output

y_j is calculated output

k is the neuron over all neurons in the layers above neuron $_j$

"Momentum term" is another parameter to speed up training without causing oscillations. This term decides the amount of the effect of previous weight changes on current weight change. The weight of the next connection by using both "learning rate" and "momentum term" is then obtained, Lippmann (1987).

$$w_{ij}(t+1) = w_{ij}(t) + \eta\delta_j x_j^{'} + \varphi(w_{ij}(t) - w_{ij}(t-1)) \qquad (2.37)$$

Where φ is "momentum term" and $0 \leq \varphi \leq 1$.

2.4.3.2 Avoiding Over-fitting

Bad generalisation by a neural network can stem from over exposure of the network to the training data set. This problem is known as over-fitting. Deciding when to end the training algorithm can have a major influence on the ability of the trained network to generalise new data sets. Training algorithms are nominally terminated when a local minimum has been attained or when the convergence rate is insignificantly low, i.e. improvement between successive iterations is zero or negligible after exposure to the training set for a certain number of epochs (cycles).

Different types of technique have been introduced to improve generalisation to avoid the over-fitting problem. Two of the widely used methods are cross-validation, otherwise known as early stopping, and Bayesian regularisation.

2.4.3.2.1 Cross-Validation

Cross-validation (or 'early-stopping') involves dividing the available data into three groups instead of two. In addition to the conventional training and test data sets, a validation set is produced. During the training process, the training data set is used to compute the network weights and biases. Simultaneously, the validation set is used to produce a validation error for the network configuration. The validation error is monitored and when the validation error continuously increases for a specified number of iterations, the training process will be terminated and the weights and biases present at the minimum validation error will be implemented for testing with a test data set. Although good results can be obtained using cross-validation, it is not particularly suited to applications with limited data. As not all of the data are used to train the model, and the training is terminated before attaining the minimum training error, the information contained in the selected data is not optimal and the network may suffer from under-constrained training.

2.4.3.2.2 Bayesian Regularisation

Another method of improving generalisation is by using the Bayesian MLP Neural Network, otherwise known as Bayesian Regularisation. Bayesian methods use probability to quantify uncertainty in inferences and the result of Bayesian learning is a probability distribution expressing our beliefs regarding how likely the different predictions are. A practical problem with MLPs is in controlling the complexity of the model (i.e. how to select the right number of neurons in the hidden layer, and control the weights and biases of the network). The Bayesian approach offers efficient tools for avoiding over-fitting and has become a viable alternative to the older, error minimisation-based approaches, MacKay (1992) and Bishop (1995b). In this method the performance function is complemented by additional terms that consist of the mean of the sum of squares of the network weights and biases as follows:

$$F(w) = \alpha E_d + \beta E_w \tag{2.38}$$

where, α and β denote control parameters which are to be optimised within the Bayesian framework of MacKay (1992) which has been successfully applied to a number of practical engineering problems.

Employing the modified performance function, described in **Eq. (2.38)** will yield a network with smaller weights and biases, thus forcing a smoother network response that is less likely to over-fit. It is assumed that the weights and biases are random variables with a Gaussian distribution. The regularisation parameters are related to the unknown variances associated with these disturbances. Analysis has shown that the optimal regularisation technique requires the determination of the Hessian matrix which necessitates intensive computation.

Alternative approximation techniques which are less calculation-intensive have been developed, such as Bayesian regularisation with the use of the Levenberg-Marquardt (LM) algorithm, Foresee and Hagan (1997). The key steps in this algorithm are:

1. Initialisation of the α and β control parameters, network weights, and biases.

2. Execute a single iteration of the LM algorithm to minimise the objective function described in **Eq. (2.38)**.

3. Determine the effective number of parameters (γ) using the Gauss-Newton approximation to the Hessian matrix available in the LM algorithm.

$$\gamma = N - 2\alpha Tr(H)^{-1} \tag{2.39}$$

where, N denotes the number of parameters and H denotes the Hessian matrix.

4. Calculate new estimates for the objective function control parameters α and β.

$$\alpha = \frac{\gamma}{2E_d(w)} \tag{2.40}$$

$$\beta = \frac{N-\gamma}{2E_d(w)} \tag{2.41}$$

5. Repeat steps 2-4 until convergence is attained.

The following factors should be checked during training for model performance:

- If γ is very close to N, then the network may be too small. Add more hidden layers and retrain.
- If the larger network has the same final γ, then the smaller network was large enough.
- Otherwise increase the number of hidden neurons.
- If the larger network is sufficiently large, then a larger network will achieve compatible values for γ, E_D and E_W.

The benefits of a regularisation technique together with the Bayesian Framework are summarised below:

- Regularisation improves generalisation.
- Bayesian Framework provides a measure of how many network parameters (weights and biases) are being effectively used by the network.
- Bayesian Framework eliminates the guesswork required in determining the optimum number of hidden neurons and consistently leads to good networks that are not over-trained.
- Hessian matrix calculation is required.
- Gauss-Newton approximation can be used to approximate the Hessian matrix.
- Computational overhead is minimal when using Levenberg-Marquardt training algorithm, as it is 10 to 100 times faster than other training algorithms.
- If either sum of the square weights or total number of effective parameters become the same two successive epochs, training may be terminated.
- Applications to practical problems demonstrate feasibility of the technique, MacKay (1992).

2.4.4 Kohonen Self-Organising Feature Maps (KSOFMs)

The unsupervised learning technique involves the use of self- organising feature maps to classify data, Kohonen (1982). The objective of a KSOFM network is to map the natural structures inherent in the input data vectors, of an arbitrary dimension N, onto a discrete map with just 1 or 2 dimensions as shown in **Figure 2.17**.

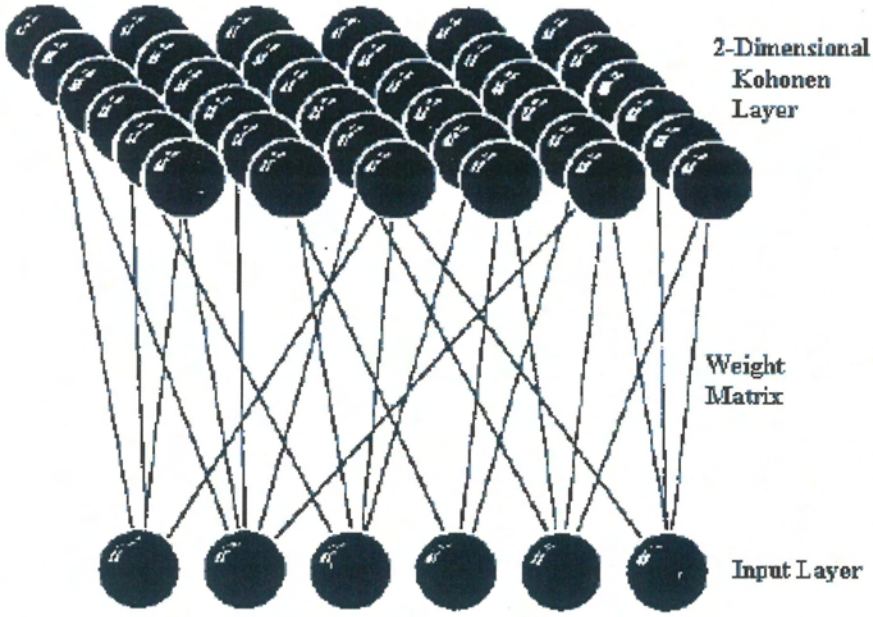

Figure 2.17 – Kohonen Self-Organising Feature Map, taken from Blaney (2008).

Patterns exhibiting similarities in the input space should be topographically arranged close to one another in the output map. These networks are particularly useful where complex high dimensional data needs to be presented in an understandable format.

The Kohonen Self Organising Feature Maps have been successfully applied to a number of practical engineering applications, Kohonen et al (1996). The KSOFM learning process comprises the following stages:

1. Initialisation of output node weights.
2. Looping of the following stages until node weights converge:

    2.1 For each data point:

        2.1.1 Present the input feature vector

        2.1.2 Calculate the similarity

        2.1.3 Determine the winning output node

        2.1.4 Locate all nodes in the neighbourhood of the winner

        2.1.5 Update the weight vectors of neighbourhood nodes

    2.2 Reduce the size of the neighbourhood (if required)

3. End learning process.

Similarity of a data point is normally determined by calculating the Euclidian distance between the input pattern and the weight vector. The network weights are exploited in

a different manner to that experienced in the Back Propagation Neural Networks: the weights are not multiplied with the input vector.

Thus, the Euclidean distance (d_i) is calculated for an input vector $\bar{p}$ and each i^{th} output node which has a corresponding weight vector $\bar{w}_i$.

$$d_i = \sqrt{(\bar{p} - \bar{w}_i)^T . (\bar{p} - \bar{w}_i)} \tag{2.42}$$

The winning output unit, or best matching unit (BMU), is simply the unit with the weight vector that has the smallest Euclidean distance to the input pattern, i.e. the most similar.

The neighbourhood of a node is defined as all nodes within a specified distance of the node on the grid. For example, in a square geometry grid, if the size of the neighbourhood is 1 then all units no more than 1 either horizontally or vertically from any unit fall within its neighbourhood. The weights of every node in the neighbourhood of the winning node, including the winning node, are updated according to Eq.2.43 thus, moving each node in the neighbourhood closer to the input data point.

$$\overline{w_i} \rightarrow \overline{w_i} + \eta(\overline{p} - \overline{w_i}) \tag{2.43}$$

Where, η denotes the step size.

As time progresses, the learning rate and the neighbourhood size are reduced. If the parameters are well chosen the final network should capture the natural clusters in the input data.

2.4.5 Application of PR Techniques to MPFM

Some of the foregoing pattern recognition techniques have previously been applied for multiphase flow measurement and analysis. The most prominent of the literature dealing with multiphase flow measurements using pattern recognition techniques is perhaps that conducted by the pioneering research work at Imperial College, London. This concept was first proposed by Darwich (1989). Here it was suggested that if the

turbulence characteristics of multiphase flow conditions are reproducible, then the flow rates of individual phases can be determined by identification of these characteristics. Using this approach a set of features was derived from the turbulent pressure signals, and pattern recognition methods were used for the identification and measurement of the individual phase flow rates in a two-phase flow. A statistical technique known as template matching was used as the pattern classifier model. A software package called ESMER was built as a result.

A 2-inch horizontal measurement spool piece comprising radially mounted pressure transducers and axially mounted capacitance and conductance sensors was constructed to perform two-phase tests with air and water. It was determined that eight features were effective in characterising the multiphase flow: three amplitude features (standard deviation, skewness and kurtosis) and five linear prediction coefficients. All eight features were extracted from pressure transducer signals but only the amplitude features were found to be discriminatory for the conductance/capacitance sensors. Template matching was employed as the pattern recognition method whereby the individual phase flow rates were identified by matching measured vectors to those in a reference database. A measurement accuracy of ±10% was reported for each of the individual phase flow rates with a confidence level of 90%.

Toral et al (1990) introduced an orifice plate to the horizontal spool piece set up by Darwich, described above, to study its ability to produce effective features for multiphase flow classification. It was reported that the presence of the orifice plate led to the production of enhanced discriminability for the extracted features.

Beg (1998) built upon previous work undertaken by Darwich using radially and axially mounted absolute and differential pressure transducers in 2-, 3-, and 4-inch horizontal multiphase flows. A new feature set was employed comprising the mean and variance from the amplitude domain, and five features from the Cepstrum domain. Template matching was the pattern recognition technique applied and it was reported that 100% of liquid phase and 93% of gas phase measurements could be obtained to within ±10 % through feature combinations. Comparisons made between

the feature maps for the different pipe sizes revealed that different turbulence signatures were obtained for the same flow conditions. Accordingly, a method of scaling was proposed based on the hydrodynamic coordinates and feature vectors. Measurement accuracy with the scaling technique was reported to be poorer than that obtained through *in situ* calibration. He also incorporated a gamma densitometer device into the measurement spool piece for the resolution of oil, water and gas flow rates in a multiphase flow. However, the gamma densitometer was just one of an array of sensors employed with the system: pressure, conductance and capacitance sensors were also exploited to predict flow regimes and individual phase flow rates in 3" and 16" diameter multiphase pipes. From each sensor, 24 feature vectors were extracted. However, these were limited to the mean, variance, minimum, maximum and a 20-bin amplitude histogram of each sensor.

Accuracies of ±10% were reported employing the gamma densitometer and ±18% from the pressure sensor for horizontal gas and liquid flows.

Akartuna (1994) undertook an experimental campaign with a 2-inch horizontal measurement spool piece with strip type capacitance sensors and pressure transducers in the slug flow regime for both two and three-phase flows. Two additional features were employed to those originally studied by Darwich: slug frequency and slug length. The template matching classification technique was compared and contrasted with a Multi Layer Perceptron neural network employing the SCG training algorithm. Akartuna reported that the MLP neural network system yielded superior classification properties when pressure and capacitance sensor fusion was employed: 97% of water cut, 90% of air velocity, and 90% of liquid velocity measurements were predicted to within ±10% relative error.

Cai (1995) proposed the development of a flow regime specific pattern recognition model using a Kohonen self-organising feature map to classify data point flow regimes and then employing a separate MLP neural network for flow rate determination for each 53 flow regimes. An F-ratio feature saliency technique was applied to facilitate the selection of an effective feature set. Phase flow rate measurement accuracies for the multi-level hierarchical system were reported to be ±5% for 100% of oil continuous data points and 95.2% of water continuous samples.

In terms of superficial velocity determination, 99.3% of gas and 100% of liquid phase superficial velocities were calculated to within ±9%.

Toral et al (1998) and Wood (2002) have described the commercial version of the ESMER multiphase flow meter developed through the aforementioned studies. Stochastic features are extracted from three differential pressure sensors (one top axial, one bottom axial and another radially mounted), impedance sensors (axially mounted on top) and a temperature sensor and input to an MLP neural network. The neural network system is trained and then validated, using the cross-validation technique to avoid over-fitting, before being subjected to tests. The individual phase flow measurements made by the ESMER meter were reported to match those yielded by the test separators to within ±10%.

A number of pattern recognition studies in multiphase flow measurement have been conducted outside of the ESMER development programme.

Goudinakis (2004) investigated the feasibility of using an MLP neural network for flow regime identification in a horizontal pipeline and an S-shaped riser for air-water flow using capacitance sensors and pressure transducers respectively. Stratified smooth, stratified wavy, bubble and slug flow regime classifications were identified using raw time-series data (fixed length window) as the input to the system. The S-shaped system was determined to accommodate long severe slugging flow cycles up to 230 seconds; while the horizontal system cycles did not take more than 10 seconds. It was reported that a delay window of 200 inputs (20 seconds of data at 10 Hz) was required for horizontal pipe regime classification, while 100 inputs (100 seconds of data at 1 Hz) was adequate for identification of the S-shaped riser's flow pattern. Nevertheless, it was identified that the excessive training time required to enable classification would prevent this technique from being suitable for practical applications.

Jama (2004) reported on the use of pattern recognition techniques using absolute and differential pressure signals from a Venturi meter to measure wet gas flow rates. A Bayesian MLP network was implemented using feature extraction from the pressure sensor signals. It was reported that by employing cross-sensor data fusion of

amplitude features, all test data points predicted the gas and liquid superficial velocities to within ±5% relative error.

Wylie et al (2006) proposed the use of an electromagnetic cavity resonator-based sensor to determine multiphase flow rates. Low power radio frequencies were transmitted across a pipeline carrying a multiphase flow and the phase fractions calculated by monitoring the shift in the resonant frequencies with different fluid properties. Neural networks were exploited to overcome the modelling complications induced through the application of the system to different flow velocities, temperatures, pressures, installations etc. Measurement accuracies of ±10% for phase fractions were reported and a measurement repeatability of 4% was claimed based on the experimental data presented.

Sheppard and Russell (1993) investigated the ability of a neural network to classify horizontal gas and liquid flow rates from the response of a gamma densitometer. No information was provided on the gamma densitometer system employed but it is reported that standard statistical parameters were extracted from the raw signals for use as the system inputs. The neural network was trained on 12 time-series covering a range of flow regimes. The pattern recognition model was firstly evaluated using unseen data from the 12 time-series used to train the network and produced gas and liquid flow rates to within a root mean square error of 13%. A second phase of analysis was undertaken using data from previously unseen flow rates; the classification accuracy was reduced to a root mean square error of 15%.

Bishop and James (1993), and Bishop (1995b), proposed a technique using gamma attenuation based on the use of three vertical and three horizontal dual-energy gamma densitometer beams installed in a parallel configuration across a pipe section. The input features to the neural network were the six path lengths measured by the gamma densitometers, and the target outputs were the volume fractions of the oil and water phases. The Quasi-Newton training algorithm was employed in these studies. It was concluded that a neural network technique based on gamma attenuation could provide a practical solution in determining component phase fractions from the gamma densitometer data.

Åbro et al (1999) documented their findings using an americium-241 source and a multibeam configuration with a neural network to identify the flow regime and the void fraction. A computer simulation model of the gamma emission and detection system was employed to create training data sets for the neural network. The input to the network was an energy spectrum for the photon range 30 to 68 keV (i.e. 38 bins of 1 keV) for single sensor investigations and an energy spectrum for the photon range 55 to 64 keV for the multi-detector experiments. Test data was collected on an 8 cm aluminium pipe using a 14 mCi americium-241 source and a CZD detector from eV Products Inc. Using a single detector position at 180° to the source, an average error of 15.8% was obtained for the void fraction measurements with a standard error deviation of 8%. Using a multi-detector setup, the inputs were parts of spectra at detector positions of 180°, 156°, and 140°. The multi-detector configurations yielded average void fraction errors of just 3% and a reduced standard error deviation of 4.2%.

Blaney (2008) reported the analysis of the use of pattern recognition techniques to correlate gamma densitometer data with the individual phase superficial velocities and the water cut with two neural network models (a single multilayer-perceptron and a multilayer hierarchical flow regime dependent model). The pattern recognition systems were trained to map the temporal fluctuations in the multiphase mixture density with the individual phase flow rates using statistical features extracted from the gamma count signals as their inputs. Initial results yielded individual phase flow rate predictions to within ±10% based on flow regime specific correlations.

2.4.6 Salinity Effects on Multiphase Flow Measurements

The term "Salinity" refers to the amount of dissolved salts that are present in water (Kg/m3). Sodium and Chlorides are the predominant ions in sea water, and the concentrations of Magnesium, Calcium and Sulphate ions are also substantial. Increased oil recovery by water injection causes changes in the produced water, since the injected water and the formation water have different salinity. There may also be horizontal and/or vertical gradients in the formation water salinity across the reservoirs, and this may cause sudden changes in the salinity of the produced water in the case of "water breakthrough", McCoy et al (1994). This problem is of increasing importance since new technology has made it economically feasible to produce marginal wells with more than 80% water content, with varying salinity levels.

Both electromagnetic and nuclear sensors exhibit changes in their response when confronted with a change in water salinity. Recalibration can usually solve the problem, but is often not convenient especially for a subsea meter; furthermore, the change in salinity needs first to be detected, Scheers and Slijkerman (1996) showed that water salinity could change significantly in a short period of time as shown in **Figure 2.18**.

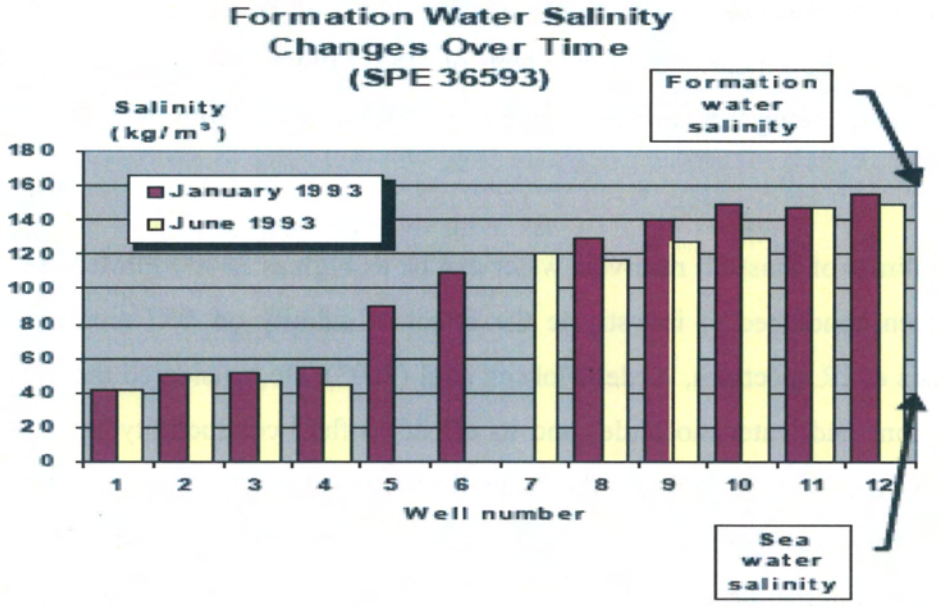

Figure 2.18 - The Salinity's of various wells from the North Sea, Scheers and Slijkerman (1996)

The salinity's of various wells from one North Sea field as measured in January and June 1993. The formation water salinity is 160 kg/m3 and the sea water salinity is 35 kg/m3. Salinity changes gradually from the formation water salinity to sea water salinity.

Johansen and Jackson (2000), used a dual mode densitometry method to measure the gas volume fraction in gas/oil/water pipe flows independent of the salinity of the water component. They applied this method to homogeneous and annular flows making use of the different responses in photoelectric attenuation and Compton scattering to changes in salinity.

The dual mode densitometry method used by Johansen and Jackson detects changes in salinity using one gamma-ray energy and two detectors. A traditional detector located outside the pipe is used to find the total attenuation coefficient. A second detector positioned between the source and transmission detector is used to measure the scatter response.

Results of the work showed that it is possible to measure the gas void fraction in homogeneously mixed multiphase flows using the dual modality densitometry principle independent of the salinity of the water. For the annular flow, the gas void fraction measurement was dependent on the salinity of the water due to the densitometer being less sensitivity to changes farther away from the source side of the pipe.

The salinity of most oil reservoir water can be as high as 30000 PPM. Some research has been conducted to investigate the effect of salinity on WC measurement with analysis of IR spectrum, Abdel-Mohsen et al (2003). He considered the interaction of NaCl ions and water molecules and its effect on fluid conductivity, specific gravity, surface tension as well as the overall effect on water fraction measurement. Considering the hydrogen bonding which is prevalent in water, the interaction between water molecules and increasing salt concentration destroys this hydrogen bonding by ionic interaction, thus forming unstable concentration of HCL and NaOH as shown below.

$$Na^{+}Cl^{-} + H^{+}OH^{-} \longrightarrow HCl + NaOH$$

The conductivity of water increases due to the formation of more polar substances such as HCl. This may also account for the increase in the dielectric constant of the mixture. With increase in the dielectric constant of the mixture, WC measuring meters such as the Microwave and Capacitance based meters are likely to read higher WC than present. Increased salinity increases the mass of the mixture, as a result, the specific gravity of the mixture increases. The increase in specific gravity implies increase in the density of water, which results to a corresponding increase in dielectric constant of the mixture.

3.4.6.3 Conductance Sensor Response

Figure 3.13 presents a typical maximum value feature response for a conductance sensor for multiphase oil, water and gas flow. The sensor's performance is severely impaired in an oil continuous flow as shown.

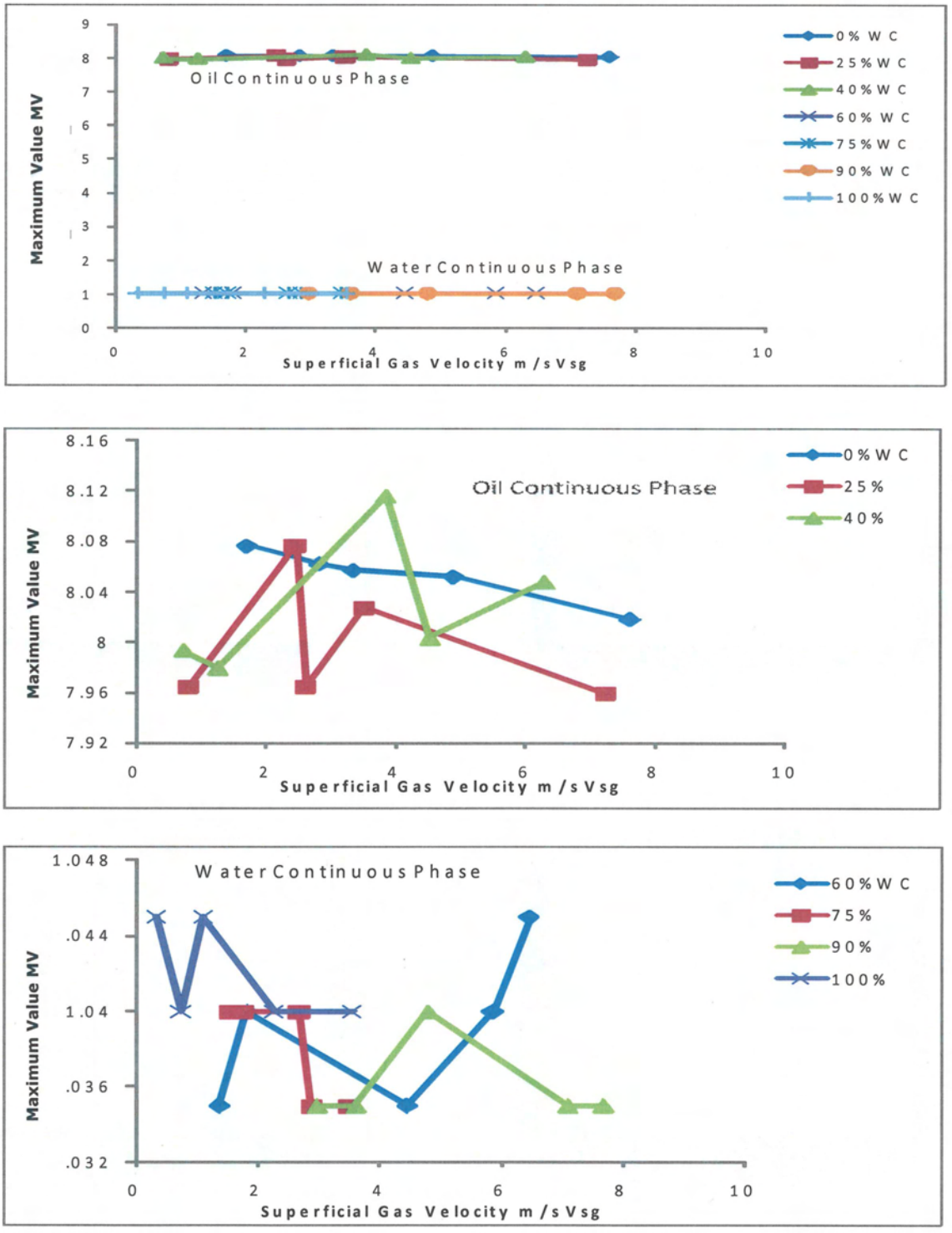

Figure 3.13 – Response of Maximum Value Conductance Feature to Water Cut

3.4.6.4 Gamma Amplitude Features

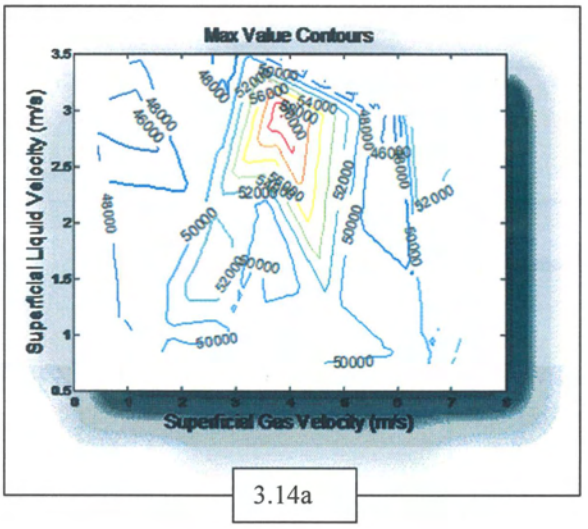

3.14a

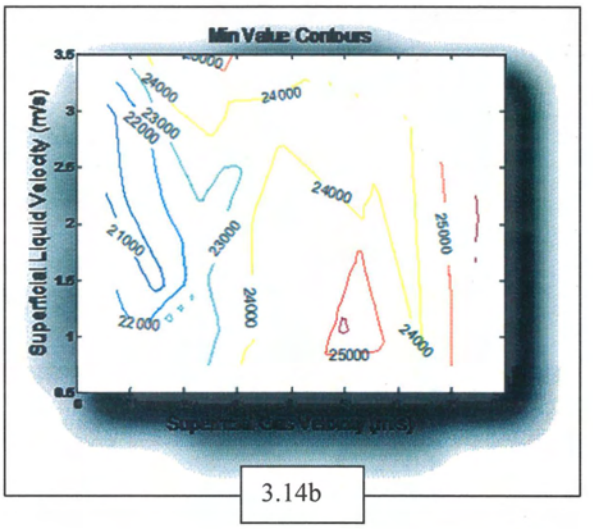

3.14b

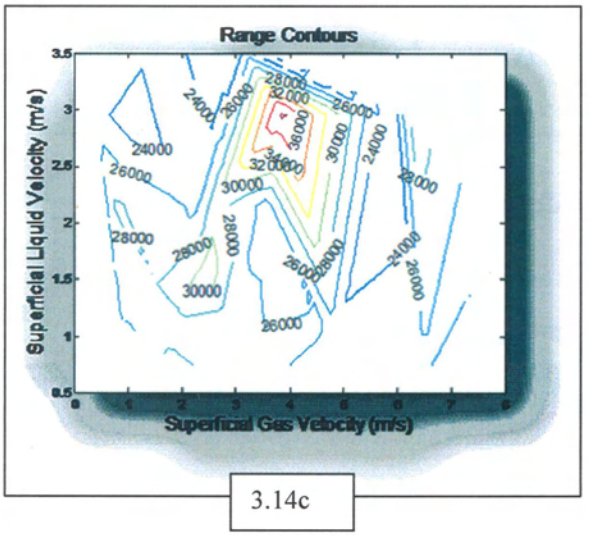

3.14c

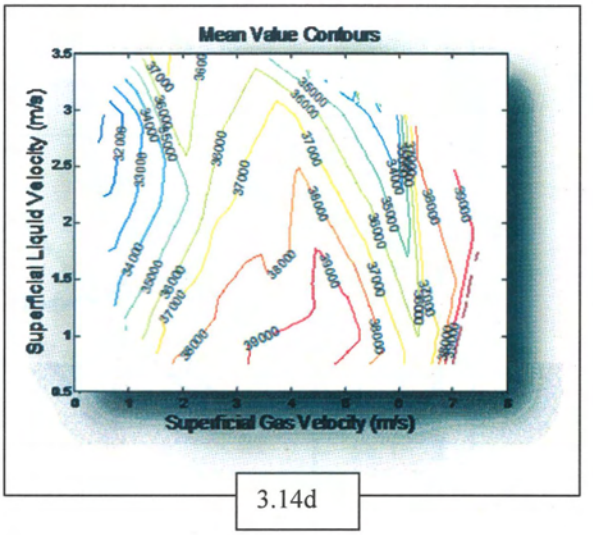

3.14d

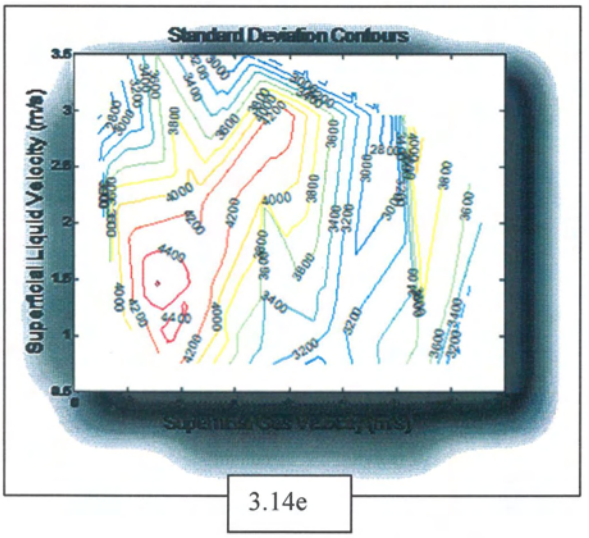

3.14e

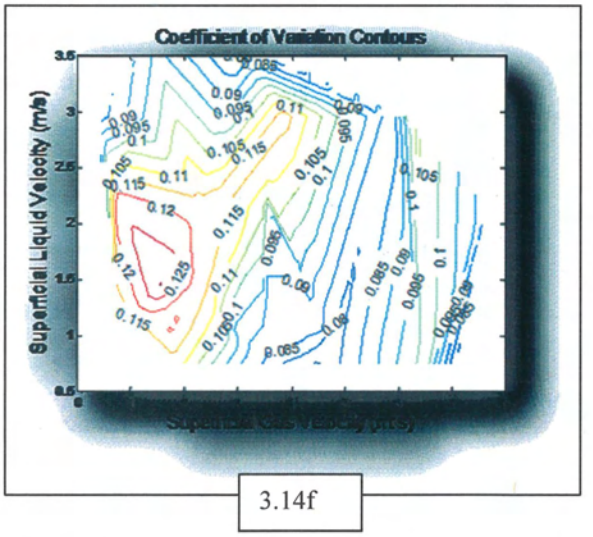

3.14f

Figures 3.14 a-f – Amplitude Features Contour Maps of Gamma Signal

3.5 Notes on Experiment and Database

It is worth stating that the sensor signal database was collected as part of the Flow Programme Work for the United Kingdom Department of Trade and Industry (DTI) now called Department of Business Enterprise and Regulatory Reform (DBERR).

In conjunction with the National Engineering Laboratory (NEL), Cranfield University designed and assembled the sensor spool piece. The response data from the sensor spool piece was collected over a wide range of oil, water and gas flow rates in NEL's Multiphase Flow Loop in East Kilbride, Glasgow. Data were collected under two different salinities of 50 and 100 g/l $MgSO_4$.

It must be noted that the differential pressure data in test numbers MU0601 to MU0616 were corrupted and appeared random and negative. (These data sets were excluded for the purpose of this research work). During subsequent tests/calibrations (MU0617 – 44), which were conducted by the author at both NEL and Cranfield University facilities, a number of techniques were used to ensure that the data collected were valid and that the sensors correctly responded to flow conditions. Sensor response as a function of time was plotted and monitored online. Test parameters such as superficial gas/liquid velocities, water cut, gas volume fraction etc. were analysed and validated through comparisons with reference conditions at regular intervals.

The author was also involved with the sensor database creation (preliminary data analysis, design of sensor signal template, report preparation etc.) at Cranfield University, through the final stages of the project.

Please refer to Appendix C for additional information on the data acquisition system.

CHAPTER 3

EXPERIMENTAL SET-UP

The recommendation of a previous survey project undertaken by Cranfield in the 1996-1999 Flow Programme, funded by the DTI's NMS programme, was the creation of a sensor database for multiphase flow. The rationale behind this was that the cost of collecting sensor responses to multiphase flows under representative conditions is high and beyond the means of research institutions and small innovative companies. Yeung et al (1998).

3.1 Sensor Spool Piece

In conjunction with NEL, Cranfield University designed and assembled the sensor spool piece. The response data from the sensor spool piece were collected over a wide range of oil, water and gas flow rates in NEL's Multiphase Flow Loop in East Kilbride, Glasgow. Data were collected under two different salinities of 50 and 100 g/l $MgSO_4$. To allow researchers to ensure that the techniques developed were installation independent, the spool piece was placed at two different locations in the flow loop where the flow regime induced by the pipe arrangement and location was expected to be different.

3.1.1 Selection Criteria

There is a wide range of sensors (both commercial and laboratory) used to study multiphase flows. They can be intrusive or non-intrusive. For better reliability and easier maintenance, non-intrusive sensors are more desirable as they are less prone to erosion, corrosion or excessive pressure drop problems. Non-intrusive sensors include:

i. absolute pressure
ii. temperature
iii. differential pressure
iv. conductance
v. capacitance
vi. gamma and x-ray
vii. microwave

viii. ultrasound

ix. infra red

The pressure and temperature sensors are primarily used to determine the average conditions at the measurement point for the estimation of fluid properties such as density, viscosity and surface tension.

In the selection of sensors to be used in the sensor array, the following criteria were considered:

i. known behaviour in oil/water/gas flows

ii. frequency (or dynamic response)

iii. complexity of sensor output processing

iv. commercial availability

v. cost

vi. non-intrusive design

vii. reproducibility

viii. ruggedness/complexity

The above criteria were then rated A, B or C with A representing the best and C being the worst as shown in **Table 3.1**.

Table 3.1 Sensor Selection Matrix, Yeung et al (2002)

SENSOR	**CRITERIA**							
	I	**ii**	**iii**	**iv**	**v**	**vi**	**vii**	**viii**
Absolute pressure	A	A	A	A	A	A	A	A
Differential pressure	A	A	A	A	A	A	A	A
Conductance	A	A	A	B	B	A	A	A
Impedance	A	A	A	B	B	A	A	A
Gamma	A	B	A	A	B	A	A	B
X-ray	A	B	B	B	C	A	A	B
Ultrasonic	B	B	B	B	B	A	B	B
Microwave	B	B	B	B	B	A	B	B
Infrared/Optical	B	C	C	B	B	A	B	B

3.1.2 The Sensor Array

Using the consideration mentioned above, a combination of sensors was selected. All the sensors and equipment are commercially available. The sensors are generic in nature and thus their response should be similar to sensors of other makes. This means that the signal analysis techniques developed by the user of the database should be applicable to other similar sensors and thus their efforts will not be restrained and restricted.

The multiphase sensor spool as shown in **Figure 3.1** below comprises sensors in the following order:

	Sensor	Distance from Densitometer
1.	Gamma ray densitometer	0
2.	Capacitance sensor 1	590 mm
3.	Conductance sensor 1	1060 mm
4.	Capacitance sensor 2	1500 mm
5.	Conductance sensor 2	1960 mm
6.	Absolute pressure transducer	2330 mm
7.	Differential pressure transducer 1	2640 mm
8.	Differential pressure transducer 2	2740 mm
9.	Thermocouple	2840 mm

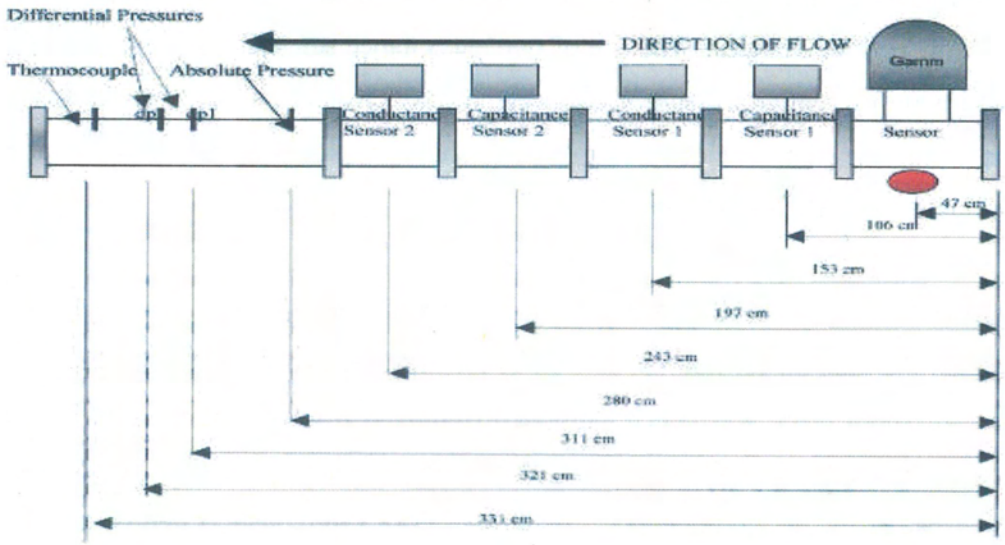

Figure 3.1 – Schematic of Sensor Spool Piece, Yeung et al (2002).

Length of spool piece is about 3.43m and weighs about 400 kg

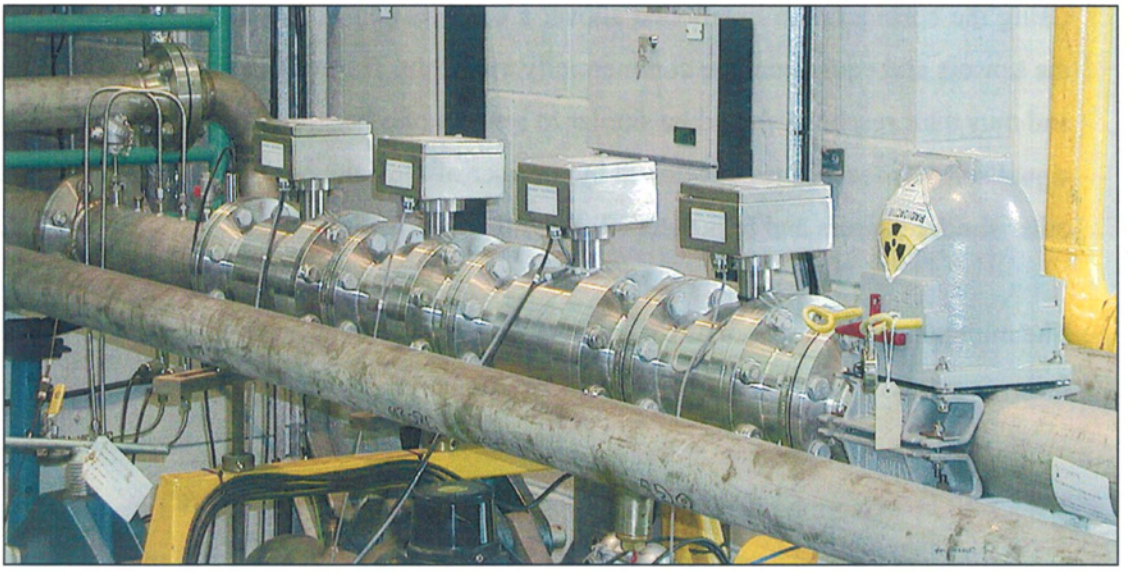

Figure 3.2 – Sensor Spool Piece mounted at NEL Test Facility, Yeung et al (2002).

The temperature and absolute pressure transducers are used to determine the properties of the mixture. The gamma ray densitometer provides a measurement of the mixture density. The capacitance and conductance sensors are needed to cope with oil continuous and water continuous flows respectively. Together with the gamma ray densitometer, the three sensors should be able to give the relative composition of the three phases. The differential pressure sensors indicate the liquid holdups and response to flow regime changes. The use of two capacitance sensors, two conductance sensors and two differential pressure transducers, allows cross correlation between the sensors to determine phase velocity, **Figure 3.2** shows a picture of the sensor spool piece mounted on the 4" flow loop at NEL.

Once the whole sensor spool piece was assembled, the sensors were calibrated for water and then oil for holdup, as well as for the height of the liquid in the pipe. The sensor spool piece was bench calibrated (removed from the flow loop). This bench calibration involved blanking both ends of the sensor spool piece with calibrated transparent flanges and gradually filling the sensor spool piece at height intervals of 1 or 2mm and recording the signals from all sensors. This method is, however, deficient considering flow pattern effects and errors generated with, say, bubbly flow etc.

3.1.2.1 Gamma Ray Densitometer

The gamma ray density gauge supplied by Ronan Engineering consists of a shielded source holder containing a radioactive Caesium^{137} source, a detector unit and a signal processing box. The source has strength of 185 MBq.

The source holder and the detector are mounted directly opposite each other across a stainless steel pipe. During operation, a beam of gamma ray is shone through the complete cross sectional area of the pipe and the process material inside it, onto the surface of the detector. The absorbed radiation is directly related to the density (or mass) of the material it went through while the transmitted radiation is inversely related to that density (or mass).

The gamma densitometer had to account for the radiation absorbed by the pipe material as well as the background radiation count. Calibration was carried out using water and air as the media, in accordance with the operating procedure supplied by the manufacturer as shown in **Figure 3.3** below. Although the output signals (i.e. 4 to 20 mA) can be assumed to be linear with the calibrated densities, the output signals are not linear to the radiation counts rates registered by the counter.

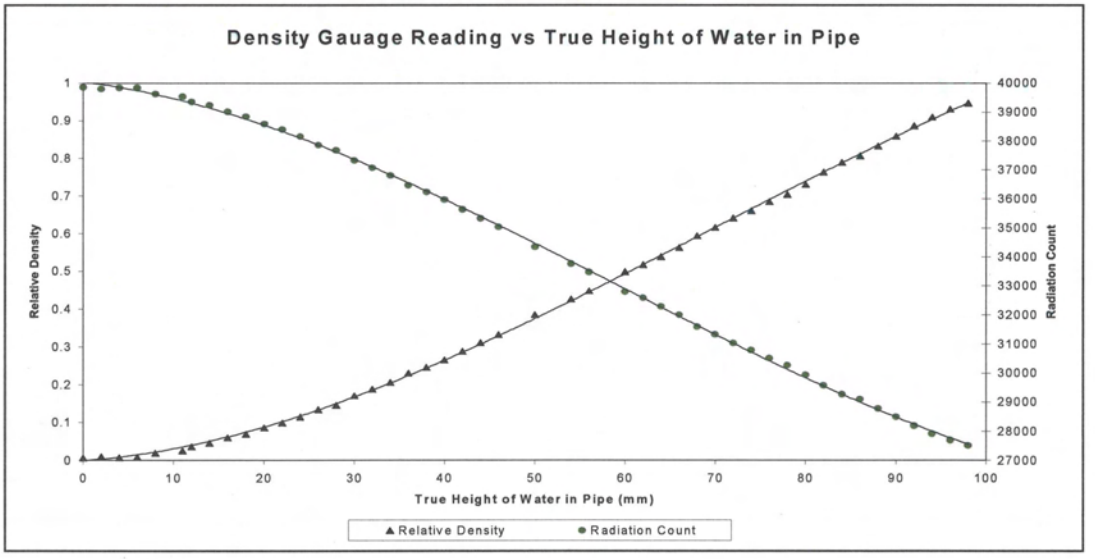

Figure 3.3 – Calibration Data for Gamma Densitometer, Yeung et al (2002).

3.1.2.2 Capacitance Sensors

The capacitance sensors are supplied by Siemens Milltronics Process Instruments B.V. in the Netherlands. Each system comprises an MFT300 flow sensor and an MFT200 detector module.

The MFT300 flow sensor is an assembly of flow-through electrodes with an attached electronics module, "the driver". The driver circuit generates the measurement signal and compensates for parasitic capacitances in sensor and cabling.

The output signals must be tuned on site for air and water so that 0V (or alternatively 4mA) will correspond to air, and 5V (or alternatively 20mA) will correspond to water. Details can be found in the instruction manual supplied by Milltronics. For simplicity, the signals were converted through the data acquisition system to show 1 for a pipe full of water and 0 for an empty pipe.

As the output signal is not linear, the performance of the sensor must then be calibrated to relate the signals to various liquid holdups. The device is capable of following the dynamic changes in the process up to 1000 samples/sec. It responds both for water and oil, although its response for the latter is much lower in signal output. **Figures 3.4 a-c** shows calibration curves for the capacitance meter.

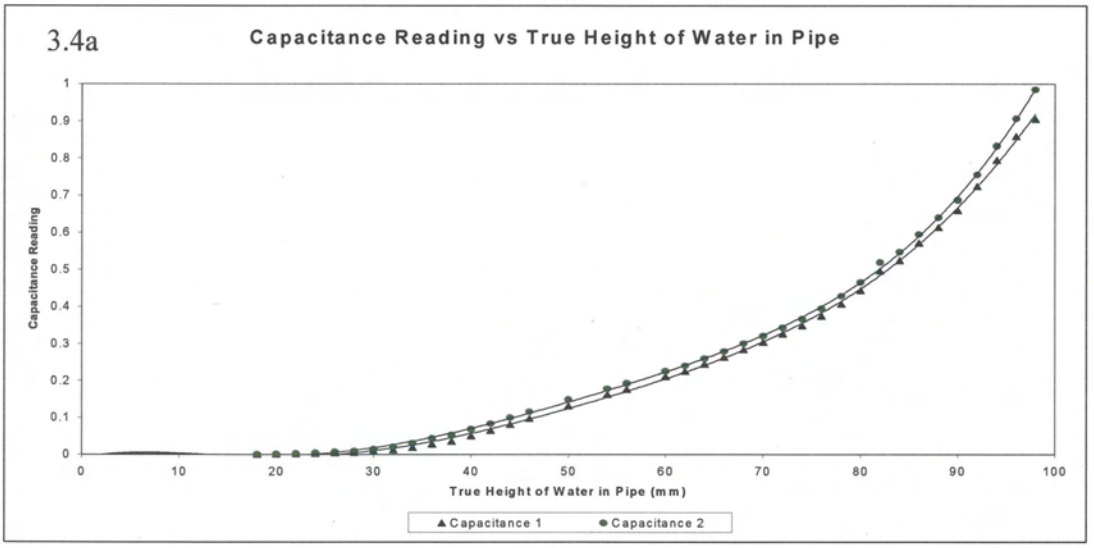

Figures 3.4a – Calibration Data for Capacitance Meter, Yeung et al (2002).

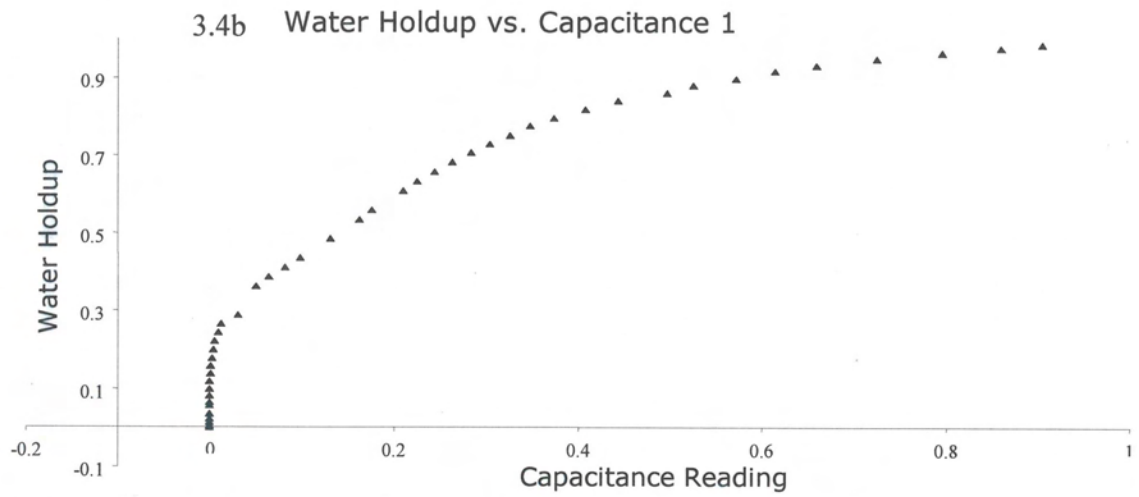

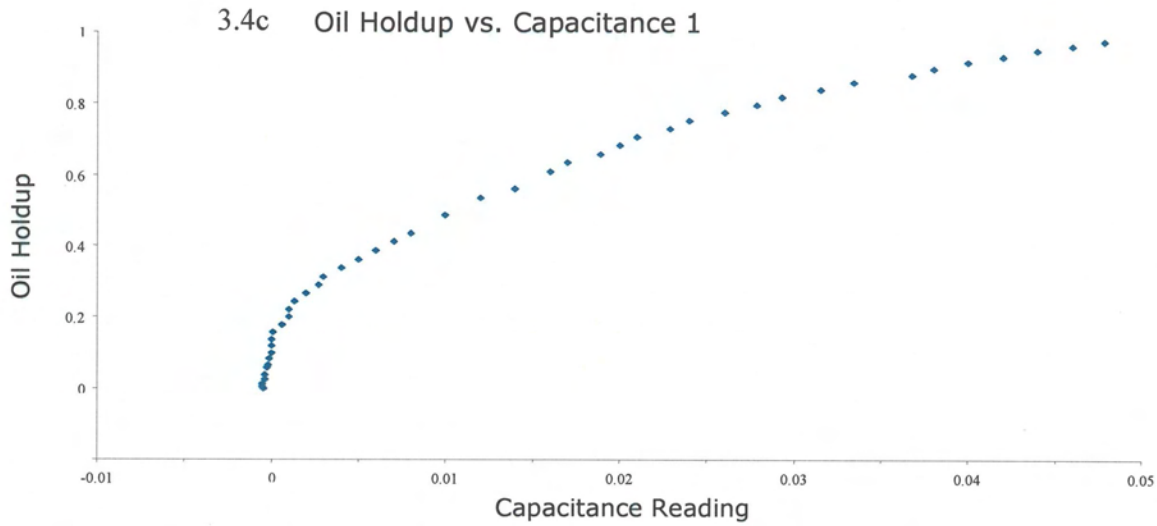

Figures 3.4 b and c – Calibration Data for Water and Oil Holdup for Capacitance 1

3.1.2.3 Conductance Sensors

The conductance sensor model MGT9500, is supplied by Siemens Milltronic Process Instruments B.V. in the Netherlands and is suitable for products with high conductivity. It uses a 60kHz signal with a current source output to allow a very small current through the product. A pair of ring electrodes applies the signal to the product and across the resistive part of the product; a voltage then builds up. This voltage is measured and used to drive the current loop signal.

The output signals from the devices are tuned to a fixed range by the supplier. Hence, a local calibration check is necessary to record the output data for water, air and also various liquid holdups. As the output signal is not linear, the performance of the sensor must be calibrated to relate the signals to various liquid holdups. The conductance sensor does not work with oil. The sensors were set to give a signal of between 7.5V and 8.2V for a pipe full of clean water and 1V for an empty pipe. This enables a clear visualisation of the two sensors and allows for cross referencing. **Figures 3.5 a-c** shows calibration curves for the conductance meter.

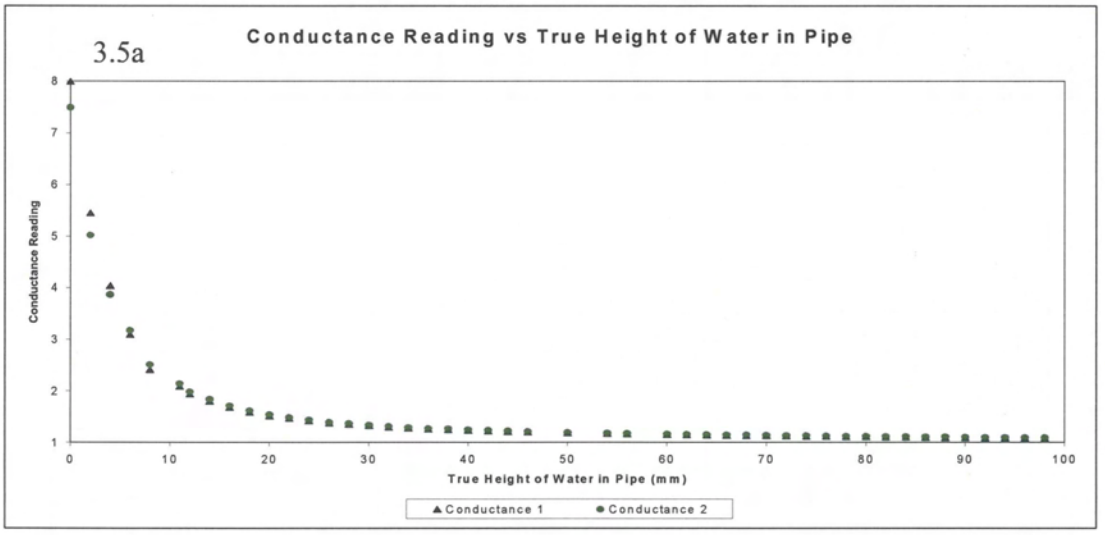

Figures 3.5a – Calibration Data for Conductance Meter, Yeung et al (2002).

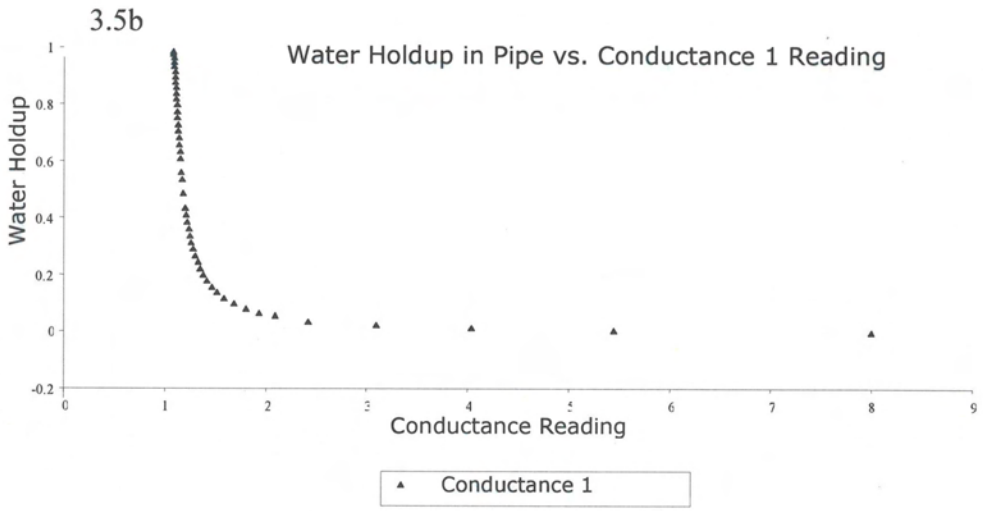

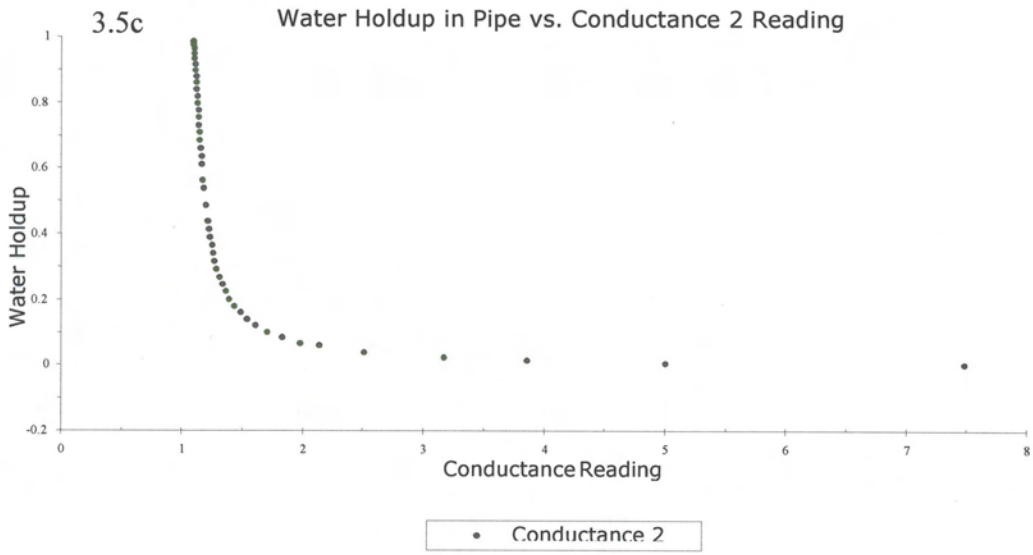

Figures 3.5b and c – Calibration Data for Water Holdup for Conductance Sensors

3.1.2.4 Differential Pressure Transducer

The differential pressure transducers model PMP 4110, supplied by Druck, are of the silicon diaphragm type. They have a range of 0.7 bar with a voltage signal from 0 to 5 Volts. They incorporate corrections for thermal induced errors, and Non-Linearity and Hysteresis of +/- 0.08%. **Figures 3.6 a-c** shows calibration curves for the differential pressure transducers.

They are installed to measure the differential pressure between the top and bottom of the pipe. When in gas/liquid stratified flows, they give the height of the liquid layer in the pipe. The distance between the two differential pressure transducers was set at one pipe diameter apart.

Due to the installation using fitting and connecting stainless steel tubes, the actual position of the transducers is about 95 to 105mm below the inside surface of the pipe. Hence, the transducer would measure 95 to 105mm H_2O for an empty pipe when the stainless steel tubes are filled with water. Therefore, the reading on the data acquisition system has to be reset to zero for an empty pipe. This can be achieved by inserting a zero offset in the data acquisition system.

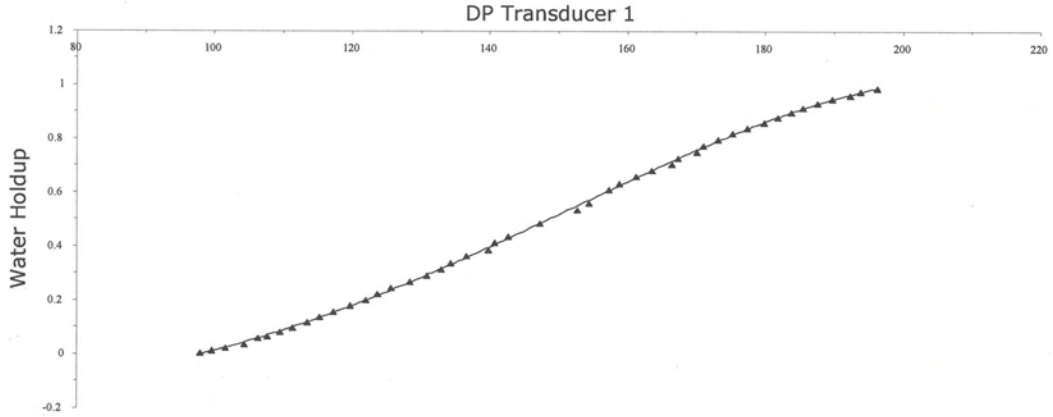

3.6a Differential Pressure Transducer 1 Readings versus Water Holdup

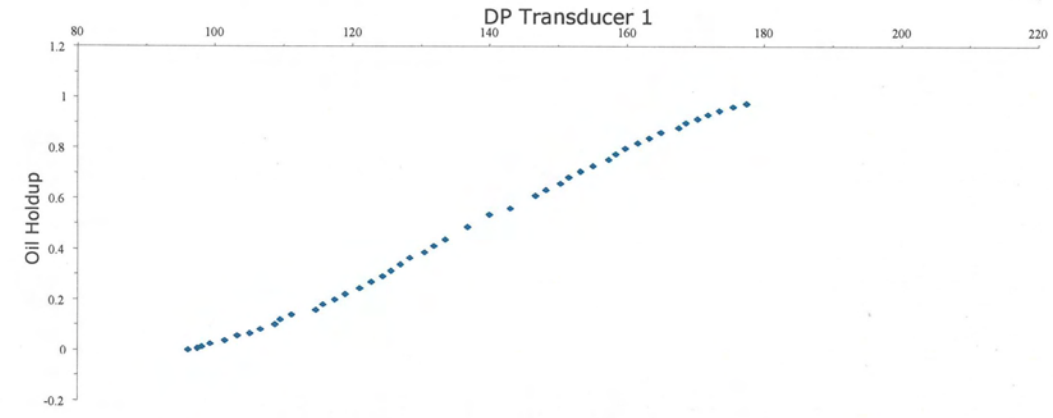

3.6b Differential Pressure Transducer 1 Readings versus Oil Holdup

Figures 3.6 a and b – Calibration Data for Water and Oil Holdup for Differential Pressure Transducer1

3.1.2.5 Absolute Pressure Transducer

The absolute pressure transducer model PMP 4010- a silicon diaphragm type, was supplied by Druck. It has a range of 20 bar and an output voltage of 0 to 5V D.C. It incorporates corrections for thermal induced errors, and Non-Linearity and Hysteresis of +/- 0.08%.

3.1.2.6 Temperature Transducer

A T-type thermocouple was used to measure the temperature in the pipe. The temperature transmitter connected to the thermocouple outputs a linear response from a voltage of 0V for 0°C to 5V for 100°C. The thermocouple has a range of -200 to 400°C and its signal response is of the order of 1 Hz.

3.2 Signal Conditioning and Data Acquisition System

The instrumentation is wired into a signal processing console/cabinet, which processes and conditions the instrument outputs into voltage signals (from 0 to 5V). The unit is custom built to house all the power supplies and individual signal conditioners for the instruments. It allows individual signal conditioners to be accessed for tuning or adjustment.

All the conditioned signals from the signal processing console are linked to an analogue-to-digital converter card through a signal distribution box. This card converts and inputs all the signals into a dedicated computer. The data acquisition software chosen for the above function is LABVIEW (from National Instruments). The data files created by LABVIEW can be input into or opened by any spreadsheet software for data analysis.

A data acquisition system was set up to monitor signals from a number of different sensors and save them to a data file at a chosen rate. During the data acquisition process, LABVIEW read a run identifier string generated by NEL's SCADA system, which was transmitted over a serial link. This identifier string triggered the start/stop of the data acquisition process.

3.2.1 Data Acquisition Software

The software controlling the data acquisition was written in LABVIEW version 6i. The software is supplied in the form of an executable file. A LABVIEW program (called a VI, or Virtual Instrument) consists of several sub-VIs. These comprise a front panel and a diagram. The front panel is made up of controls and indicators whose function is to control the flow of data into and out of the VI. Every sub-VI executes during each loop of the main program. A MENU allows the user to view the front panel of key VI's during program execution. Some of these contain controls that may be operated to perform certain functions.

3.2.2 Data Acquisition System Hardware

The DAQ hardware comprises of a 16-channel analogue-to-digital converter (A/D converter) card and a timer/counter card. Both of these are installed in PCI slots in the computer chassis **Figure 3.7** shows the data acquisition system hardware, while **Figure 3.8** illustrates the data cable connection. Their outline specifications are as follows:

A/D converter

Type:	PCI-MIO-16E-4
No. channels:	16 Single-ended or 8 differential (selectable)
Speed:	250 kS/s in single channel operation
Input Range:	±10V

Timer/Counter

Type:	PCI 6601
No. Counters:	4
Speed:	10MHz
Input Range:	±10V

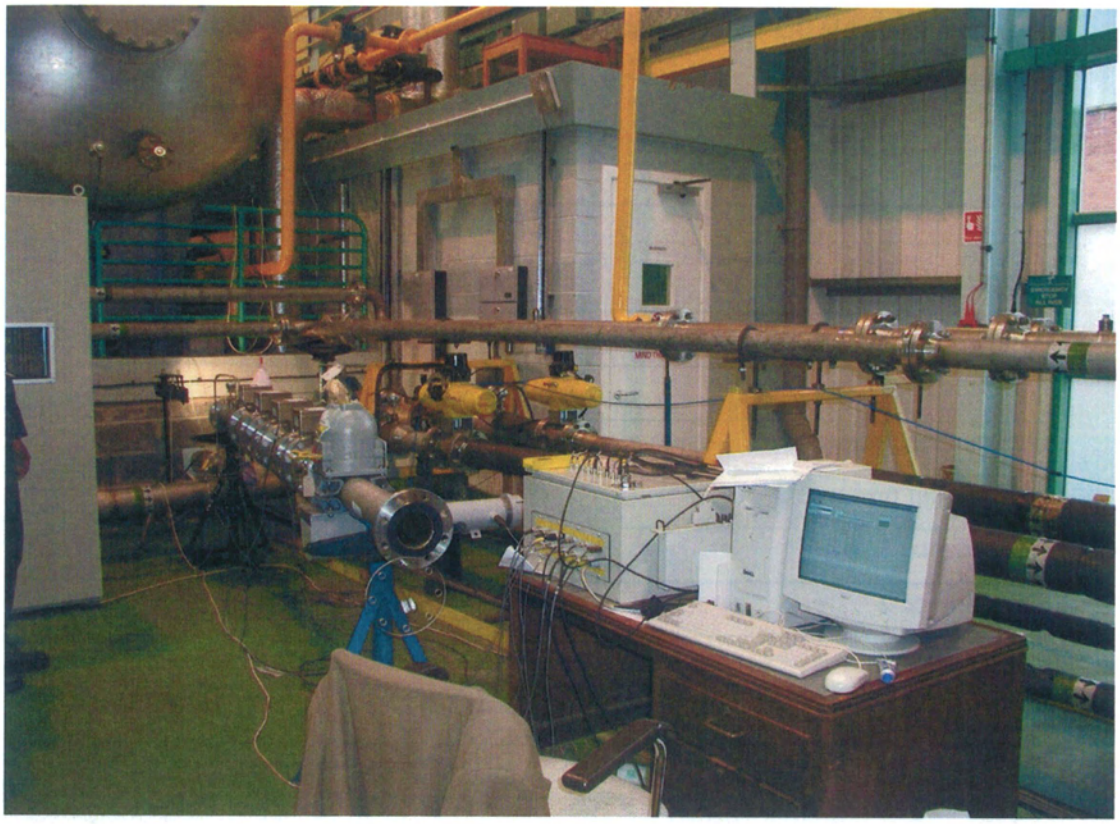

Figures 3.7 – Test area at NEL Facility showing the DAQ System, Yeung et al (2002).

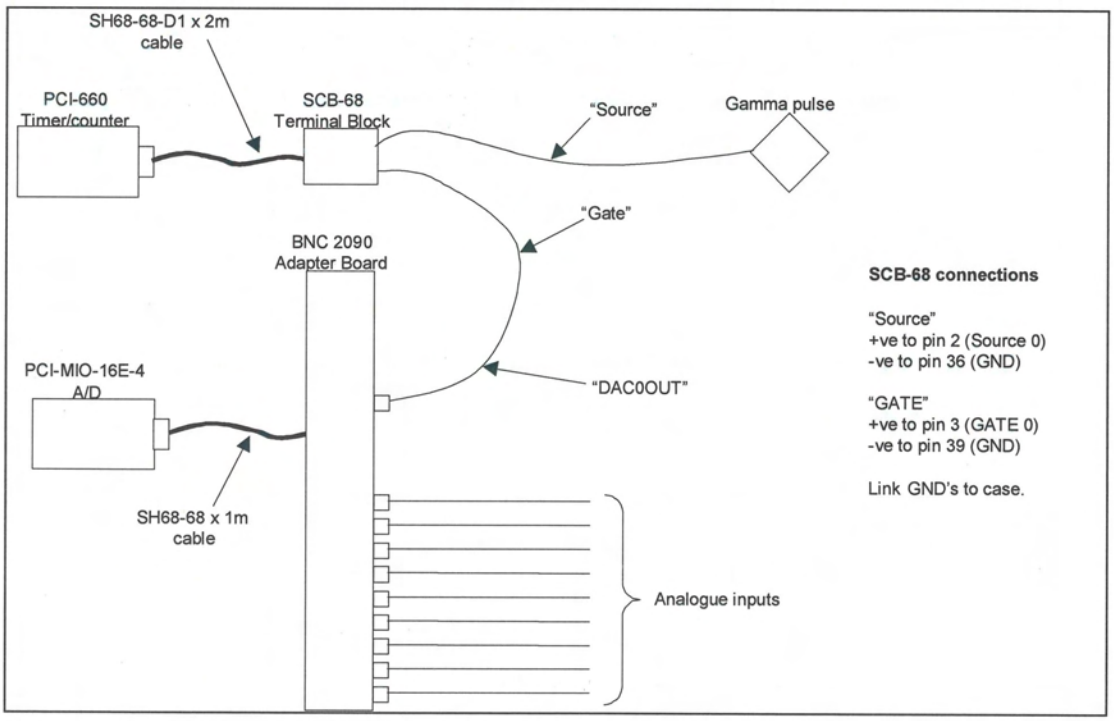

Figure 3.8 – Data cable connection for Data Acquisition System, Yeung et al (2002).

The details in **Table 3.2** below relate to the information the data acquisition program interprets:

Table 3.2 Voltage Output for Measured Parameters

Measured parameter	**Sensor output**
Temperature	0 – 5V D.C.
Absolute pressure	0 – 5V D.C.
Differential Pressure 1	0 – 5V D.C.
Differential pressure 2	0 – 5V D.C.
Capacitance 1	0 – 5V D.C.
Capacitance 2	0 – 5V D.C.
Conductivity 1	0 – 5V D.C.
Conductivity 2	0 – 5V D.C.
Gamma densitometer 2	TTL-type pulses (typically 4V peak)

The response of the temperature sensor is of the order of 1 Hz. That of the 'Gamma densitometer 1' output is 8 Hz (internal circuitry gives a minimum response time of 125 ms). The response of the rest of the sensor group is of the order of several kHz. Although the instrumentation associated with the gamma densitometer 2 output may generate pulses with a width of less than 1 μs (1 MHz), the minimum width observed in practice was approximately 7.5 μs (133 kHz). However, it was not possible to vary the data acquisition rate for each channel as the hardware used would not allow it and even if it had been possible, time and keeping the different channels in the data file would have been difficult. During subsequent analysis, the user must be aware of the limitations of each sensor.

3.2.3 Data File Structure

The data file is in ASCII format and can be read directly into a spreadsheet. However, as the sampling rate is 250 Hz, the file is fairly large. Earlier versions of spreadsheet programs like Microsoft Excel will not be able to display all the 75,000 rows of data. Only 65,536 rows of data can be displayed. However, the 75,000 rows of data do not pose any problem for other data editing software or mathematical programs (e.g. MATLAB etc).

3.3 Three Phase Facility at NEL

Figure 3.9, below shows the Multiphase facility, with the test section inset.

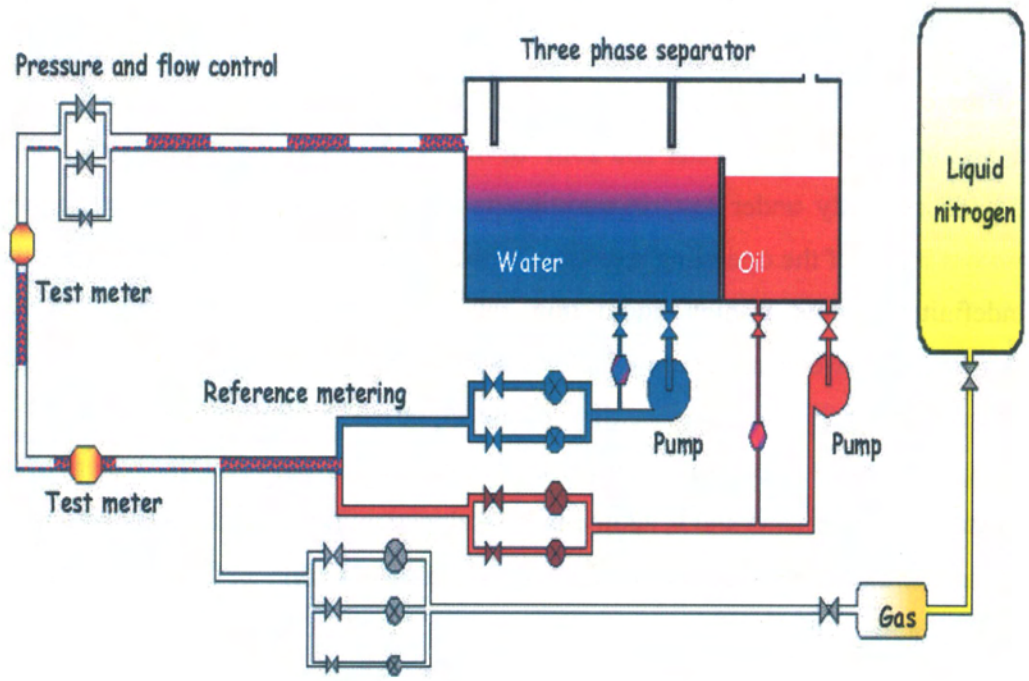

Figure 3.9: Schematic of NEL Multiphase Flow Facility

The multiphase facility is based around a 3-phase separator, which contains the working bulk fluids. The oil and water are recycled around the test facility using two variable speed pumps. For safety reasons, nitrogen is used as the gas phase and can be delivered at up to 0.5 kg/s by evaporation of liquid nitrogen on demand. The delivery pressure of the nitrogen is up to 12 bar at the point of injection. After passing through the test section, the nitrogen is vented to atmosphere from the separator, schematic of the NEL Flow loop is shown in **Figure 3.9** above.

The different oils and waters used are stored in tanks under the separator and in tanks kept outside the building. When a fluid change is required the separator is drained and the new fluid is pumped into the separator. The facility is manufactured entirely from stainless steel and can thus utilise brine substitutes and dead crudes as the

working fluids in addition to de-ionized water and refined oils. The oil used for this test is a mixture of Forties and Beryl crude oil – D80, topped to remove light ends and increase flashpoint to about 75°C, with kerosene added to restore original viscosity (approx. 33° API gravity).

At the centre of the facility is a large three-phase gravity separator, which contains approximately $35m^3$ of water and $25m^3$ of oil. This acts as the storage vessel for the liquids currently under test, in addition to separating the fluids for recirculation. Across much of the operating envelope of the facility, the liquids can be recirculated indefinitely, while at high liquid flow rates (especially oil-continuous flows) the degree of cross-contamination of the oil and water usually means that flow must be paused for a period to allow settling of the liquids. The separator is equipped with pumps and piping to allow transfer of settled liquids between the water, oil and mixture compartments and is additionally equipped with heat exchangers which allow the temperature of the oil and water to be maintained within ±1 °C over the range of approximately 10° to 40°C.

The facility operation is controlled by an automated SCADA system, which allows a single operator to control the entire facility from a PC workstation. The PC is linked to the PLC and Cranfield's Data Acquisition System via an Ethernet connection, which permits a response time from command to action of less than one second. The PLC is linked to all the field instruments on the facility.

A 4" Perspex visualisation section is installed immediately upstream of the sensor spool piece.

3.3.1 Flow Regime Map

The flow rates of nitrogen, water and oil were varied so that a wide range of water cut and GVF (gas void fractions) could be obtained for the tests.The first data sets from the sensor spool piece were obtained from Test Section 1, at a location on the flow loop where the full flow regime had been generated. The sensor spool piece was then moved to a location further upstream (Test Section 2), where the flow regime had not been fully developed before repeating some of the test conditions.

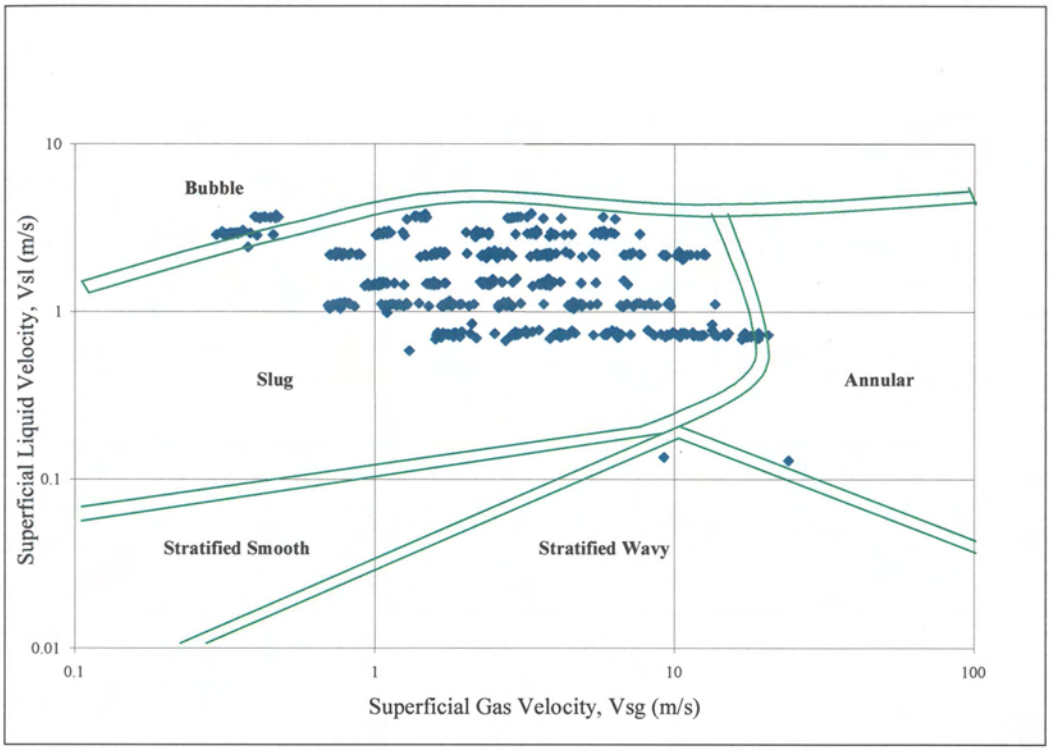

Figure 3.10 – Flow Regime Map showing the Matrix of Data Collected, Yeung et al (2002).

Figure 3.10 shows the full test matrix plotted on a flow regime map. This is a flow regime map of NEL, typical of flow regimes generated by the flow loop.

Test numbers MU0601 to MU0619 were carried out using a water salinity of 50 g/l $MgSO_4$ while test numbers MU0621 to MU0637 were carried out using a water salinity of 100 g/l $MgSO_4$ at the first location (i.e. location of fully developed flow regime). MU0638 to MU0644 were carried out using a water salinity of 100 g/l $MgSO_4$ at the second location where the flow regime was not fully developed.

3.4 Experiments

At the start of each day of tests, the height of liquid in the pipe measured by the differential pressure transducer was adjusted to zero, under no-flow and dry conditions. This process was necessary due to drifting of the zero offsets experienced over time and was achieved by adjusting the offset value of the differential pressure transducer in the data acquisition system.

The operation of the NEL multiphase facility is computer automated. The requested flow rates are set through the SCADA system, where a control loop then adjusts the flow rates according to the input flow rates and measured pressure and temperature at the point of metering. For each test, when each flow condition was generated, it was left to stabilise for five minutes to allow the flow regime to fully develop, before any data were collected.

After the flow had been allowed to stabilise for five minutes, the "start recording" and "stop recording" signal would be sent from the NEL data acquisition system to the Cranfield data acquisition system. During the data collection process, NEL's data acquisition system records the flow conditions while Cranfield University's data acquisition system records the sensor response. The test files are date and time-stamped, and individual test points are also time-stamped. The data acquisition duration for each test condition was five minutes at a frequency of 250Hz.

3.4.1 Data Collection and Raw Data Processing

For each multiphase flow experiment, the data collected were stored simultaneously into two separate files with two different computers. One of the computers was storing the outputs from the instruments on the spool piece and the other computer (at NEL) was storing information of the flow rates for the phases involved, before the spool piece. Both computers were also recording every time step at which a sample was recorded.

The data were later merged using a VI on LABVIEW platform to generate single files, containing the reference measurements with corresponding signals response of the flow conditions. The data were stored in files with the following file structure:

The first seven rows form the file header for the reference measurements. The reference measurement data are split into nine columns A to I:

A. Test Point
B. Number of Records
C. Temperature (T), °C
D. Mean Pressure, bar(g)
E. Oil Flow, l/s
F. Water Flow, l/s
G. Gas Flow, l/s
H. Water cut, %
I. Gas Fraction, %

Rows 9 – 15 form the file header for the test rig signals response, which are split into 10 columns A – J.

3.4.2 "Spool Piece" Signals Responses are as follow:

A. Time in seconds
B. Temperature (T1), °C
C. Absolute Pressure (P3), bar(a)
D. Differential Pressure 1 (d.p.1), mmH_2O
E. Differential Pressure 2 (d.p.2), mmH_2O
F. Capacitance 1 (Cap.1) – 0 for air and 1 for full of water
G. Capacitance 2 (Cap.2) – 0 for air and 1 for full of water
H. Conductivity 1 (Cond.1) – 8.2 for empty and 1 for full of water
I. Conductivity 2 (Cond.2) – 7.5 for empty and 1 for full of water
J. Transmitted Gamma radiation counts, ctr

3.4.3 Sensor Response Database

A total of 531 test conditions were recorded during the test programme. This included test conditions carried out mainly in slug flow regimes, different water salinities, and the two test locations. Overall, there is almost 2.7 GB of data recorded.

Tests numbers MU0601 to MU0619 were carried out using water with a salinity of 50 g/l $MgSO_4$. It must be noted that the differential pressure data in test numbers MU0601 to MU0616 were corrupted and appeared random and negative. However, data from all other sensor in the file were unaffected and hence accurate.

Tests MU0621 to MU0637 were carried out with the higher salinity solution of 100 g/l $MgSO_4$ using the same test matrix.

The last set of data, i.e. tests MU0638 to MU0644, with the new spool piece location, and where the distance between the sensor spool piece is very close to the supply line did not have enough time to allow the flow regime to fully develop.
In addition, the database also contains:

1. A <readme.txt> file, which gives a general description of the database.

2. A <TEMPLATE.xls> file, in Microsoft Excel format, a spreadsheet which contains the full details of all the data files. This template allows the users to view the summary of any of the data set and to sort and locate any data in accordance with their preference in terms of any flow conditions, flow regimes, etc. The file also contains charts specially prepared to allow the users to view the data and the trends graphically.

3. An <instruction.txt> file, which is a set of simple to follow instructions to the users to view the data using the graphs in the <TEMPLATE.xls> file

3.4.4 Reference Measurements

The reference measurements sheet as shown in **Table 3.3** contains the following information for all the tests points:

1. File Name
2. Test Point
3. Number of Records
4. Mean Temperature, °C
5. Mean Pressure, Bar(g)
6. Oil Flow, l/s
7. Water Flow, l/s
8. Gas Flow, l/s
9. Water Cut, %
10. Gas Fraction, %
11. Superficial Liquid Velocity, m/s
12. Superficial Gas Velocity, m/s
13. Flow Pattern
14. Salinity of Water
15. Location of Sensor Spool Piece

3.4.5 Sensor Signals

Sensor signals are displayed in Columns A to I.

Columns M to P display the following computations:

V_{sl} – Superficial Liquid Velocity, m/s

V_{sg} – Superficial Gas Velocity, m/s

V_{so} – Superficial Oil Velocity, m/s

V_{sw} – Superficial Water Velocity, m/s

Table 3.3 Abridged Signals Database Reference & Test Measurements indicating Salinity and Spool Piece Location, Yeung et al (2002).

			Reference Measurements							Test Meter Measurements				
File Name	Test Point	No. Records	Mean Temp degC	Mean Pressure Bar g	Oil Flow l/s	Water Flow l/s	Gas Flow l/s	Water Cut %	Gas Fraction %	Superficial Velocity Liquid m/s	Superficial Velocity Gas m/s	Flow Patte	Salinity	Spool Piece Location
MU0601	1	100	38.35	1.18	5.848	0.058	98.721	0.99	94.35	0.717	11.99	SLUG	50g/l MgSO4	1
MU0601	2	100	39.06	3.61	6.299	0.062	50.878	0.98	88.89	0.772	6.18	SLUG	50g/l MgSO4	1
MU0601	3	100	39.06	2.35	17.987	0.172	102.442	0.95	84.94	2.205	12.44	SLUG	50g/l MgSO4	1
MU0601	4	100	39.66	5.75	5.727	0.054	34.387	0.94	85.61	0.702	4.18	SLUG	50g/l MgSO4	1
MU0601	5	100	39.79	5.19	9.321	0.088	22.988	0.93	70.96	1.142	2.79	SLUG	50g/l MgSO4	1
MU0601	6	100	40.39	5.74	5.992	0.056	14.350	0.92	70.35	0.734	1.74	SLUG	50g/l MgSO4	1
MU0601	7	100	39.49	5.60	6.185	0.058	27.644	0.92	81.58	0.758	3.36	SLUG	50g/l MgSO4	1
MU0601	8	100	39.25	3.69	17.943	0.140	62.765	0.77	77.63	2.196	7.62	SLUG	50g/l MgSO4	1
MU0601	9	100	38.81	3.36	9.240	0.069	68.101	0.75	87.97	1.130	8.27	SLUG	50g/l MgSO4	1
MU0601	10	100	37.75	0.97	5.740	0.042	143.765	0.73	96.13	0.702	17.46	SLUG	50g/l MgSO4	1
MU0601	11	100	39.57	5.04	8.858	0.064	40.363	0.72	81.90	1.083	4.90	SLUG	50g/l MgSO4	1
MU0601	12	100	39.97	5.75	8.848	0.062	23.472	0.70	72.48	1.082	2.85	SLUG	50g/l MgSO4	1
MU0601	13	100	40.14	5.72	9.078	0.064	14.223	0.70	60.87	1.110	1.73	SLUG	50g/l MgSO4	1
MU0602	1	100	41.78	0.69	0.909	7.999	80.094	89.79	89.99	1.082	9.73	SLUG	50g/l MgSO4	1
MU0602	2	100	40.77	2.14	0.685	5.468	88.923	88.87	93.53	0.747	10.80	SLUG	50g/l MgSO4	1
MU0602	3	100	40.55	0.91	0.694	5.439	157.212	88.69	96.25	0.745	19.09	SLUG	50g/l MgSO4	1
MU0602	5	100	41.44	5.24	13.511	4.937	13.761	26.76	42.72	2.240	1.67	SLUG	50g/l MgSO4	1
MU0602	6	100	40.76	3.85	6.974	2.247	63.103	24.37	87.25	1.120	7.66	SLUG	50g/l MgSO4	1
MU0602	7	100	39.28	1.61	4.675	1.463	124.647	23.83	95.31	0.745	15.14	SLUG	50g/l MgSO4	1
MU0602	12	20	39.32	0.87	4.839	1.374	81.367	22.11	92.91	0.754	9.88	SLUG	50g/l MgSO4	1
MU0602	13	100	37.99	1.64	4.657	1.312	139.337	21.98	95.89	0.725	16.92	SLUG	50g/l MgSO4	1
MU0602	14	20	42.81	0.47	3.747	0.061	0.000	1.60	0.00	0.462	0.00	SLUG	50g/l MgSO4	1
MU0603	1	100	41.87	1.87	1.782	16.188	63.429	90.08	77.92	2.182	7.70	SLUG	50g/l MgSO4	1
MU0603	2	100	41.89	2.49	4.536	13.453	92.977	74.78	83.79	2.184	11.29	SLUG	50g/l MgSO4	1
MU0603	3	100	42.28	1.06	2.448	6.718	78.131	73.30	89.50	1.113	9.49	SLUG	50g/l MgSO4	1
MU0603	4	100	41.23	1.29	1.631	4.408	142.632	72.99	95.94	0.733	17.32	SLUG	50g/l MgSO4	1
MU0603	5	100	41.78	0.84	2.537	3.628	141.348	58.85	95.82	0.749	17.16	SLUG	50g/l MgSO4	1
MU0603	6	100	43.10	0.80	3.727	5.330	79.391	58.85	89.76	1.100	9.64	SLUG	50g/l MgSO4	1
MU0603	7	100	43.30	2.44	7.426	10.515	98.029	58.61	84.53	2.179	11.90	SLUG	50g/l MgSO4	1
MU0603	9	100	41.35	1.88	9.953	6.933	87.765	41.06	83.86	2.050	10.66	SLUG	50g/l MgSO4	1
MU0603	11	100	38.76	0.95	3.512	2.337	139.871	39.96	95.99	0.710	16.98	SLUG	50g/l MgSO4	1
.	.	.	.	.	.	.	.	.	.	.	.	.	.	.
.	.	.	.	.	.	.	.	.	.	.	.	.	.	.
MU0641	1	100	35.62	5.04	0.954	8.156	21.953	89.53	70.67	1.106	3.656	SLUG	100g/l MgSO4	2
MU0641	2	100	35.33	4.93	0.977	8.283	5.953	89.45	39.13	1.124	1.729	SLUG	100g/l MgSO4	2
MU0641	3	100	35.76	5.00	0.968	8.202	37.233	89.44	80.24	1.114	5.517	SLUG	100g/l MgSO4	2
MU0641	4	100	38.43	5.29	6.706	2.418	13.646	26.50	59.93	1.108	1.951	SLUG	100g/l MgSO4	2
MU0641	6	100	37.13	4.84	9.018	3.243	28.132	26.45	69.64	1.489	3.810	SLUG	100g/l MgSO4	2
MU0641	7	100	37.50	5.35	9.090	3.261	18.583	26.41	60.07	1.500	2.652	SLUG	100g/l MgSO4	2
MU0641	8	100	38.39	5.27	6.803	2.437	9.134	26.37	49.71	1.122	1.405	SLUG	100g/l MgSO4	2
MU0641	9	100	37.96	4.23	6.926	2.449	35.326	26.12	79.03	1.138	4.587	SLUG	100g/l MgSO4	2
MU0641	10	100	38.34	5.38	9.107	2.784	7.527	23.41	38.76	1.444	1.252	SLUG	100g/l MgSO4	2
MU0642	1	100	36.72	5.05	2.400	21.548	2.706	89.98	10.15	2.908	2.945	SLUG	100g/l MgSO4	2
MU0642	2	100	37.12	5.05	2.431	21.413	15.977	89.80	40.12	2.895	4.540	SLUG	100g/l MgSO4	2
MU0642	3	100	36.57	5.44	1.819	15.790	11.409	89.67	39.32	2.138	3.303	SLUG	100g/l MgSO4	2
MU0642	4	100	37.23	4.98	2.470	21.426	25.231	89.66	51.36	2.902	5.665	SLUG	100g/l MgSO4	2
MU0642	5	100	36.51	3.28	1.839	15.841	61.302	89.60	77.62	2.147	9.367	SLUG	100g/l MgSO4	2
MU0642	6	100	37.43	5.36	3.109	26.416	3.649	89.47	11.00	3.585	3.651	SLUG	100g/l MgSO4	2
MU0642	7	100	37.63	5.24	3.185	26.964	20.569	89.44	40.56	3.661	5.772	SLUG	100g/l MgSO4	2
MU0642	8	100	36.65	4.89	1.951	16.303	27.514	89.31	60.12	2.216	5.320	SLUG	100g/l MgSO4	2
MU0642	9	100	36.36	5.21	1.941	16.106	6.141	89.25	25.39	2.191	2.701	SLUG	100g/l MgSO4	2
MU0642	10	100	38.50	5.25	13.594	5.112	17.696	27.33	48.61	2.271	2.769	SLUG	100g/l MgSO4	2
MU0642	11	100	39.17	5.11	13.586	4.643	12.084	25.47	39.86	2.214	2.031	SLUG	100g/l MgSO4	2
MU0643	1	100	39.67	1.26	3.422	2.456	120.432	41.78	95.35	0.714	14.922	SLUG	100g/l MgSO4	2
MU0644	1	100	40.50	2.50	3.533	2.495	75.105	41.39	92.57	0.732	9.423	SLUG	100g/l MgSO4	2
MU0643	2	100	40.03	3.83	5.394	3.802	53.366	41.35	85.30	1.117	6.942	SLUG	100g/l MgSO4	2
MU0644	2	100	40.20	4.98	7.286	5.074	29.139	41.05	70.22	1.501	4.154	SLUG	100g/l MgSO4	2
MU0643	3	100	40.46	5.02	5.382	3.742	34.751	41.02	79.21	1.108	4.674	SLUG	100g/l MgSO4	2
MU0644	3	100	40.30	5.08	7.305	5.018	18.766	40.72	60.36	1.496	2.888	SLUG	100g/l MgSO4	2
MU0643	4	100	40.68	4.60	3.607	2.470	23.939	40.65	79.75	0.738	3.207	SLUG	100g/l MgSO4	2
MU0643	5	100	40.38	4.91	7.133	4.880	8.114	40.62	40.31	1.459	1.578	SLUG	100g/l MgSO4	2
MU0643	6	100	40.72	5.06	5.428	3.686	13.955	40.45	60.49	1.107	2.142	SLUG	100g/l MgSO4	2
MU0643	7	100	38.51	4.74	3.494	2.327	13.506	39.98	69.88	0.707	1.923	SLUG	100g/l MgSO4	2
MU0643	8	100	40.58	5.20	5.309	3.526	8.961	39.91	50.35	1.073	1.516	SLUG	100g/l MgSO4	2
MU0643	9	100	40.64	4.60	10.541	7.624	29.372	41.97	61.79	2.206	4.492	SLUG	100g/l MgSO4	2
MU0643	10	100	40.85	5.29	10.687	7.673	13.024	41.79	41.50	2.229	2.513	SLUG	100g/l MgSO4	2
MU0643	11	100	40.54	5.50	10.882	7.115	6.088	39.53	25.28	2.185	1.603	SLUG	100g/l MgSO4	2

3.4.6 Typical Sensor Signal Response

Some typical sensor signal's response displaying the differential pressure, capacitance, conductance, and gamma count are presented in **Figures 3.11 – 3.14.** This enabled the visual description of sensor behaviour to flow changes, and provided the basis for data analysis and neural network application in subsequent chapters.

3.4.6.1 Differential Pressure Transducer

The DP vs time chart displays a plot of the differential pressure signals for the two DP transducers namely dp1 and dp2 in mmH_2O.

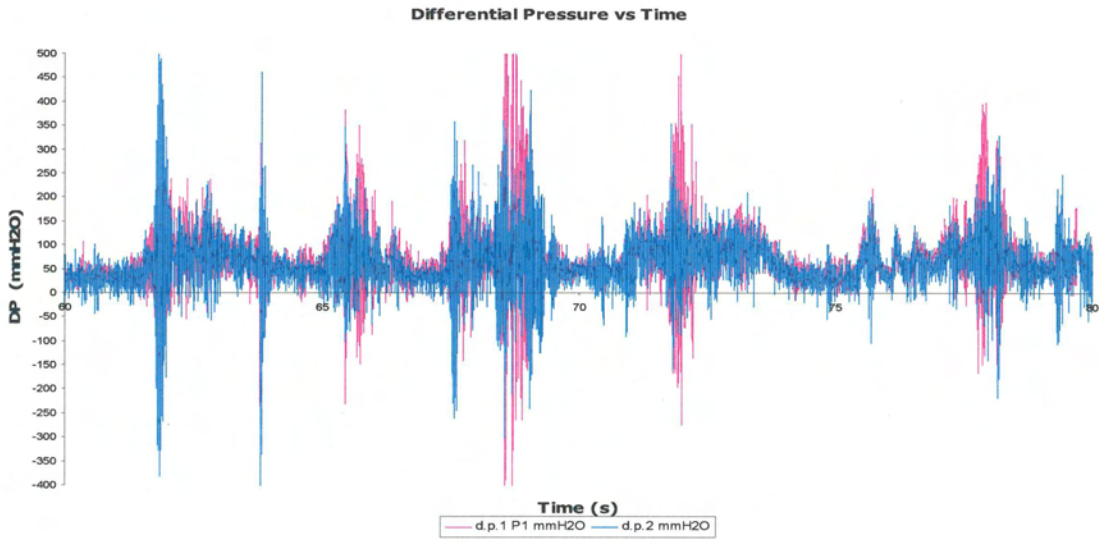

Figure 3.11 – Plot of Differential Pressure (DP) vs. Time

3.4.6.2 Capacitance Sensor Response

Capacitance vs. time chart, **Figure 3.12a** below displays the plot of Capacitances 1 & 2 in typical slug flow conditions. **Figure 3.12b** shows a calibration curve with water, the values for the capacitance have been non-dimensionalised, i.e. a capacitance reading of 0 indicates an empty pipe, and a reading of 1 indicates that the pipe is full of water.

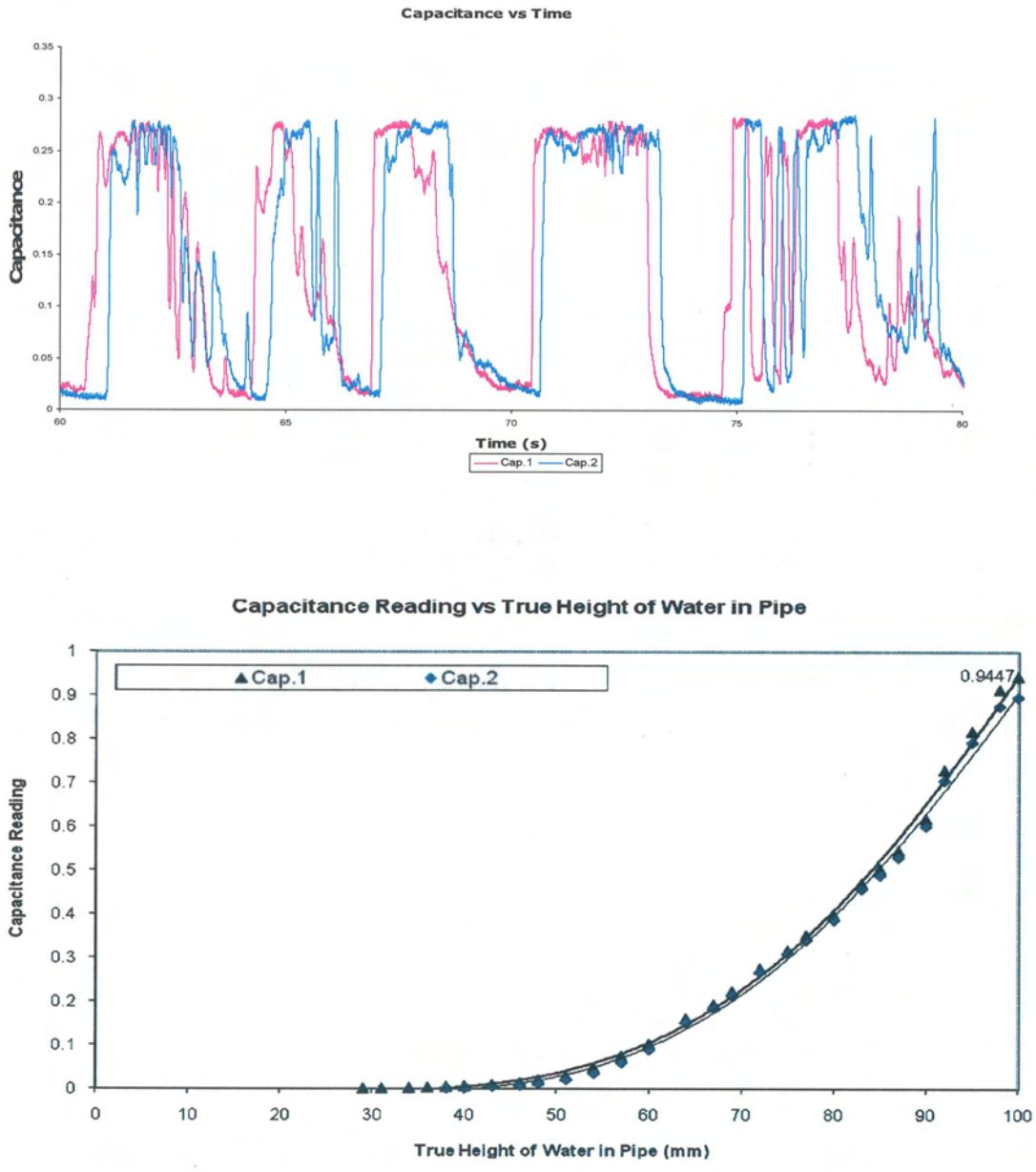

Figure 3.12 (a) and (b) – Plots of Capacitance (a) vs. Time, (b) vs. True Height of Water

3.4.6.3 Conductance Sensor Response

Figure 3.13 presents a typical maximum value feature response for a conductance sensor for multiphase oil, water and gas flow. The sensor's performance is severely impaired in an oil continuous flow as shown.

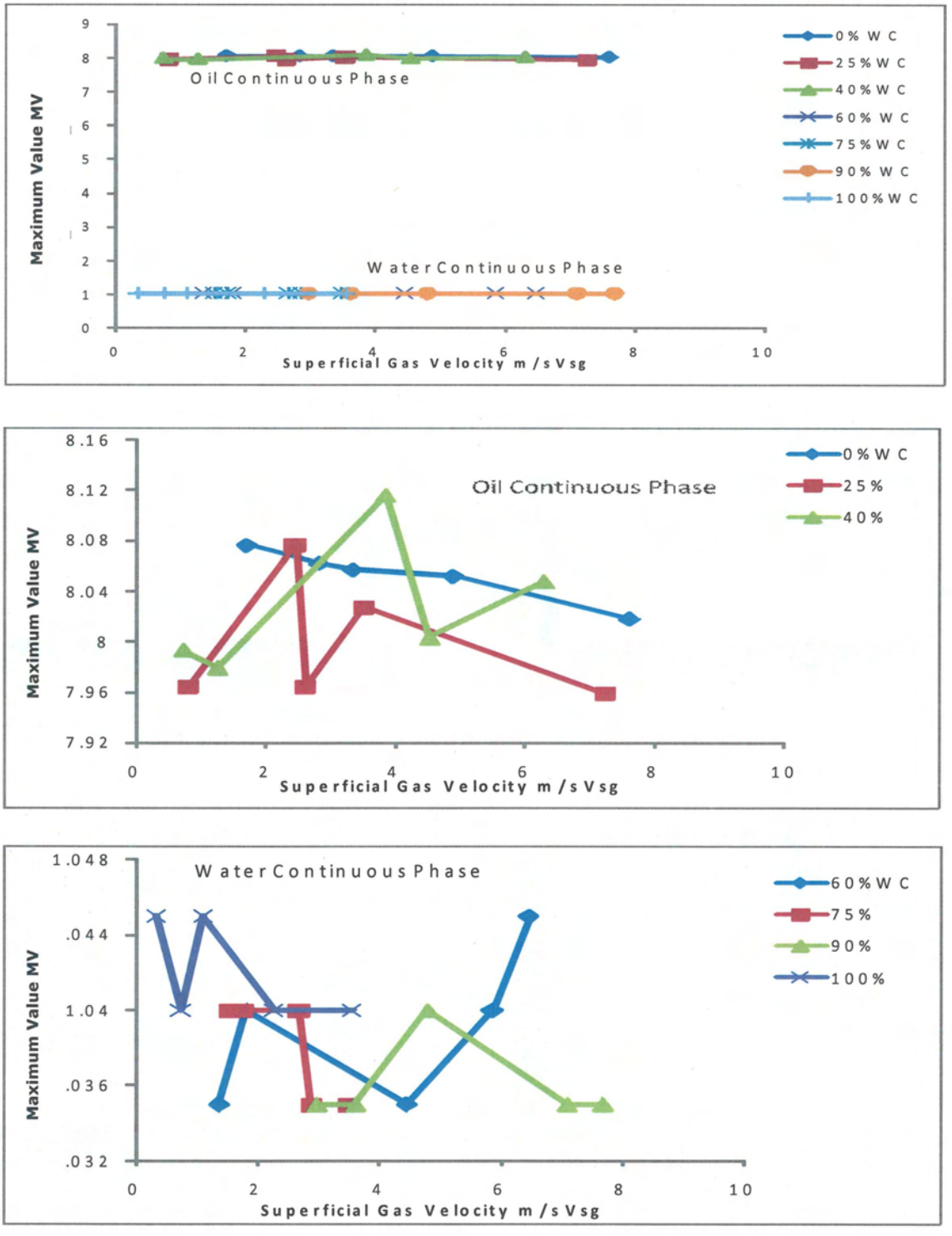

Figure 3.13 – Response of Maximum Value Conductance Feature to Water Cut

3.4.6.4 Gamma Amplitude Features

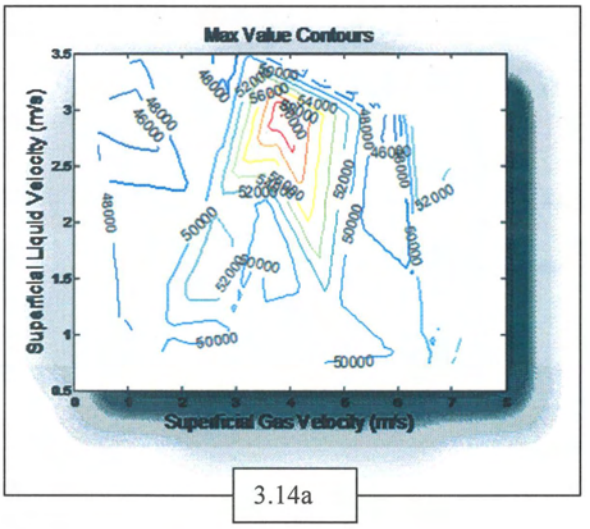

3.14a

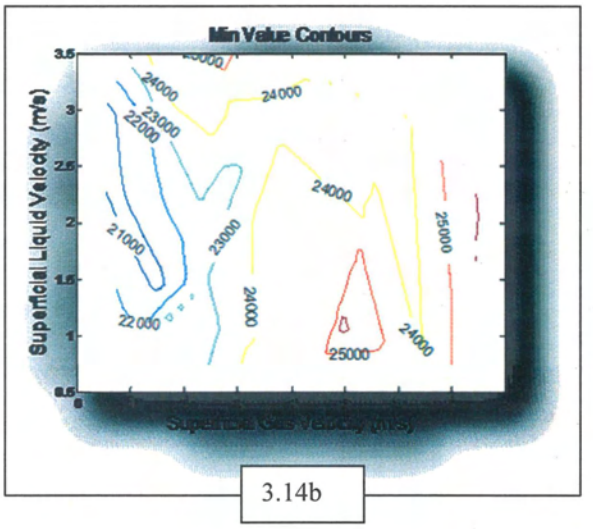

3.14b

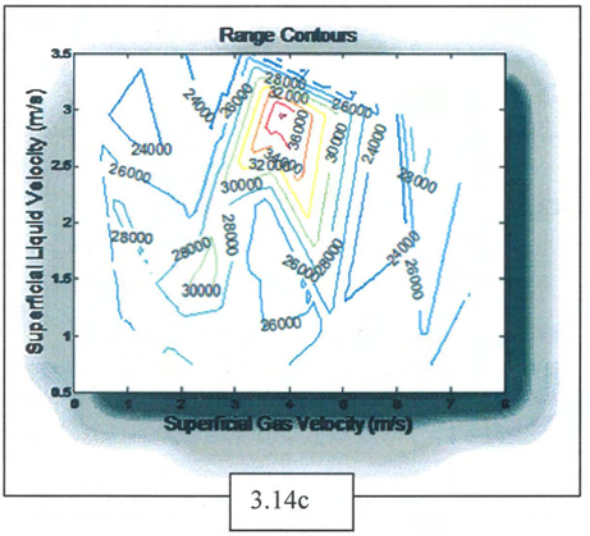

3.14c

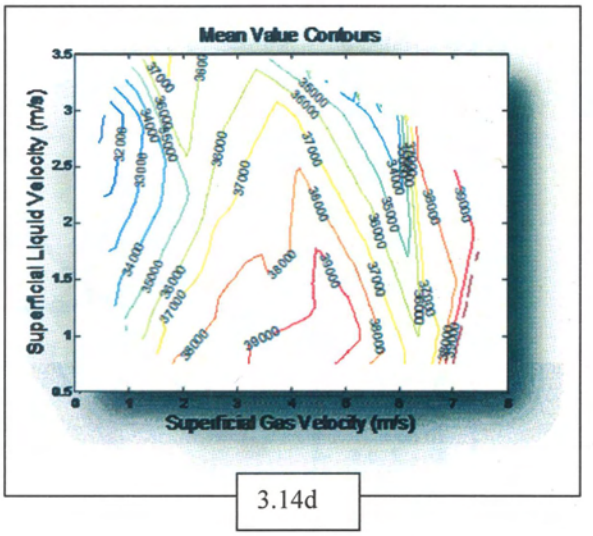

3.14d

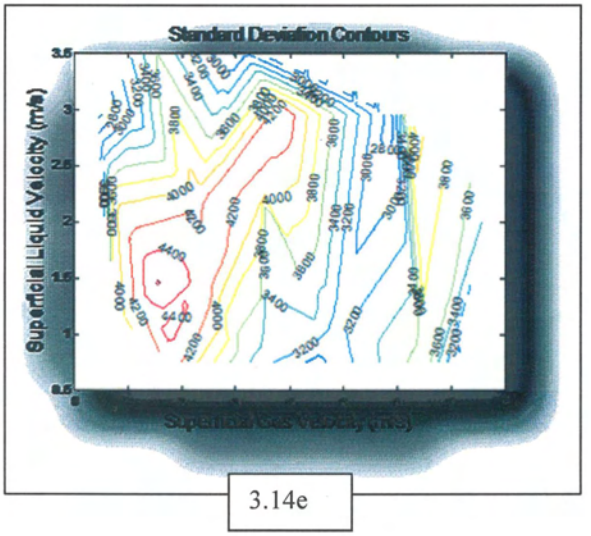

3.14e

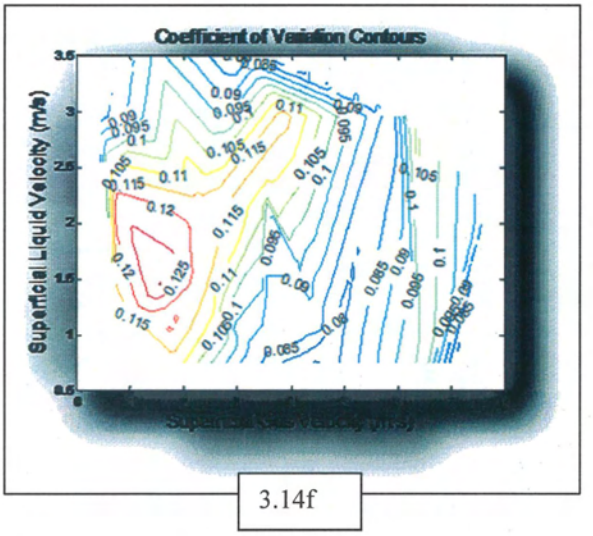

3.14f

Figures 3.14 a-f – Amplitude Features Contour Maps of Gamma Signal

3.5 Notes on Experiment and Database

It is worth stating that the sensor signal database was collected as part of the Flow Programme Work for the United Kingdom Department of Trade and Industry (DTI) now called Department of Business Enterprise and Regulatory Reform (DBERR).

In conjunction with the National Engineering Laboratory (NEL), Cranfield University designed and assembled the sensor spool piece. The response data from the sensor spool piece was collected over a wide range of oil, water and gas flow rates in NEL's Multiphase Flow Loop in East Kilbride, Glasgow. Data were collected under two different salinities of 50 and 100 g/l $MgSO_4$.

It must be noted that the differential pressure data in test numbers MU0601 to MU0616 were corrupted and appeared random and negative. (These data sets were excluded for the purpose of this research work). During subsequent tests/calibrations (MU0617 – 44), which were conducted by the author at both NEL and Cranfield University facilities, a number of techniques were used to ensure that the data collected were valid and that the sensors correctly responded to flow conditions. Sensor response as a function of time was plotted and monitored online. Test parameters such as superficial gas/liquid velocities, water cut, gas volume fraction etc. were analysed and validated through comparisons with reference conditions at regular intervals.

The author was also involved with the sensor database creation (preliminary data analysis, design of sensor signal template, report preparation etc.) at Cranfield University, through the final stages of the project.

Please refer to Appendix C for additional information on the data acquisition system.

CHAPTER 4

THE USE OF A NEURAL NETWORK FOR MULTIPHASE FLOW MEASUREMENT

4.1 Feature Analysis

Time series plots from the sensor signals were employed to ensure that the data collected were valid and that the sensors correctly responded to varying flow conditions. Sensor responses as a function of time were plotted and monitored online, so that any sensor malfunctioning could be detected immediately. The reference measurements are also continuously monitored on the system. The sensor spool piece has a pair of sensors each for the capacitance, conductance, and differential pressure, which enabled cross referencing between the sensors to ensure data validity.

The electronics in the signal processing box for the gamma densitometer scan the transmitted radiation every 125 ms (8 Hz) and calculate an average of the signal for every second. This characteristic of the instrument makes it unsuitable for certain flow conditions (e.g. short slug and bubbly flow). Hence, it is more appropriate to use the raw data from the densitometer before the processing, which gives the radiation transmitted through the processing material onto the detector in the form of counts or pulses, which are sampled every 1 msec (1 kHz). These counts can be converted to density values afterwards.

A more detailed analysis of the sensor signal was carried out to validate and further ensure that the sensors were functioning correctly to the pre-defined test conditions.

Figure 4.1 is a typical slug flow time domain representation of a capacitance 1 sensor at 6.0l/s liquid flow, 25% water cut, 70 gvf, and **Figure 4.2** is also a time series representation of capacitance 2 under the same conditions. This enabled cross referencing to ensure data quality.

Similarly, **Figure 4.3** shows response of gamma output signal as a function of time (10 seconds) when subjected to the same flow conditions as the capacitance sensors.

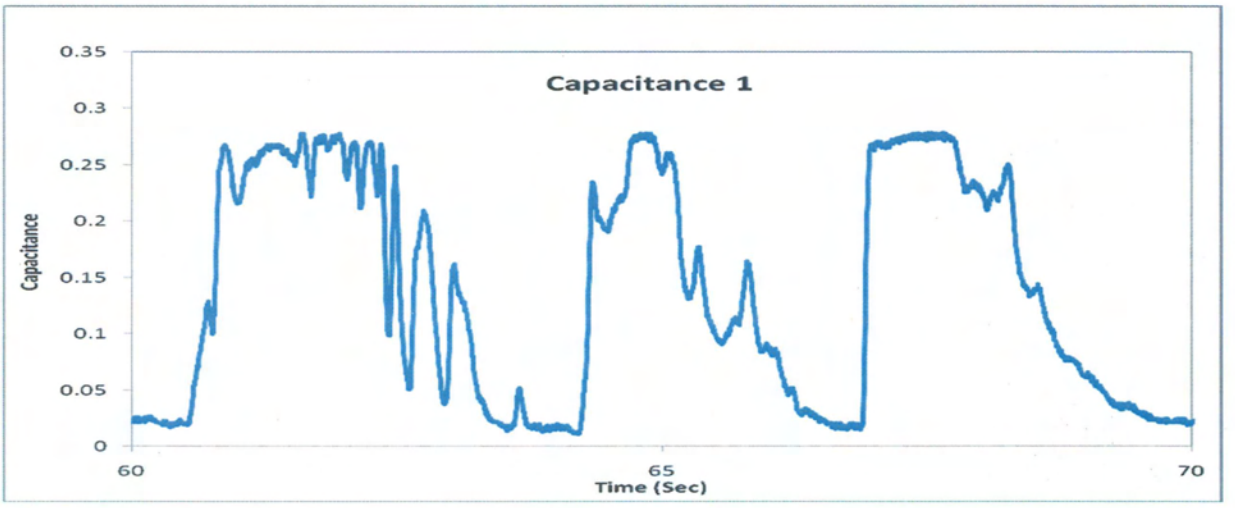

Figure 4.1 Capacitance 1 Response at 6.0 l/s liquid, 25% water cut, 70 gvf

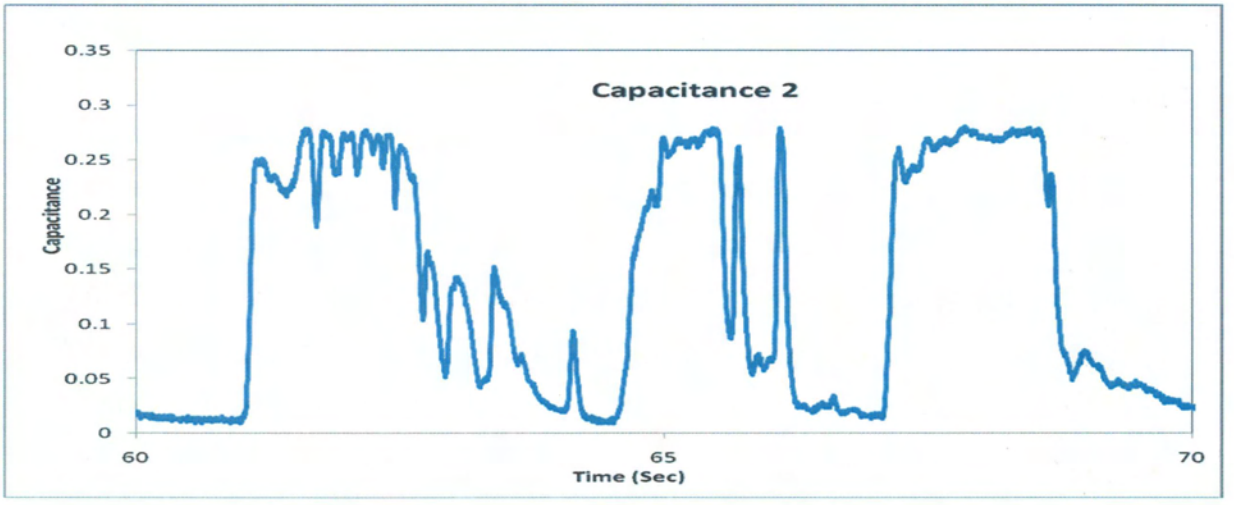

Figure 4.2 Capacitance 2 Response at 6.0 l/s liquid, 25% water cut, 70 gvf

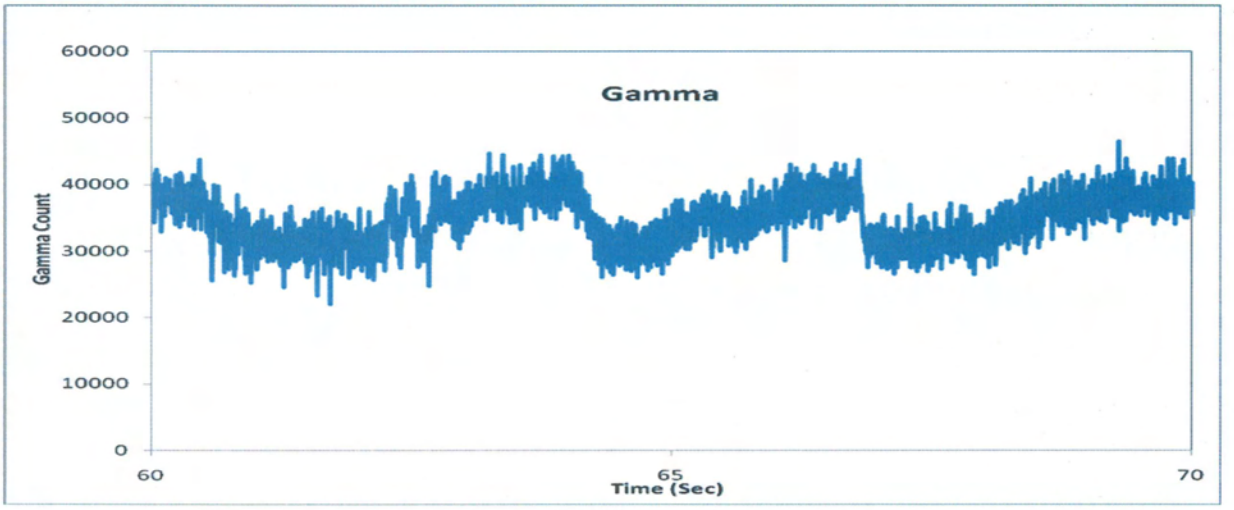

Figure 4.3 Plot of Gamma Count vs Time

Identification of density fluctuations in the multiphase flows is obvious from the series of peaks and troughs in the amplitude of the output signals. For high-density, liquid-rich, fluid segments, the number of gamma photons absorbed by the fluid increases. Accordingly, the magnitude of the detector unit's output signal decreases. Conversely, the signal magnitude will increase for low-density, gas-rich, fluid segments where the number of photons absorbed by the multiphase mixture decreases. When analysed over a short period (e.g. 10 – 70 seconds), the raw signal traces provide a useful visual indication of the flow features present in the multiphase flow pipeline.

As the gas loading increases, the troughs produced by the passing slug increase first in amplitude and then in width. The troughs present in the signals' amplitude represent the passage of slug structures through the measurement section: the lower the amplitude of the signal trough, the smaller the slug length, with large troughs inferring a large slug passage. Trough width provides an indication of the slug height: higher slug structures will induce a wider trough. However, the width of the trough will also be dependent on the slug velocity.

4.1.1 Feature Extraction

The sheer volume of raw sensor signals data could not be practically handled by a neural network system. There are two main reasons why the raw signals data could not be used: in the first instance a neural network with too large a number of input parameters and corresponding weights and biases would be required to populate the input space. e.g. measurement period of 5 minutes, a 75,000-dimensional input space (5 minutes x 60 seconds/minute x 250 Hz) is generated. Secondly, previous studies in the application of pattern recognition techniques confirmed that the discriminatory information in multiphase flow measurements lies with the feature extraction principle. Darwich (1989), Bishop (1995b), Jama (2004), and Blaney (2008).

Consequently a feature extraction approach was adopted as part of the initial data preprocessing. With the help of digital signal processing techniques, there are an infinite number of features that can be extracted from different information domains. In the current study a number of features were extracted from time and frequency domains.

Statistical parameters from the sensor signals were analysed on the basis of their relationship with multiphase flow characteristics. The central moments, Linear Prediction Coefficients (LPCs), and Linear Spectral Frequencies (LSFs) were evaluated for various test conditions.

These features were extracted from the sensor signals for the two salinity levels ie 50g/l MgSO4 and 100g/l MgSO4, and the two test sections.

A variety of statistical features were also analysed using contour mapping to determine their discriminability. Contour plotting facilitated visual examination of an input feature's response to variations in any one of the target output variables. **Table 4.1** lists the features selected for examination.

Table 4.1 Features Selected for Investigations based on Feature Analysis

		Information Domain		
Feature	**Symbol**	**Amplitude**	**LPC**	**LSF**
Mean Value	AV	X		
Standard Deviation	SD	X		
Coefficient of Variation	CV	X		
Coefficient of Skewness	CS	X		
Coefficient of Kurtosis	CK	X		
Signal Total Energy	E_T	X		
Linear Prediction Coefficient 2	LPC2		X	
Linear Prediction Coefficient 3	LPC3		X	
Linear Prediction Coefficient 4	LPC4		X	
Linear Prediction Coefficient 5	LPC5		X	
Linear Prediction Coefficient 6	LPC6		X	
Linear Prediction Error	E_R		X	
Line Spectral Frequency 1	LSF1			X
Line Spectral Frequency 2	LSF2			X
Line Spectral Frequency 3	LSF3			X
Line Spectral Frequency 4	LSF4			X
Line Spectral Frequency 5	LSF5			X

The LP coefficients are obtained from standard linear prediction analysis, based on blocks of input samples. The autoregressive model is employed due to its comparative simplicity and computational efficiency. **Equation (4.1)** below shows how the residual error *e(n)* is associated with LP coefficients..

$$e(n) = x(n) - \sum_{k=1}^{p} a_k x(n-k) \tag{4.1}$$

Where:

e(n) is the residual error, *x(n)* is the actual signal, *p* denotes the number of past output samples being considered by the model, which is also representative of the order of the linear prediction function and a_k is the $(k+1)$th LP coefficient.

A simple test to obtain the optimal linear predictor order p is to check the variation of the residual error with the predictor order, which will almost be flat for $p > p_0$, where p_0 is the optimal linear predictor order.

There are two widely used methods for estimating the LP coefficients, which are the autocorrelation and the covariance method, Golub and Loan (1989). Both methods choose the short-term filter coefficients in such a way that the residual error is minimised using the least square technique. When the autocorrelation method is used a Toeplitz matrix, where all elements along a given diagonal are equal is generated which unlike the covariance method guarantees the stability of the synthesis filter. This allows the linear equations that arise from the least-squares formulation to be solved by the Levinson-Durbin recursion algorithm, presented by Golub and Loan (1989).

The relationship between two random variables called correlation, gives a measure of the average dependency of the two signals. The correlation between pairs of signal sample is known as an autocorrelation (AC). The autocorrelation function of a signal is an average measure of its time domain properties given by:

$$r_{xx}(\tau) = \lim_{T=\infty} \frac{1}{T} \int_{-T/2}^{T/2} x(t)x(t+\tau)dt \tag{4.2}$$

Where r_{xx} is autocorrelation function, τ is time shift known as lag. When the autocorrelation technique is used to compute the LP coefficients as described above, the sample correlation function can be calculated first. There are no requirements to do extra calculations to obtain the autocorrelation coefficients, AC. This method was adopted to estimate the LP coefficients 2 – 6 using MATLAB.

Under different flow conditions of gas and liquid, a variation in energy and spectral characteristics can occur in a short time interval. Therefore there will be a change in the LP coefficients in consecutive blocks of sensor waveforms. Since LP coefficients provide a simple and effective method of representing different signals in terms of the

small number of parameters, they can be used not only as a way of data compression but also as a supply for different statistical features for different flow conditions. The feature-set response and variation with respect to specific waveform of differential pressure, absolute pressure, capacitance, conductance and gamma sensors were examined by using distribution/contour-mapping techniques. The line spectral frequencies are a representation of the LP parameters in the frequency domain and they have a shorter dynamic range of values, and hence have better quantisation ability than LP parameters. The LSFs were also evaluated for their discriminatory ability for different flow conditions using contouring techniques.

A number of methods were initially tested for pre-processing the input feature vectors:

- One method was to normalise the input features to the pattern classifier so that they fall in the range of [-1, 1].

- Another normalisation technique was to equalise the magnitude and dynamic range of each feature by applying zero mean and unit-variance normalisation to the feature vectors. Here the data values are centred (i.e. subtract the mean values from the data values in order to obtain centred anomalies) and then divided by their standard deviations to obtain a normalised data having zero mean and unit variance.

- A third pre-processing technique was to transform the input feature vectors, which are uncorrelated and orthogonal to each other, into a new feature space by the use of principal component analysis (PCA). A MATLAB routine called PREPCA was used for this purpose. Those components, which contribute only a small amount to the total variance in the data set, can be eliminated.

The classification accuracies obtained from the above three pre-processing techniques were compared using feature vectors extracted from each information domain for each sensor as well as a combination of different feature vectors.

Reference output target values were obtained from the test facility's reference measurements. The output targets employed were the gas and liquid superficial phase velocities (Vsg and Vsl respectively) and the liquid phase water cut (WC).

A Back Propagation Neural Network was constructed to predict the individual phase flow rates and water cut, and assesses the effects of salinity and test location on the measurement accuracy of the measurement system.

The results indicated that in terms of normalisation methods, the zero mean and unity standard deviation technique result in much better classification accuracy than the simple technique of scaling the data in the range of [-1, 1]. This may be due to the fact that the former technique ensures that all features are given equal emphasis by equalising the magnitude and dynamic range of each feature, i.e. by applying zero mean and unit-variance normalisation to the feature vectors.

It is common practice in many applications to use a principal components analysis (PCA) method to guide the choice of a subset of features from a larger candidate set. It was considered necessary to verify its applicability in the current research work, hence the application of PCA was carried out and its classification accuracies compared against the above-mentioned normalisation techniques. It transpired that when PCA was used to orthogonalise the input features so that they were uncorrelated without feature reduction, its accuracies were compatible to those obtained when the input features were normalised with zero mean and unity standard deviation. The second trial of PCA was to employ it in dimensionality reduction mode, such that those transformed feature vectors that contribute less than a predefined percent (typically 0.1%) to the overall variability were eliminated. As shown in **Figure 4.4**, the dimensionality reduction by PCA reduces the classification accuracies of the network as those features with the least variance are eliminated. It was observed that this trend in PCA performance was consistent regardless of the type of sensor(s) and feature vectors used.

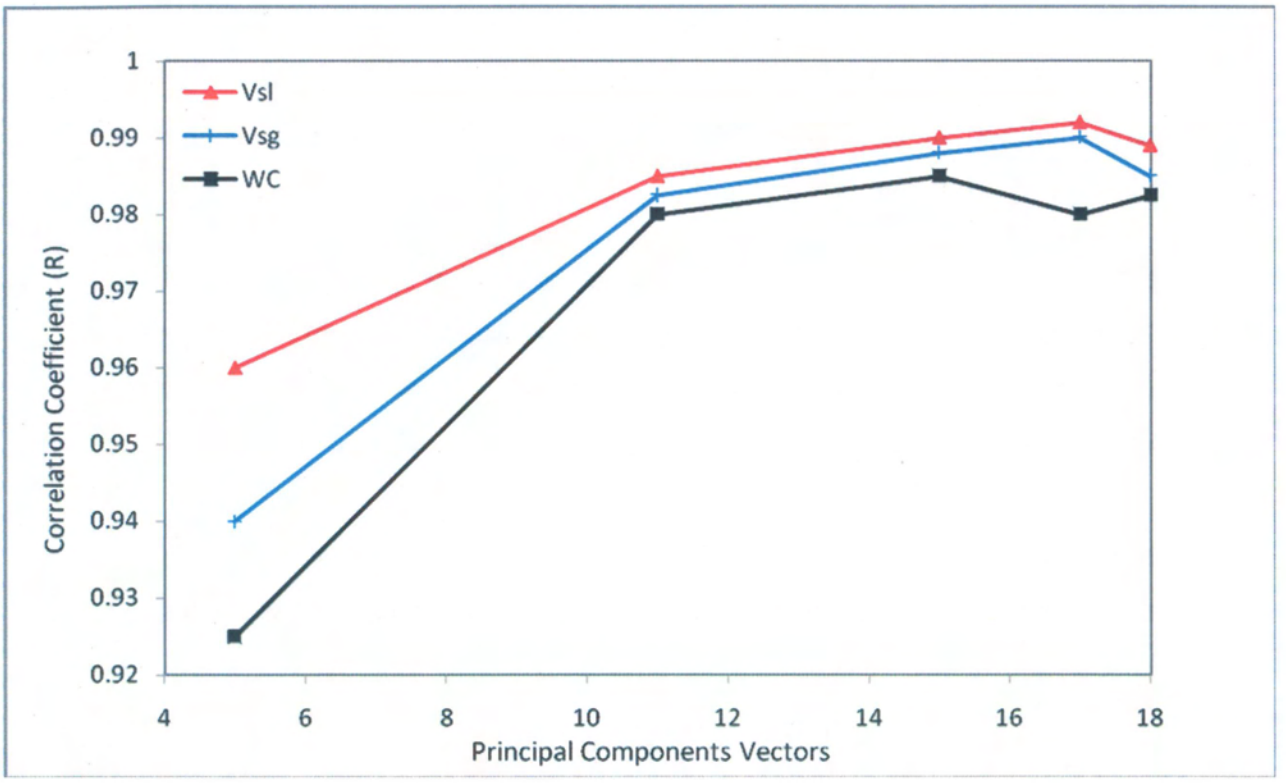

Figure 4.4: Evaluation of Principal Component Analysis (PCA)

The preliminary feature pre-processing exercise showed that the decorrelation and high measures of statistical significance provided by the first few principal component axes are no guarantees of having the best subset of features. PCA finds feature combinations that model the variance of a data set, but these may not be the same features that separate the classes, i.e. the PCA components that model the largest contributions to the data set variance may work poorly for pattern recognition and may not be suitable for discriminating between underlying classes as applied to the current study. It was also seen that the popular practice of ignoring the lower-order PCA components in order to achieve dimensionality-reduction resulted in losing some of the discriminatory information in the data.

It can be stated that in applications similar to the current study, wherein features from the raw data are extracted have been considered useful, the use of PCA processing is not recommended because of its computational complexity without necessarily achieving improved classification accuracies. Due to the limitations of PCA encountered in the current study, it was omitted from the present pattern recognition system. In certain applications, however, when the input data has high dimensions and

there are no obvious features which can be extracted from it, the input dimensionality must nevertheless be reduced in order to limit the number of free parameters in the pattern classifier; in these cases PCA may be a suitable technique to apply for dimensionality reduction.

The Zero Mean and Unit-Variance (ZMUV) normalisation procedure was applied to the input features in this study, as a pre-processing technique feature. This serves to equalise the magnitude and range for each feature, but leaves the relative overlap between the different features unchanged.

It is important to visualise each feature's variation over the flow domain of interest. A useful technique, which facilitates feature trend visualisation, is contour plots. This technique allows the visualisation of three-dimensional data on two-dimensional plots. A contour plot of vector Z over (X, Y) plot treats the values in Z as heights above a plane.

The contours are the level curves of the feature vectors over the intersection grid values of superficial gas and liquid velocities. This provides the ability to visualise how each feature is responding to the changes in flow conditions. It is necessary to select a suitable number of contour levels, as too many contours would render the technique ineffective for providing the required visualisation, while too few contours would not capture the overall feature spectrum. Fifteen linearly spaced contour levels including minimum and maximum of each normalised feature were considered as the optimum for feature trend visualisation purposes. The contour plots represent the normalised features, as this will be the input to the neural network.

4.1.1.1 Gamma Count Signal

Figures 4.5a-f displays the normalised feature distribution maps of the central moments, of the gamma count signal.

The mean value (MV) gamma count was observed to increase with increasing superficial gas velocity (Vsg) due to the decreasing average mixture density, **Figure 4.5a**. At low Vsg the water cut influences the mean count in a manner one would expect: the lowest water cuts yielding higher mean values. However, at Vsg in excess of 4 m/s the influence of the water cut on the mean value diminishes as high and low water cut data points intermingle.

The standard deviation feature increases with increasing superficial liquid velocity, **Figure 4.5b**. In general, increasing the water cut led to a decrease in the standard deviation. It is hypothesised that phase inversion in the liquid phase may induce this increased variation in the measurements.

The coefficient of variation (CV), **Figure 4.5c,** feature exhibits a linear decrease with increased Vsl, but lesser response to Vsg until 3m/s. The feature responds most markedly with higher liquid loading.

The coefficients of skewness (CS) and kurtosis (CV) features are shown in **Figures 4.5d and e**. In general, both the skewness and kurtosis decreased with increasing Vsl and Vsg. The feature response of the total signal energy (E_T) starts at superficial gas velocity above 2.5 m/s below which the feature appears to be flat. From a pattern recognition viewpoint, this will mean that this feature will not provide discriminatory ability for the current test conditions below 2.5 m/s Vsg.

The feature distribution maps of the Linear Prediction Coefficients (LPC) of the gamma count are shown in **Figures 4.6a-f.**

Increasing superficial liquid velocity had little effect on the magnitude of the LPC2 and LPC3 values but the variation between different data points with the same Vsg but different superficial liquid velocity diminished. The magnitudes of the LPC2 and

LPC3 values are a function of Vsl. The data points produced increasing LPC2 and LPC3 magnitude values for higher Vsl. From the data, it was hypothesised that liquid phases with significant water/oil content were susceptible to phase inversion that produce a characteristic response to the gamma signal depending on the water cut.

LPC4, LPC5 and LPC6 yielded similar reactions to the different multiphase flows, **Figures 4.6c, d and e**. As observed for LPC2 and LPC3, the magnitudes of the LPC4, LPC5 and LPC6 values displayed no significant dependence on the Vsg value but the variation between the data points for different Vsl decreased with increasing superficial gas velocity.

The linear prediction coefficient error (ER) demonstrated an approximately linear relationship with the Vsg, increasing in magnitude with increasing superficial gas velocity, **Figure 4.6f**. The LPC error influences on the Vsg indicated increasing sensitivity from 2.5 m/s Vsg.

Figures 4.7a-e displays the feature distribution maps of the Line Spectral Frequencies (LSF) of the gamma signal. The first line spectral frequency (LSF1) appears to be influenced by increasing superficial liquid velocity, with most noticeable liquid dependency seen as superficial gas velocity of 4 m/s (Vsg). The feature has no significant visible trends associated with higher Vsg.. The LSF1 feature is shown to be strongly sensitive to hydrodynamic flow changes.

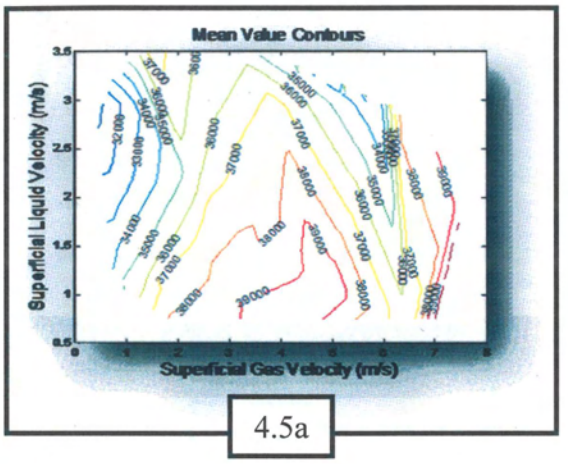

4.5a

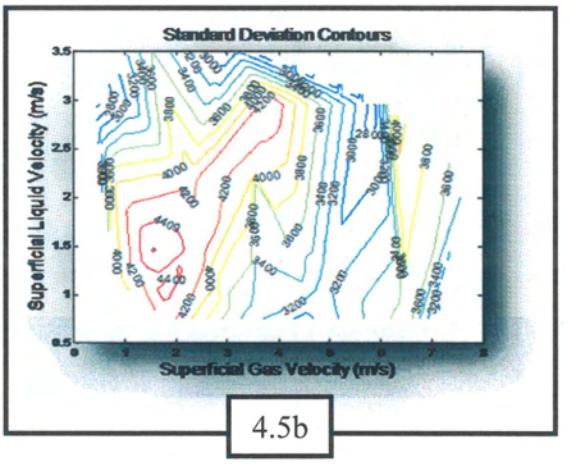

4.5b

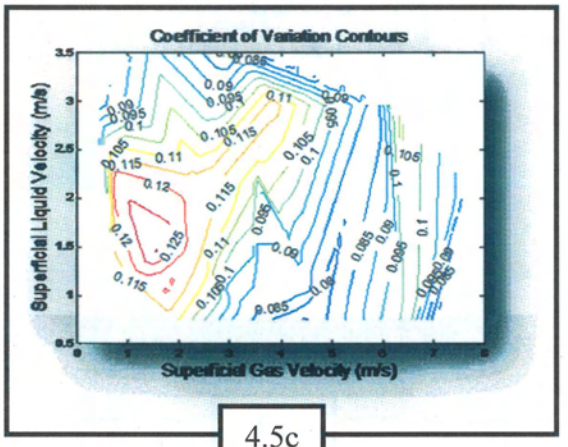

4.5c

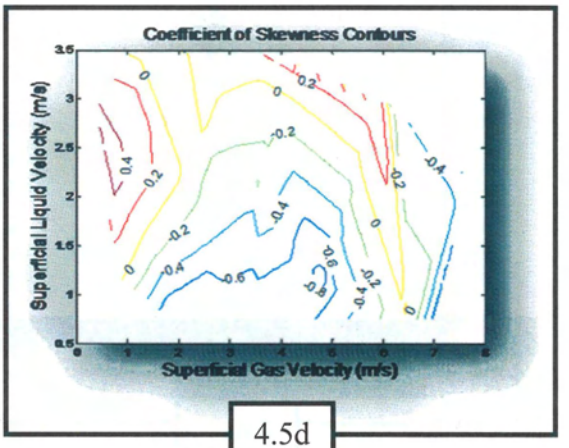

4.5d

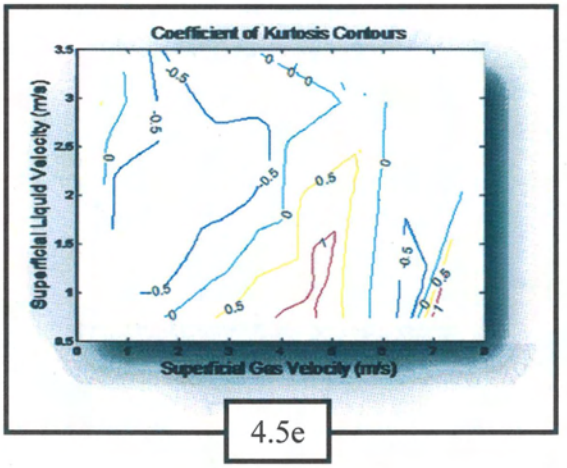

4.5e

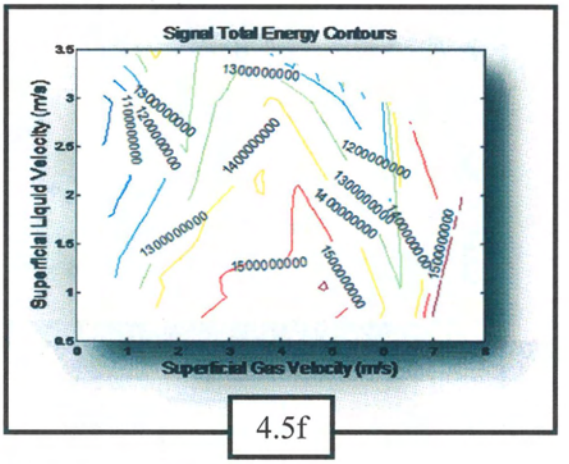

4.5f

Figures 4.5 a-f, Amplitude Feature Distribution Maps of Gamma Signal

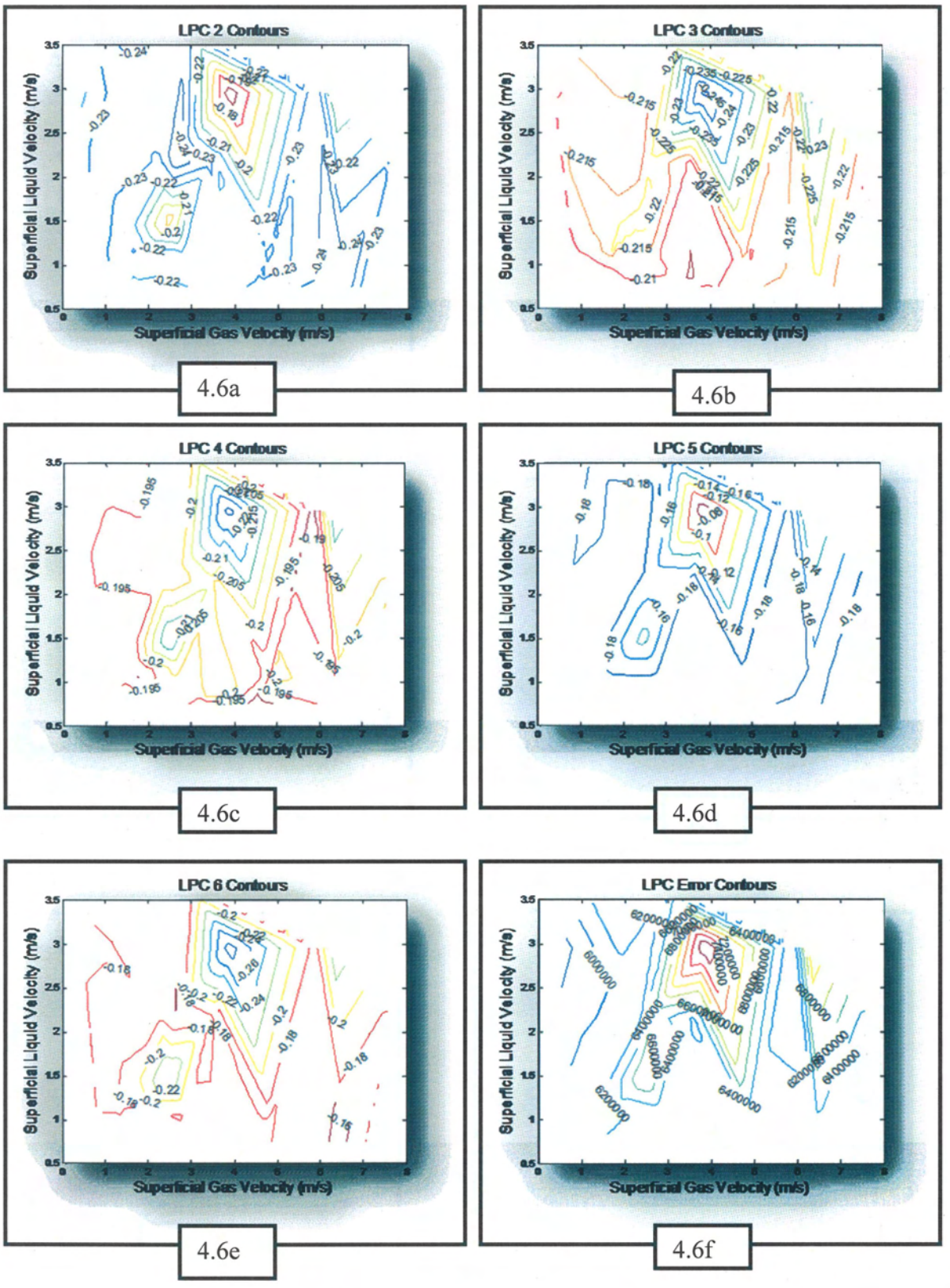

Figures 4.6 a-f, LPC Feature Distribution Maps of Gamma Signal

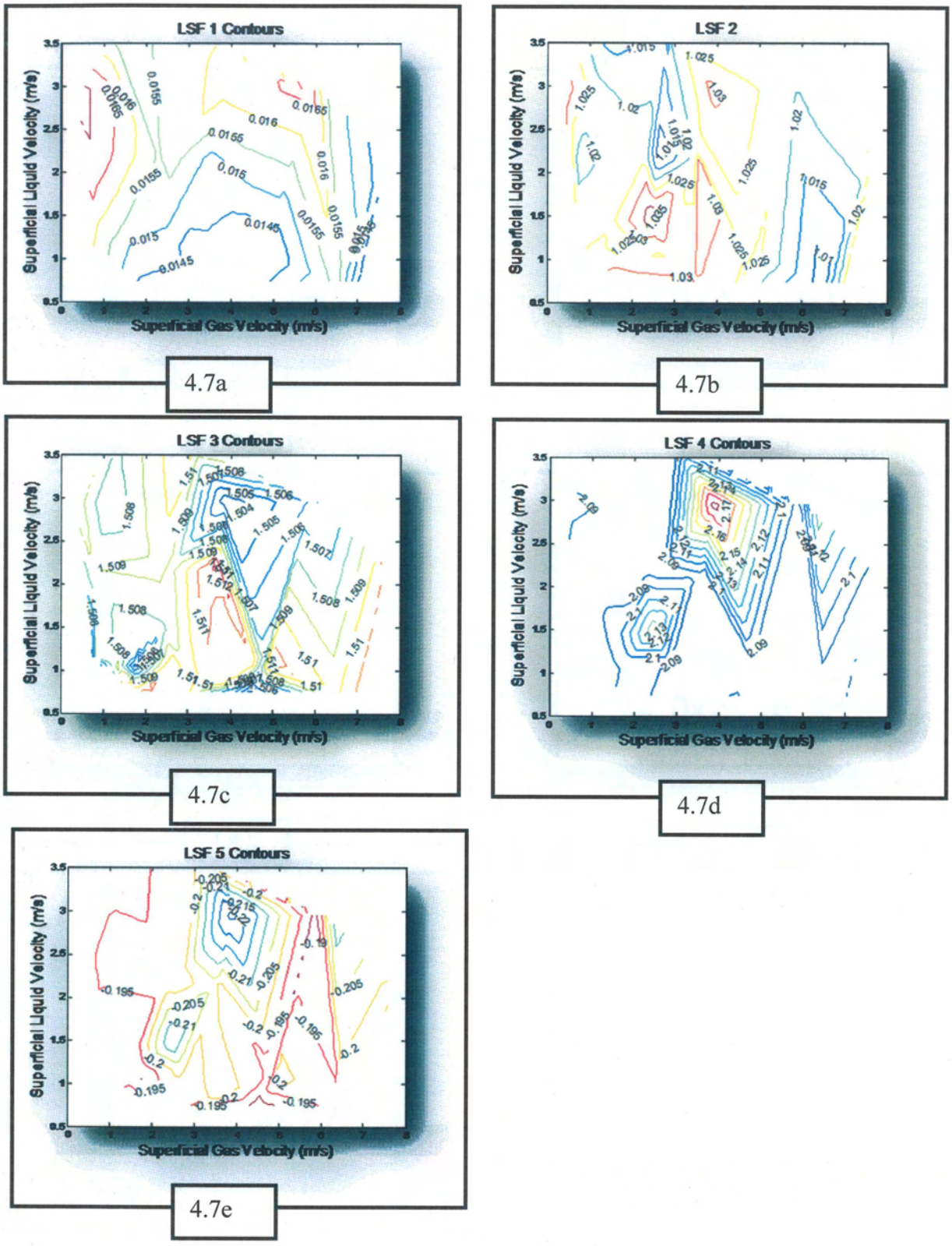

Figures 4.7 a-e, LSF Feature Distribution Maps of Gamma Signal

Conductance Features

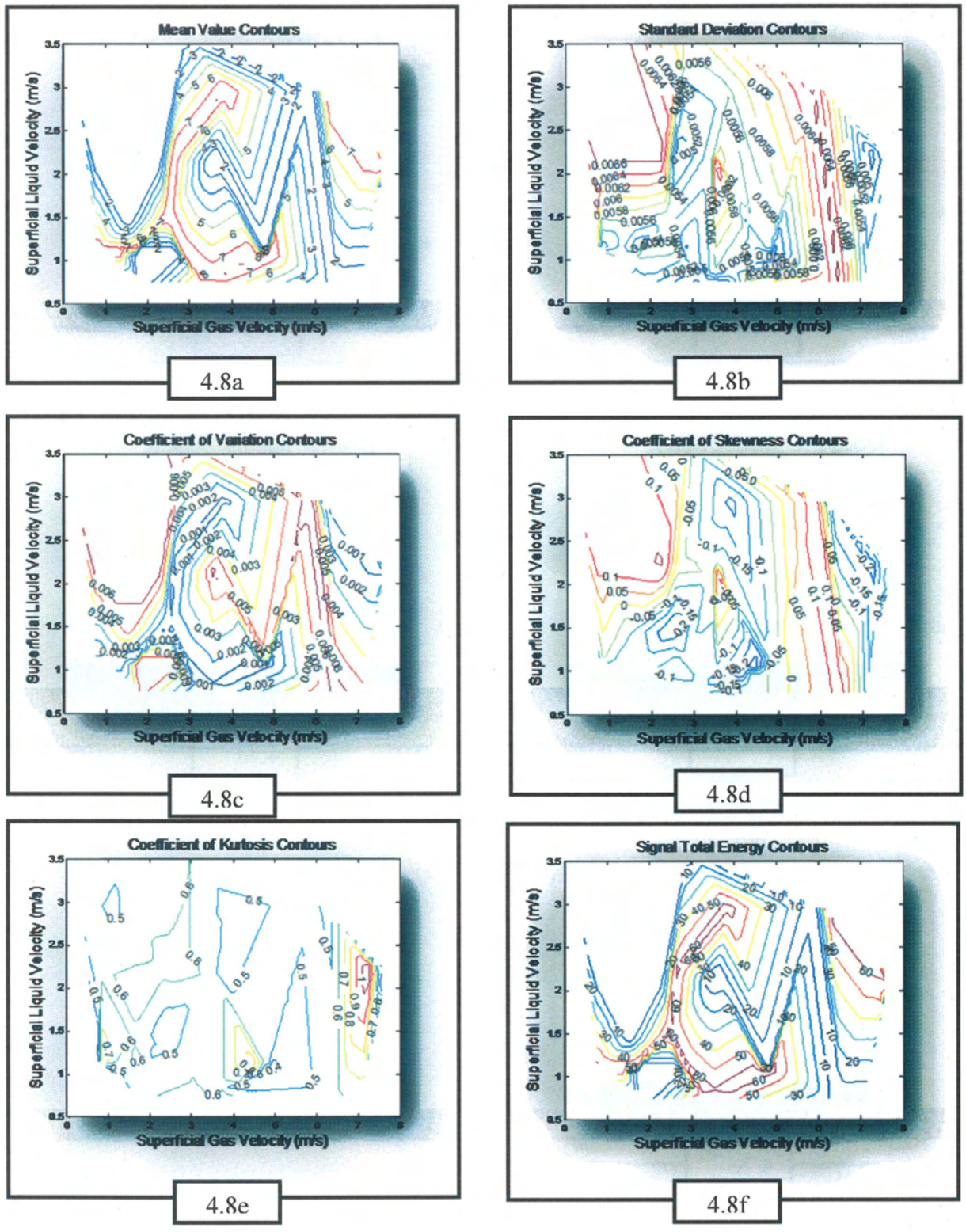

Figure 4.8a-f, Amplitude Features Distribution Maps of Conductance Signal

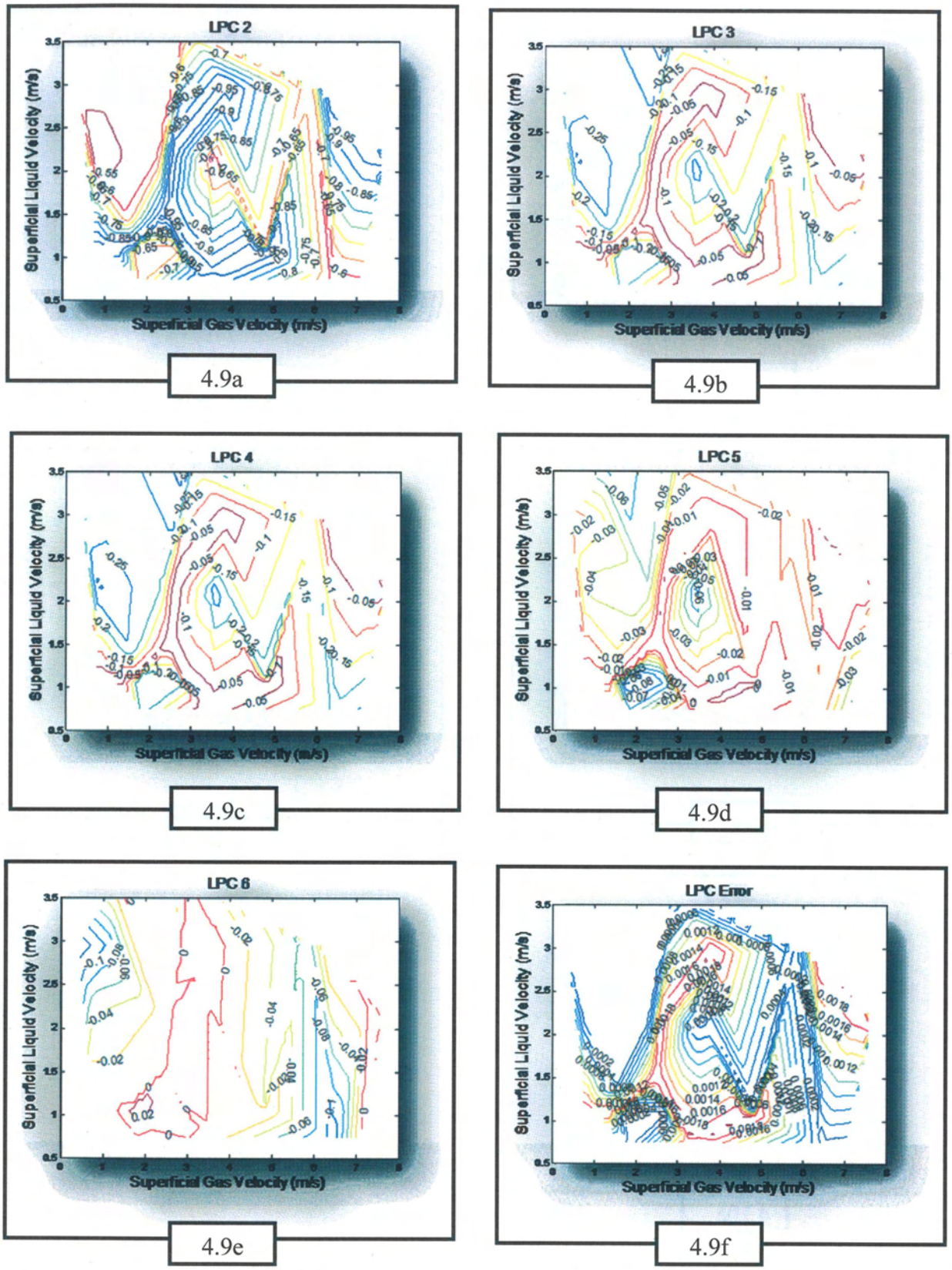

Figure 4.9a-f, LPC Feature Distribution Maps of Conductance Signal

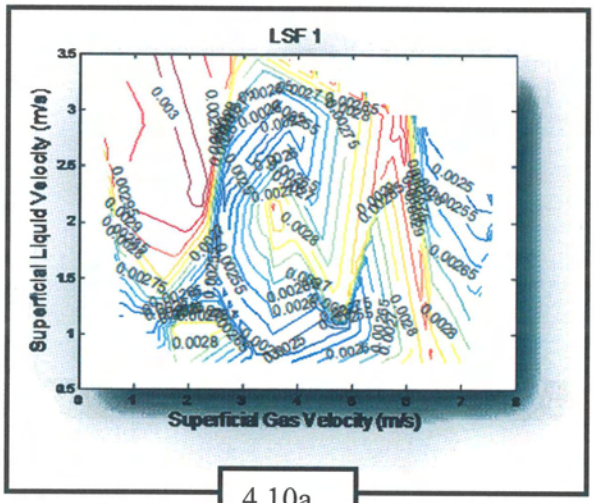

4.10a

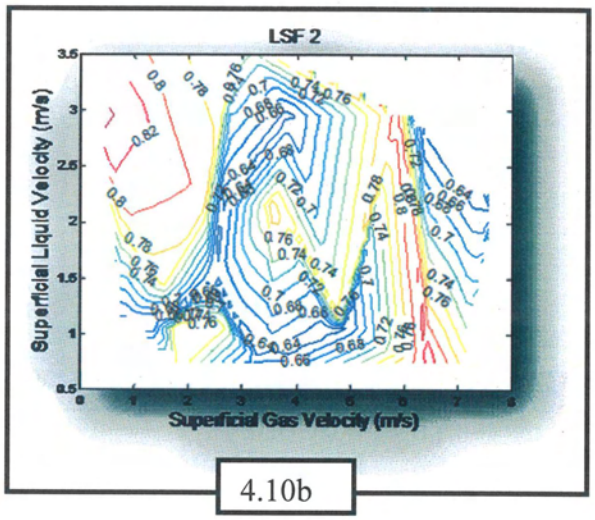

4.10b

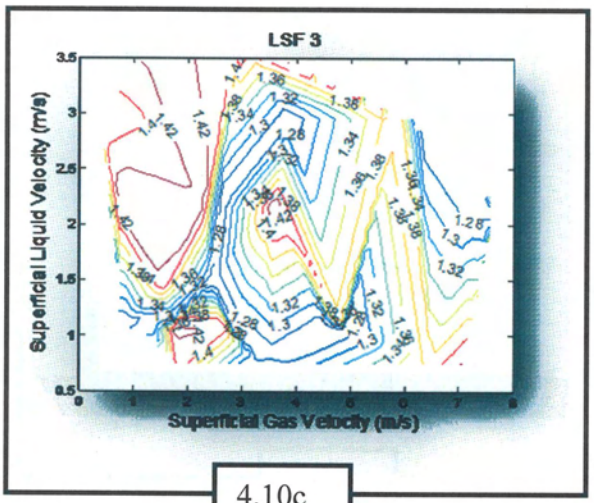

4.10c

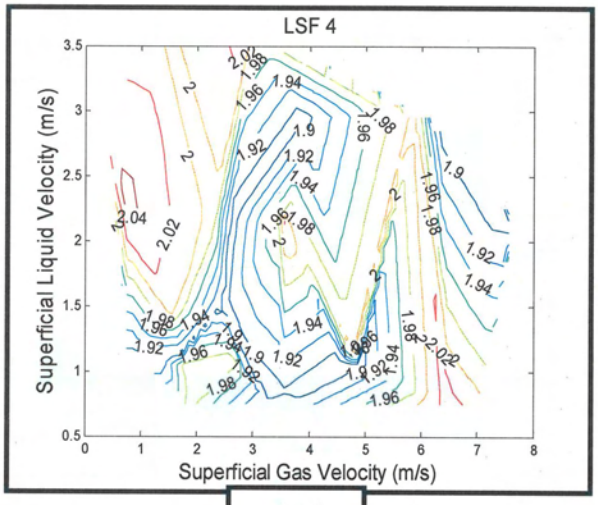

4.10d

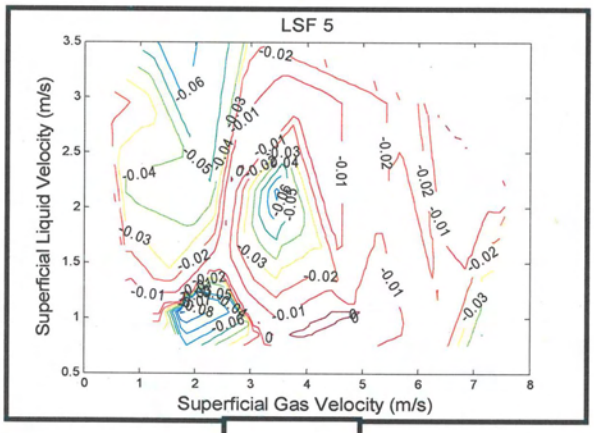

4.10e

Figure 4.10a-e, LPC Feature Distribution Maps of Conductance Signal

Another statistical analysis technique employed to visualise and extract features with discriminatory capabilities to multiphase flow, was to plot the central moments, linear prediction coefficients (LPCs), and linear spectral frequencies (LSF) against the superficial gas velocity with varying water cut. Typical plots are presented in **Figures 4.11-4.12**, showing scatter plots of the conductance signal indicating the responses to multiphase flow.

The feature responses clearly indicate the sensor functions only at water cuts of 60% and above. This information is important in excluding the conductance signal features in subsequent measurements for oil continuous flow conditions.

The standard deviation also increased with Vsg as the measurement range increased. In general, increasing the water cut led to increases in the standard deviation. However, the largest standard deviations were obtained for test points with a water cut of 75%.

The skewness and kurtosis exhibited a linear decrease with Vsg until Vsgs of 75% or greater were attained. In general, both the skewness and kurtosis increased with increasing water cuts.

Increasing the Vsg had little effect on the magnitude of the LPC2 and LPC3 values. However, the variation between different data points with the same Vsg but different water cuts diminished. **Figures 4.12a-f** also indicate the conductance performance as a function of water cut.

LPC4, LPC5 and LPC6 yielded similar reactions to the different multiphase flows. As observed for LPC2 and LPC3, the magnitudes of the LPC4, LPC5, and LPC6 values displayed no significant dependence on the Vsg value but the variation between the data points for different water cuts decreased with increasing Vsg. The water cut was the major influence on the LPC magnitudes, with phase inversion effects being prominent.

The linear prediction coefficient error (ER) demonstrated an approximately linear relationship with the Vsg, increasing in magnitude with increasing Vsg.

A decrease in magnitude of the LSF1 parameter was observed with increasing Vsg, particularly for Vsgs in excess of 60%, **Figure 4.13a**. Water cut was observed to exhibit a significant influence on the LSF1 magnitude.

LSF2 and LSF4 yielded similar responses to the multiphase flows demonstrating no detectable reaction to variations in the Vsg, **Figures 4.13b-d**. The variation between parameter magnitudes with water cut for data points of equivalent Vsgs decreased with increasing multiphase flow Vsgs.

The LSF3 and LSF5 coefficients decreased in magnitude with increasing Vsg, **Figures 4.13 e** and **f**. In this instance, the variation between data points of different water and equivalent Vsg was observed to be at a minimum for Vsg >75%.

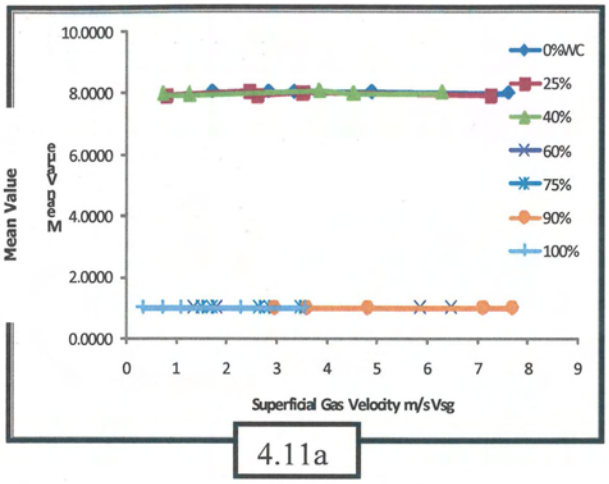

4.11a

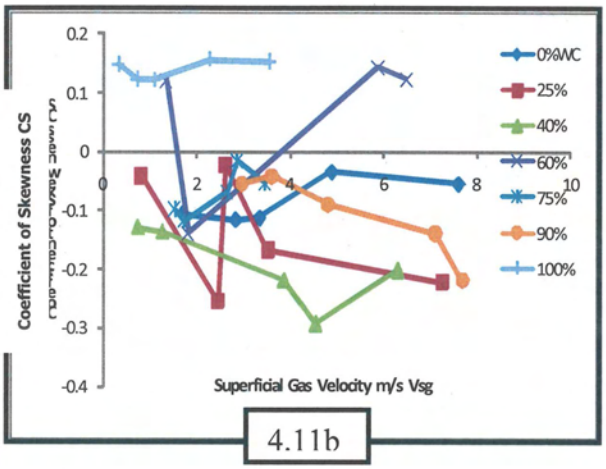

4.11b

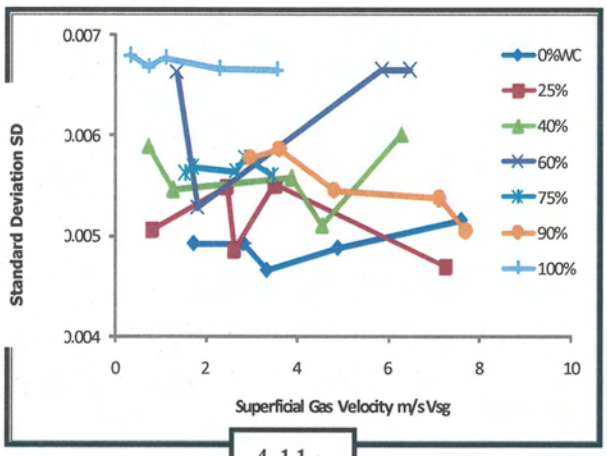

4.11c

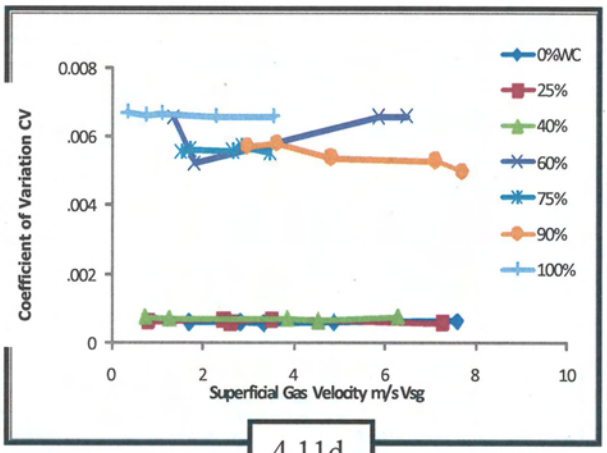

4.11d

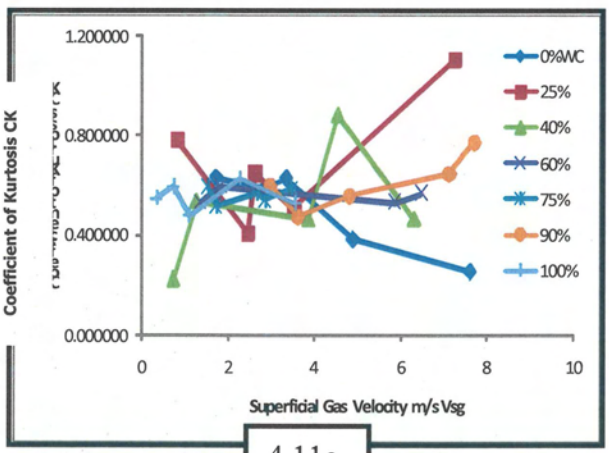

4.11e

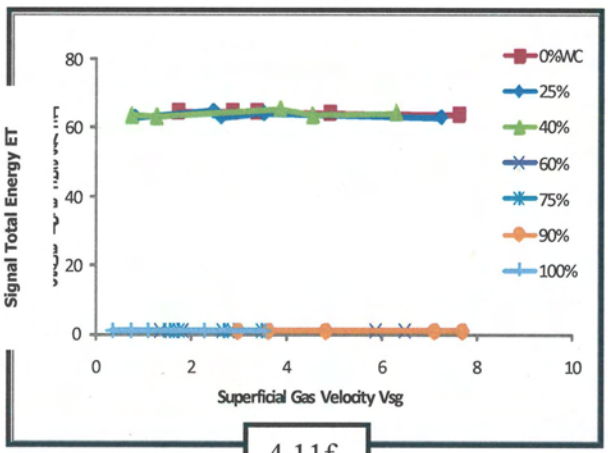

4.11f

Figure 4.11 Central Moments Line Scatter Plots of Conductance Signal

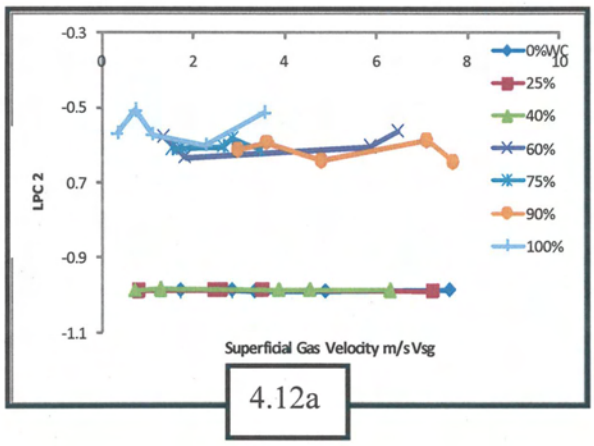

4.12a

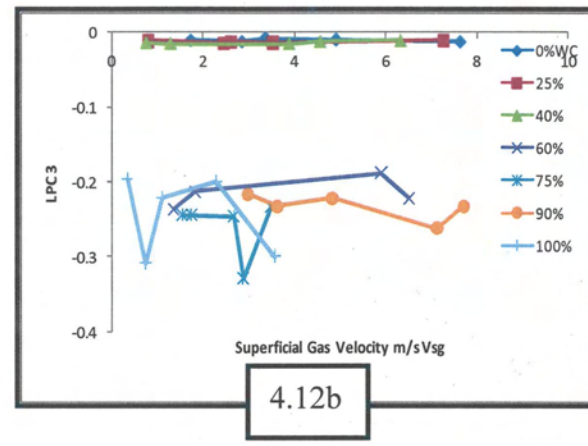

4.12b

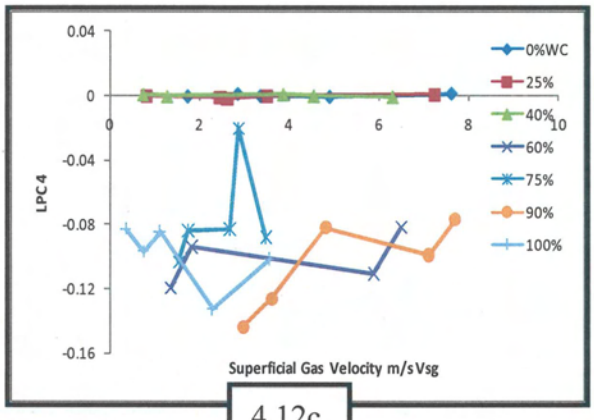

4.12c

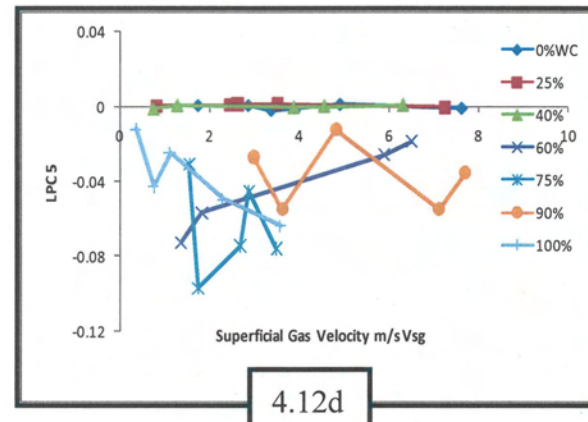

4.12d

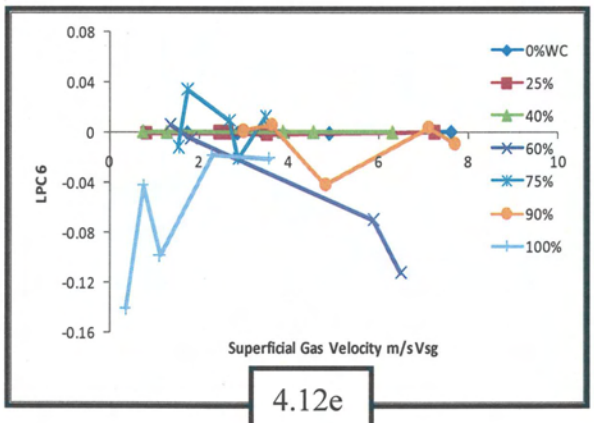

4.12e

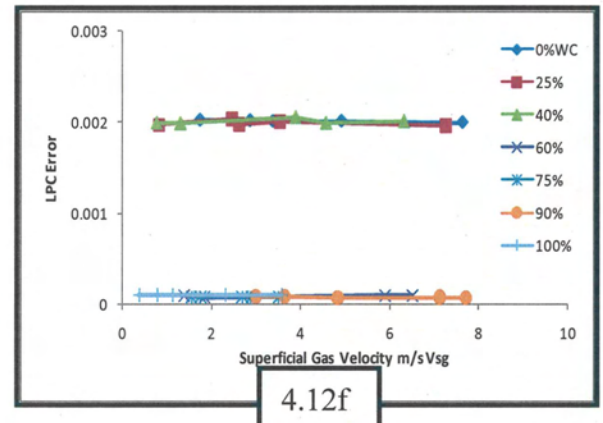

4.12f

Figure 4.12 LPC Line Scatter Plots of Conductance Signal

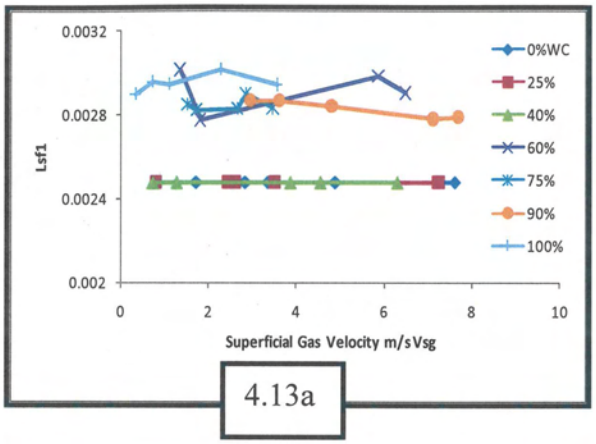

4.13a

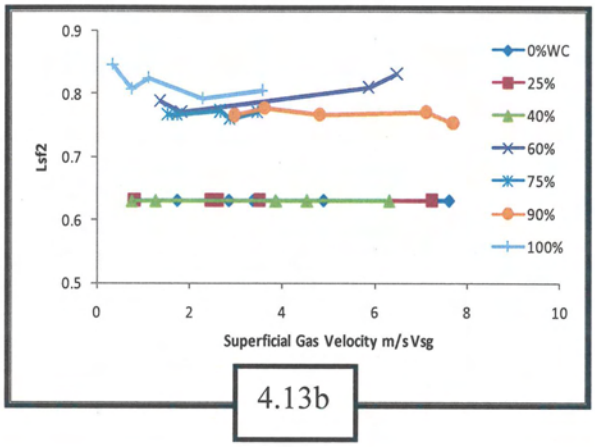

4.13b

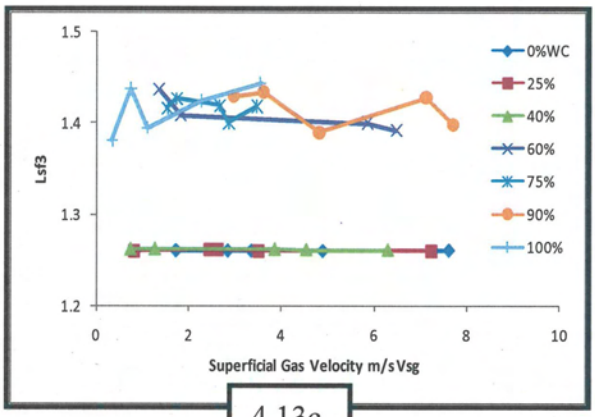

4.13c

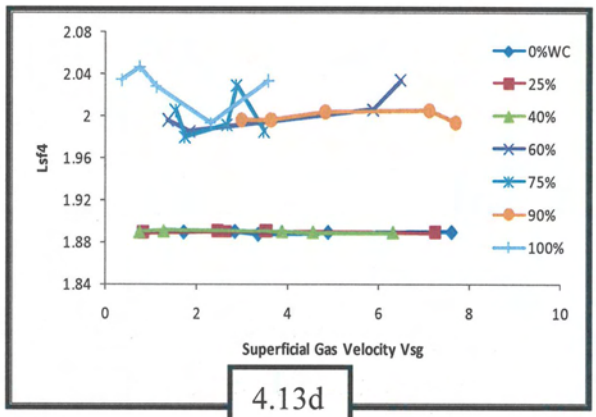

4.13d

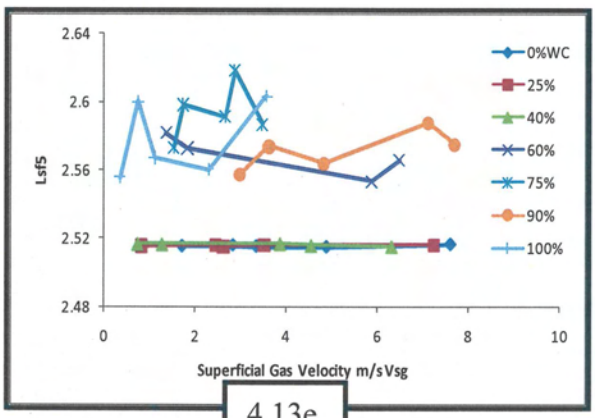

4.13e

Figure 4.13 LSF Line Scatter Plots of Conductance Signal

4.1.1.2 Capacitance Features

The same techniques were employed for the capacitance sensor to extract features in both oil continuous and water continuous flow conditions, as the sensor is proven to function in both conditions, Darwich (1989).

The capacitance signal contains strong information about the dynamic structure of the flow. The passage of slugs exerts a direct effect on the signal.

In addition to the similar features obtained to the conductance signal, two features were derived (Appendix B) from the capacitance signals; these features are the "slug frequency" and "slug length" indicating the physical characteristics of the flow to which they are roughly related. The numbers of peaks in the signal were counted as "slug frequency" and the average widths of these peaks in time domain were calculated as "slug length".

The “slug frequency” of the capacitance signal shows a stable increasing trend with increasing liquid velocity up to 2.0 m/s. Above 2.0 m/s liquid velocity, it seems that the feature is not affected. The “slug length” displays a better trend up to 1.0 m/s liquid and 7.0 m/s gas velocity. The feature does not respond to higher liquid velocities.

The mean value does not carry much information above 1.6 m/s liquid velocity. Also, the liquid velocity lines indicate that this feature is not sensitive to gas velocity. However, the standard deviation presents a decreasing trend with increasing liquid velocity with the exception of the low liquid velocity region. Unlike other transducers, the standard deviation feature of the capacitance exhibits a steady trend.

The coefficient of skewness decreases with increasing liquid velocity. However, after about 3.0 m/s velocity, the feature loses its sensitivity to liquid velocity. The coefficient of kurtosis does not respond to either the liquid or the gas velocity.

The linear prediction coefficients do not carry too much information about liquid or gas velocity. At high liquid velocity, the second coefficient shows a decreasing trend with increasing liquid velocity.

Similarly, a decrease in magnitude of the LSF1 parameter was observed with increasing Vsg particularly for Vsgs. LSF2 and LSF4 yielded similar responses to the multiphase flows demonstrating no detectable reaction to variations in the Vsg. The LSF3 and LSF5 coefficients also decreased in magnitude with increasing Vsg.

4.1.1.3 Differential Pressure

The mean value (MV) feature displays a definite and unbiased response to both gas and liquid velocities across the whole flow conditions examined. The standard deviation (SD) feature displays a flat response in the low flow rates, but only up to a liquid velocity of 2.5 m/s. However, at a superficial gas velocity of 3 m/s, and as the liquid velocity is increased beyond 2.5 m/s, which corresponds to the slug flow regime, the SD feature contours curl upwards and continue with this trend throughout the slug flow regime. This behaviour suggests that the feature is flow regime dependent.

The coefficient of variation (CV) feature appears to be more affected by the liquid loading than by gas velocity. The feature responds most markedly to the hydrodynamic changes of the slug flow regime.

Both the coefficient of skewness (CS) and coefficient of kurtosis (CK) show a strong dependency on liquid loading in the slug flow regime as they are seen to attain higher feature values. The coefficients of skewness and kurtosis show a decreasing trend with increasing liquid velocity up to 1.0 m/s. The coefficient of kurtosis feature displays a difference at lower liquid flow rates (0.7 m/s). The feature at lower liquid flow rates tends to follow the same trend at flow rates under 6 m/s gas velocities. However, above 6 m/s the feature is not effective.

The trend response of the total signal energy (E_T) starts at a liquid velocity above 1.6 m/s. Below this point, the feature does not appear to have any trends which, from a

pattern recognition viewpoint, will mean that this feature will not provide any discriminating ability for the current test condition.

The first line spectral frequency (LSF1) appears to be influenced by the liquid loading with most noticeable liquid dependency seen in the slug flow. The LSF1 feature appears to be strongly sensitive to hydrodynamic flow changes in most flow conditions.

Both the LSF4 and LSF5 demonstrate similar response behaviors to changes in flow conditions. These features do not appear to have a traceable response in the area having liquid velocity between 1.5 and 3 m/s.

4.1.1.4 Absolute Pressure

Unlike the differential pressure sensors, the AP sensor measures the absolute pressure at the test section. It should therefore be expected that some of the features extracted from this sensor would have a different distribution map to the aforementioned differential pressure sensors. The amplitude feature distribution maps of the absolute pressure signal are as would be expected, the MV feature contours increase linearly with the increase in liquid loading and gas velocity and have a uniform feature distribution to both gas and liquid superficial velocities across the whole flow conditions, a trend which is similar to those exhibited by both of the above differential pressure sensors.

The standard deviation (SD) feature has a flat trend distribution. However, as the liquid loading is increased above 2.5 m/s and in the slug flow, the feature contours start to curl upwards, and at higher Vsgs, the contours begin to decline and become flat as the gas velocity is increased beyond 6 m/s. The SD feature distribution is quite similar to those exhibited by the Differential Pressure.

The CV feature of the absolute pressure sensor is responding most markedly to the liquid loading, particularly above 4.5 Vsg, and 3 m/s Vsl, where, similarly to the SD feature, the contours curl upwards. As with the SD feature, the CV feature also has most of its high feature values in the same flow conditions. The CS and CK features

display a rather scattered distribution over the flow domain, and it is not possible to draw any definitive conclusions from their trend behaviour. The feature distribution maps of the total signal energy (E_T) are quite similar to those of the MV feature, and unlike the differential pressure sensors, the AP sensor has a uniform sensitivity distribution across the whole flow test conditions.

4.2 Multiphase Flow Parameters Prediction

In this study, features derived from pressure, capacitance, conductance and gamma sensors were used as input nodes of the network. Superficial liquid and/or gas velocities and water cut (three-phase flow) corresponding to each feature vector were employed as output nodes. The identification scheme applied in this study is shown in Figures 4.14a-c.

There are currently many neural network software packages available including both commercial packages and public domain software. These packages range from a simple demonstration of introductory software to large commercial packages supporting a range of network architecture and training algorithms. Many of the commercial packages interface with standard spreadsheets from which they obtain their input data. This provides a flexible environment for designing, training and testing the neural network without requiring a heavy investment in software development. An example of such software, which is used in this research, is MATLAB.

An added advantage of MATLAB is that it is an integrated technical computing environment that combines data acquisition, signal processing, statistical techniques, neural networks, high level of programming language, and many more functionalities. The open architecture makes it easy to use MATLAB and companion products to explore data and create custom tools that provide early insights and competitive advantages. The version of MAT LAB that was used for this work is 7.1

4.2.1 Overview of PR Workflow and Approach to Multiphase Metering

Once an effective number of features have been identified, the next step is to map these features from the feature vectors to the superficial gas and liquid velocities (volumetric flow rates). The exact form of this mapping is to be determined from a data set of reference measurements.

Figure 4.14a shows a generic workflow of the main elements involved in the pattern recognition approach for the multiphase flow metering involved in this work.

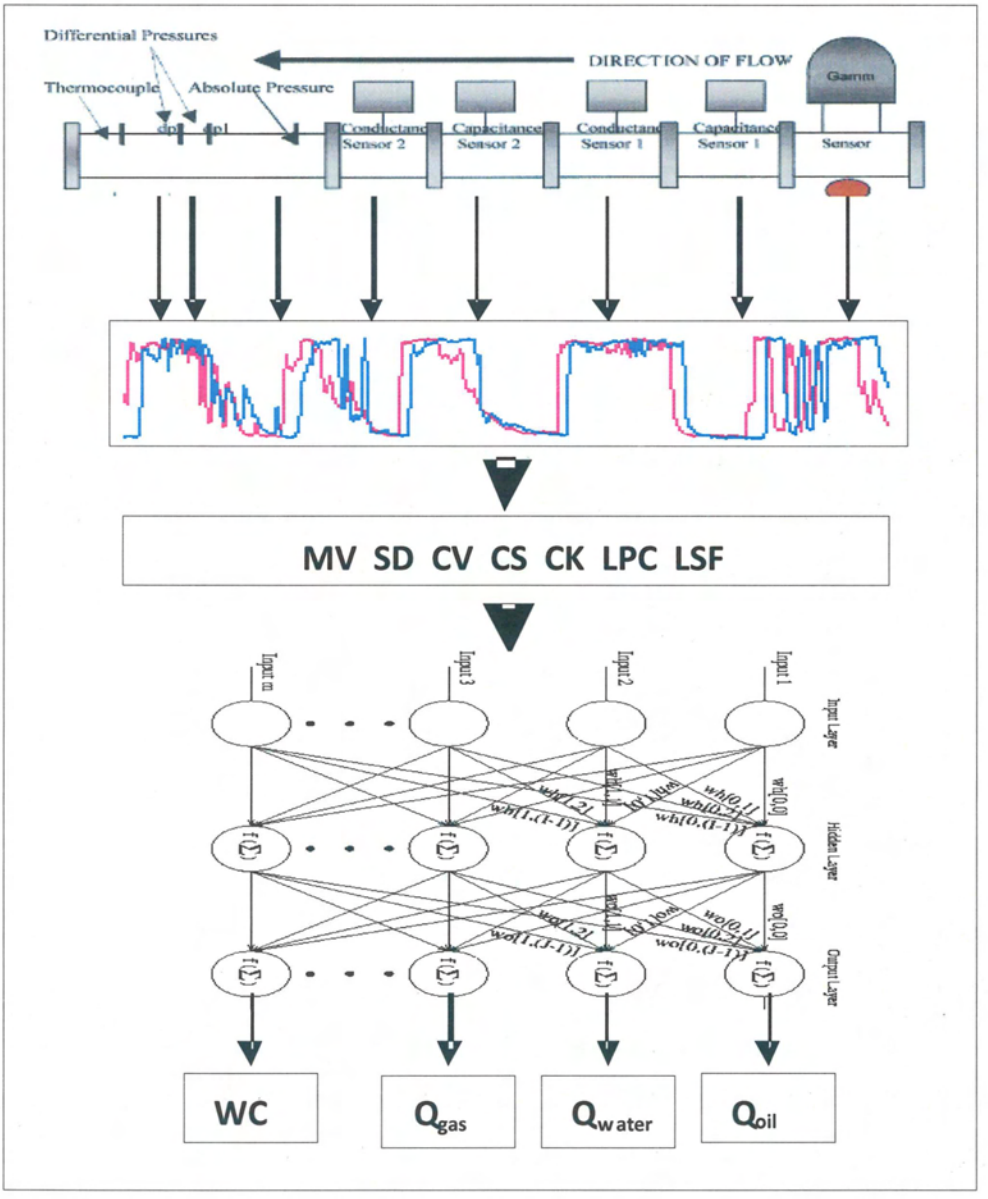

Figure 4.14a Pattern Recognition Approach to Multiphase Flow Metering

The data was sub-divided into training and test data. Having trained the systems with some correct examples of system inputs and desired outcome, the performance of the network had then to be appraised by independent test data, not seen previously by the network. The available data were classified into training and test set, **Figure 4.14b.**

Some data were reported corrupted, please refer to 3.4.2, thus limiting available data for evaluation of the salinity effects under the same operating conditions. However, the availability of a pair of sensors for the differential pressure, capacitance and conductance, enabled the use of one data set for training and another for testing. Since the data corruption was only limited to the differential pressure sensors (signals for DP sensors appeared random and negative), signals from all the other sensors from the file runs were available for investigations with the 50g/l MgSO4 solution.

The work described here is for the higher salinity case, i.e. 100g/l $MgSO_4$ solution. Preliminary investigations demonstrated that 89 training points and 37 test points provided an appropriate training to test the data

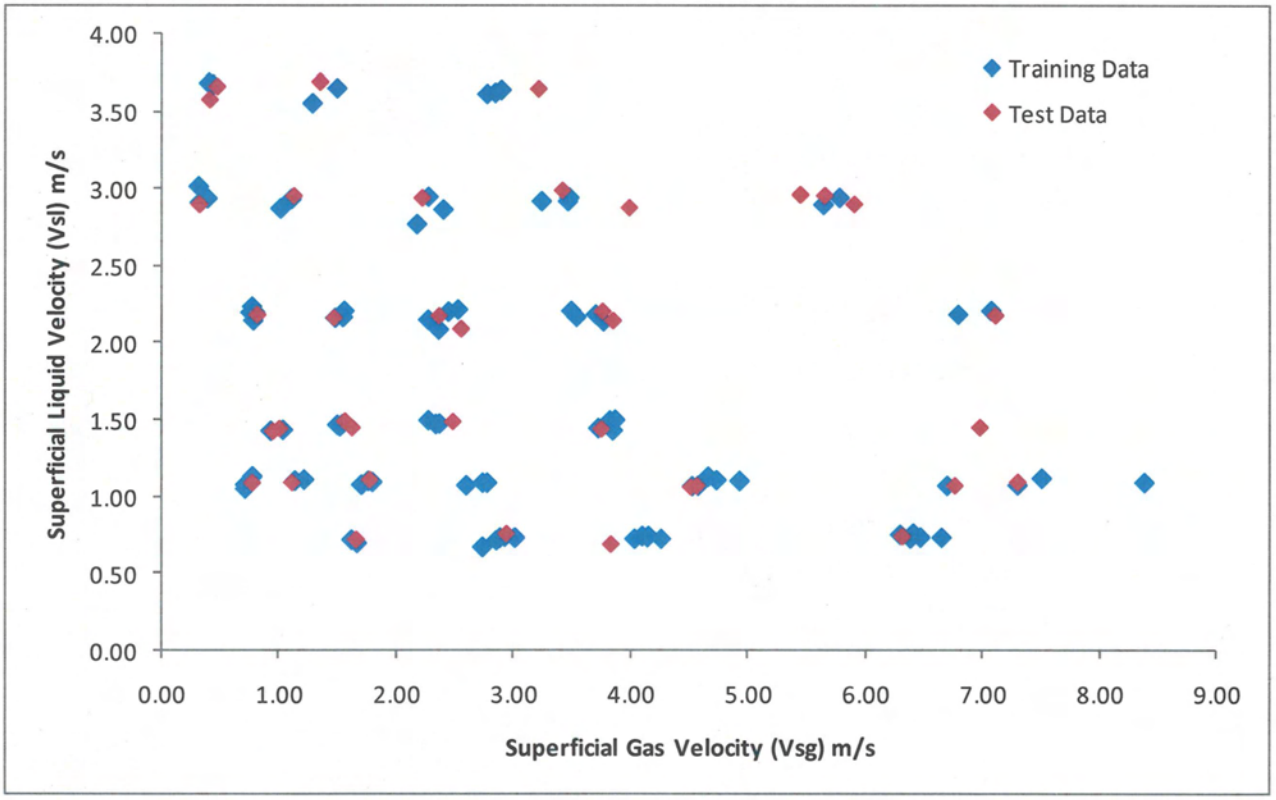

Figure 4.14b Training (Calibration) and Test (Measurement) Data

Figure 4.14c illustrates the mechanism conceived and applied to design, train, and then test the Back Propagation Neural Network's generalisation performance with previously unseen data.

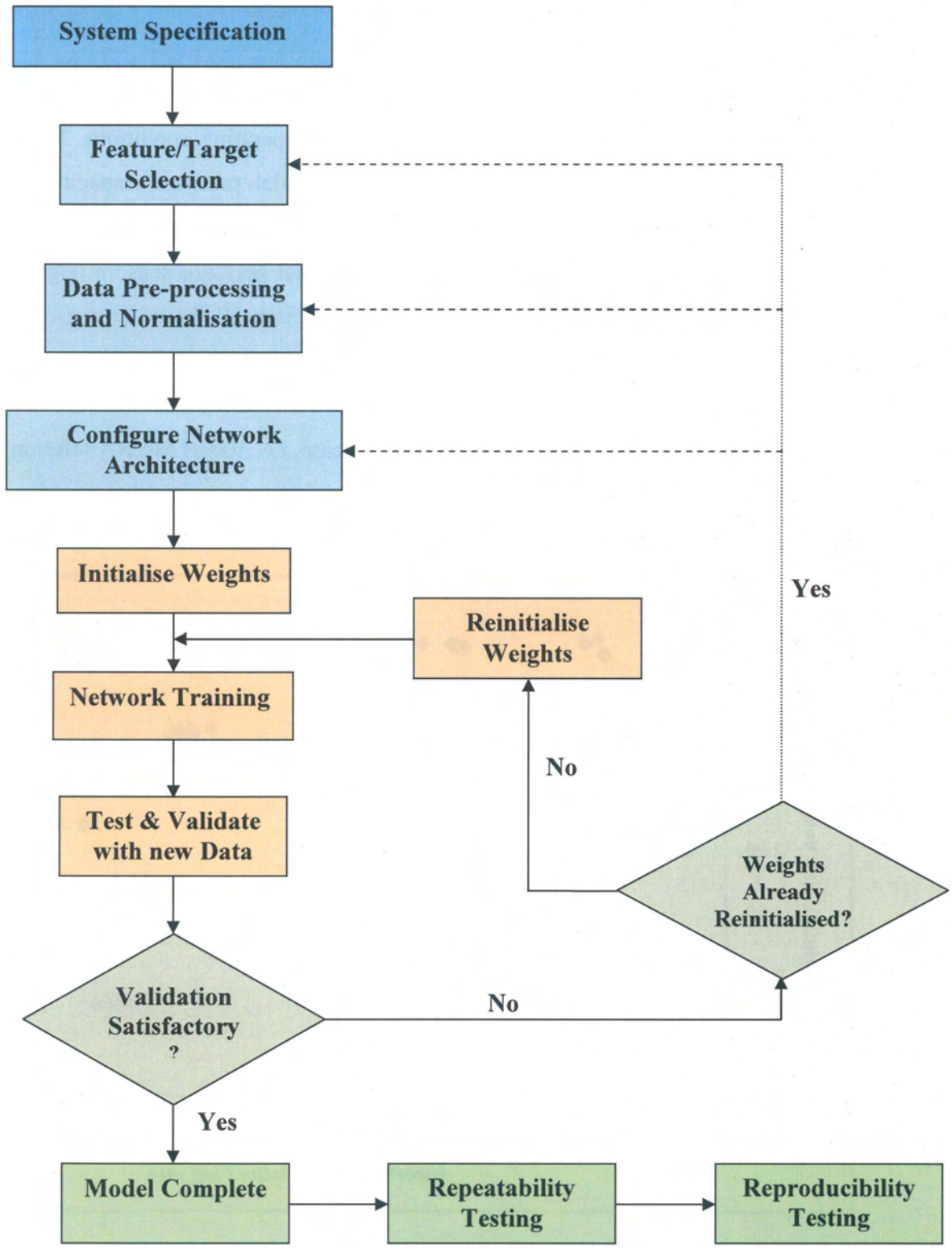

Figure 4.14c Neural Network Design, Training, and Testing Scheme

Choosing the number of neurons in the hidden layer depends on the complexity of the underlying function, which the neural network is attempting to approximate. If there are too many hidden neurons, the danger exists that the training set is simply memorised, while on the other hand a neural network with too few hidden neurons will not generalise well to new data sets. In most of the applications involving a neural network, the network configuration is found by trial and error, starting with a small number of neurons and different sets of random, initial weight values. However, in this study, the Bayesian regularisation technique was evaluated and found to successfully optimise the number of hidden neurons needed for classification in an automated manner.

The Levenberg-Marquardt (LM) algorithm was found to give the best classification results. This training algorithm minimises a combination of squared errors and weights to determine the best configuration for network generalisation.

However, it was noticed that when new data, previously unseen by the network was introduced, the generalisation ability of this algorithm was badly affected. This problem is commonly referred to as over-fitting.

Different types of technique have been introduced to improve generalisation to avoid the over-fitting problem. The two most widely used methods are cross-validation, otherwise known as early stopping, and regularisation. Both of these techniques were tested during the current research study. Although cross-validation was found to improve generalisation, its performance was significantly inferior to the Bayesian regularisation technique. A contributing factor to the poor performance of the cross-validation technique could be attributed to the fact that sub-dividing the available data into three sub-sets (training, validation and testing) results in a reduced training set. Hence the information contained in the selected samples is not optimally used and the risk of under-constrained training increases. Furthermore the cross-validation technique involves many trial and error runs to optimise the number of neurons in the hidden layer. For these reasons, the Bayesian regularisation technique is preferred for this study.

One feature of the Bayesian regularisation technique is that it provides a measure of how many network parameters (weights and biases) are being effectively used by the network. As seen in **Figure 4.15**, the final trained network uses approximately 124 parameters, i.e. weights and biases in the neural network.

This effective number of parameters should remain approximately the same, no matter how large the total number of parameters in the network becomes. (This assumes that the network has been trained for a sufficient number of iterations (epochs) to ensure convergence).

It is clear that the algorithm has truly converged if the Sum Squared Error (SSE) and Sum Squared Weights (SSW) are relatively constant over several iterations, which is true in this case as shown in **Figures 4.15a** and **4.15b** respectively. When this occurs, a decision may be made to terminate the training and retain the weights and biases for network testing

When the network's repeatability accuracy is satisfactory, then the network is used for measurement of new data. **Figure 4.16** shows the repeatability performance of the neural network trained with amplitude features extracted from all the sensors. The plots are a linear regression fit between the experimentally measured velocities and the neural network prediction results. The linear regression fit shows that the network achieves excellent repeatability results and therefore can be used for the measurement of the new data.

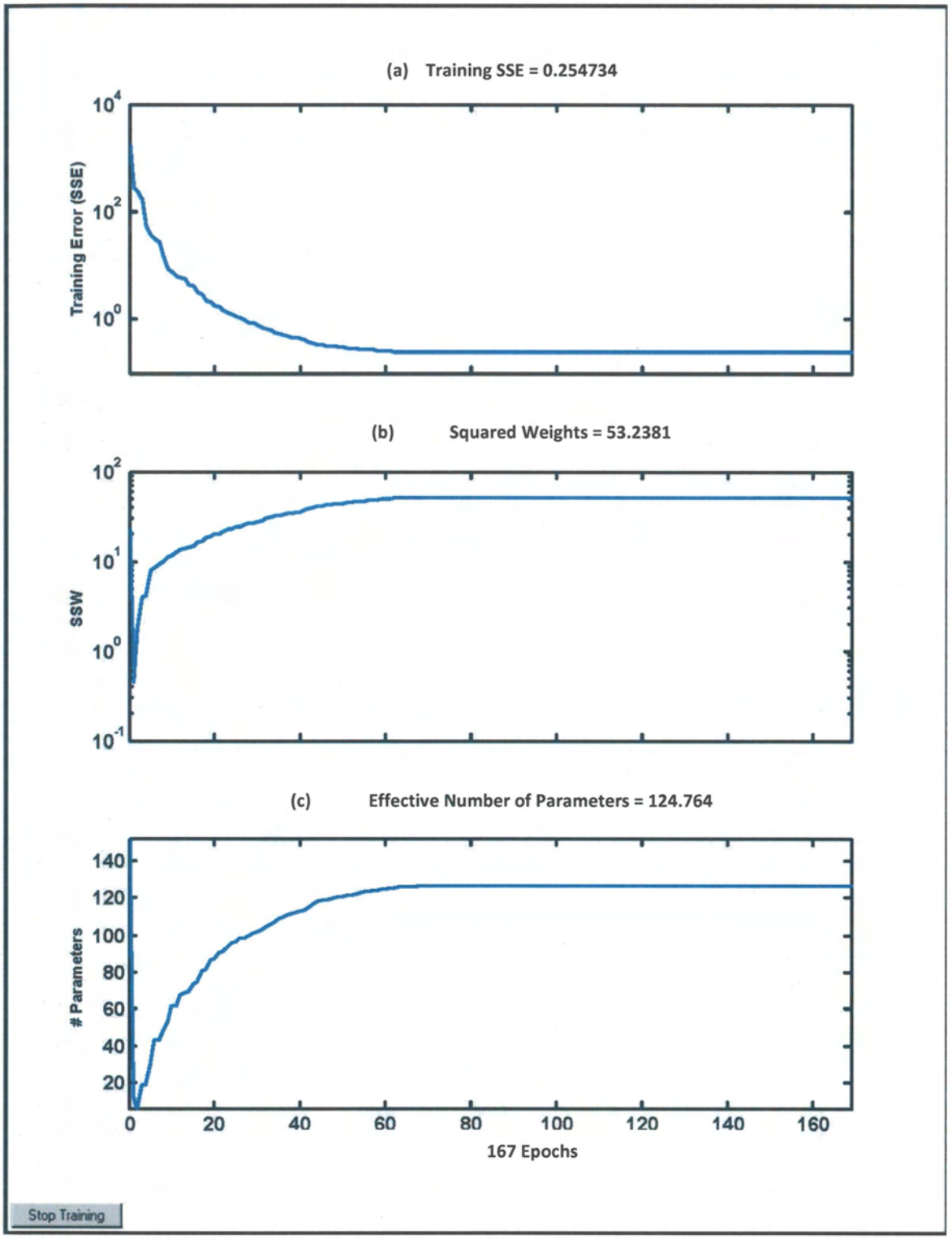

Figure 4.15 Neural Network Training and Optimisation

Prior to testing the network on new and previously unseen data, it is important to evaluate its repeatability capabilities (i.e. test the network on the same data that it is being trained with).

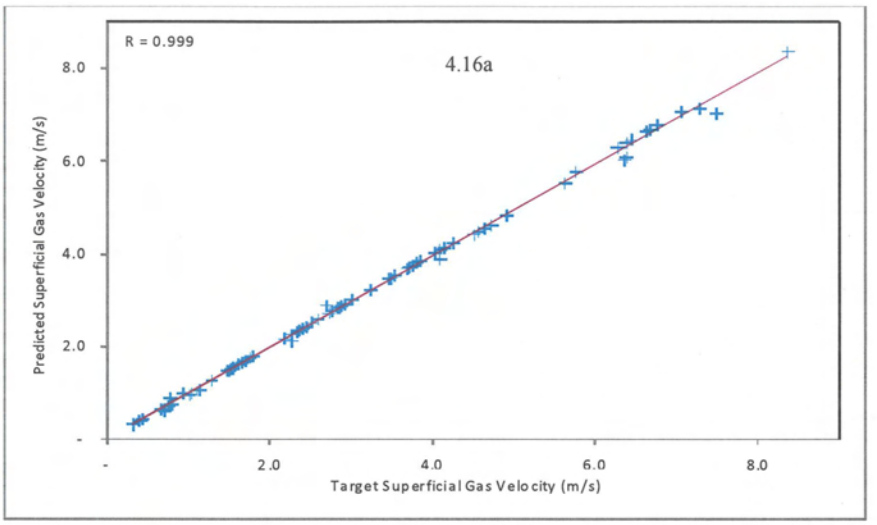

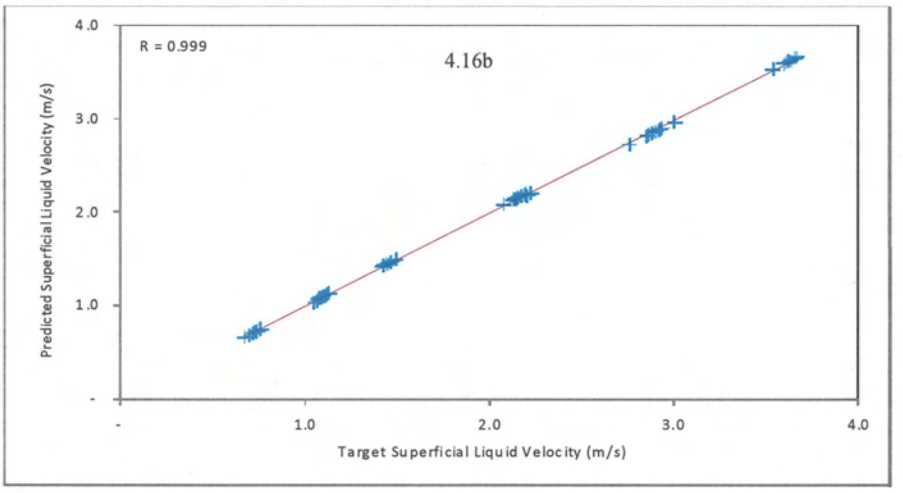

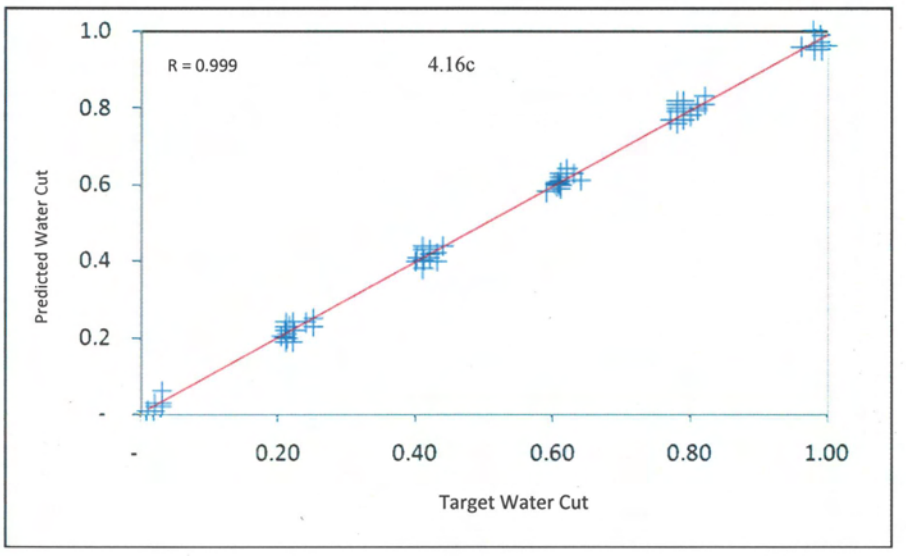

Figures 4.16a-c, Repeatability Tests of the Back-Propagation Neural Network, (a) Vsl, (b) Vsg and (c) Water Cut Prediction Performances

4.2.2 Network Architecture Definition

The final network architecture was defined as [n – 10 – 3]. This denotes the number of neurons in each of the layers:

- n – the number of input feature vectors (variable)
- 10 – the number of neurons in the hidden layer (fixed)
- 3 – the number of output neurons i.e. one each for the target (fixed)

However, for phase velocity determination using the individual and/or combination of the sensor signal features, the water cut output node was simply removed and preliminary investigations revealed that the network performance remained unchanged.

4.2.3 Test Parameters

At the preliminary testing stage, it was observed that the neural network performance varied as a function of the number of input features, i.e. the more input features presented, the higher the quality of the network prediction in terms of accuracy. There were a vast number of input vector permutations possible with the 85 extracted features for all the five sensors, plus the additional 51 features, for other pairs of sensors.

Previous work on the use of feature extractions with multiphase flow observed that an efficient method of feature vector construction was obtained through combining features of each of the information domains and this was verified through preliminary investigations, Jama (2004). This method provides a systematic methodology for comparing the discriminatory abilities of the various information domains across the different spectra, **Table 4.2**.

Table 4.2 – Input Feature Vector Sets for Analysis (One Sensor)

No.	Feature Domain	Training Data	Test Data
1	Amplitude Features	6 x 89	6 x 37
2	Linear Prediction Coefficients (LPC)	6 x 89	6 x 37
3	Line Spectral Frequencies (LSF)	5 x 89	5 x 37
4	All (Amplitude + LPC + LSF)	17 x 89	17 x 37

The 126 signal data points collected were divided so that 89 were utilised for neural network training and the remaining 37 were exploited for testing purposes, **Figure 4.17**.

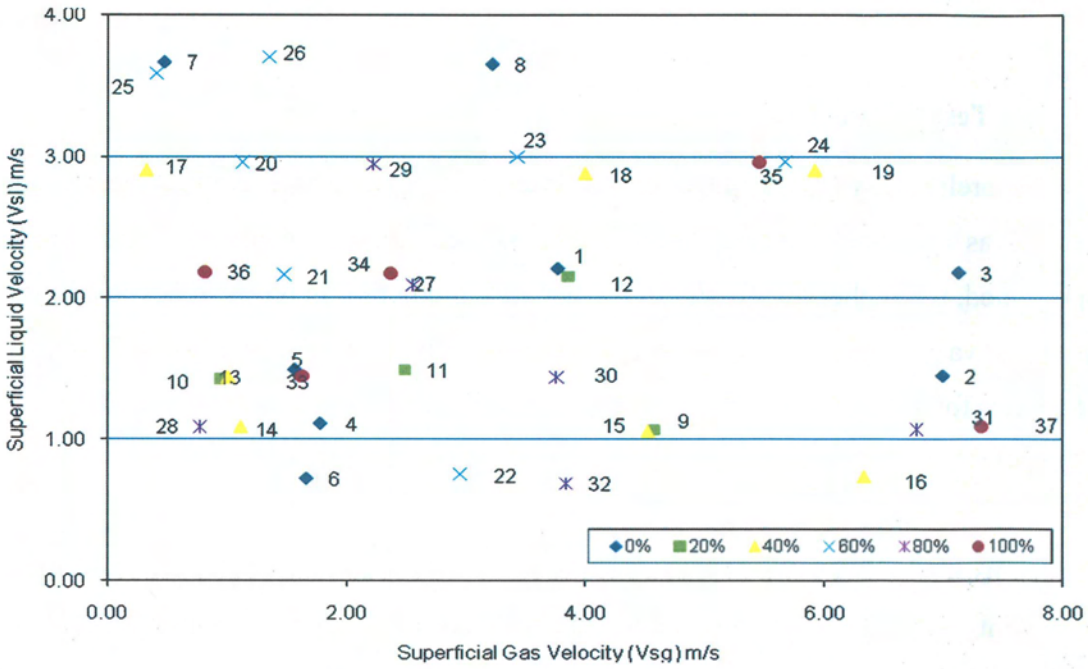

Figure 4.17 - Test Data Matrix

Target accuracy in this work was set at ±5% for each of the target outputs. The measurement error was calculated as a relative error over the range of measurement defined as:

$$E_r = \frac{y_{i(predicted)} - y_{i(measured)}}{y_{range}} \times 100\% \qquad (4.3)$$

Where, y_i denotes the variable of interest and y_{range} denotes the measurable range, i.e. $y_{max} - y_{min}$. This method for calculating the relative error has been widely used to express the classification performance of several pattern recognition based multiphase flow measurement systems Darwich (1989), Beg (1998), Jama (2004).

4.2.4 Multiphase Flow Measurement Results

The predictions of the neural network for determination of liquid and gas superficial velocities from the information domain using the features shown in **Table 4.2**, as well as water cut from the features of the pair of capacitance and conductance sensors and the single gamma densitometer are discussed below. **Table 4.3** contains a summary of the flow rate and water cut prediction performance, utilising the best performing feature for each of the sensor signals.

4.2.4.1 Absolute Pressure

Flow rate measurement results obtained for both the liquid and gas velocity predictions with Absolute Pressure Features are presented in **Figures 4.18 - 4.21**.

(a) Liquid Superficial Velocity

For the liquid phase measurements, the amplitude feature vectors and the feature fusion case do well on determining the liquid superficial velocity by achieving 88 and 100% of the test points to within ±5% error band. Results for DP pressure and fusion of all pressure sensor features are shown and will be discussed in section 4.2.4.6.

(a) Gas Superficial Velocity

Figure 4.20 presents the gas superficial velocity measurements from the neural network models, derived by the Absolute Pressure Features. The results indicate that gas superficial velocity measurement accuracies were significantly poorer than those obtained for the liquid phase.

The line spectral frequency (LSF) feature vectors resulted in the best measurement accuracy, with 65% measurement accuracy.

While the network was trained successfully for liquid velocity, most of the prediction errors for gas velocity appeared at the higher liquid velocity extremities of the flow.

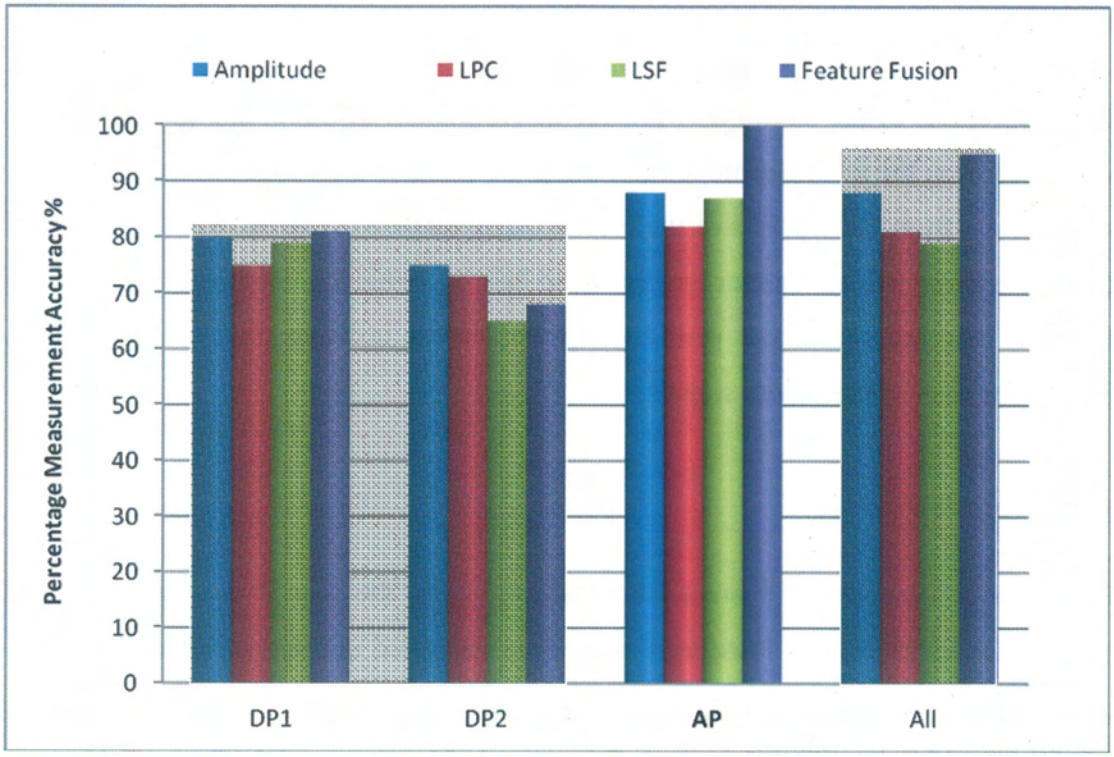

Figure 4.18 – Percentage Measurement Accuracy for Superficial Liquid Velocity for Absolute Pressure Feature Vectors

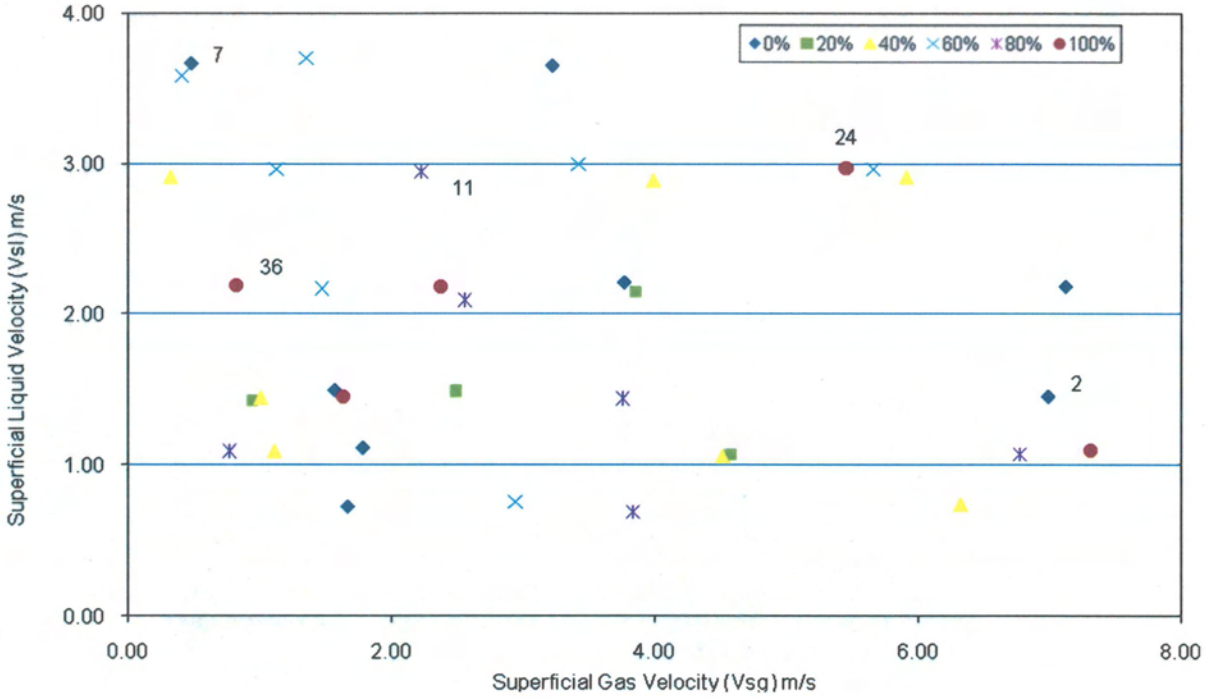

(a)

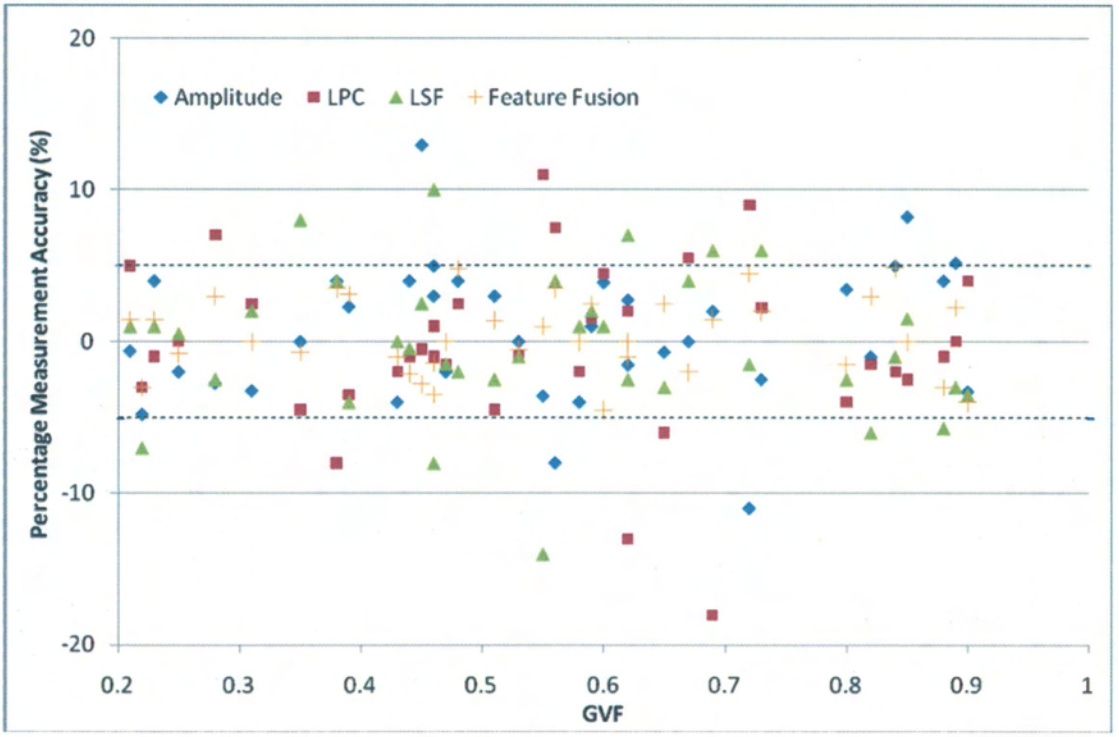

(b)

Figure 4.19 – Percentage Liquid Distribution for Absolute Pressure Features (a) GVF Plot (b) Outlying Test Point Matrix Location for Amplitude Errors

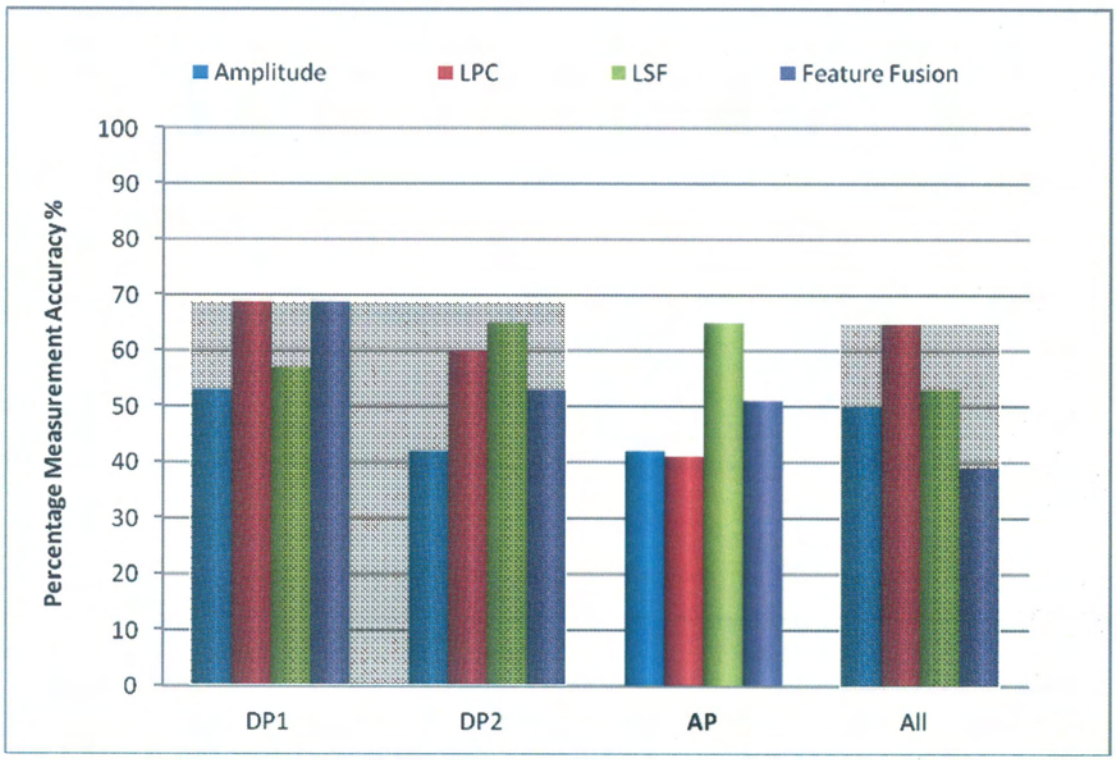

Figure 4.20 – Percentage Measurement Accuracy for Superficial Gas Velocity for Absolute Pressure Feature Vectors

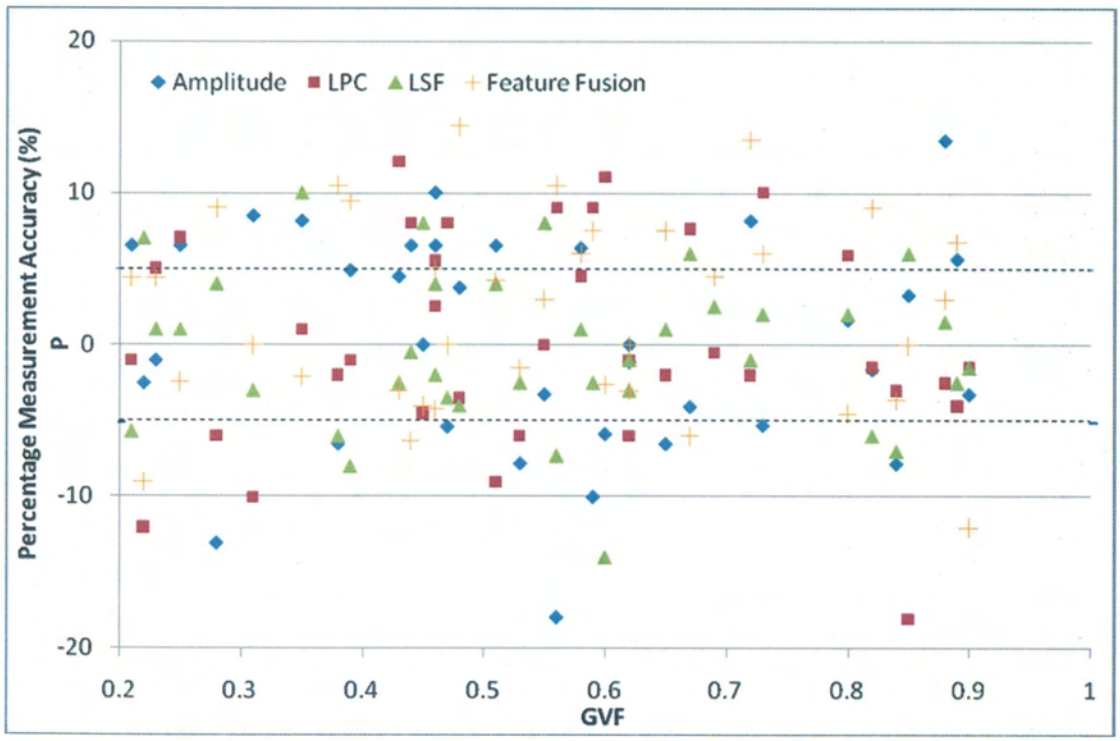

(a)

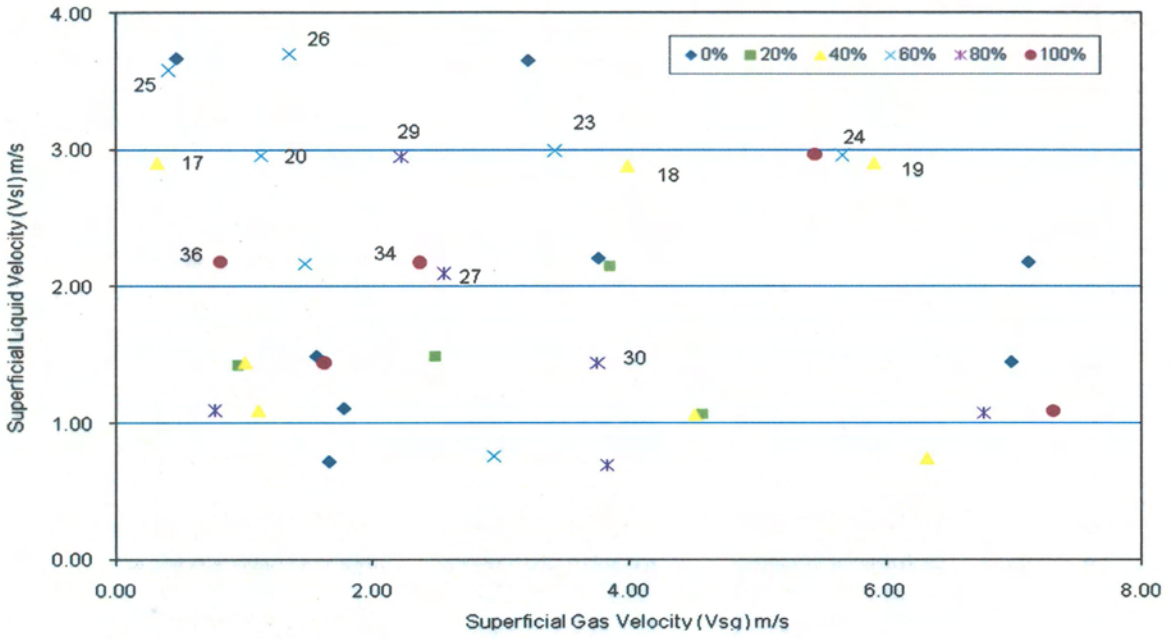

(b)

Figure 4.21 – Percentage Gas Distribution for Absolute Pressure Features (a) GVF Plot (b) Outlying Test Point Matrix Location for LSF Errors

4.2.4.2 Differential Pressure

(a) Liquid Superficial Velocity

Figure 4.22 shows a summary of the flow rate measurement performance by different feature vectors of the differential pressure signals. The results obtained were within the target accuracy (±5%) for the liquid superficial velocity measurements. It can be seen that the measurement variable's performance is described by three sets of plots, one for DP1, and another for DP2, and a third showing the results for All i.e. both DP1 and DP2 signal features (This will be discussed in section 4.2.4.6). Results demonstrated that feature fusion input vectors from DP1 provided the strongest discriminatory abilities for liquid superficial velocity determination. The amplitude features showed strong liquid velocity classification capabilities for the DP2 signal. In general, the DP1 features produced better liquid superficial velocity predictions than those of DP2.

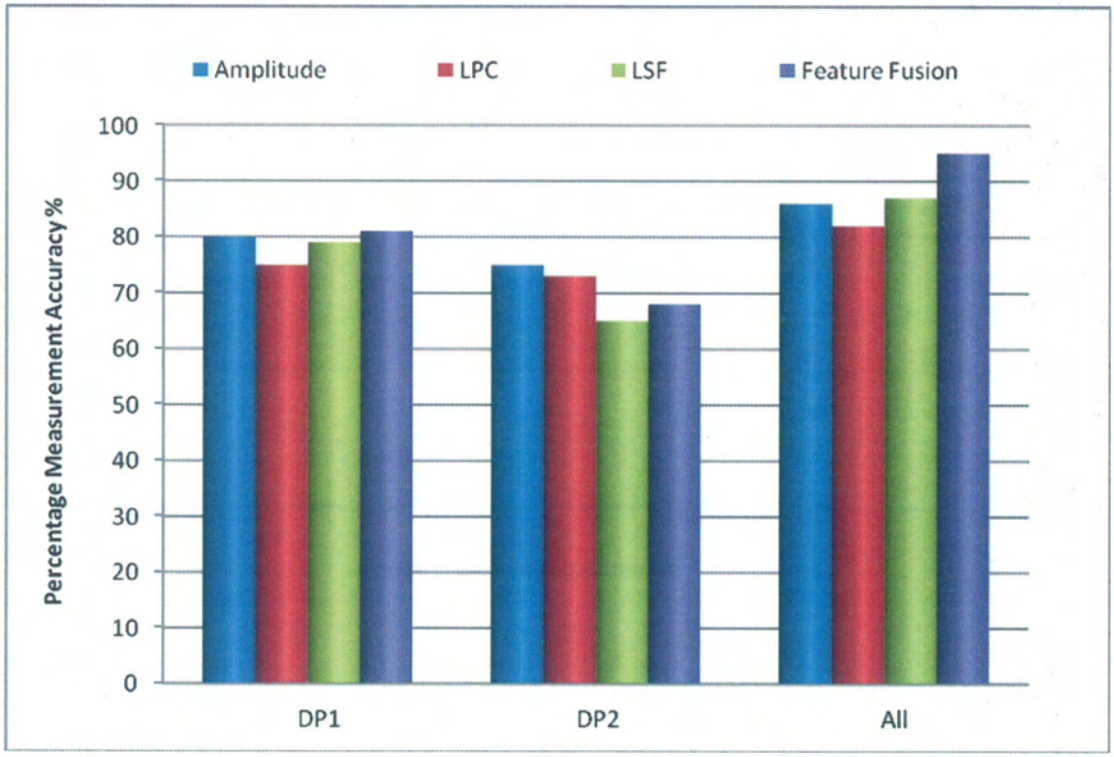

Figure 4.22 – Percentage Measurement Accuracy for Superficial Liquid Velocity for DP Feature Vectors

The contrast in measurement error distribution obtained by different feature vectors is indicative of the fact that different features respond differently to the same flow conditions as explained previously and therefore their combination should lead to better measurement accuracies, as confirmed by **Figure 4.22**.

Two subset plots are used for the visualisation of the network classification results. The first subset plots the measurement errors as a function of gas volume fraction (GVF). The second is a plot of the actual test matrix (used for testing the network) with superficial gas velocity on the x-axis and superficial liquid velocity on the y-axis. The data points on the plots show the exact locations of the measurements and the measurement error at those locations.

Figure 4.23 (a) displays the error distribution plot as a function of the gas void fraction for the feature fusion input vectors. The best overall performance was obtained from the vector comprising feature fusions of All the Differential Pressure features: 97% of test data points were predicted within ±5% of their target values.

Figure 4.23 (b) illustrates the test conditions for the outlying data point; test point 28 from DP2 has the highest error, with a prediction error of +18%. The error is not significant in comparison to the results obtained for the other test points and cannot be attributed to any one particular systematic source and must therefore be inherent in the network. It is anticipated that increasing the quantity of training data utilised during the training phase would lead to an increase in the liquid velocity determination accuracy.

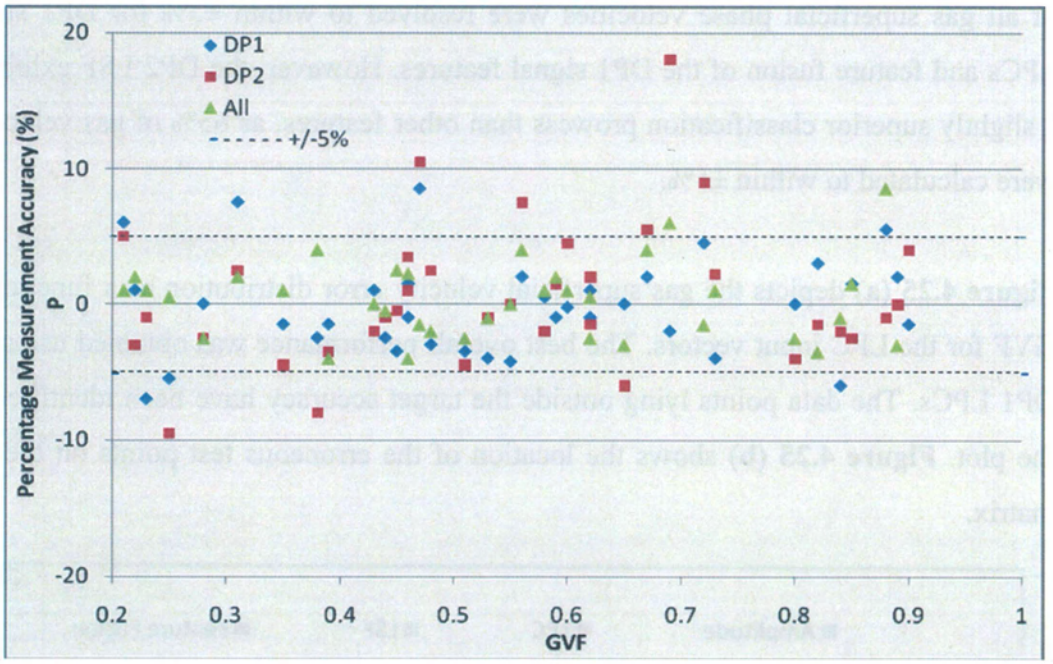

(a)

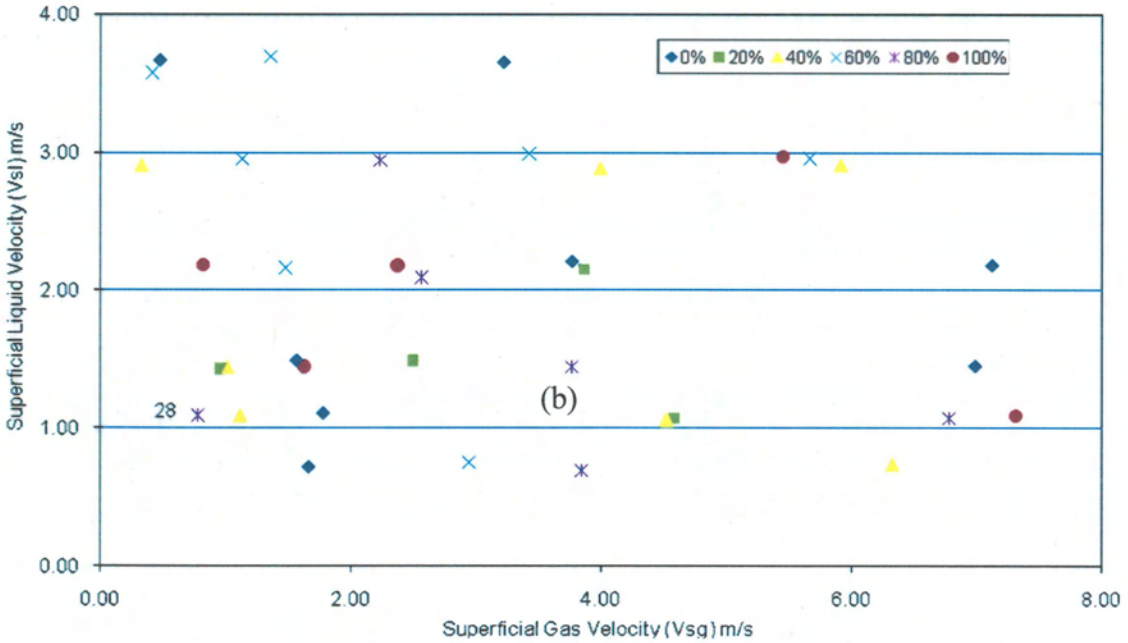

(b)

Figure 4.23 – Percentage Liquid Distribution for Feature Fusion (a) GVF Plot (b) Outlying Test Point Matrix Location

(b) Gas Superficial Velocity

Figure 4.24 presents the gas superficial velocity measurements obtained from the neural network models. Gas superficial velocity measurement accuracies were significantly poorer than those obtained for the liquid phase.

With the gas velocity measurements, the linear prediction coefficients and feature fusion provided the best discriminatory properties for gas velocity determination. 69% of all gas superficial phase velocities were resolved to within ±5% for DP1 signal LPCs and feature fusion of the DP1 signal features. However, the DP2 LSF exhibited a slightly superior classification prowess than other features, as 65% of gas velocities were calculated to within ±5%.

Figure 4.25 (a) depicts the gas superficial velocity error distribution as a function of GVF for the LPC input vectors. The best overall performance was obtained using the DP1 LPCs. The data points lying outside the target accuracy have been identified on the plot. **Figure 4.25 (b)** shows the location of the erroneous test points on the test matrix.

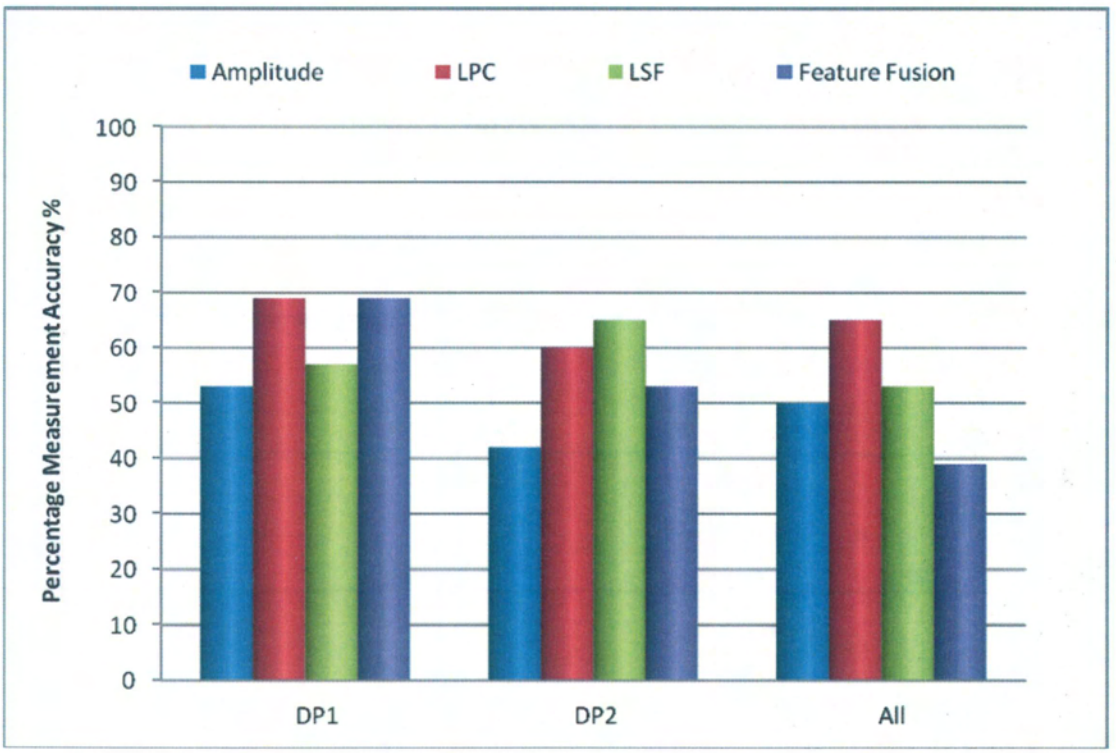

Figure 4.24 – Percentage Measurement Accuracy for Superficial Gas Velocity for DP Feature Vectors

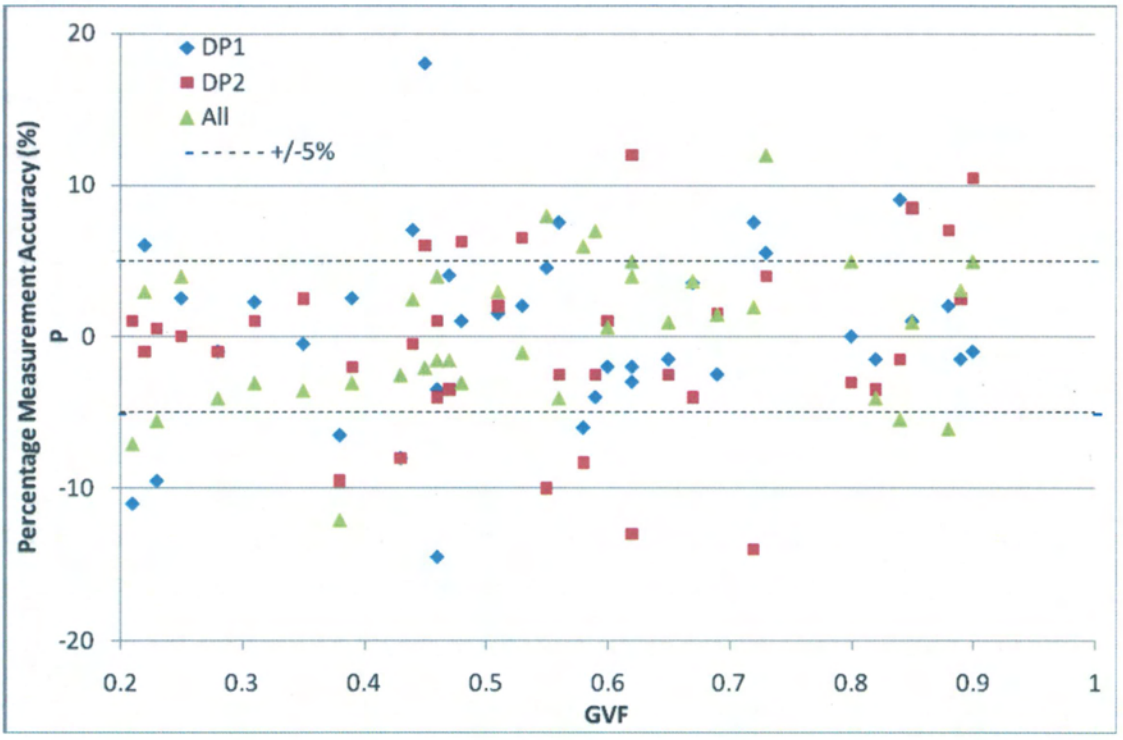

(a)

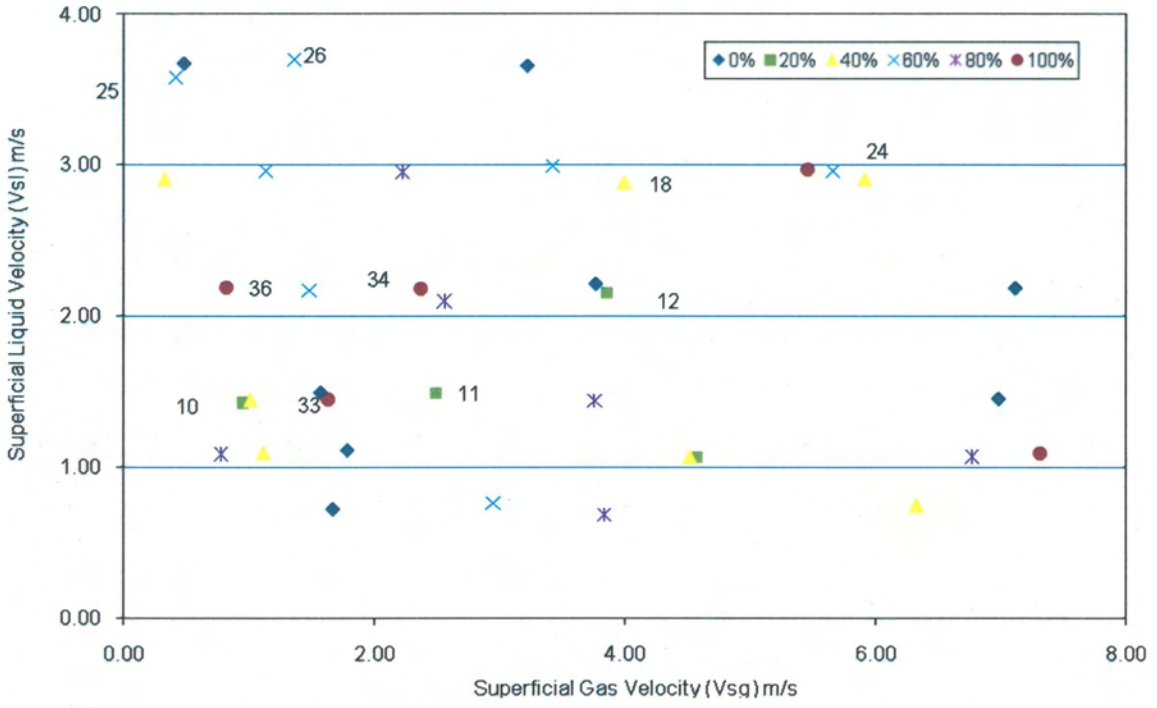

(b)

Figure 4.25 – Percentage Gas Distribution for (DP1) LPC (a) GVF Plot (b) Outlying Test Point Matrix Location

The performance of different feature vectors is clearly different in the gas phase. It is interesting to see that the feature fusion vector for the combined DP1 and DP2 features performs poorly on the gas velocity measurement with 39% measurement accuracy. This indicates that the intuitive approach of 'bigger the feature dimension the better the pattern classifier' accuracy does hold true here, or perhaps the network did not converge and just displaying results for the local minimum. These results show generally when comparing the measurement accuracy obtained by different feature vectors, the feature fusion vectors perform best for both liquid and gas velocity measurements for single DP transducer features.

From the above discussion, it may be concluded that if only a single differential pressure sensor is available for phase flow measurements on the spool piece, then feature fusion vectors for the single transducer should be used for the liquid and gas volumetric measurements. This also underlines the fact that neural network generalisation performance is heavily influenced by the type of feature vectors used and that the formation of a large calibration database in terms of feature vectors does not necessarily lead to improved measurement accuracy.

4.2.4.3 Capacitance

(a) Liquid Superficial Velocity

Figure 4.26 presents a summary of the liquid superficial velocity measurements obtained from the neural network models for both capacitance 1 and capacitance 2 features. The amplitude and feature fusion features provided the best discriminatory properties for liquid velocity determination. 78% of all liquid superficial phase velocities (Vsl) were resolved to within ±5% for amplitude features of capacitance 1, and 74% Vsl with feature fusion signal features of capacitance 2.

(b) Gas Superficial Velocity

Figures 4.27 summarises the results obtained within the target accuracy (±5%) for the gas superficial velocity measurements.

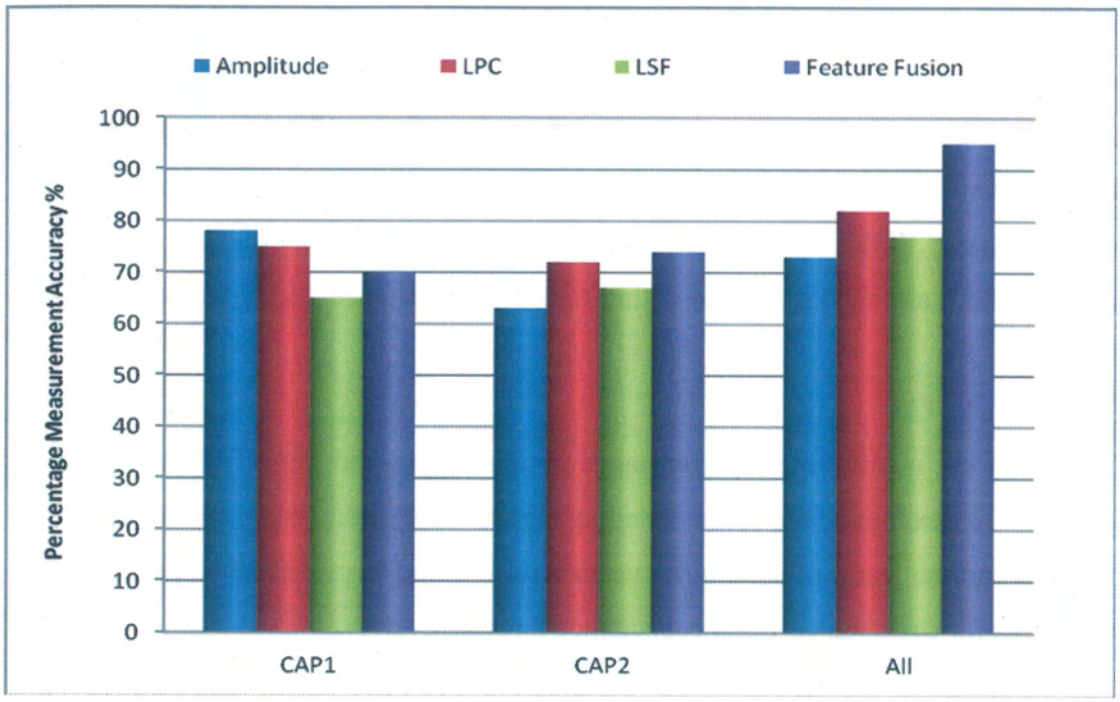

Figure 4.26 – Percentage Measurement Accuracy for Superficial Liquid Velocity for Capacitance Feature Vectors

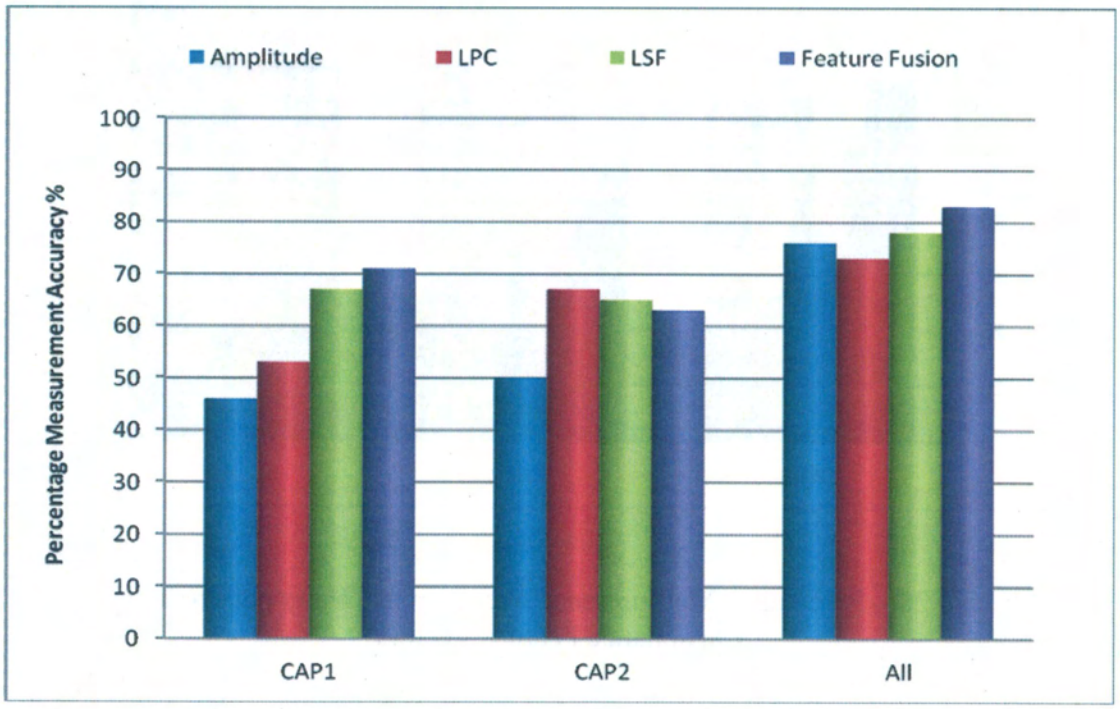

Figure 4.27 – Percentage Measurement Accuracy for Superficial Gas Velocity for Capacitance Feature Vectors

Results demonstrated that feature fusion input vectors provided the strongest discriminatory abilities for gas superficial velocity determination for capacitance 1. The LPC features also showed strong gas velocity classification capabilities for capacitance 2. The results obtained using an input vector comprising feature fusion features were: 71% of the data points were predicted within the ±5% target for capacitance 1, and 67% predicted within ±5% for capacitance 2 LPC features.

(c) Water Cut

The water cut measurement performance obtained from the input feature and signal permutations examined are summarised in **Figure 4.28**. In this instance, the amplitude features and the feature fusion input vectors were found to provide the optimal output responses for capacitance 1 and capacitance 2 respectively.

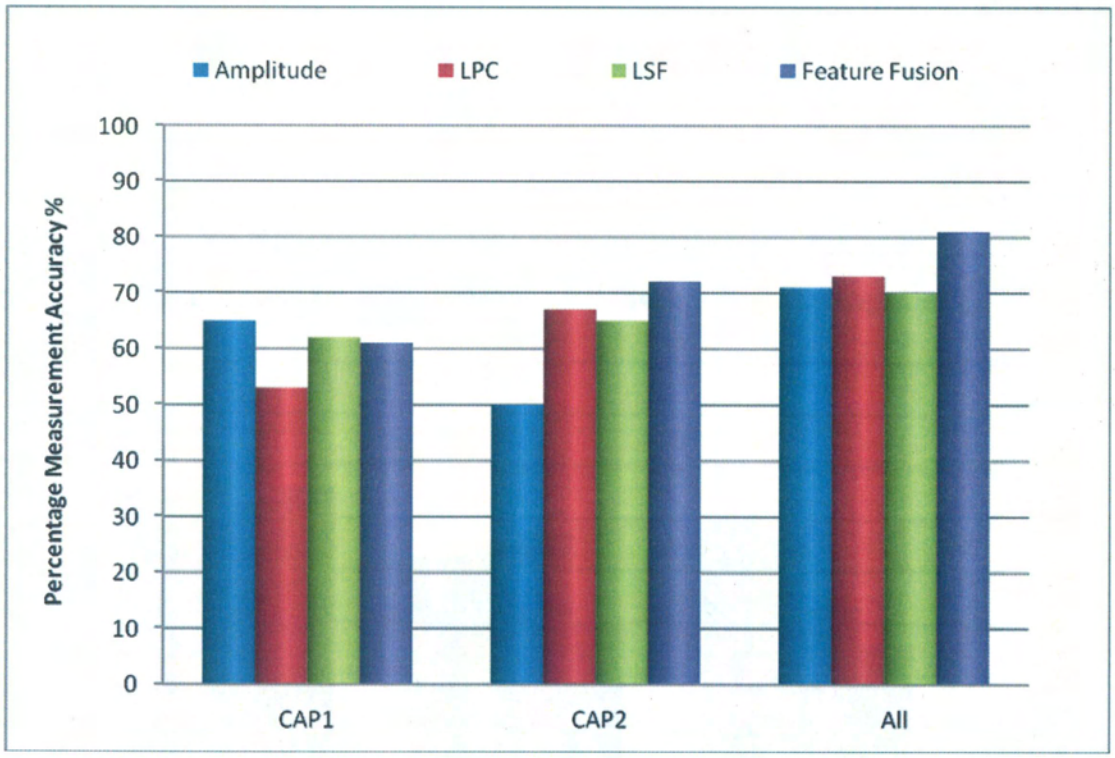

Figure 4.28 – Percentage Measurement Accuracy for Water cut Prediction - Capacitance Feature Vectors

It can be seen that prediction error increases as water cut increases. The testing of the neural network models showed that 65% were predicted within the target accuracy of ±5% with amplitude features of capacitance 1, and 72% accuracy with feature fusion vectors of capacitance 2.

When liquid and gas velocity information was checked at points where the highest prediction error occurred, it was observed to lie at the low liquid velocities and high water cut – see **Figure 4.29**.

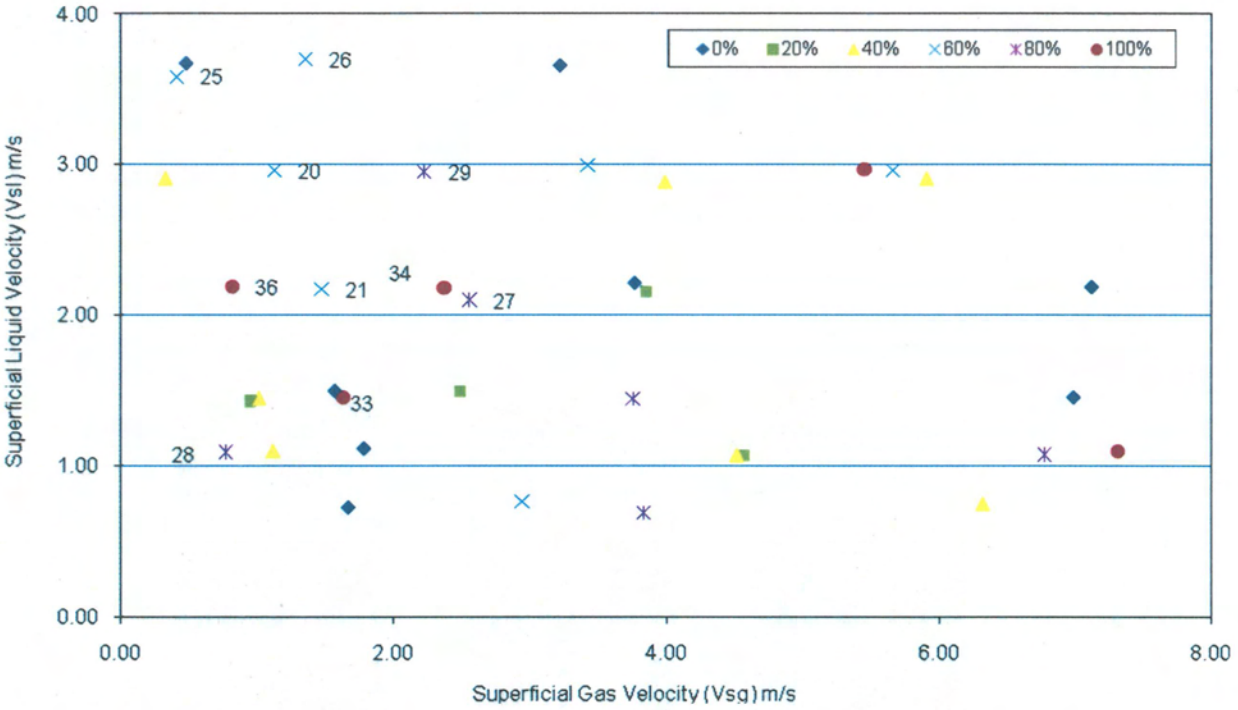

Figure 4.29 – Outlying Test Point Matrix Location for Feature Fusion Errors – Capacitance 2 (Water cut Determination)

4.2.4.4 Conductance

(a) Liquid Superficial Velocity

Figure 4.30 presents the liquid superficial velocity measurements obtained from the neural network. Liquid superficial velocity measurement accuracies were significantly poorer than those obtained for the capacitance features, especially at water cut ≤60%.

The linear prediction coefficients and feature fusion provided the best discriminatory properties for liquid velocity determination for conductance 1 and conductance 2 respectively. 69% of all liquid superficial phase velocities were resolved to within ±5% for the LPCs features of conductance 1, and the feature fusion results for conductance 2 signal features Vsl predictions was 67%, i.e. within the ±5% target.

Figure 4.31 depicts the liquid superficial velocity error distribution as a function of GVF for the LPC input vectors for conductance 1. The data points lying outside the

target accuracy have been identified on the plot and have been observed to be in high liquid, low water cut flow conditions. (This confirms the conductance's poor performance in oil continuous flow multiphase conditions.)

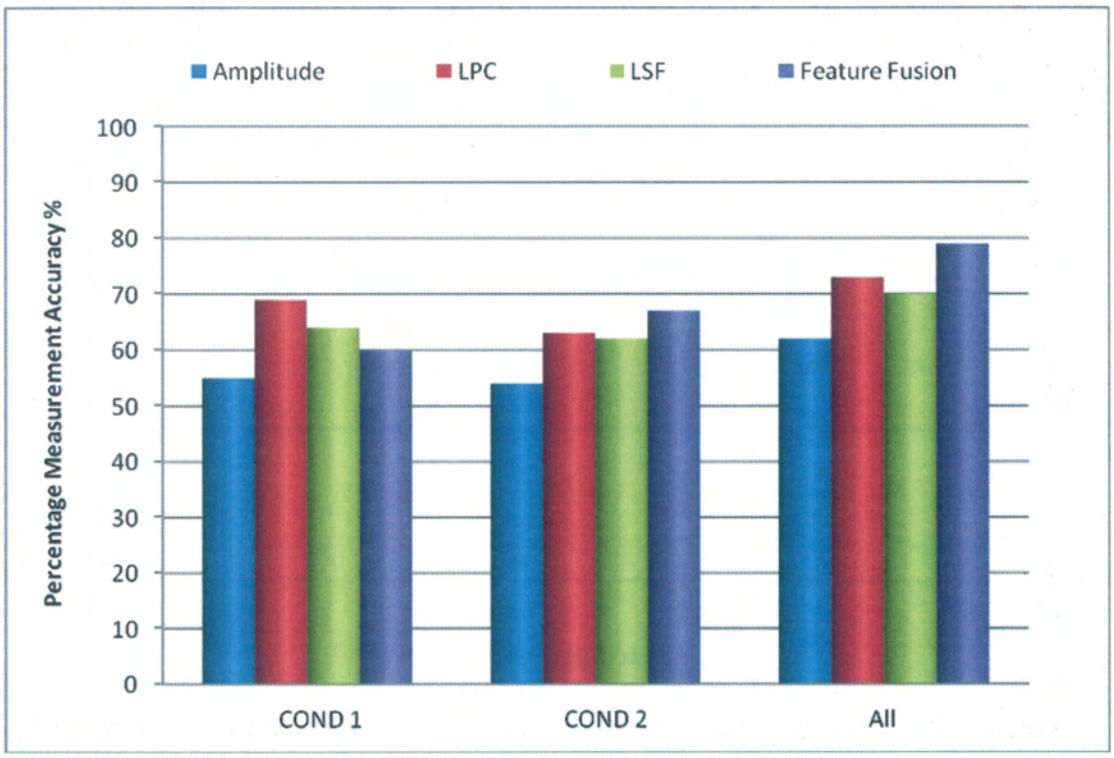

Figure 4.30– Percentage Measurement Accuracy for Superficial Liquid Velocity for Conductance Feature Vectors

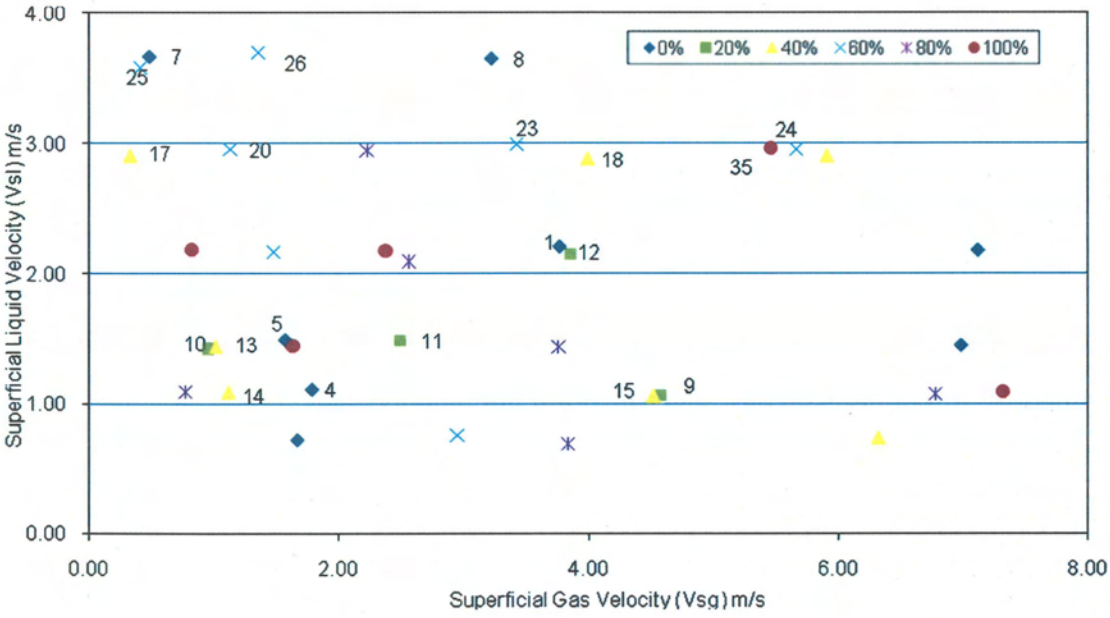

Figure 4.31 – Outlying Test Point Matrix Location for Feature Fusion Errors – Conductance 1 (Vsl Prediction)

(b) Gas Superficial Velocity

Figure 4.32 summarises the results obtained within the target accuracy ±5% for the gas superficial velocity measurements. The measurement variable's performance is described in the plot below.

Results demonstrated that LSF input vectors provided the strongest discriminatory abilities for gas superficial velocity determination for conductance 1 meter. However, for conductance 2, feature fusion vectors showed stronger gas velocity classification capabilities. Similar to the liquid predictions, the conductance features produced poorer gas superficial velocity predictions than capacitance signal features.

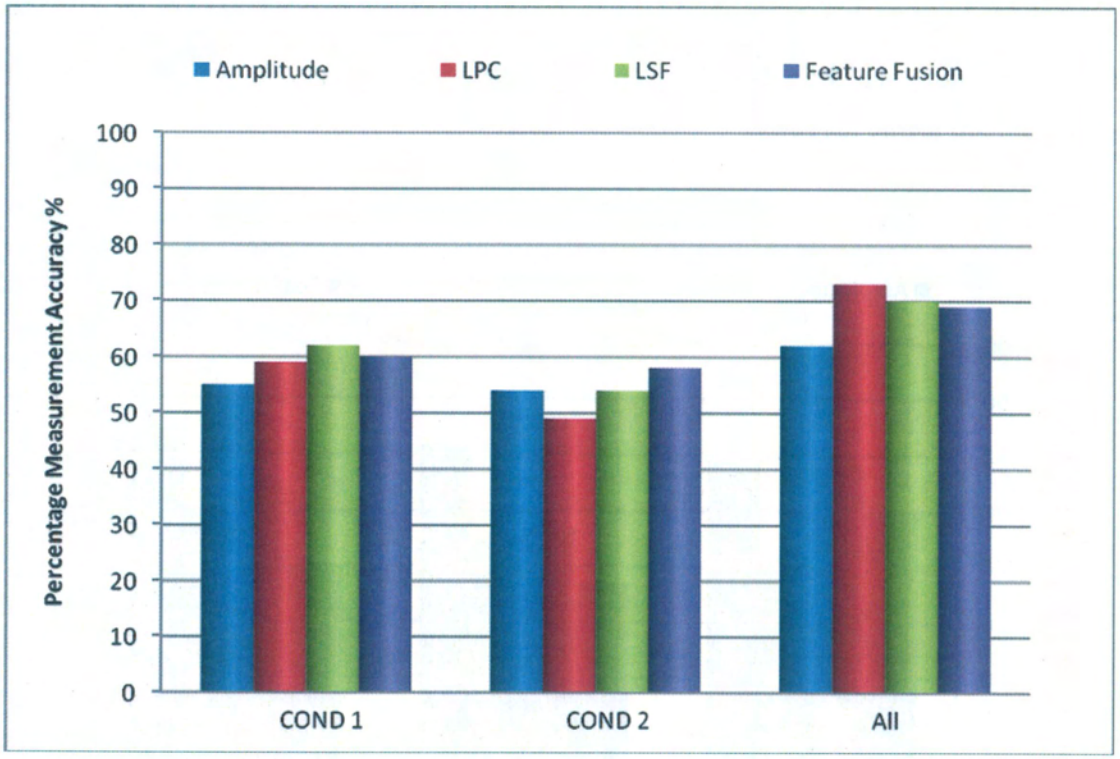

Figure 4.32 – Percentage Measurement Accuracy for Superficial Gas Velocity for Conductance Feature Vectors

(c) Water Cut

Performance obtained for water cut measurement from the input feature and signal permutations examined are summarised in **Figure 4.33**. In this instance, the LPC features and the feature fusion input vectors were found to provide the optimal output responses for conductance 1 and conductance 2 respectively.

It can be seen that prediction error decreases as water cut increases. Testing of the neural network showed that 78% were predicted within the target accuracy of ±5% with LPC features of conductance 1, and 82% accuracy with feature fusion vectors of conductance 2.

When liquid and gas velocity information was checked at points where the highest prediction error occurred, they were observed to lie at the high liquid velocities and low water cut, see **Figure 4.34,** indicating the test points at which water cut measurement errors occurred.

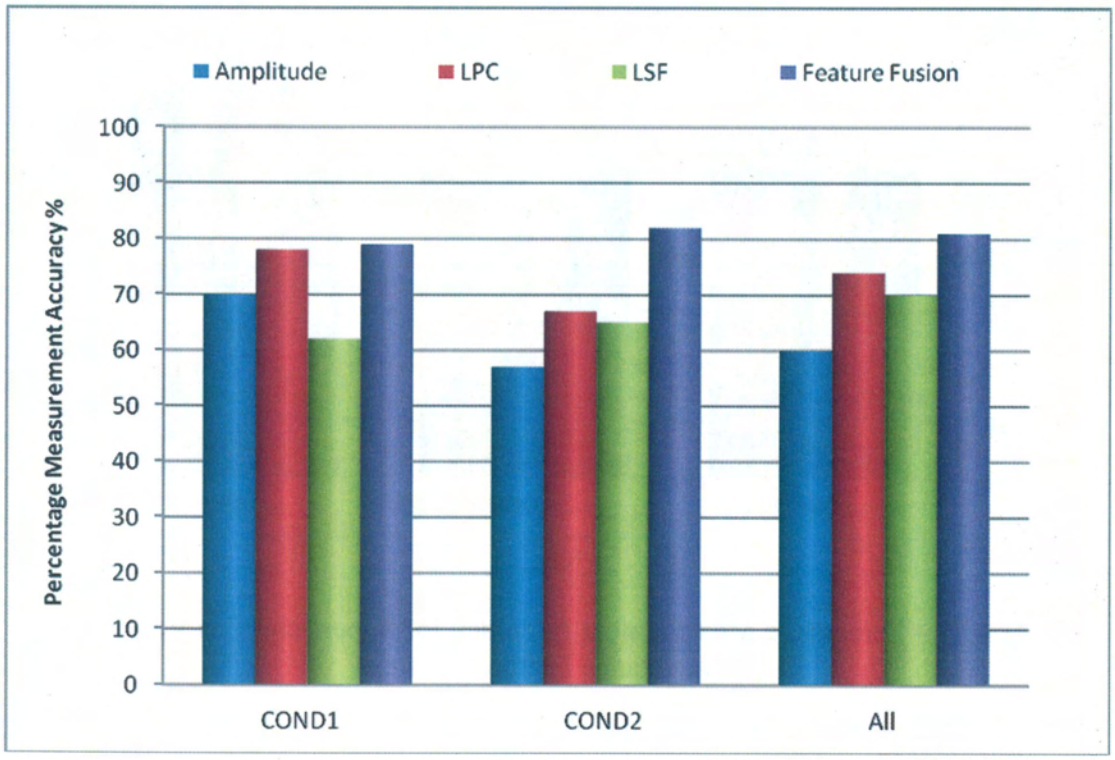

Figure 4.33 – Percentage Measurement Accuracy for Water Cut Prediction - Conductance Feature Vectors

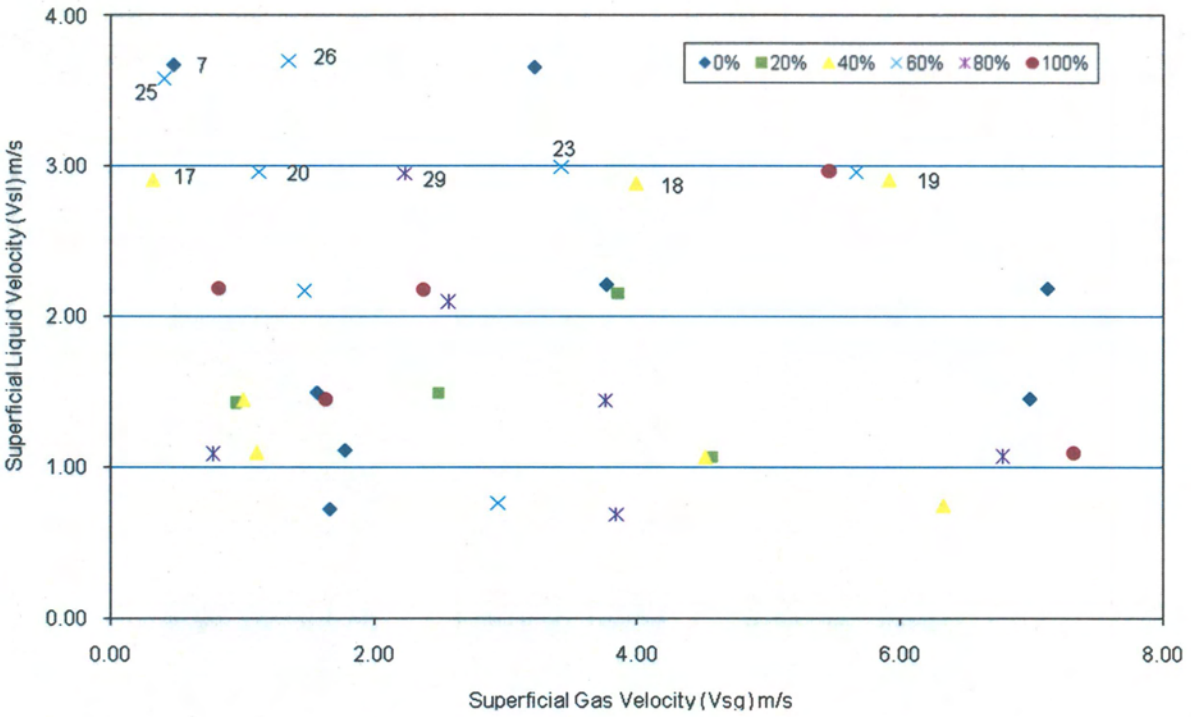

Figure 4.34 – Outlying Test Point Matrix Location for Feature Fusion Errors – Conductance 2 (Water cut Determination)

4.2.4.5 Gamma

(a) Liquid Flow Rate Measurement

Figure 4.33 shows a summary of all the measurements obtained from the neural network model from the gamma feature vectors.

Liquid superficial velocity measurement accuracies indicated 71% of the data points were best predicted with the LSF feature vectors within the target accuracy of ±5%.

(b) Gas Flow Rate Measurement

Gas flow rate prediction results demonstrated that amplitude feature input vectors provided the strongest discriminatory abilities for gas superficial velocity determination. In general, the results obtained produced the best predictions so far for Vsg measurements within the target of ±5% compared to results from all individual sensors.

(c) Water Cut Measurement

The water cut measurement performances obtained from the input features examined are presented below; the amplitude feature input vectors were found to provide the best output accuracies, with 81% of the test data points meeting the specified target within ±5%.

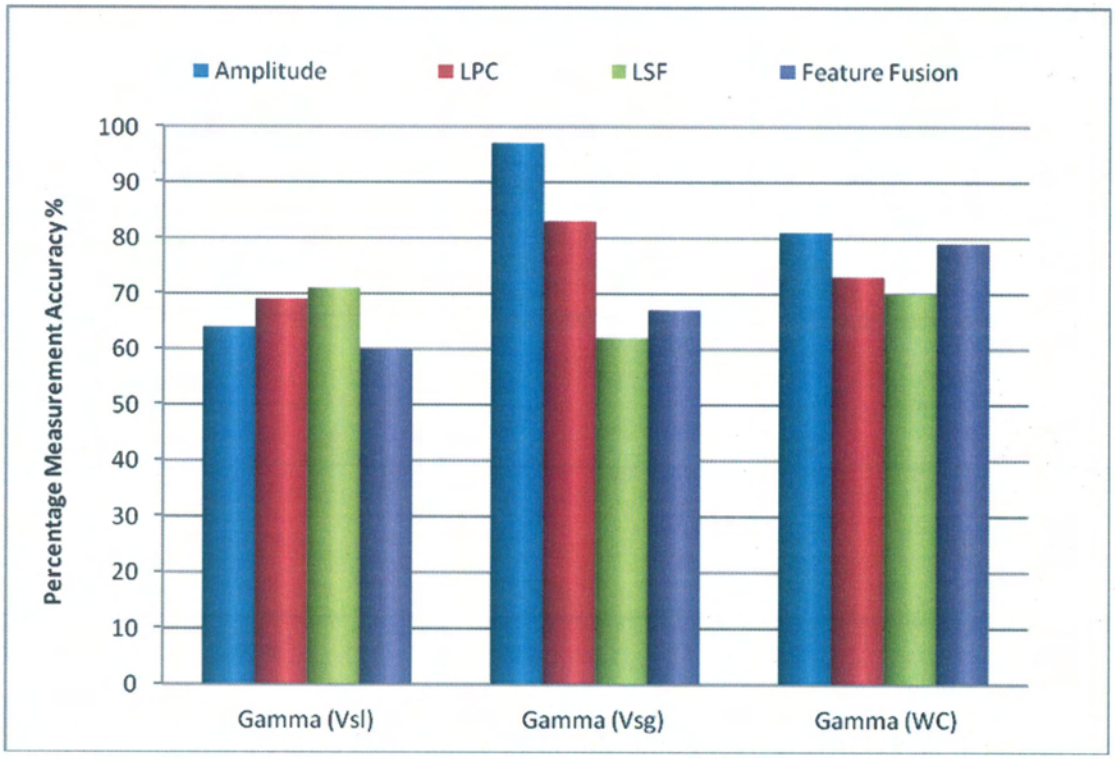

Figure 4.35 – Percentage Measurement Accuracy – Gamma Features for Vsg, Vsl and Water cut (WC)

4.2.4.6 Gas Void Fraction

Besides the velocity and water cut measurements, the neural network predicted the Gas Void Fraction (GVF) using the same methodology. The GVF was simply obtained by removing the water cut node and replacing it with GVF as the target output. The Capacitance, Conductance and Gamma Feature vectors were trained and tested for GVF measurements; **Figures 4.36 (a)** and **(b)** show a summary of the results obtained.

(a)

(b)

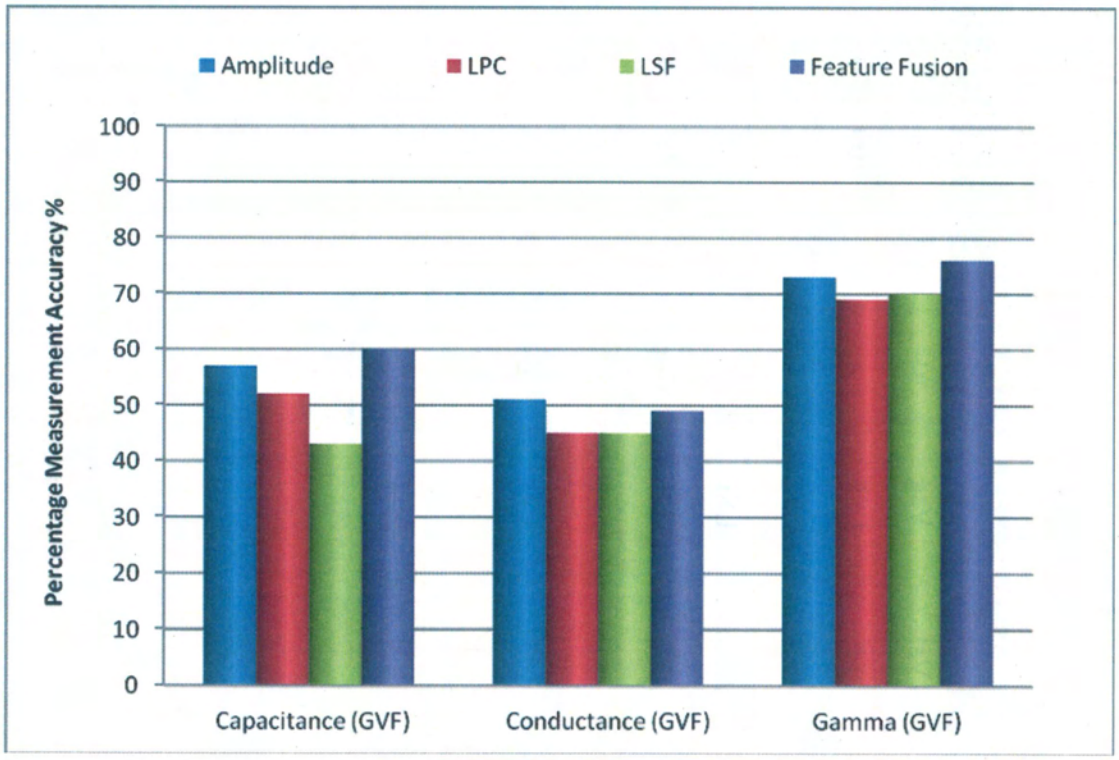

Figures 4.36 (a) and (b) – GVF Measurement Results for with Capacitance, Conductance and Gamma Features

Table 4.3 – Summary of Sensor Prediction Performance

Sensor(s)	Best Performing Feature				e ≤ 5% (%)				5% < e ≤ 10% (%)				10% < e ≤ 20% (%)			
	Vsl	Vsg	WC	GVF	Vsl	Vsg	WC	GVF	Vsl	Vsg	WC	GVF	Vsl	Vsg	WC	GVF
AP	FF	LSF	-		100	65	-		0	32	-		0	3	-	
DP1	FF	LPC	-		81	68	-		19	24	-		0	8	-	
DP2	Amp.	LSF	-		75	65	-		20	24	-		5	11	-	
Capacitance 1	Amp.	FF	Amp.	FF	78	71	65	60	18	29	26	20	4	0	4	17
Capacitance 2	FF	LPC	FF		74	67	71		22	30	28		6	3	1	
Conductance 1	LPC	LSF	LPC	Amp.	69	62	78	51	28	33	20	38	3	5	2	11
Conductance 2	FF	FF	FF		67	58	82		25	25	17		8	17	1	
Gamma	LSF	Amp.	Amp.	FF	71	97	81	76	27	3	10	19	2	0	9	5

4.2.5 Comparison of Sensor-Feature Prediction Performance

The superficial liquid and gas velocity measurement performance of each sensor, and water cut predictions from the capacitance and conductance sensors have been presented. There were varying levels of measurement accuracy achieved by the different information domains of the six sensors. A summary of the forgoing results and analysis has been presented in **Table 4.3** and **Figures 4.37 – 4.39**. The accuracies provided here are the overall measurement accuracies for the multiphase flow conditions at 100 g/l $MgSO_4$ salinity level, at test section 1. As shown in **Figure 4.37**, the fused feature vectors of the absolute pressure achieved the best measurement accuracy on the prediction of the liquid flow rate. The same fusion feature vectors of the differential pressure 1 and conductance 1 sensors follow this lead.

On the gas flow rate measurement results, **Figure 4.38**, the amplitude features of the gamma sensor accomplished the highest measurement accuracy. From the above results it may be concluded that when comparing the six sensors, the fusion and amplitude feature vectors achieve the best flow rate classification accuracy.

Similarly the feature fusion and amplitude vectors of the conductance 2 and gamma sensors achieved the best performance in predicting water cut with measurement accuracies of 82 and 81%, **Figure 4.39**.

For the Gas Void Fraction (GVF) prediction, the back propagation neural network prediction performance was highest with the feature fusion vectors of the gamma signal with 76% of the data points within the target accuracy of ±5%. This was followed by 60% performance, again with feature fusion vectors of the capacitance, and finally only 51% of the conductance signal was predicted within the target accuracy of ±5% with the amplitude vectors, **Figure 4.40**.

This information is important in optimising the network prediction with cross sensor fusion in the following section. The analysis will be useful in the salinity change investigations in chapter 5.

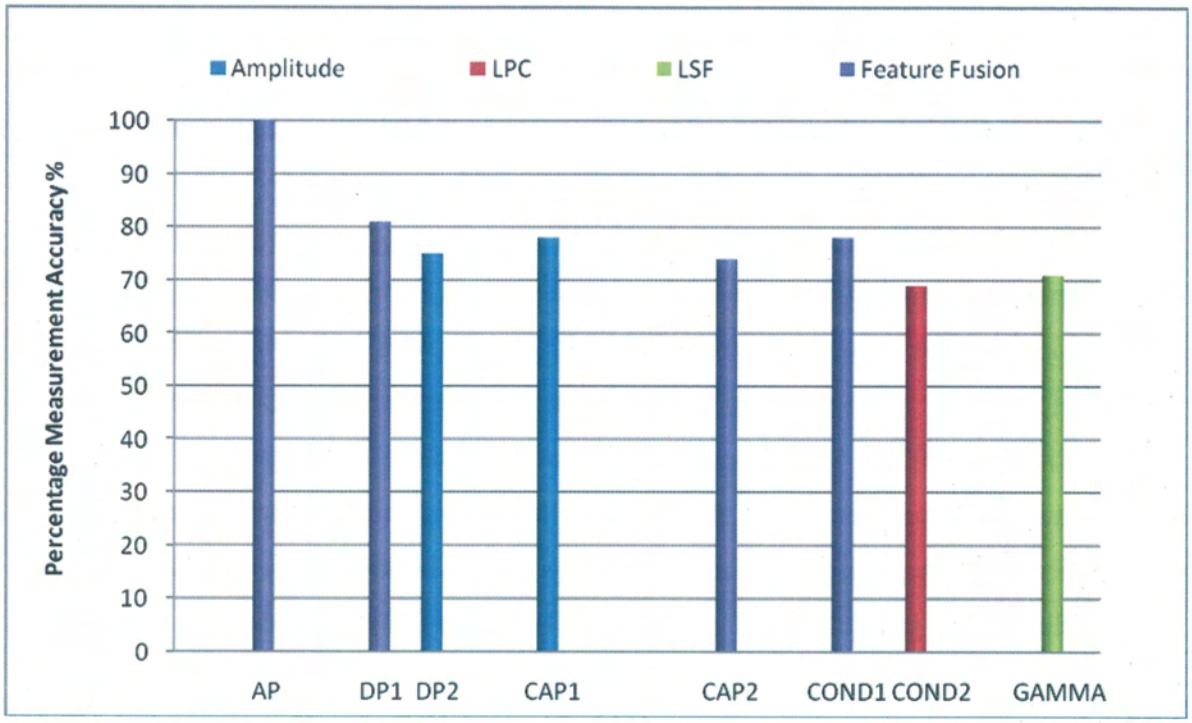

Figure 4.37 Sensor-Feature Performances for Vsl Prediction

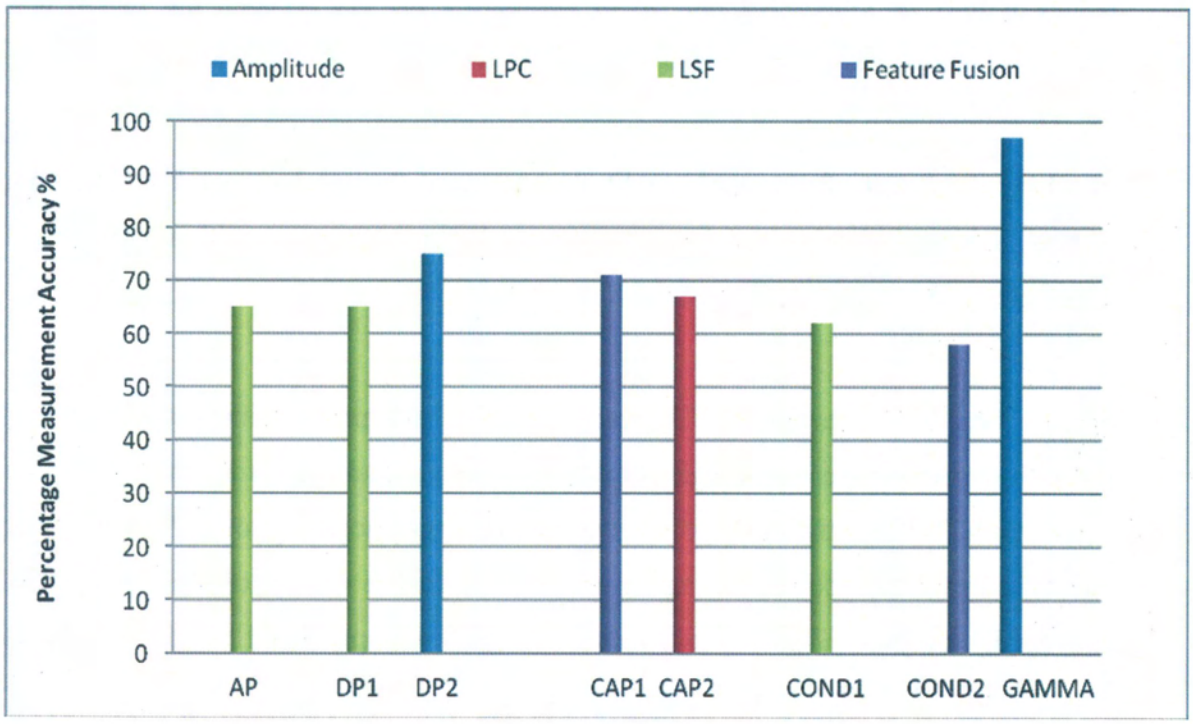

Figure 4.38 Sensor-Feature Performances for Vsg Prediction

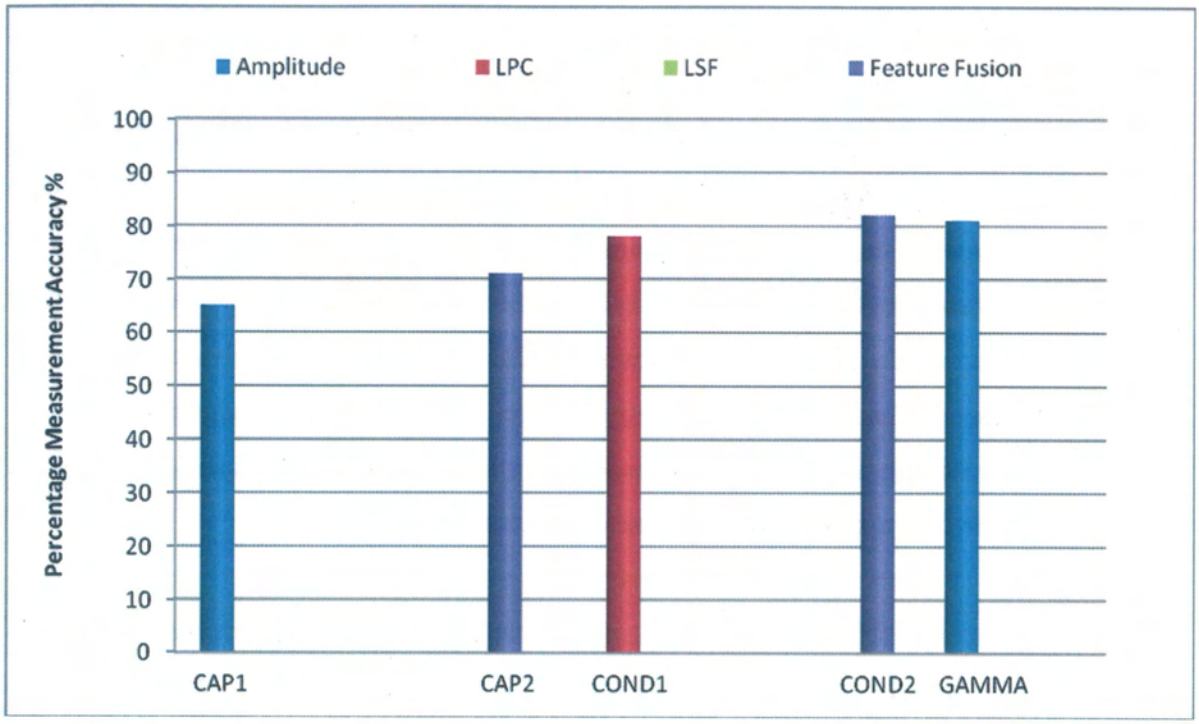

Figure 4.39 Sensor-Feature Performances for WC Prediction

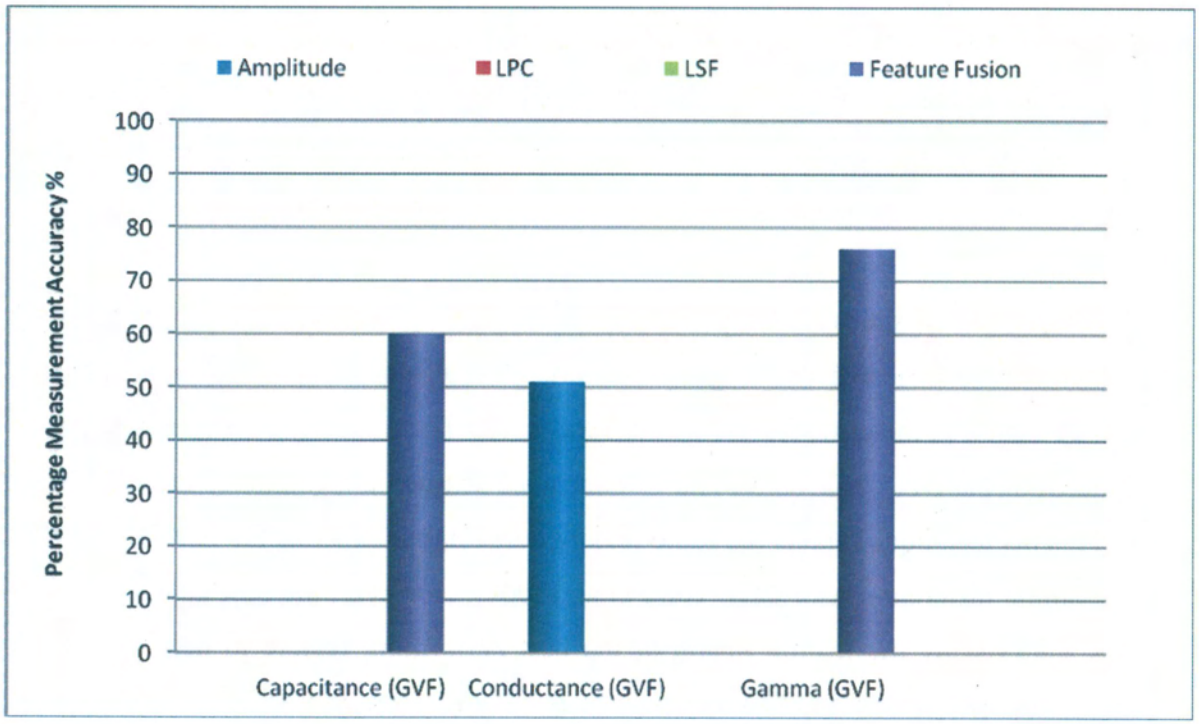

Figure 4.40 Sensor-Feature Performances for GVF Prediction

4.2.6 Multiphase Measurement using Cross-Sensor Data Fusion

From the foregoing results and discussions, it is clear that the neural network model's prediction ability is dependent on the type of feature vector combinations used as well as sensor type. The above results indicated that if the flow information from different sensors is fused together, then there is a potential of achieving greater measurement accuracies in all the test conditions studied. This potential is primarily due to the fact that each sensor has a defined operating range, outside which its accuracy reduces, and by combining and fusing stochastic features from different sensors, the overall accuracy for flow rate measurement may be extended.

There are many different ways that sensor data fusion can be achieved and many of these were tested during initial test screens in the current study. These included extracting the same feature (e.g. AV DP, AV Capacitance and AV Absolute Pressure etc.) from each sensor and fusing them together to form feature vectors to be input to the neural network model. Other trials included extracting different features (e.g. AV DP, LPC Capacitance and LSF Conductance, etc) and constructing a set of input feature vectors. The feature fusion of each feature domain was also tested, whereby the amplitude features from Cap.1, Cond.1 and DP1 sensors were combined to form a total of 18 feature vectors. Similar procedures were also conducted for the linear prediction coefficient (LPC) and the line spectral frequencies (LSF).

A comparison of the network performance when using the above different feature combinations, indicated that a good network generalisation can be achieved when feature fusion of the same feature domain was used. That is to say, fuse the amplitude features of the DP, Capacitance and Conductance sensors, and similarly the LPC and LSF. This technique retains the same feature domain, but expands the feature size by combining different sensor data, Toral et al, (2004). However, the best generalisation was achieved by the feature fusion of the best performing feature to determine the multiphase parameter. **Table 4.4** shows the resultant features chosen in this study for the study of cross-sensor data fusion.

Table 4.4: Cross-Sensor Data Fusion Feature Vectors

Multiphase Parameter	Sensor	Selected Features	Feature Size
Vsl	Absolute Pressure	Feature Fusion	17 x 37
	Differential Pressure 1	Feature Fusion	17 x 37
	Capacitance 1	Amplitude	6 x 37
	Conductance 1	Feature Fusion	17 x 37
	Gamma	LSF	5 x 37
			62 x 37
Vsg	Absolute Pressure	LSF	5 x 37
	Differential Pressure 2	Amplitude	6 x 37
	Capacitance 1	Feature Fusion	17 x 37
	Conductance 1	LSF	5 x 37
	Gamma	Amplitude	6 x 37
			39 x 37
WC	Capacitance 1	Feature Fusion	17 x 37
	Conductance 2	Feature Fusion	17x 37
	Gamma	Amplitude	6 x 37
			40 x 37
GVF	Capacitance 1	Feature Fusion	17 x 37
	Conductance 2	Amplitude	6 x 37
	Gamma	Feature Fusion	17 x 37
			40 x 37

A summary of results from the cross sensor data fusion is given in **Table 4.5**. The results are in terms of percentage accuracy classified by the neural network within ±5 % measurement error.

Table 4.5: Cross-Sensor Data Fusion Measurement Performance

Multiphase Parameter	Percentage Measurement Accuracy
Superficial Liquid Velocity (Vsl) m/s	**100%**
Superficial Gas Velocity (Vsg) m/s	**98%**
Water Cut	**98%**
Gas Void Fraction (GVF)	**95%**

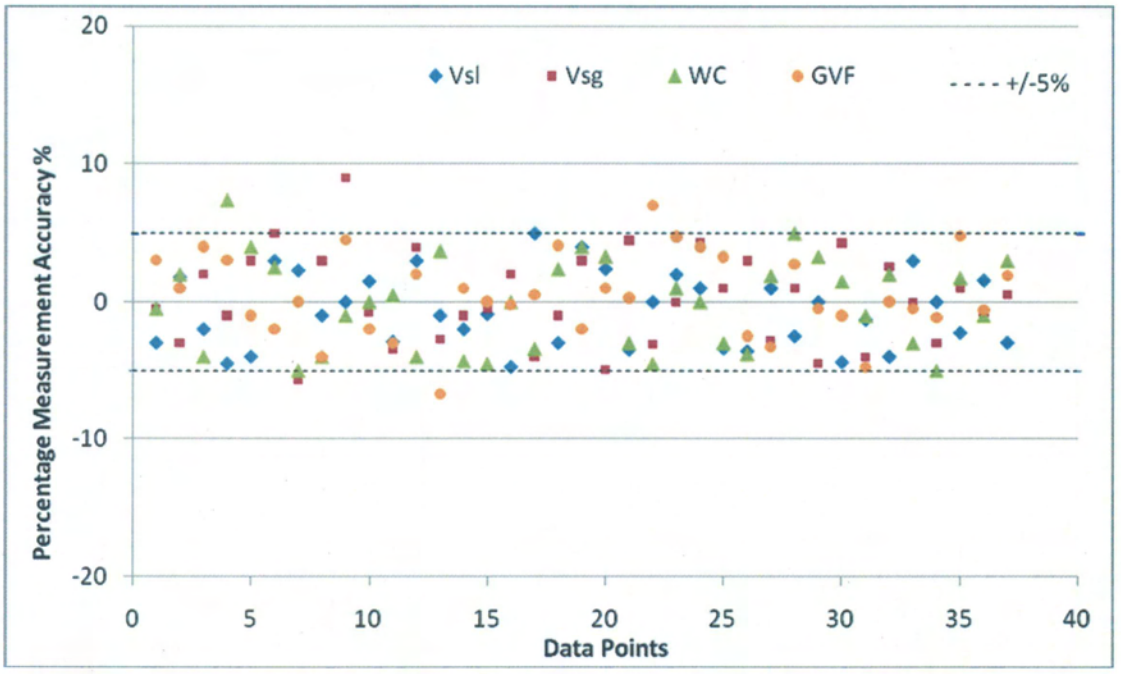

Figure 4.41 Cross-Sensor Data Fusion Measurement Results

4.3 Measurements Performance at Test Location 2

The pattern recognition system that has been developed in this research study is based on data collected at test location 1, as shown on the NEL schematic (**Fig. 3.9, Section 3.3**), with the 100g/l $MgSO_4$ Solution. It is expected that there will be a difference in operating pressure between the two test locations as a result of a pressure drop along the flow line. **Figures 4.42 and 4.43** show a plot of the Absolute Pressure against Superficial Gas Velocity for the various Superficial Liquid Velocities; the Absolute Pressure is shown to increase with the Superficial Liquid Velocity. The maximum pressure at the two test sections are indicated on the plots; further analysis revealed an average pressure drop of 0.5 bars across all the test points in section 1, relative to test section 2. The effect of change in operating pressure on the pattern recognition developed will be investigated below.

For the purpose of this study, 30 data points have been singled out for comparison purposes. **Figure 4.44** shows the data points that were selected from test sections 2, on the Vsl vs. Vsg plot.

In evaluating the network performance with test location changes, three scenarios were considered.

- The first scenario is to train the network with the data at test location 1, while testing its generalisation performance with data at test location 2.

- The second scenario is to train the network with data combined from both test sections 1 and 2, while testing its generalisation performance with data at test section 2.

- The third scenario is to train the network with data gathered at test location 2, and evaluate its generalisation performance with data from the same test location i.e. test location 2.

Figures 4.45a-c show the relative measurement errors obtained with the above three scenarios. It is evident from these plots that the network results are subject to significant errors in scenarios 1 and 2, but have slightly better results in scenario 2 than 1 (**Figures 4.45a and 4.45b**), obviously due to the presence of data from the same test section. However, with scenario 3, the network performance is seen to improve, achieving results close to those obtained from the best generalisation in test section 1. i.e. the feature fusion of the best performing features (Section 4.2.6). It is presumed that the performance achieved in scenario 3 is not the same or even better than the results from test location 1 as a result of far less available data points from the test location, thus reducing the training to test ratio.

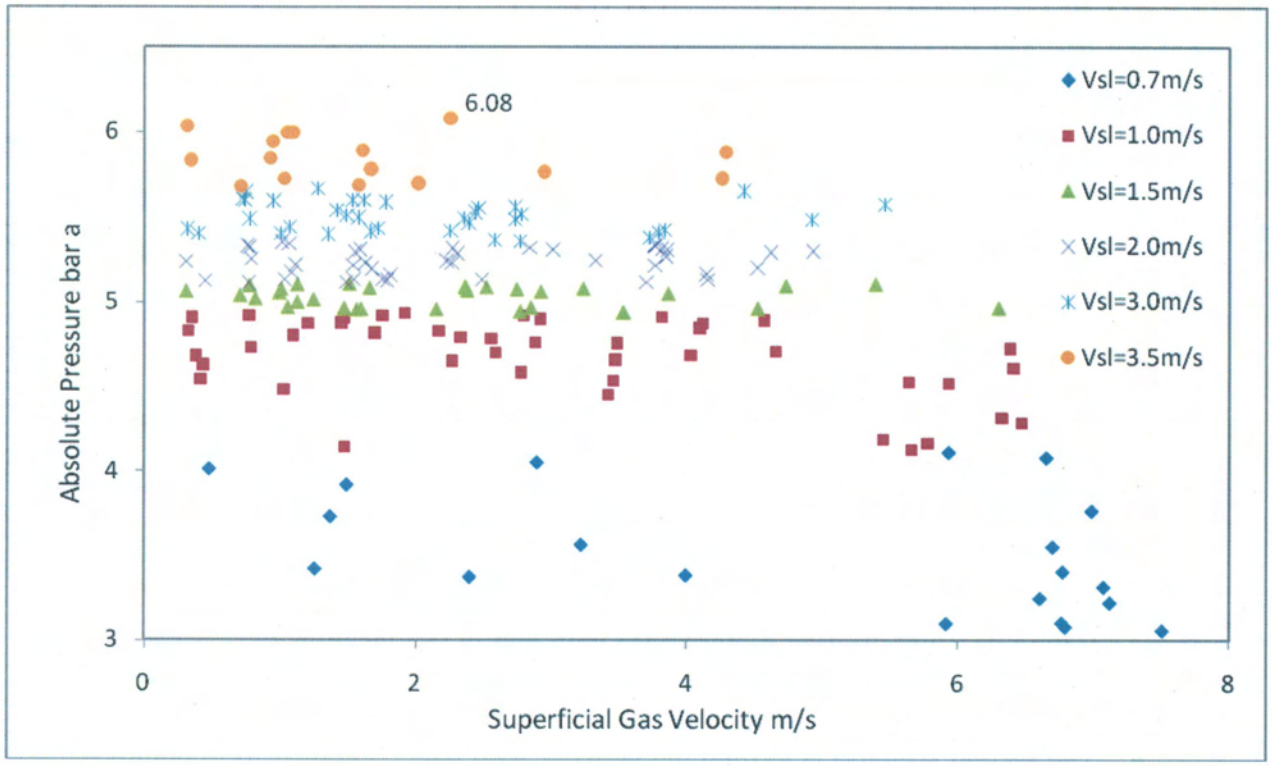

Figure 4.42 Plot of Absolute Pressure vs. Superficial Gas Velocity – Test Section 1

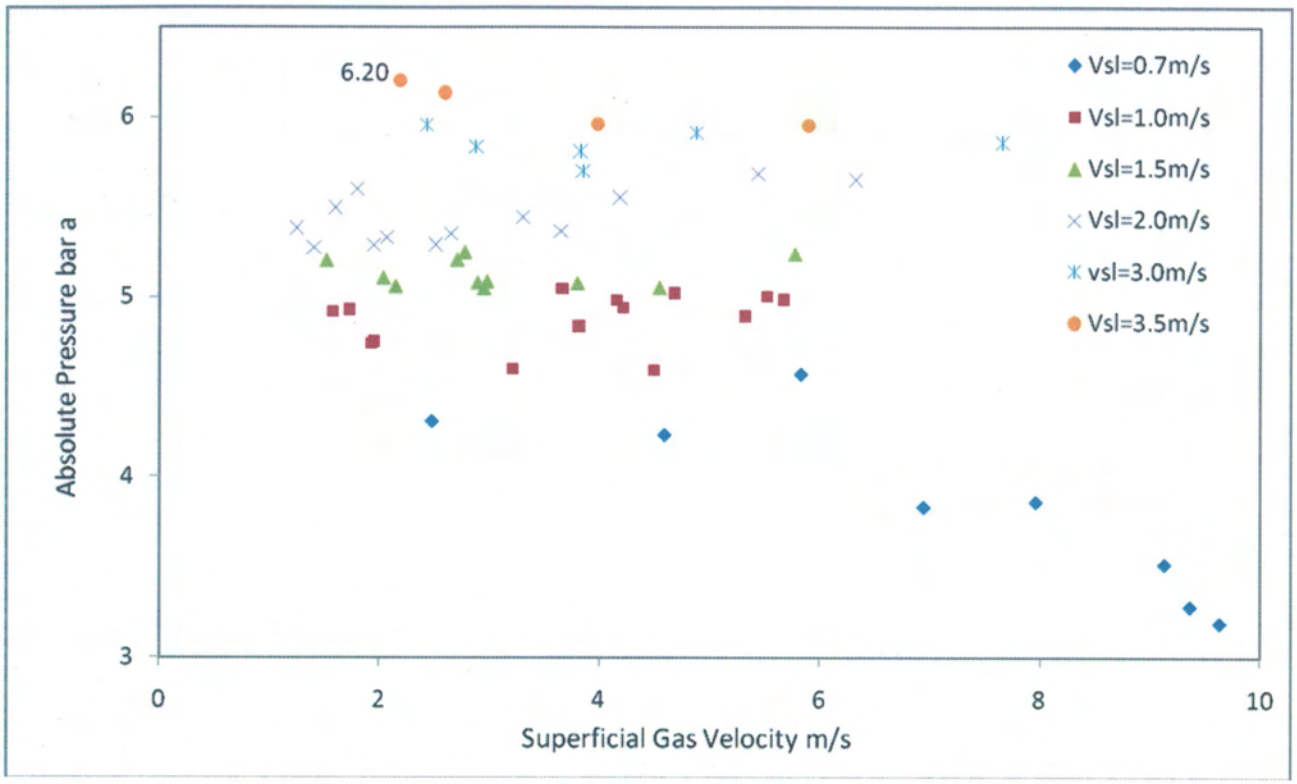

Figure 4.43 Plot of Absolute Pressure vs. Superficial Gas Velocity – Test Section 2

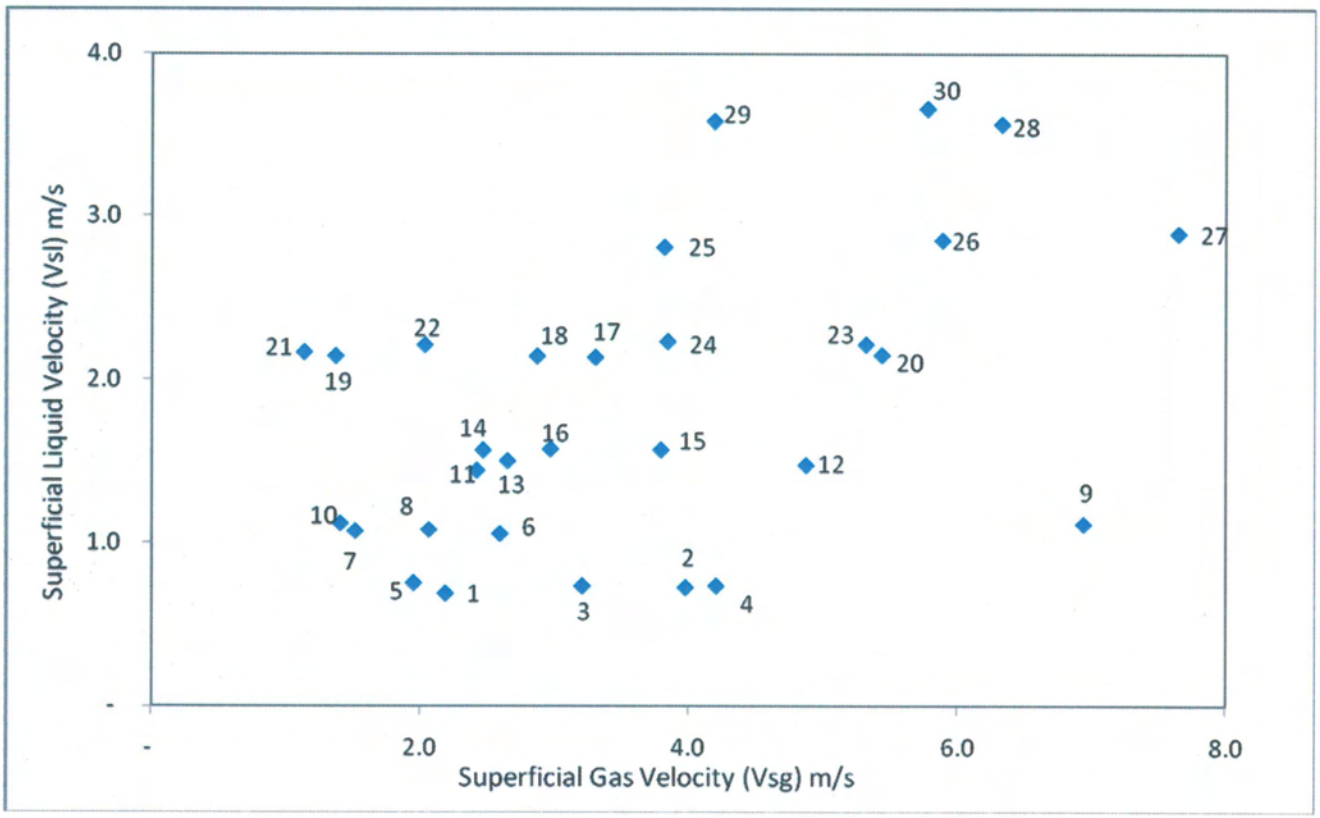

Figure 4.44 Test Data Matrix – Test Section 2

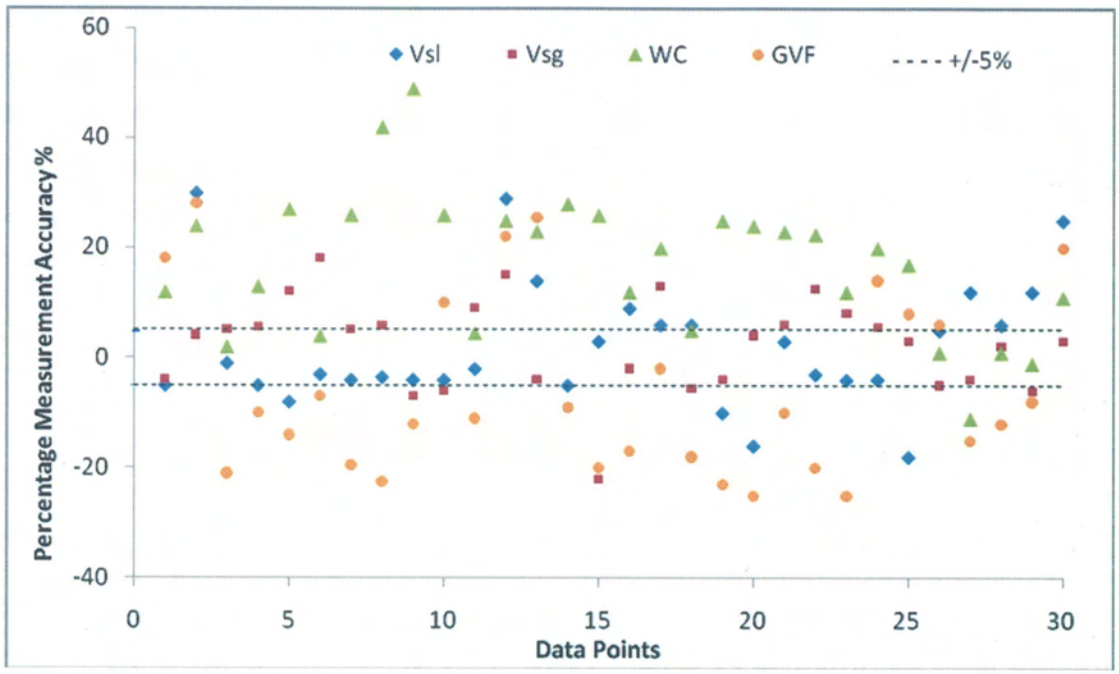

Figure 4.45 (a) Scenario 1 Measurement Results

Figure 4.45 (b) Scenario 2 Measurement Results

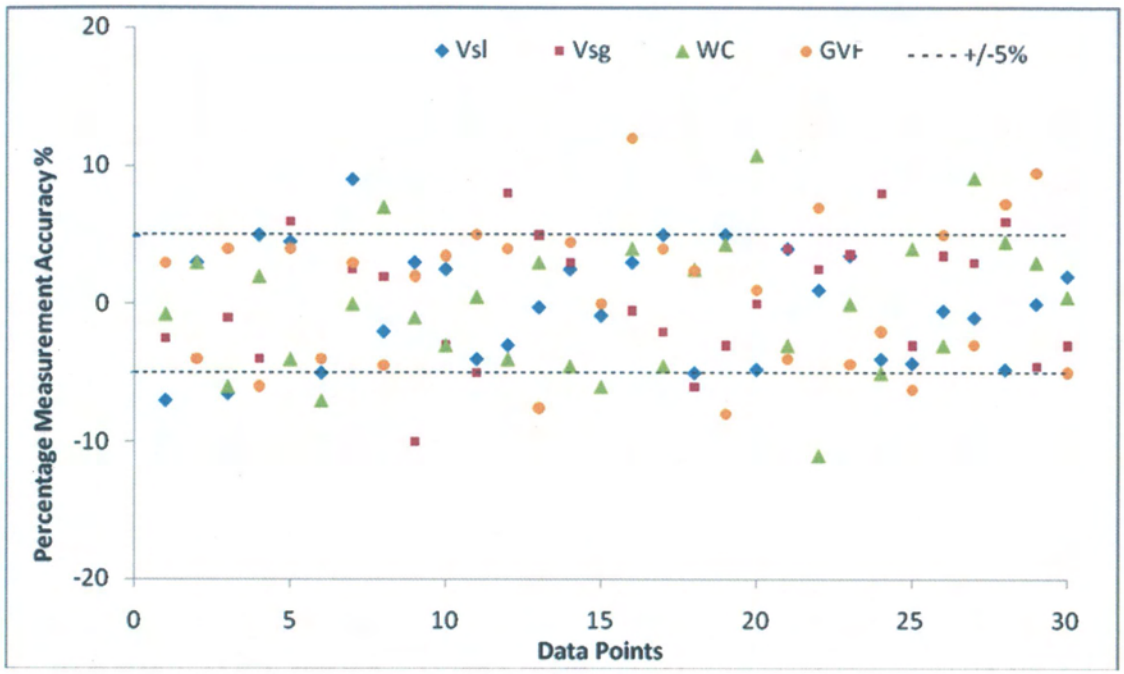

Figure 4.45 (c) Scenario 3 Measurement Results

Table 4.6: Test Section 2 Measurements Performance

Multiphase Parameter	Percentage Measurement Accuracy
Superficial Liquid Velocity (Vsl) m/s	90%
Superficial Gas Velocity (Vsg) m/s	80%
Water Cut	77%
Gas Void Fraction (GVF)	73%

CHAPTER 5

SALINITY EFFECTS ON MULTIPHASE FLOW MEASUREMENTS

The presence of salt in multiphase fluid causes the water phase of the fluid to become more conductive; this conductivity affects the dielectric constant, resistivity and capacitance of the fluid measurements. The conductivity of water increases due to the formation of more polar substances, which causes the increase in the dielectric constant of the mixture and with this increase, multiphase flow parameter measurements are likely to read higher than actual conditions. Increased salinity also increases the mass of the mixture, and as a result, the specific gravity of the mixture increases which implies an increase in the density of water, resulting in a corresponding increase in the dielectric constant of the mixture, Scheers and Slijkerman (1996), Johansen and Jackson (2000).

Due to the high solubility of salt in water, the direct impact of salinity on multiphase flow measurement is on the water cut measurement. Produced fluids having a low water cut consist of a stream of oil with water droplets suspended in it; this is called an oil continuous flow. Produced fluids having a high water cut consist of a stream of water with oil droplets suspended in it; this is called a water continuous flow. Whether the flow is water continuous or oil continuous matters when the effect of salinity is considered.

Another complicating factor is that it is quite possible to have a well producing fluid that has an erratic water cut. The overall bulk conductivity of the fluid increases as the proportion of conductive water in the fluid increases. This, coupled with the fluid changing back and forth from oil continuous to water continuous, as well as the underlying salinity of the water phase of the fluid changing, gives rise to a very challenging measurement environment in which the water cut and bulk conductivity of the fluid can change dramatically and unpredictably.

The performance of multiphase measuring instruments is affected by this major, naturally occurring condition, as indicated in **Figures 5.1 – 5.3**. This study was conducted with two levels of salinity (50 and 100 g/l $MgSO_4$).

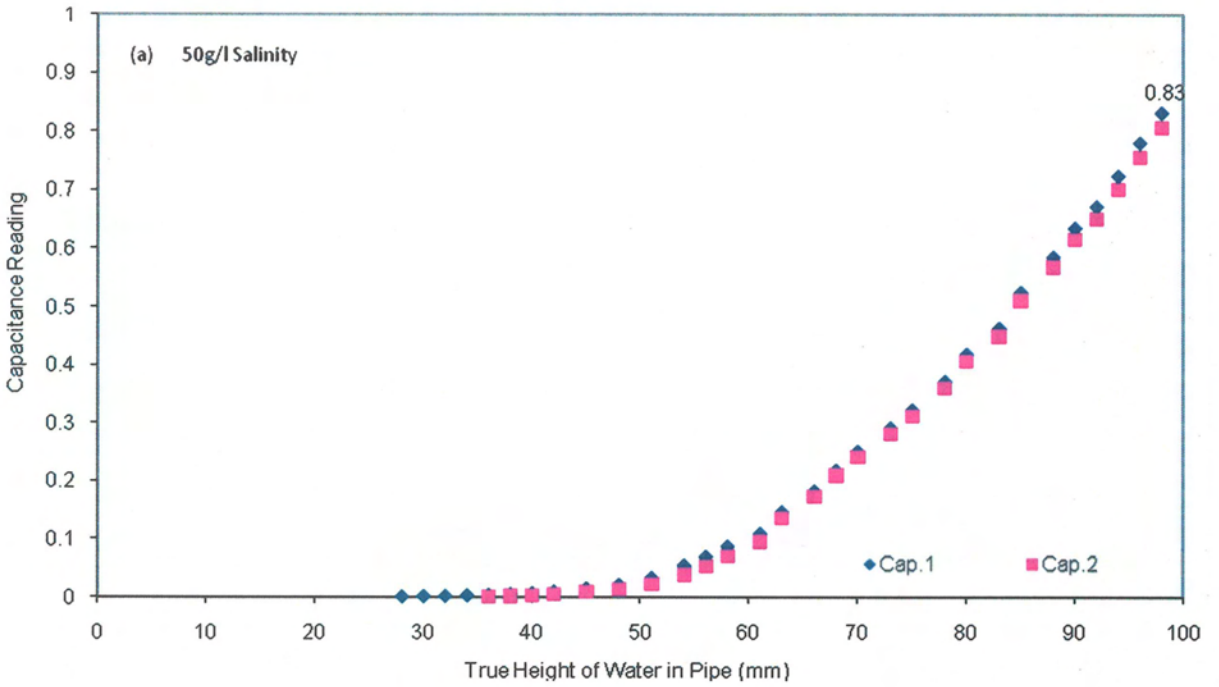

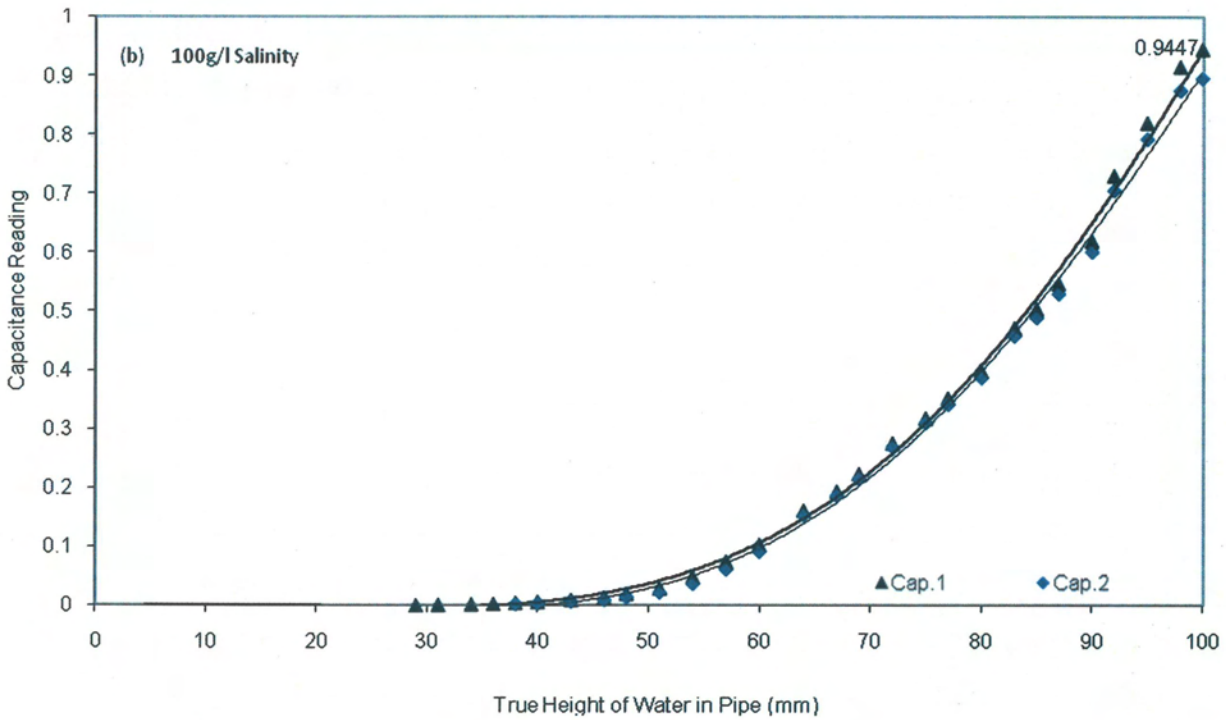

Figures 5.1a and b Capacitance Reading vs True Height of Water in Pipe (a) 50 g/l Salinity, (b) 100 g/l Salinity

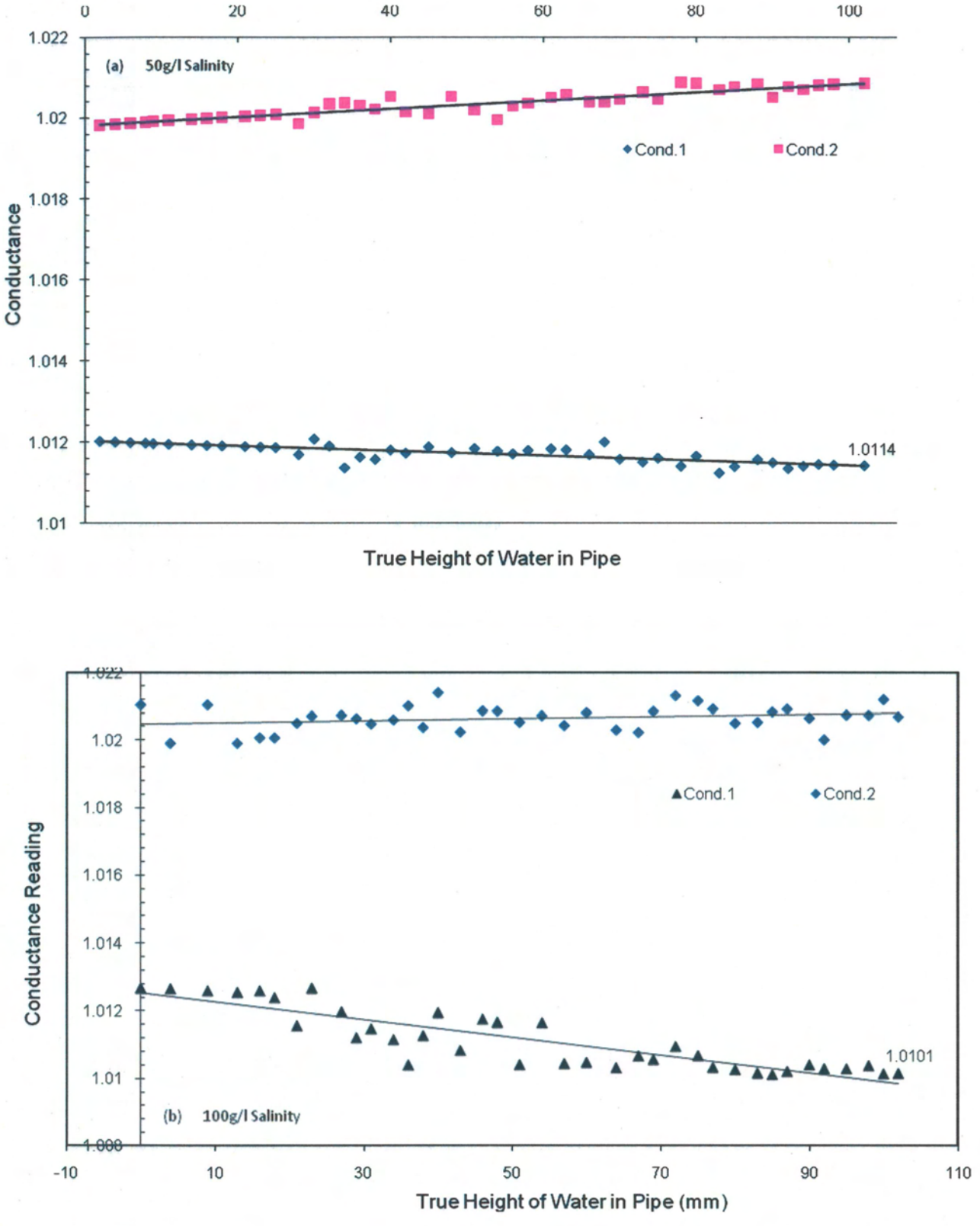

Figures 5.2a and b Conductance Reading vs True Height of Water in Pipe (a) 50 g/l Salinity, (b) 100 g/l Salinity

Figure 5.3 Average Gamma Count vs. Water Cut for 50, and 100 g/l Salinity

5.1 Identification of Salinity Change

A useful application of neural networks is their ability to classify data. Self-organising maps can examine a series of data points and group them according to some underlying characteristic property. These networks are particularly useful in multiphase flow measurements where complex high dimensional data need to be presented in an understandable format.

Change in salinity was analysed by coupling a multilevel hierarchical neural network, shown in **Figure 5.4**. The data points are classified according to the two salinity levels using a Kohonen self-organising feature map (KSOFM) (review of KSOFMs was presented in **Chapter 2.4.4**.) and the identification of the phase flow parameters is achieved through the employment of a second layer of the Back Propagation Neural Network (BPNN): one each for the two salinity levels, i.e. 50 g/l solution is referred to as Salinity 1 (S1), while the 100 g/l solution is Salinity 2 (S2).

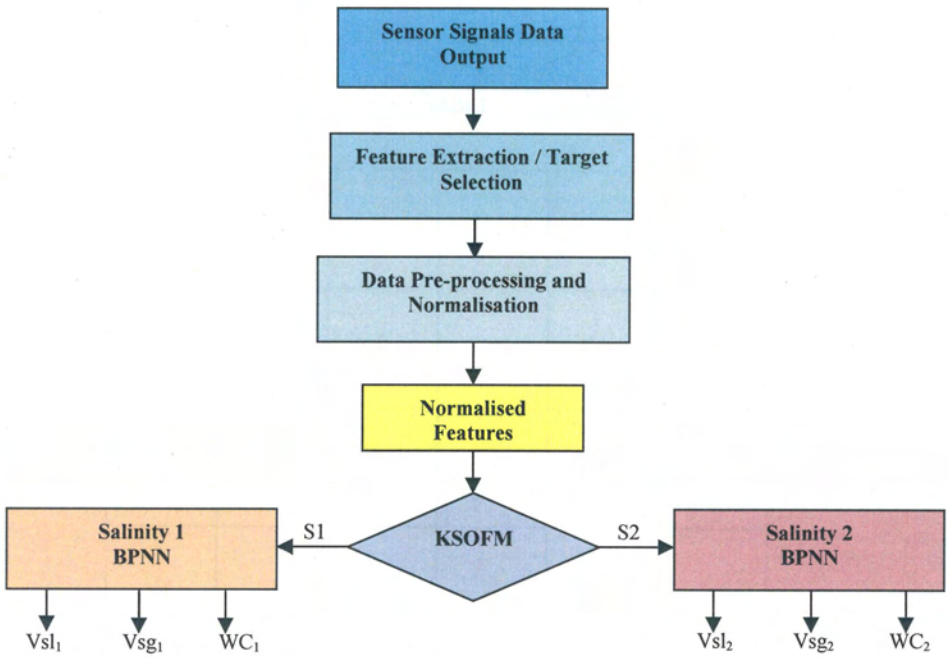

Figure 5.4 – Salinity Dependent Pattern Recognition Model

If the correlations between the extracted feature inputs and the target outputs are indeed salinity dependent then reduced error magnitudes should be observed for the output parameters trained with data from the same salinity level, in comparison to those obtained using training data from a different salinity level.

5.1.1 Salinity Classification Model

The combined signal features were utilised to classify the data points, based on salinity. Each input data point to the KSOFM comprised the signal's feature vectors comprising Amplitude, LPC, and LSF features of the capacitance, conductance and gamma sensors. The data points were labeled with their associated salinity levels (S1 for 50 g/l and S2 for 100 g/l solutions respectively).

An empirical approach was adopted to determine the optimal magnitude for the output grid. Several grid configurations were analysed. It was found that too large a grid resulted in the creation of redundant nodes, whereas, too small a grid yielded overlapping flow patterns. It was established that a 6 × 5 grid was best suited for the data set.

The KSOFM learning algorithm was applied, and the node topology shown in Figure 5.5 was obtained.

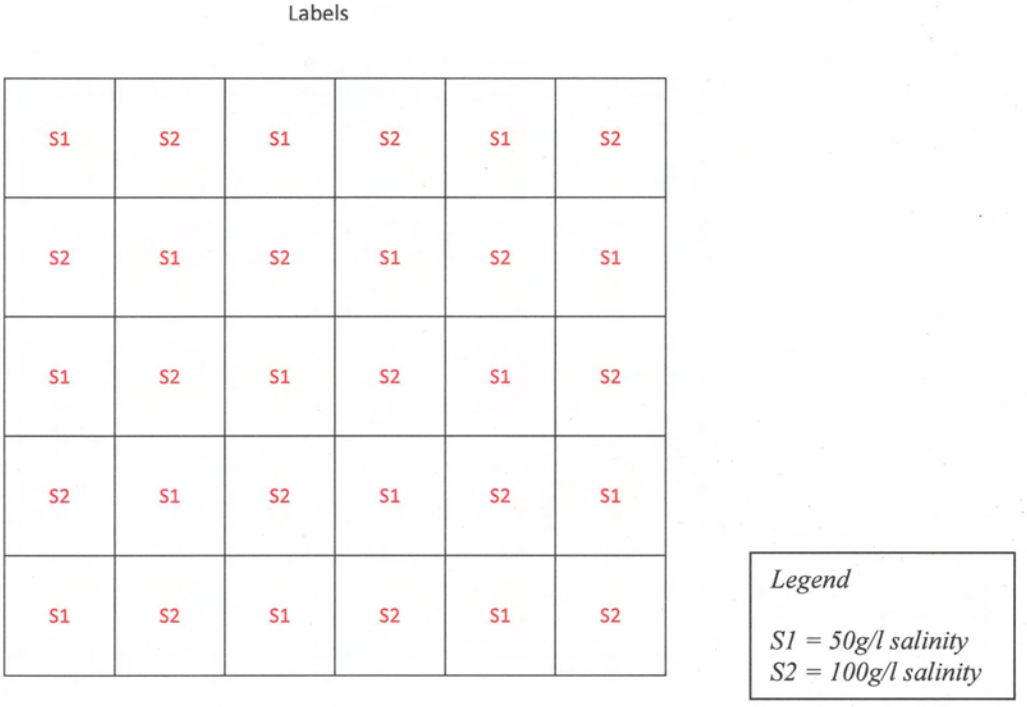

Figure 5.5 – Salinity Identification by KSOFM

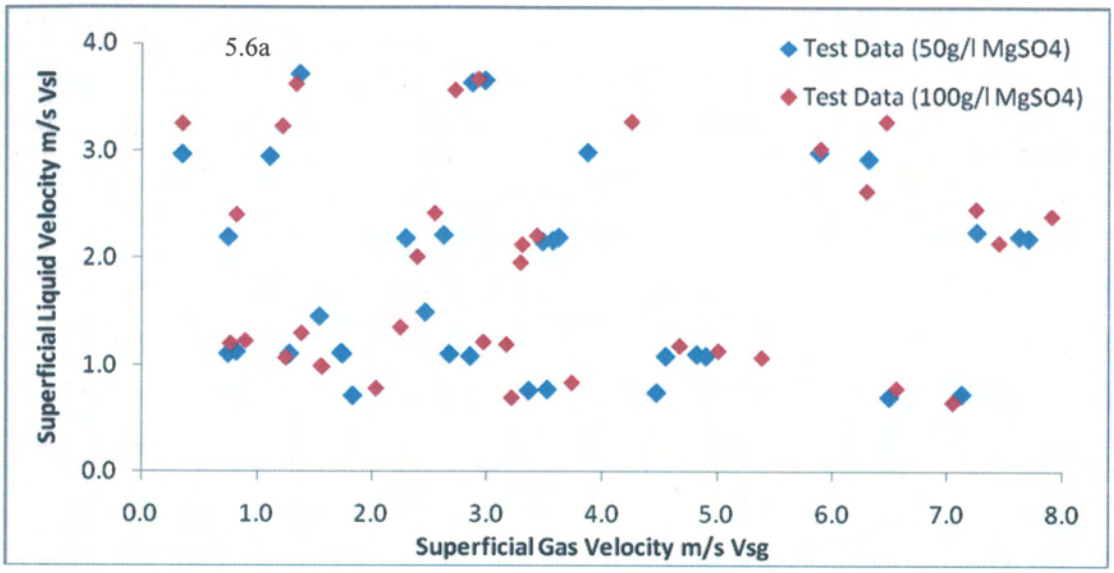

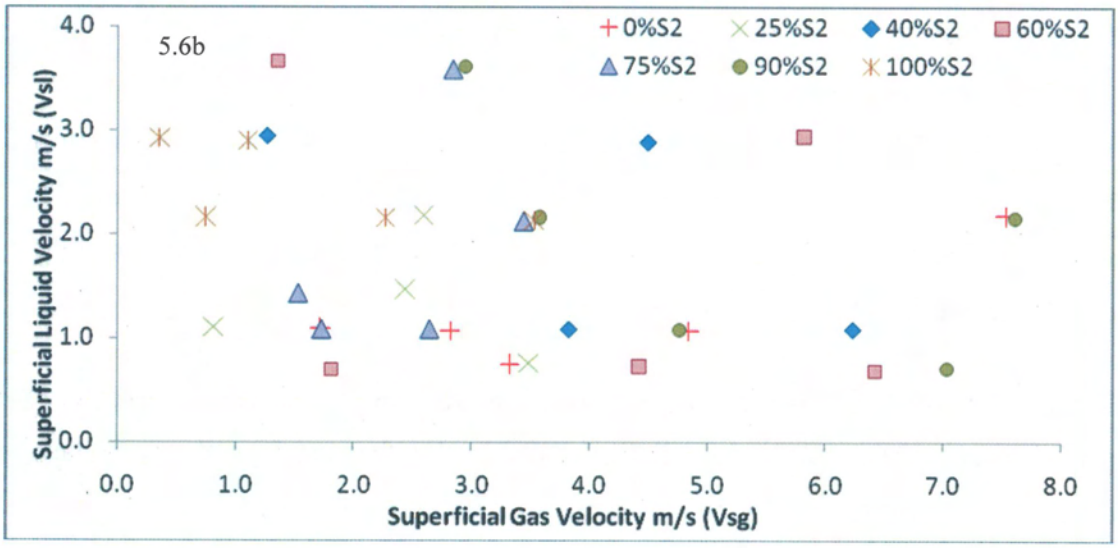

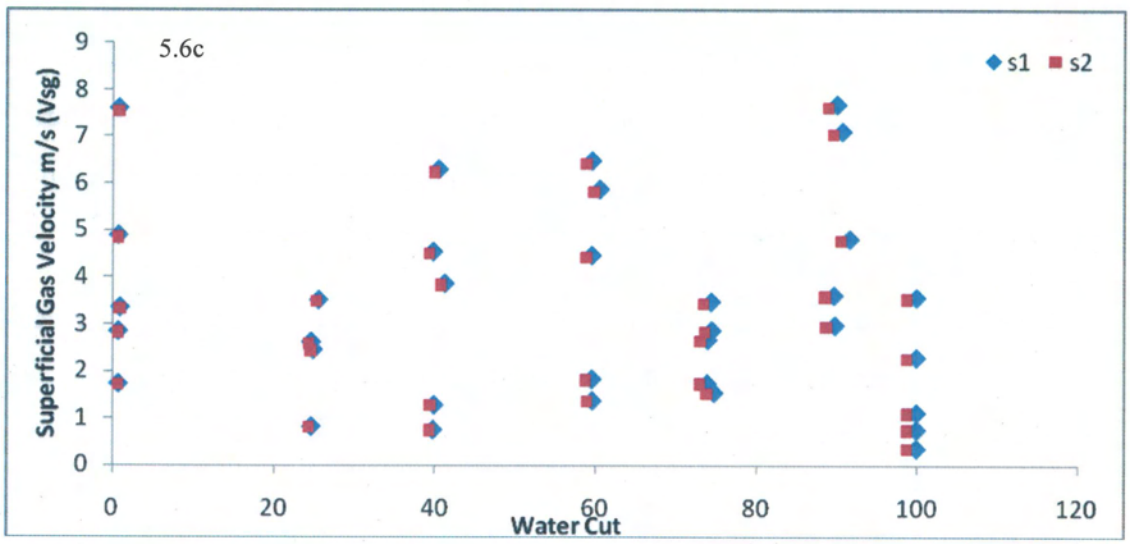

Figures 5.6 a-c – Plots of Test Data Points used for Salinity dependence investigations

The KSOFM was able to locate different underlying patterns in the input vectors and the topological arrangement of the output grid relates well to the salinity level classification undertaken with the formation of two distinct salinity levels on the output grid: S1 for the 50g/l and S2 for the 100g/l solutions.

After training the neural network on one set of training data, the predictions of data points for both salinity levels could be compared and contrasted. It was hypothesised that if the relationship between the input features and output variable is salinity dependent, good prediction performance would be seen for test points that share a common salinity with the training data, whilst poor performance would be witnessed for test points of the unseen salinity.

5.1.2 Salinity 2 (S2) Back Propagation Neural Network (BPNN)

The salinity 2 BPNN was trained on the 100 g/l salinity training data. Based on the results obtained from extensive preliminary repeatability tests, the architecture of the salinity 2 BPNN was defined to be [n – 8 – 3]. All other parameters were as per the original single BPNN model used in chapter 4.

Table 5.1 (page 178), contains a summary of the flow rates and water cut prediction performance, obtained from the salinity 2 BPNN using features from the capacitance, conductance, gamma sensors, as well as fused features from all the sensor signals.

5.1.2.1 Liquid Superficial Velocity

Figures 5.7 and **5.8** display the liquid superficial velocity measurement results obtained from the salinity 2 BPNN using a range of different input signal features. **Figure 5.7** illustrates the network performance for the salinity 2 test points; while **Figure 5.8** depicts the prediction results for the salinity 1 test points.

Figure 5.7 shows the best predictions from the salinity 2 test point's liquid superficial velocities were predicted within the specified target accuracy of ±5% using the following four combinations:

- Capacitance – Feature Fusion 96%
- Conductance – Feature Fusion 86%
- Gamma – LSF 78%
- All Signals Fusion – Feature Fusion 100%

Figure 5.8 illustrates the comparatively poor measurements predictions exhibited for the salinity 1 test points. The network had been trained to classify input features according to the function derived in a learning process conducted entirely with salinity 2 data points and predicted the salinity 1 data points according to this function. This comparatively poor performance illustrates the salinity dependence of the relationship between the extracted features and the target outputs.

Figure 5.9(a) displays the errors associated with each of the test data points for the neural network predictions conducted employing feature fusion of all sensors as the input features. The data points exhibiting errors in excess of ±5 are labelled. One can observe the relationship between the measurement error and the water cut (WC): as the test point WC increases, the fluid's bulk conductivity increases and the larger the probability and magnitude of the error in the liquid's superficial velocity prediction. A significant majority of all liquid velocity measurements at WCs greater than 60% were under-predicted with respect to their target.

The locations of the outlying test data points classified outside the target accuracy are shown on the test matrix, **Figure 5.9(b)**.

5.1.2.2 Gas Superficial Velocity

Figures 5.10 and **5.11** depict the gas superficial velocity measurements prediction results obtained from the salinity 2 BPNN for the S2 and S1 test data points respectively.

Figure 5.10 illustrates that gas velocity salinity 2 prediction accuracies were not as high as those obtained for the liquid phase measurement. This observation agrees with what was witnessed for the single-BPNN System evaluated previously in chapter 4, where gas phase measurements were observed to be less accurate than the liquid phase parameter determination. The best prediction results were obtained from the feature fusion, which proved to be the strongest input feature group. Optimal classification of the gas superficial velocities was obtained exploiting the amplitude feature of the gamma signal: 85% of salinity 2 test points were predicted within ±5%.

Figure 5.11 shows the prediction results for the salinity 1 data points. Again, salinity 1 classification by the salinity 2-trained network was considerably poorer than the

salinity test results reinforcing the hypothesis that input feature/output correlations are a strong function of salinity.

Significant errors were obtained across the WC range for both salinity 2 and salinity 1 test points. There is a definite increase in error magnitude with increasing WC but this increase was much less pronounced than that observed for the liquid velocity measurements.

As the raw sensor signals are dominated by the passage of slugs, features extracted from the signals will encode mainly data from the passage of slug elements. Features representative of the gas phase properties are likely to exhibit smaller variations that are drowned out by the more dominant liquid structure induced signal features.

5.1.2.3 Water Cut

Figures 5.12 and **5.13** display the water cut measurements observed employing the salinity 2 network for the salinity 2 and salinity 1 test points respectively.

Figure 5.12 indicates that the conductance signal feature fusion and the amplitude features provided the strongest performances. By employing the feature fusion features extracted from the conductance signal, 95% of the salinity 2 test data points were successfully resolved within the ±5% target accuracy.

Figure 5.13 illustrates that the salinity 1 test data points were not well predicted using the function derived from the salinity 2 network training, demonstrating the salinity dependent nature of the water cut parameter correlation. This trend was seen for all three output variables suggesting that the superficial phase velocities and the water cut have a strong salinity specific relationship with the statistical features extracted from the raw signals.

There was also an increasing frequency and magnitude of error with increasing tests point for WC outside the target error specification of ±5%. The recurrence of this phenomenon reinforces the salinity sensitivity of the nonlinear regression modelled by the network. Nevertheless, significant errors in the salinity 2 test data points were also attained across the whole WC range of salinity 2.

It is hypothesised that the prediction of all data points into just two salinity levels may be an over-simplification of the system and may not facilitate accurate representation

of underlying relationships owing to the presence of more than two characteristic input features – output interactions in production situations – as variations in water salinity in oil and gas producing fields are shown to be much more complex in terms of the ions and concentration levels.

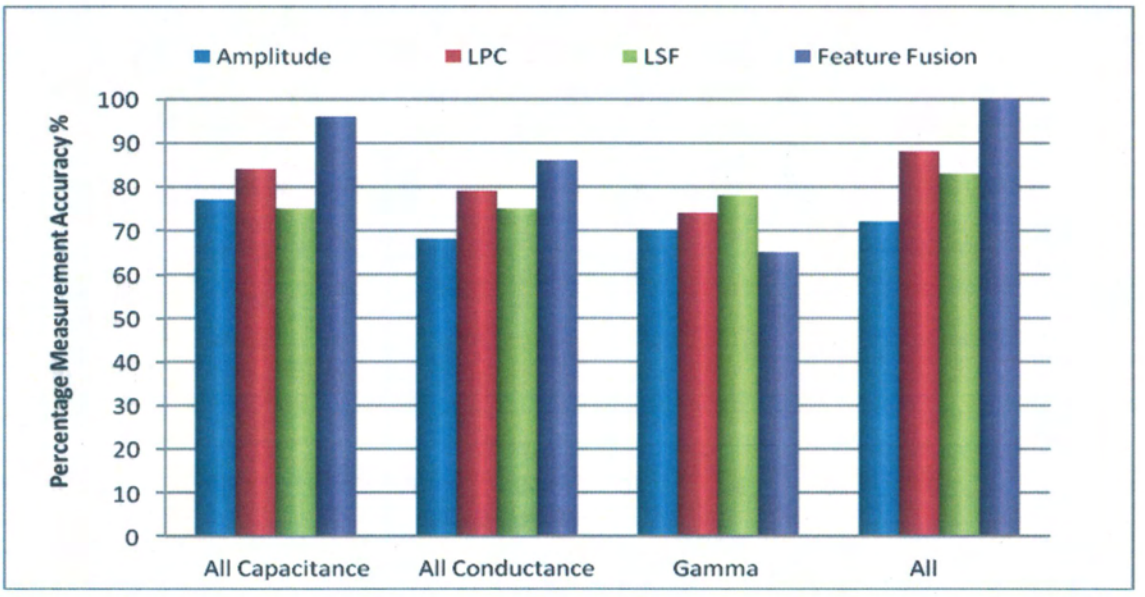

Figure 5.7 – Salinity 2 BPNN: Percentage Measurement Accuracy for the Superficial Liquid Velocity of Salinity 2 Test Points

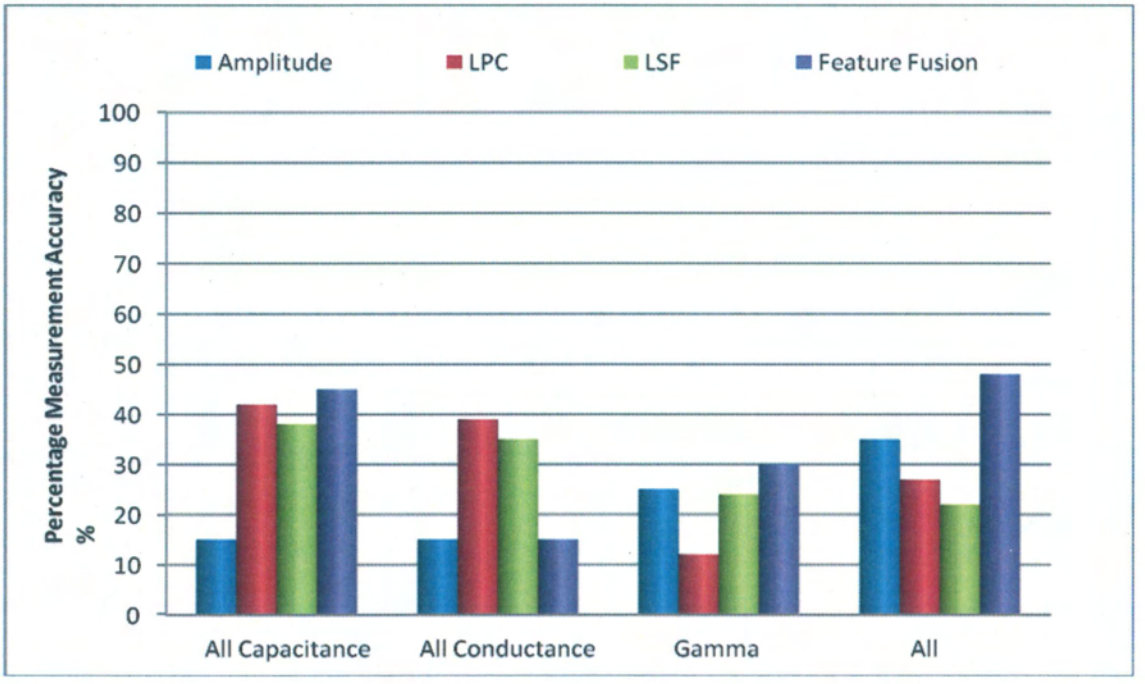

Figure 5.8 – Salinity 2 BPNN: Percentage Measurement Accuracy for the Superficial Liquid Velocity of Salinity 1 Test Points

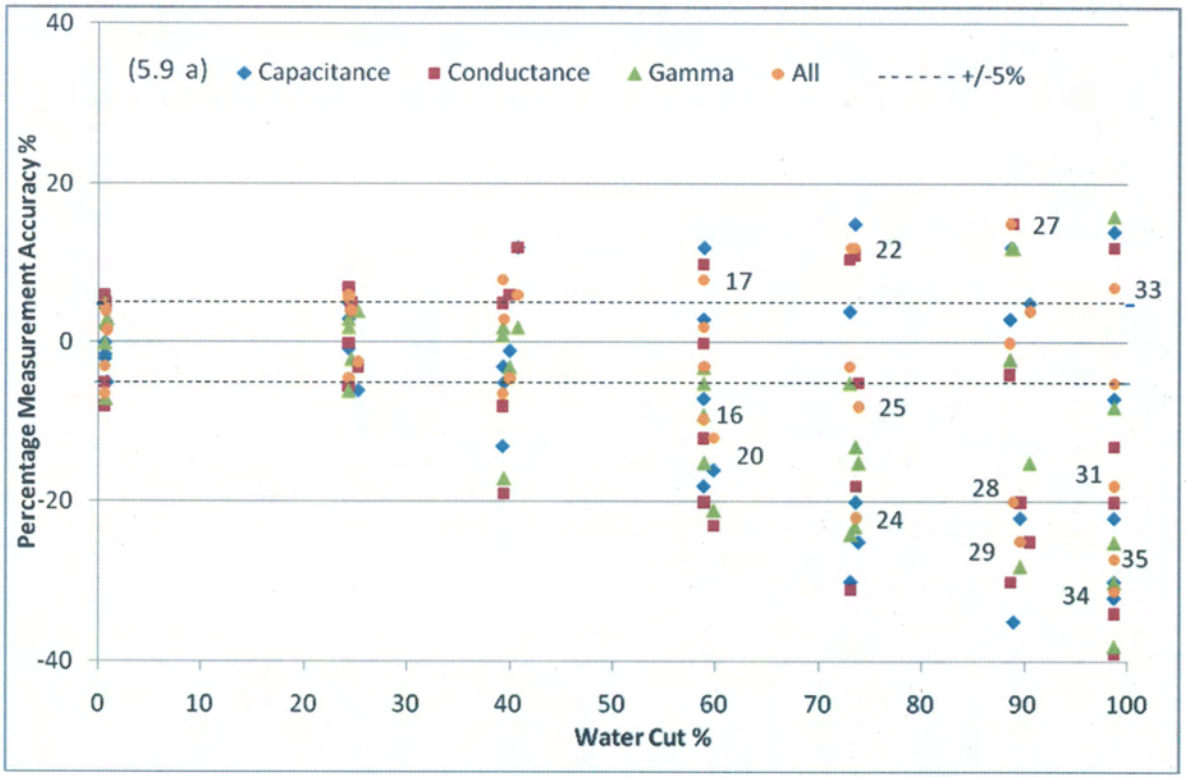

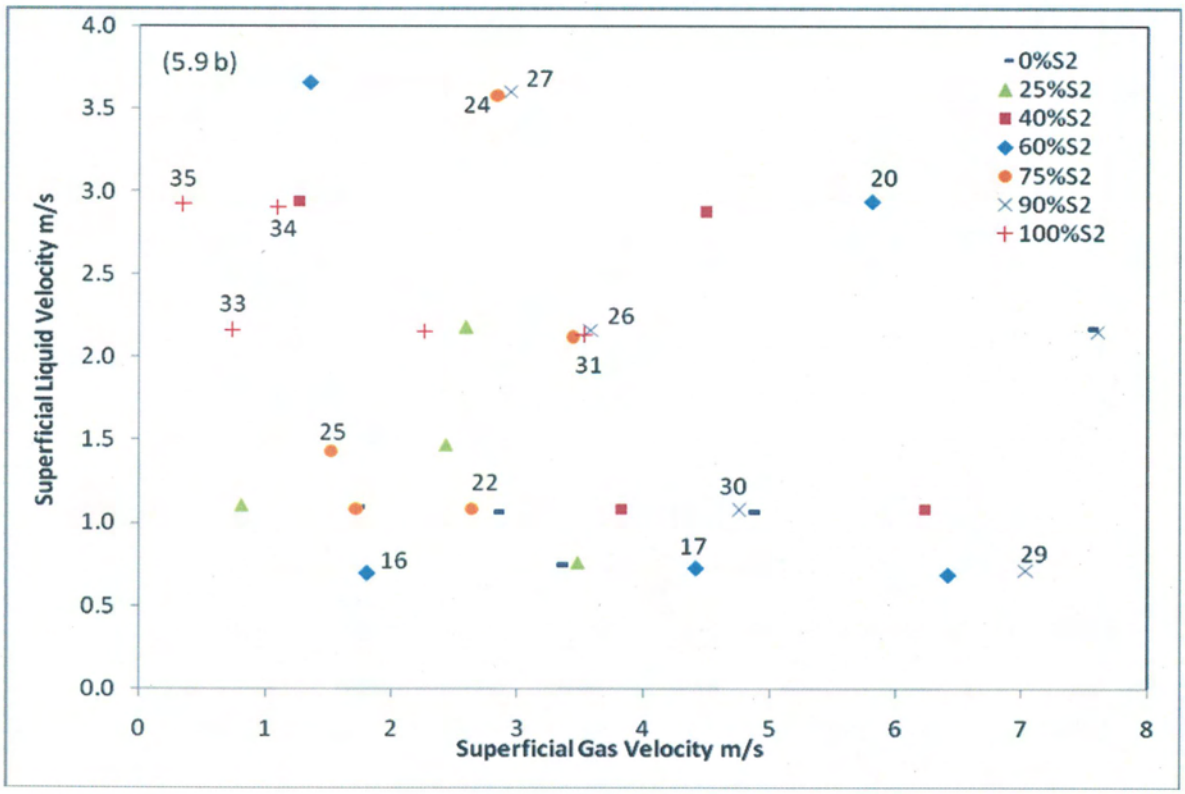

Figures 5.9 (a) and (b) – Salinity 2 BPNN: Percentage Liquid Error Distribution for Feature Fusion of All Sensors (a) Water Cut Plot (b) Outlying Test Point Matrix Location

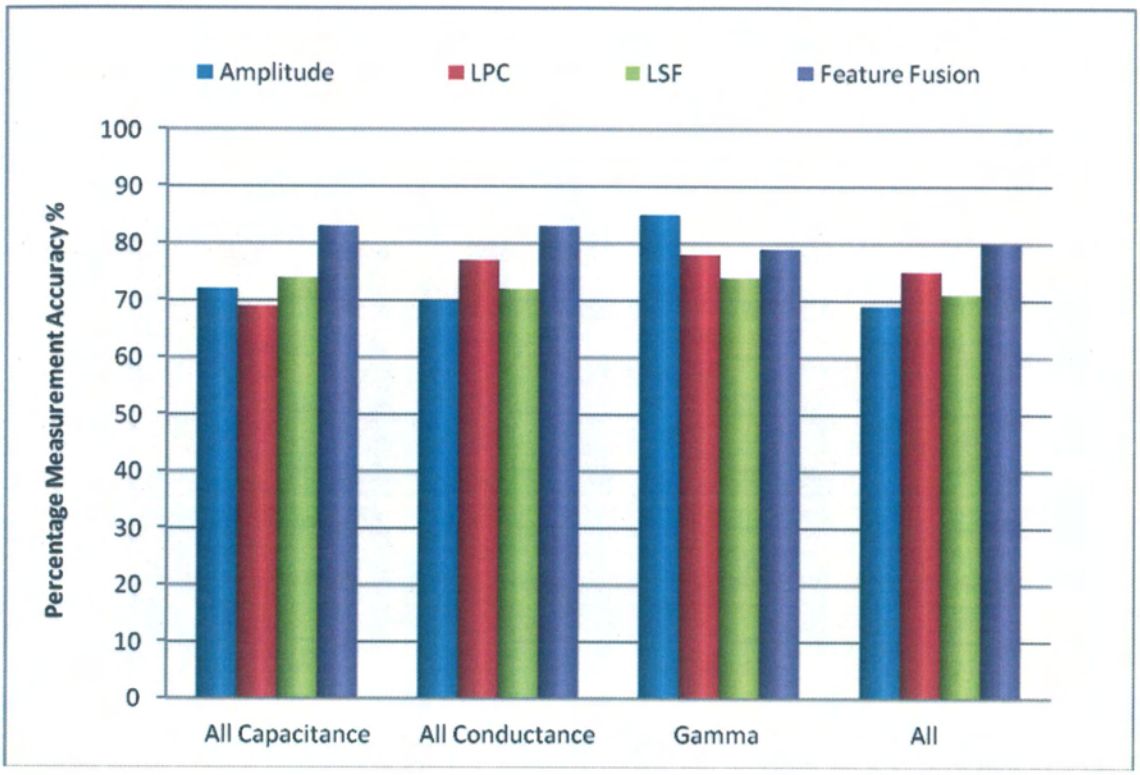

Figure 5.10 – Salinity 2 BPNN: Percentage Measurement Accuracy for the Superficial Gas Velocity of Salinity 2 Test Points

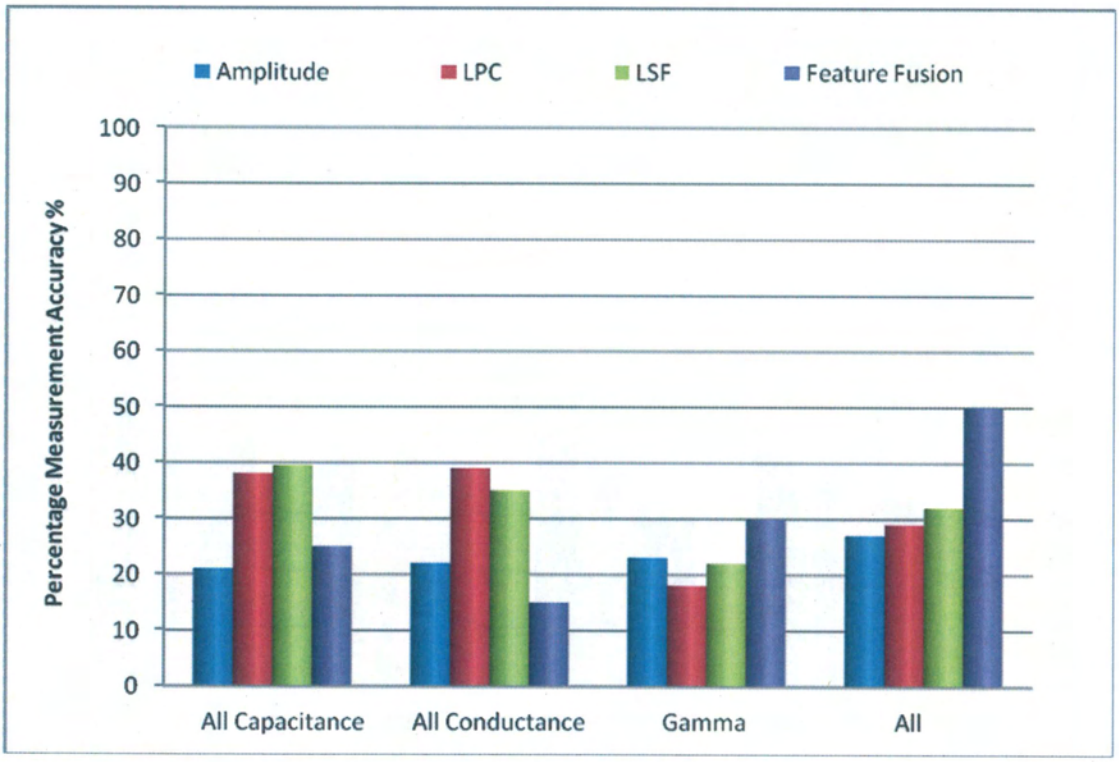

Figure 5.11 – Salinity 2 BPNN: Percentage Measurement Accuracy for the Superficial Gas Velocity of Salinity 1 Test Points

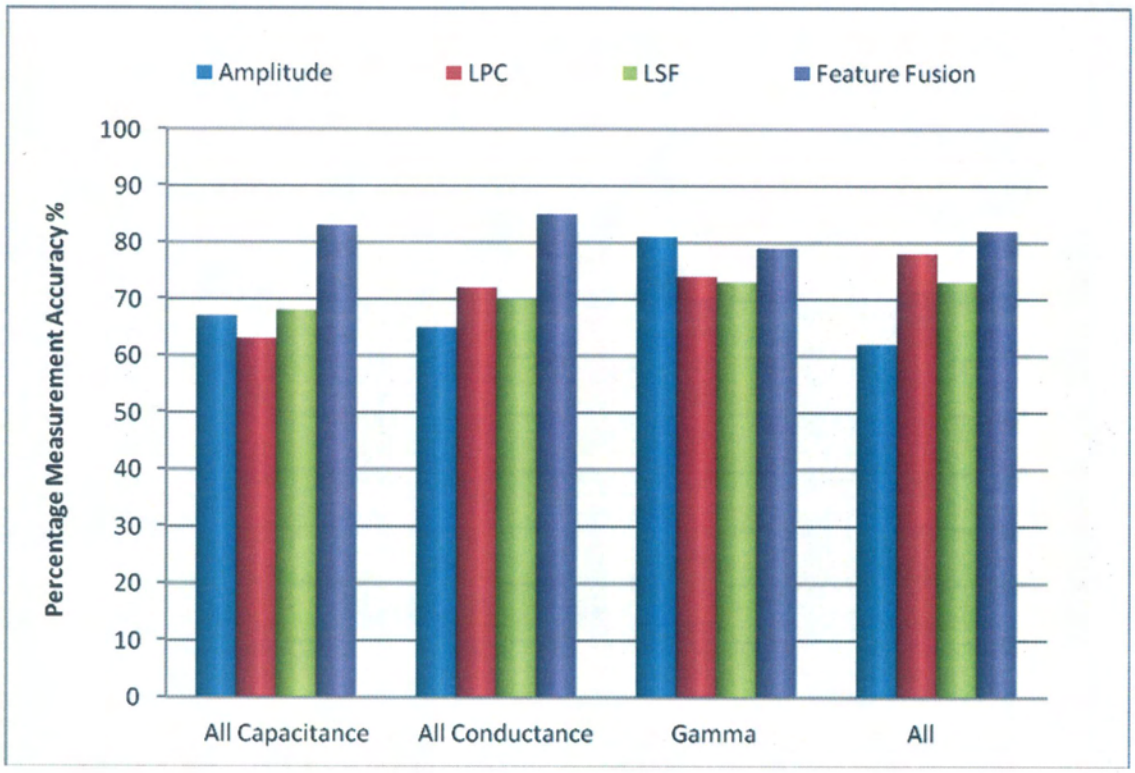

Figure 5.12 – Salinity 2 BPNN: Percentage Measurement Accuracy for the Water Cut of Salinity 2 Test Points

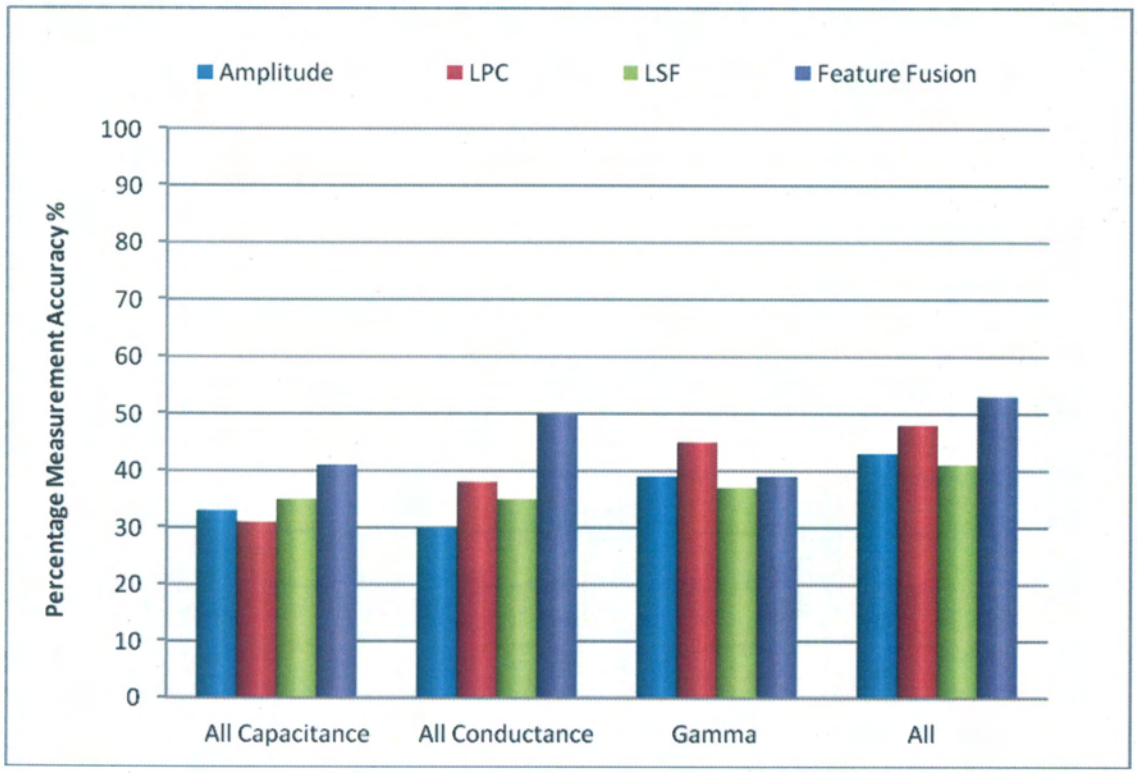

Figure 5.13 – Salinity 2 BPNN: Percentage Measurement Accuracy for the Water Cut of Salinity 1Test Points

5.1.3 Salinity 1 (S1) Back Propagation Neural Network (BPNN)

Similarly, the Salinity 1 BPNN was trained with 50g/l solution data from features extracted from the capacitance, conductance and gamma sensors. The network architecture was also defined to be [n – 8 – 3]. All other parameters were as per the original single BPNN. The trained network (50 g/l solution data) was presented with the same test data set, a mixture of salinity 2 and salinity 1 test points.

Table 5.2 (page 178), contains a summary of the flow rates and water cut prediction performance, obtained from the Salinity 1 BPNN using features from the capacitance, conductance, gamma sensors, as well as fused features from all the sensor signals.

5.1.3.1 Liquid Superficial Velocity

Figures 5.14 and **5.15** display the liquid superficial velocity measurement results acquired from the salinity 1 neural network using a variety of different input signal and feature combinations from the sensor signals.

Figure 5.14 illustrates the network performance for the salinity 1 test points; the best performance was yielded exploiting the feature fusion features of the capacitance signal: 98% of salinity 1 data points were predicted within the target accuracy of ±5%. Furthermore, 90% of salinity 1 liquid velocities were also obtained for fused LSF features of the conductance and gamma signals and 96% from the fused LPC from all signals.

Figure 5.15 presents the salinity 2 data point results for the salinity 1 trained network. As anticipated, the salinity 2 predictions observed were relatively poor, reinforcing the hypothesis that different underlying relationships exist between features and flow parameters for each of the salinity levels. In all cases, less than 52% of salinity 2 test points were predicted within the specified target accuracy of ±5%.

5.1.3.2 Gas Superficial Velocity

Figures 5.16 and **5.17** show the gas superficial velocity measurement results obtained from the salinity 1 BPNN for the salinity 1 and salinity 2 test points respectively.

Figure 5.16 illustrates that the salinity 1 gas superficial velocity predictions were better than those obtained for the salinity 2 in the salinity 2 BPNN: 98% of salinity 1 data points were predicted within ±5% of their target outputs employing the feature fusion input vectors of the all signals. Based on the results obtained, it would appear that the gas phase exerts a larger influence on the signal in the higher salinity data points.

Figure 5.17 exhibits the gas measurement results for the salinity 2 test points. Although accurate predictions were obtained for salinity 1, this model obviously does not transfer well to salinity 2 data points; typically, 70% of salinity 2 test points produced errors outside the target threshold.

Figure 5.18(a) presents the measurement errors obtained for each of the test data points using the feature fusion group as the input features. The all feature fusion signal data points exhibiting errors in excess of ±5% have been identified. It can be seen that at high WCs (>60%) superficial gas velocity predictions were outside the desired ±5% target accuracy range. Increasing the WC of the test point, thus increasing its bulk conductivity characteristics, results in increased error in frequency and magnitude.

Figure 5.18(b) indicates the location of the erroneous test points on the test matrix and reinforces the salinity sensitivity of the salinity 1 trained network: all off-specification measurements reside in the salinity 2 data points.

5.1.3.3 Water Cut

Figures 5.19 and **5.20** display the water cut measurements observed employing the salinity 1 data trained BPNN for salinity 1 and salinity 2 test points respectively.

Figure 5.19 illustrates the improvement in the performance yielded in the water cut determination through the employment of a salinity dependent model. By exploiting the amplitude features of the capacitance signal, 100% of salinity 1 test points were measured within ±5% of their target output. Strong water cut predictions were witnessed for all input signals studied using the amplitude features.

Figure 5.20 demonstrates the poor water cut determination measurement yielded for salinity 2 test points from salinity 1 trained network, reiterating the salinity specificity of the models developed in the multilevel hierarchical neural network system.

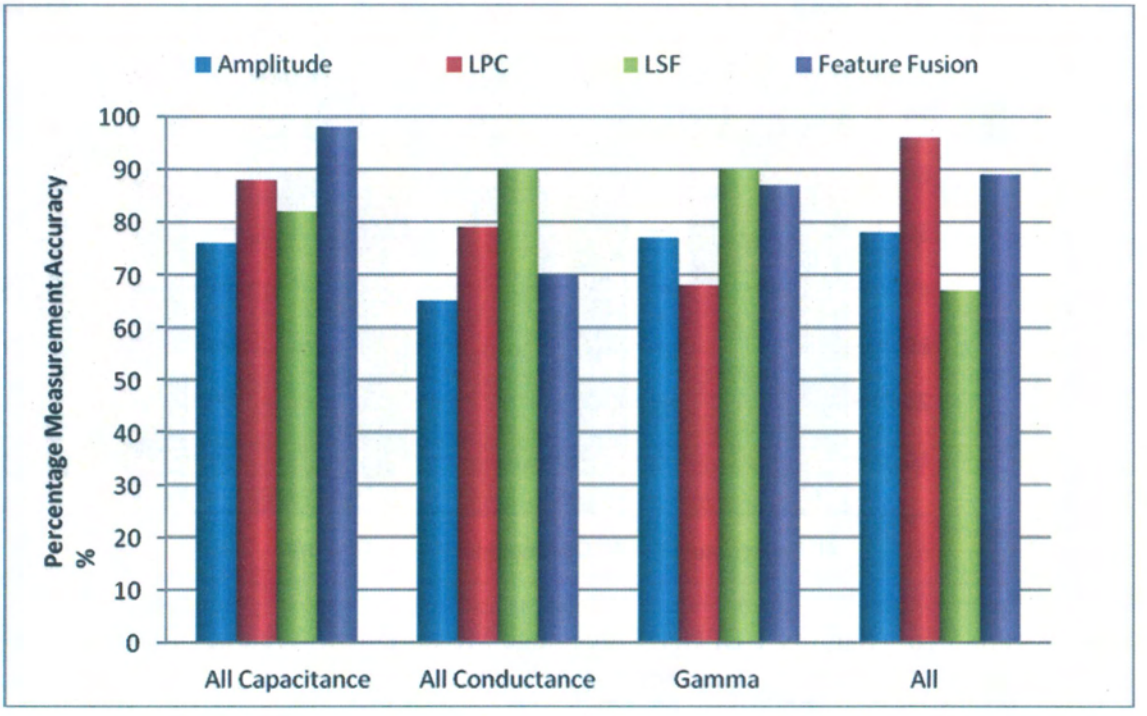

Figure 5.14 – Salinity 1 BPNN: Percentage Measurement Accuracy for the Superficial Liquid Velocity of Salinity 1 Test Points

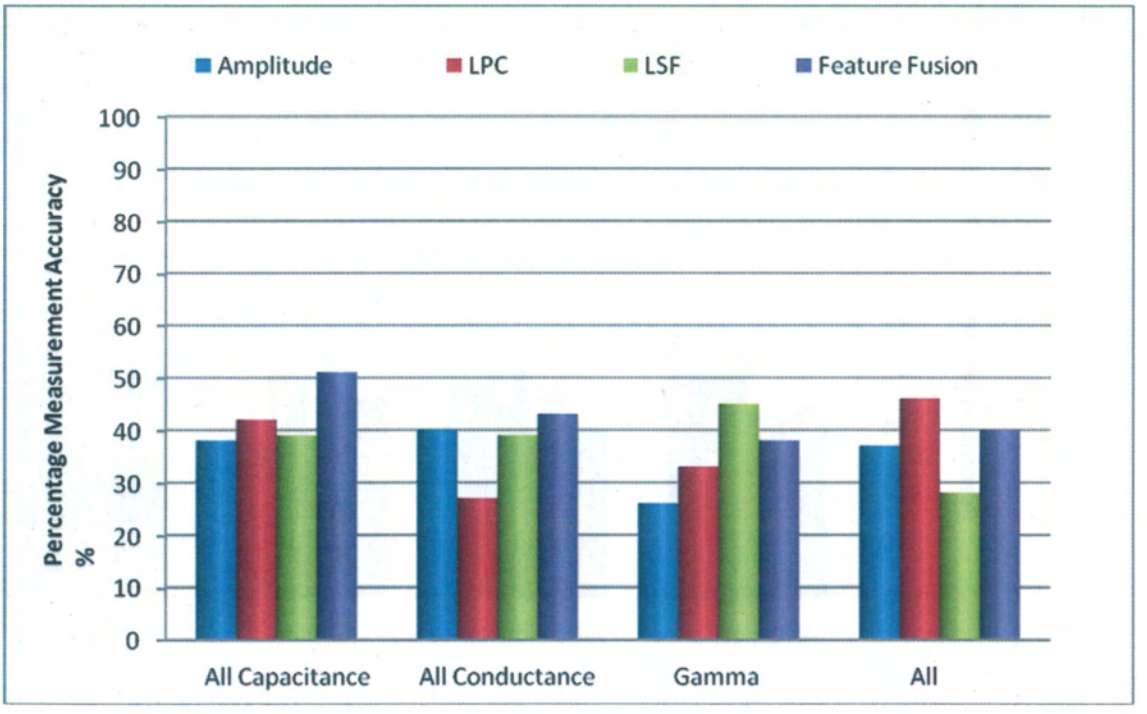

Figure 5.15 – Salinity 1 BPNN: Percentage Measurement Accuracy for the Superficial Liquid Velocity of Salinity 2 Test Points

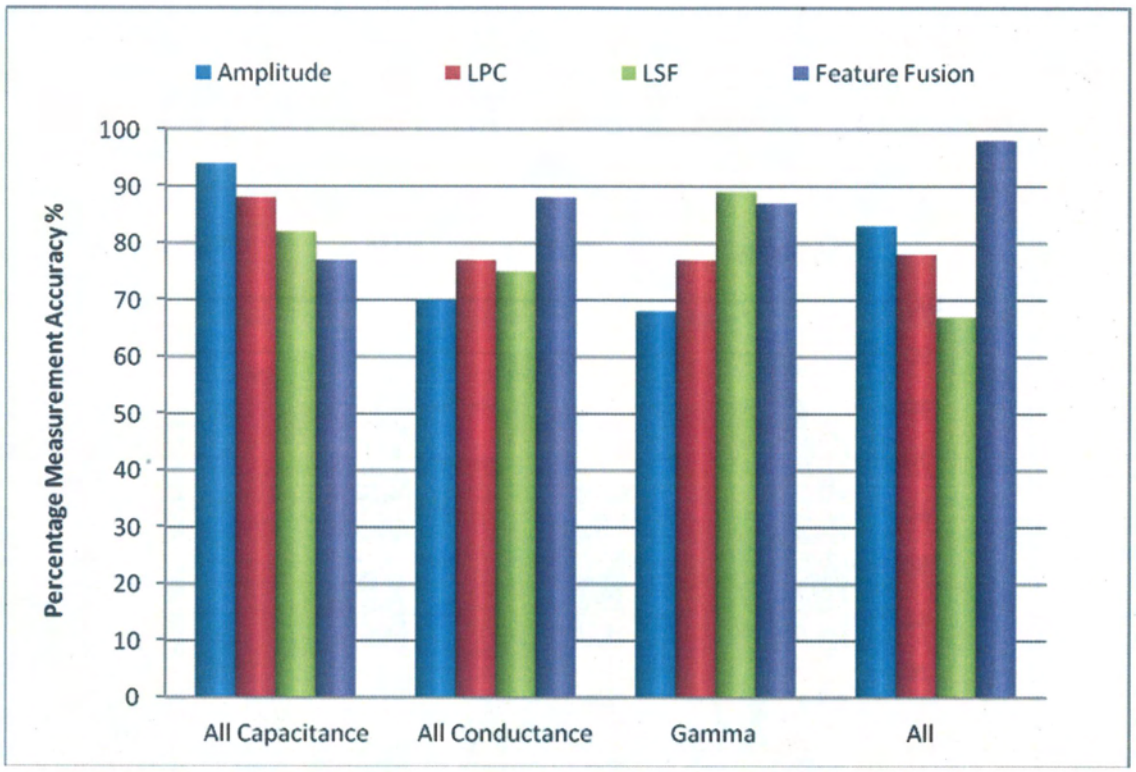

Figure 5.16 – Salinity 1 BPNN: Percentage Measurement Accuracy for the Superficial Gas Velocity of Salinity 1 Test Points

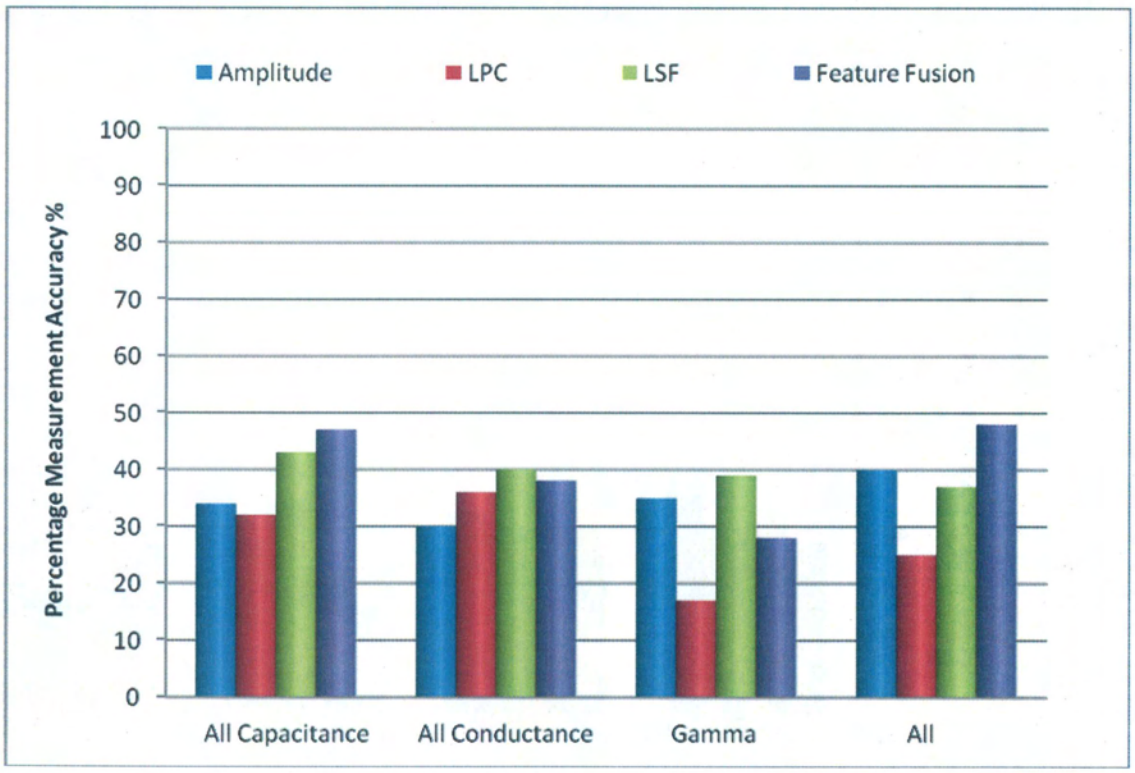

Figure 5.17 – Salinity 1 BPNN: Percentage Measurement Accuracy for the Superficial Gas Velocity of Salinity 2 Test Points

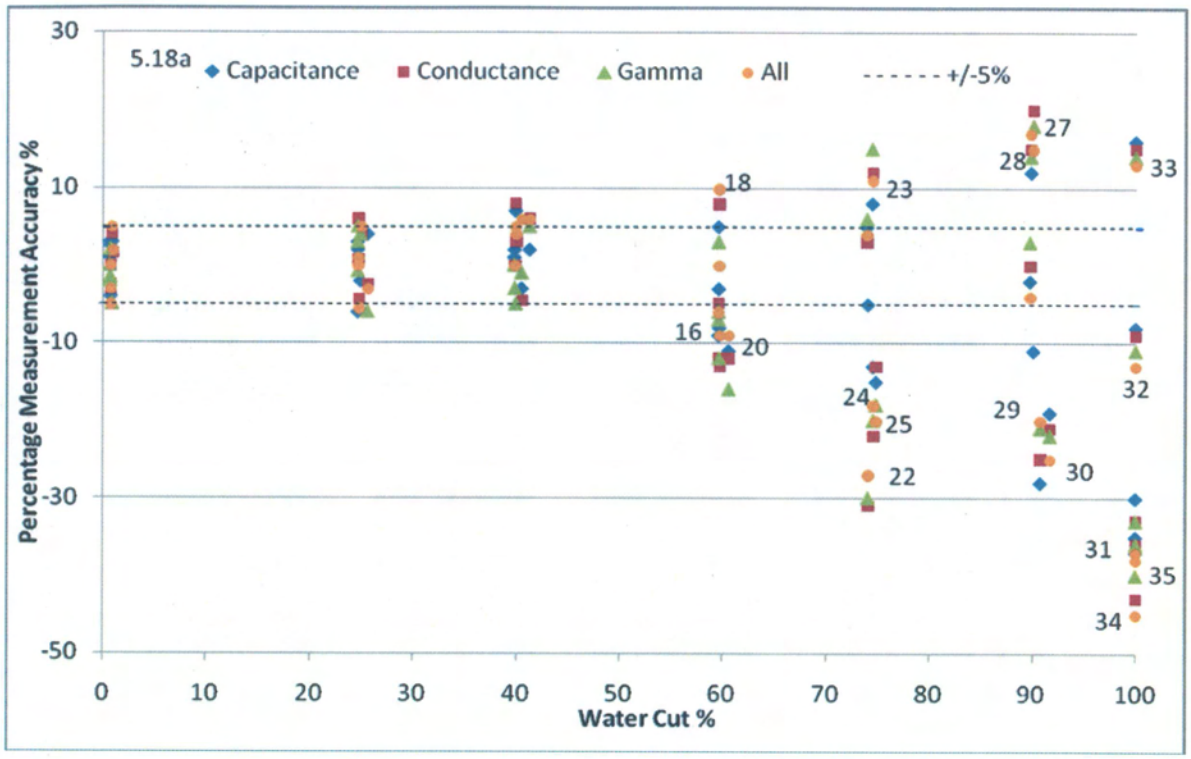

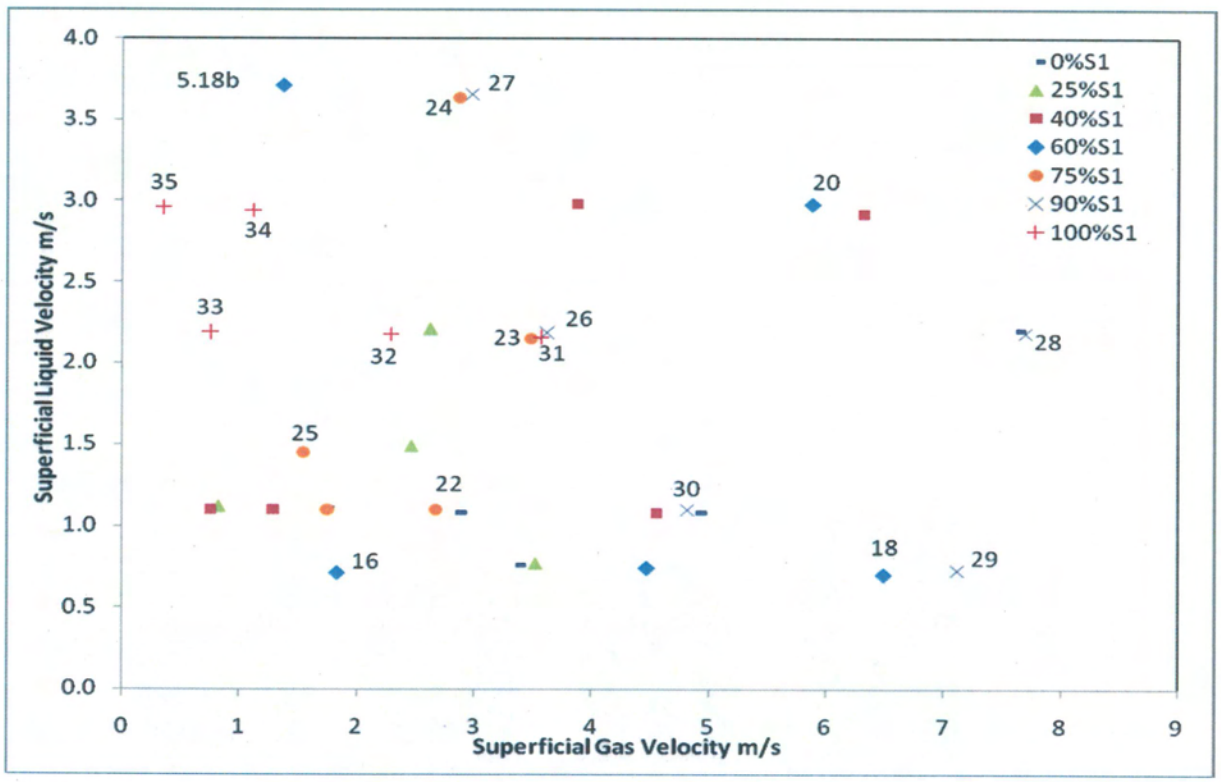

Figures 5.18 (a) and (b) – Salinity 1 BPNN: Percentage Gas Error Distribution for Feature Fusion of All Sensors (a) Water Cut Plot (b) Outlying Test Point Matrix Location

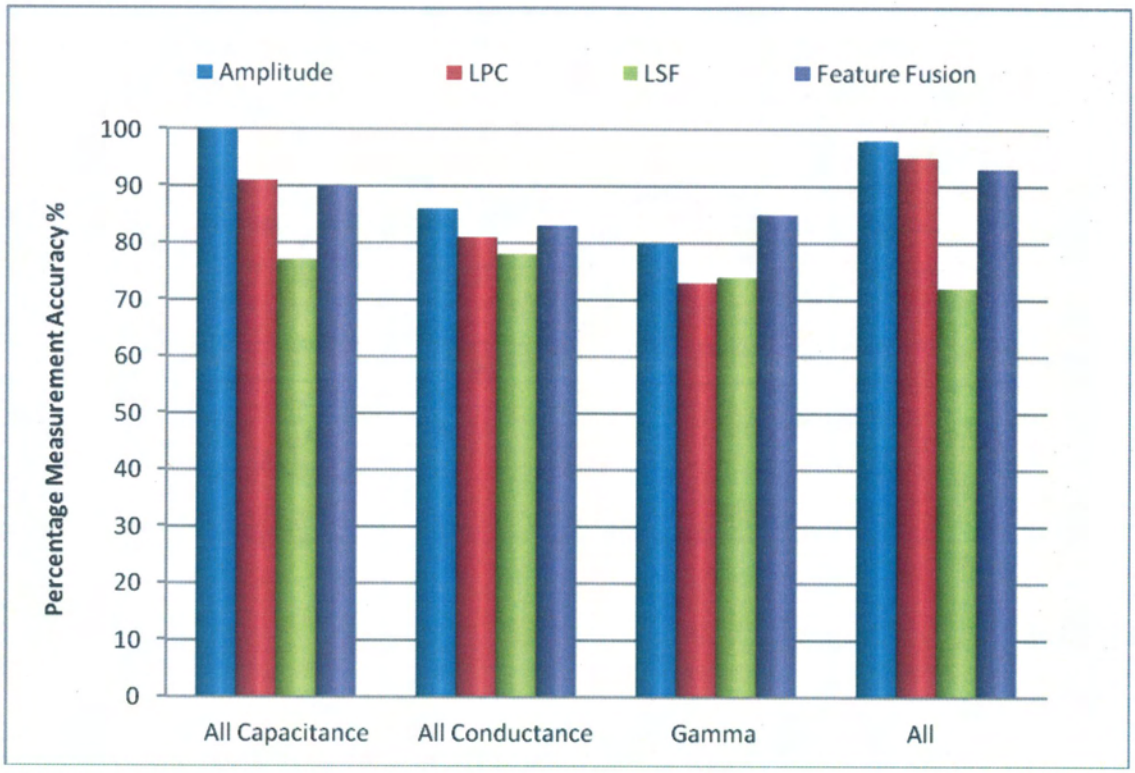

Figure 5.19 – Salinity 1 BPNN: Percentage Measurement Accuracy for the Water Cut of Salinity 1Test Points

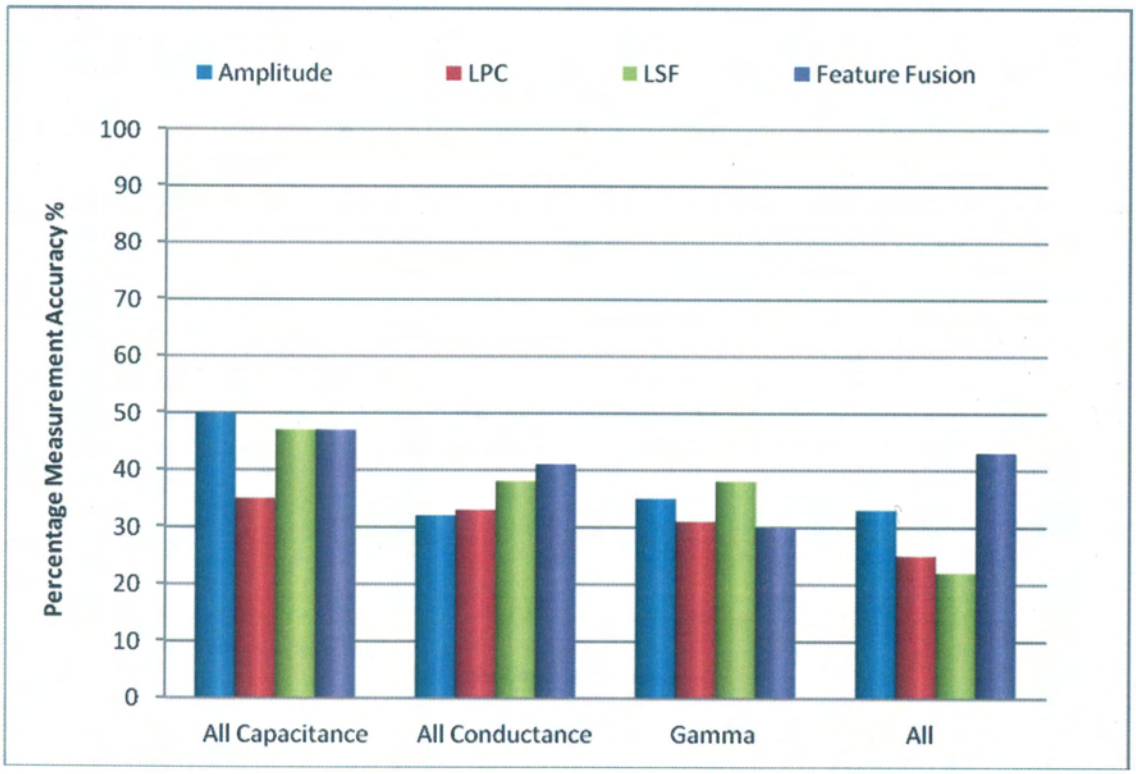

Figure 5.20 – Salinity 1 BPNN: Percentage Measurement Accuracy for the Water Cut of Salinity 2 Test Points

5.1.4 Summary of Results from Salinity Effects on Multiphase Measurements

Tables 5.1 and 5.2, contain a summary of the flow rates and water cut prediction performance, obtained from the Salinity 2 and Salinity 1 BPNNs respectively, using features from the capacitance, conductance, gamma sensors, as well as fused features from all the sensor signals. It can be seen that each individual salinity specific BPNN yielded good results for test points of the same salinity as the training data and that poor prediction of those test points belong to the alien salinity level. These findings support the hypothesis that each salinity level exhibits its own characteristic correlations between statistical features of the sensor's signals and the multiphase flow parameters. The implication is that a salinity sensor is required, if salinity is varying.

Table 5.1 – Summary of Measurements Prediction Results of Salinity 2 BPNN

Sensor(s)	Best Performing Feature			Salinity 2 BPNN (S2 training data) e ≤ 5% (%)			Salinity 2 BPNN (S1 training data) e ≤ 5% (%)		
	Vsl	Vsg	WC	Vsl	Vsg	WC	Vsl	Vsg	WC
All Capacitance	FF	FF	FF	96	83	83	45	39_{LSF}	41
All Conductance	FF	FF	FF	86	83	95	40_{Amp}	39_{Amp}	50
Gamma	LSF	Amp	Amp	78	85	81	25_{FF}	30_{FF}	45_{LPC}
All Sensors	FF	FF	Amp	100	80	92	48	50	55_{FF}

Table 5.2 – Summary of Measurements Prediction Results of Salinity 1 BPNN

Sensor(s)	Best Performing Feature			Salinity 1 BPNN (S1 training data) e ≤ 5% (%)			Salinity 1 BPNN (S2 training data) e ≤ 5% (%)		
	Vsl	Vsg	WC	Vsl	Vsg	WC	Vsl	Vsg	WC
All Capacitance	FF	Amp	Amp	98	94	100	51	47_{FF}	50
All Conductance	LSF	FF	Amp	90	88	86	43_{FF}	40_{LSF}	41_{FF}
Gamma	LSF	FF	FF	90	89	85	45	39_{LSF}	38_{LSF}
All Sensors	LPC	FF	Amp	96	98	98	46	48	43_{FF}

CHAPTER 6

6 DISCUSSION

6.1 Application of Simple Sensors and Signal Analysis for Multiphase Measurement

This chapter examines the performance of pattern recognition systems that have been constructed to model the non-linear relationship between the stochastic features extracted from each sensor and multiphase flow parameters. The system was constructed and tested for its effectiveness in enabling the meter to measure the individual liquid and gas flow rates, water cut and gas volume fraction without prior knowledge of the measured parameters. Performance of the system was evaluated based on two locations of the spool piece on the flow loop as well as two salinity levels.

A pair each of Differential Pressure sensors (DP1 and DP2, mounted axially), Capacitance (Cap.1 and Cap.2), Conductance (Cond.1 and Cond.2), one single-beam Gamma Densitometer, and Absolute Pressure and Temperature sensors were installed on a horizontal spool piece (see Figure 3.1 for the location of sensors). The test matrix covered mainly a three phase (oil, water and gas) slug flow. Data were collected under two different salinities of 50 and 100 g/l $MgSO_4$, and the spool piece was placed at two different locations in the NEL flow loop. The results presented showed that each of the sensors responds uniquely to different flow conditions.

6.1.1 Feature Extraction

Stochastic features have been extracted from the sensors in three information domains (Amplitude, Linear Prediction Coefficients (LPC), and Line Spectral Frequencies (LSF)). Features were normalised by applying Zero Mean and Unit-Variance (ZMUV) normalisation, which equalises the magnitude and dynamic range of each feature, so that they are given equal emphasis. Further data preprocessing was not found useful as it resulted in the loss of some of the discriminatory information present in the data as well as reduced classification accuracy.

The feature contouring analysis showed that there is a clear relationship between stochastic features and multiphase flow parameters (Superficial Gas and Liquid Velocities, Water Cut and Gas Volume Fraction). All features displayed a strong dependency on liquid loading and gas velocity. There is clear evidence from the contour plots that an input-output mapping exists between the above stochastic features and the corresponding multiphase flow parameters.

The plots also revealed that the feature distributions confirmed the limitations of conductance sensor function with oil continuous flow. The change in feature trends is more pronounced at water cuts below 60%.

The observed feature behaviour indicates that if pattern recognition system is developed which is trained/calibrated upon a data (feature vectors) set gathered, say, under particular pressure or salinity conditions, and the system experiences a change, then the system may not be expected to perform satisfactorily.

6.1.2 Neural Network Structure

The pattern recognition techniques were illustrated in Figures 4.14 (a) and (c) (chapter 4). The raw data were measured with sensors indicated on the spool piece. The multiphase flow parameters measurement system is composed of feature vectors extracted from the amplitude, linear prediction coefficients and line spectral frequencies. A BPNN model is used as the pattern classifier.

The BPNN prediction model used in this study has shown that it is possible to construct an input-output mapping between the stochastic features and the corresponding multiphase flow parameters. The exact form of this mapping is determined from a data set of labelled examples (i.e. training data).

Another advantage of the BPNN is that, unlike traditional neural networks which require a dedicated validation subset to minimise overfitting, the Bayesian technique controls model complexity (overfitting) automatically using only the training data. Furthermore the Bayesian approach improves generalisation and provides a measure of how many network parameters (weights and biases) are being effectively used by the network.

It also eliminates the guesswork required in determining the optimum number of hidden neurons and consistently leads to good networks that are not over-trained. A sigmoid non-linear transfer function was used in the hidden layer and a linear transfer function in the output layer. The structure of the network was kept constant, with the only variable being the size of the input nodes, which is directly controlled by the type of feature vectors used. This allowed an objective methodology to be developed upon which the performance of the sensors and feature vectors to be compared. The back propagation neural network was tested for the backward reproducibility of the individual phase flow rates and water-cuts from the derived features. The results of tests confirmed the applicability of neural networks in on-line flow rate measurement.

The multiphase flow parameter prediction results obtained vary considerably depending on which feature combinations and sensors were used. The results were also heavily influenced by flow conditions.

6.1.3 Results of Individual Sensor Performances

6.1.3.1 Absolute Pressure

The Absolute Pressure (AP) performance for the liquid flow rate indicated that the amplitude and feature fusion vectors have all successfully predicted a liquid velocity relative measurement error of ± 5 %, by achieving 88 and 100% respectively. It can be concluded that if only the AP were to be used for liquid flow rate measurement, then only the extraction of amplitude features should be considered.

The line spectral frequency (LSF) feature vectors resulted in the best measurement accuracy, with 65% for the gas superficial velocity. While the network was trained successfully for liquid velocity, most of the prediction errors for gas velocity appeared at the higher liquid velocity extremities of the flow.

6.1.3.2 Differential Pressure

From the DP transducers results, it may be concluded that if a single differential pressure sensor only is available for phase flow measurements on the spool piece, then feature fusion vectors for the single transducer should be used for the liquid and gas volumetric measurements.

This also underlines the fact that neural network generalisation performance is heavily influenced by the type of feature vectors used and that the formation of a large calibration database in terms of feature vectors does not necessarily lead to improved measurement accuracy.

6.1.3.3 Capacitance

The flow rate measurement results obtained by the different feature vectors extracted from the capacitance sensors showed that the amplitude and feature fusion features provided the best discriminatory properties for liquid velocity determination. 78% of all liquid superficial phase velocities (Vsl) were resolved to within ±5% for amplitude features of capacitance 1, and 74% Vsl with feature fusion signal features of capacitance 2. The feature fusion vectors also predicted 71% gas velocity within ±5%.

The same amplitude and feature fusion vectors were found to provide the optimal output for the water cut measurements from both capacitance sensors. Hence either of these two feature vectors may be recommended to be used for the simultaneous measurement of gas and liquid flow rates as well as the water cut, with the capacitance signals.

6.1.3.4 Conductance

The conductance sensor results obtained from the liquid superficial velocity measurement accuracies were significantly poorer than those obtained for the capacitance features, especially at water cut ≤60%. LPC and feature fusion provided the best discriminatory properties for liquid velocity determination for conductance 1 and conductance 2 respectively. 69% of all liquid superficial phase velocities were resolved to within ±5% for the LPC features of conductance 1, and the feature fusion results for conductance 2 signal features Vsl predictions was 67%, i.e. within the ±5% target.

It was observed that the liquid superficial velocity error distribution was a function of water for the LPC input vectors for conductance 1. The data points lying outside the target accuracy have been identified on the plot and have been observed to be in high liquid, low water cut flow conditions. This confirmed the conductance's poor performance in oil continuous flow multiphase conditions.

The conductance sensor results demonstrated that LSF input vectors provided the strongest discriminatory abilities for gas superficial velocity determination for the conductance 1 meter. However, for conductance 2, feature fusion vectors showed stronger gas velocity classification capabilities. Similar to the liquid predictions, the conductance features produced poorer gas superficial velocity predictions than the capacitance signal features.

It was also observed that prediction error of the conductance vectors decreased as water cut increased. Testing of the neural network showed that 78% was predicted within the target accuracy of ±5% with LPC features of conductance 1, and 82% accuracy with feature fusion vectors of conductance 2.

When liquid and gas velocity information was checked at points where the highest prediction error occurred, they were observed to lie at the high liquid velocities and low water cut.

6.1.3.5 Gamma

For the Gamma Densitometer, liquid superficial velocity measurement accuracies indicated 71% of the data points were best predicted with the LSF feature vectors within the target accuracy of ±5%. Gas flow rate prediction results demonstrated that amplitude feature input vectors provided the strongest discriminatory abilities for gas superficial velocity determination. In general, the results obtained produced the best predictions so far for Vsg measurements within the target of ±5% compared to results from all individual sensors. The water cut measurement performances obtained from the input features of the gamma signal indicated that the amplitude feature input vectors provided the best output accuracies, with 81% of the test data points meeting the specified target within ±5%.

It may be concluded that, when comparing the overall measurement performance of the sensors and the four different feature vectors, the Absolute Pressure (AP) and the Differential Pressure 1 sensor (DP1) achieved the best measurement results for the liquid phase, with the best features vectors being the feature fusion vectors. However, in terms of the gas phase, the best results were obtained from the Gamma Amplitude vectors which achieved a better performance than the other sensors.

Also the feature fusion and amplitude vectors of the conductance 2 and gamma sensors achieved the best performance in predicting water cut.

The Gas Void Fraction (GVF) prediction performance was highest with the feature fusion vectors of the gamma signal with 76% of the data points within the target accuracy of ±5, followed by the capacitance achieving 60% with feature fusion.

From the above discussions, it may be concluded that when comparing the eight sensors, the fusion and amplitude feature vectors achieved the best flow rate and water cut prediction accuracies.

6.1.4 Results of Cross Sensor Fusion

In terms of cross sensor data fusion, the pattern recognition prediction accuracy depends on the types of sensor combined and which types of feature are fused together. The results obtained indicated that if the flow information from different sensors is fused together, then there is a potential of achieving greater measurement accuracies in all the test conditions studied. This potential is primarily due to the fact that each sensor has a defined operating range, outside which its accuracy reduces, and by combining and fusing stochastic features from different sensors, the overall accuracy for flow rate measurement may be extended.

A comparison of the network performance when using the different feature combinations indicated that a good network generalisation can be achieved when feature fusion of the same feature domain is used. i.e. when the amplitude features of the DP, Capacitance and Conductance sensors, and similarly the LPC and LSF were fused.

However, the best generalisation was achieved by the feature fusion of the best performing feature to determine the multiphase parameter. From the features chosen in this study for cross-sensor data fusion, the results have shown that a better generalisation can be achieved by selecting the best performing features for the cross sensor fusion, as against the more traditional fusion of the same domain. A remarkable performance was seen, whereby the overall results for both liquid and gas velocity predictions were 100% and 98%, within the target accuracy of ±5

respectively. The water cut performance of 98% and GVF predictions also improved significantly to 95% within the specified accuracy.

6.1.5 Location Effects on Multiphase Measurements

The flow rate measurement results by different feature vectors showed that the metering system developed in this study is affected by the change in location of the spool piece. However, at the same time, the results showed that if sufficient calibration data are provided in the two locations of the spool piece, then the system could be made independent of the test location. In other words, the same pattern recognition model could be used in different test locations, provided the system is adequately calibrated.

The results from the study of location effects showed that when the pattern recognition metering system developed here is subjected to a flow condition that was not part of the calibration data, then the system showed significant measurement errors. If substantially alien data is presented to the network (as represented by introducing new flow conditions here) then it will be prone to significant errors. The availability of a controlled test rig or validated and wide-ranging field data should allow the collection of extensive data under a sufficiently wide range of conditions to ensure that the network performs satisfactorily in the field in case unexpected flow conditions develop. However, in situations where the system is expected to experience a sudden change of operating conditions outside the calibration database, a detection system may be considered, which should decide when a feature set does not represent any known measurement parameters.

In terms of operating pressure changes, this would require the provision of training data, which is collected under the system's operating pressure, and if possible some data in extreme conditions (Min and Max expected operating pressure). The operating pressure would normally fluctuate and vary by a small amount and the pattern recognition system should be expected to extrapolate well in these conditions.

In cases where the system is expected to experience sudden and large operating pressure changes, the absolute pressure measurements should be monitored closely,

and if they change significantly from a predefined threshold, the system should be turned into a calibration mode and retrained.

6.1.6 Salinity Effects on Multiphase Measurements

The multi-level hierarchical neural network model with salinity dependent BPNNs yielded measurement accuracies that match superficial phase velocity and water cut predictions from the cross data fusion performance discussed earlier. The Salinity 2 BPNN feature fusion of the three sensors (Capacitance, Conductance and Gamma) yielded the best liquid flow measurement, performing at 100% within the specified accuracy of ±5%, while the fusion and amplitude features of the combined sensors in Salinity 1 BPNN yielded 98% each for the gas velocity and water cut predictions respectively.

Comparing the two salinity dependent BPNNs, it was observed that each individual network yielded good results for test points of the same salinity as the training data and poor prediction of those test points belonged to the alien salinity condition.

These findings support the hypothesis that each salinity level exhibits its own characteristic correlations between statistical features of the sensor signals and the multiphase flow parameters. During testing of the two-salinity multi-level hierarchical networks, results obtained reinforced the salinity specificity of the feature correlations with the multiphase flow properties. Good predictions were obtained for test points sharing a common salinity with the BPNN training data, while test points from a differing salinity were poorly predicted.

It was also observed that a relationship between the measurement error and the water cut exists, whereby as the test point WC increases, the fluid's bulk conductivity increases and the larger the probability and magnitude of the error in the liquid superficial velocity classification. A significant majority of all liquid and gas velocity measurements at WCs greater than 60% were under-predicted with respect to their target.

The results suggest that prior to applying pattern recognition techniques to real world applications in the field, the system must be calibrated with data collected under a

sufficiently wide range of conditions (e.g. line pressure, flow regimes, fluid properties, salinity levels, etc).

A possible technique of incorporating a novelty detection algorithm into the PR measurement system is given as part of possible extensions of the current research work (see chapter 7 – Future Work). The absolute pressure, conductance for water continuous, and capacitance for oil continuous multiphase flows can be used as part of a novelty detection system to monitor the system operating pressure and salinity levels, and if this is significantly outside the system calibration database, a decision should be made about whether to continue the measurement or retrain the pattern recognition system with the new developing conditions. For example, the sensitivity coefficient for salinity influences on the water cut measurement can be given as a % variation of water cut per % change in salt content.

6.2 Meter Performance Compared with Existing Commercial MPFM

6.2.1 Accuflow

The AMMS has been employed by Chevron Texaco in the Lost Hills and Cymric Fields in California, USA, since 1996. Shen and Riley (1998). Chevron Texaco reported AMMS volumetric liquid measurements to within 2% of those of the test separator and agreement to within 3% was obtained for the liquid phase water cut. No gas phase measurements were performed.

6.2.2 Agar

The Agar multiphase flow meter is said to have performed to its specifications (±10% of the reading for gas, oil and water) in numerous fields worldwide, up to 99.99% GVF, McNulty and Beg (1997), Agar and Farchy (2002). Conoco (USA) have tested the Agar MPFM for high GVF under controlled field conditions on its Lafayette (Louisiana, USA) test loop and found it to be accurate to ± 12% when compared with single-phase measurements.

6.2.3 ESMER

In 2002, ESMER was field tested by Sarawak Shell Berhad in Malaysia over a 20-month period. Cai et al (FLOMEKO – 2004). In a series of well tests, the meter's measurements were compared against those obtained from a conventional test separator. Good repeatability and trending of the meter against different production rates and flow patterns were reported and it was claimed that ESMER measurements matched the separator measurements to within ±10% for wells which were inside the operating envelope. However, it was noted that the accuracy of the meter deteriorated in well tests located at the boundary of the MPFM's operating envelope and with the passage of time.

6.2.4 FlowSys

Laboratory testing of the FlowSys meter was undertaken at the National Engineering Laboratory (NEL), Hall (2000). The test matrix comprised a number of points with liquid and gas flow rates ranging between 0-60 m^3/h and 0-340 m^3/h respectively. Liquid phase and oil flow rate measurements obtained were within a relative uncertainty band of ±5%. However, for test points with a GVF greater than 70%, or water cuts in excess of 75%, large deviations from the reference values were observed. The gas flow rate measurements were found to be within ±20% across a large proportion of the operating envelope.

6.2.5 Multiphase Meters AM mpm

Field validation tests were undertaken in January 2007 on the Gullfaks A field operated by Statoil and reported gas and oil flow rate measurement accuracies to within ±8% and ±3% respectively across the full range of GVFs and WLRs Scheers and Wee (2007).

6.2.6 Phase Dynamics CCM

In 2001, Phase Dynamics reported the field testing of the CCM unit on 1152 wells in the BP operated Milne field in Alaska using a conventional separator for reference measurements. Measurement accuracies of ±5% were claimed for the gas flow rate, liquid flow rate and liquid phase water cut, Phase Dynamics Inc. (2008).

6.2.7 Roxar

Field tests of the MPFM 1900Vi meter were undertaken by the Gulf of Suez

Petroleum Company (GUPCO) in Egypt on seven wells, Leggett et al (1996). During testing, the flow regime observed was noted to range from severe slugging through to annular owing to the dynamics of the gas-lift production system employed (the average GVF ranged between 93 and 98%). It was reported that gas and liquid phase flow rates were measured to within ±10%, relative to the test separator, for GVFs in the range 93 – 96%. Significant errors were reported for liquid flow rate measurements in tests where the GVF was in excess of 96%.

6.2.8 Schlumberger Vx

Laboratory testing of the PhaseWater Vx meter was also undertaken at the National Engineering Laboratory (NEL), Letton et al (1997). The test matrix comprised a number of points with GVFs ranging from 0 to 95%. Liquid phase and oil flow rate measurements were produced within a relative uncertainty band of ±10% and water cut readings had an associated absolute error of ±6%. No quantification of the gas phase measurement performance was reported.

Table 6.1 – Performance of Current PR Meter Compared with Commercial MPFMs

Meter	Performance			Comments
	Vsl	Vsg	WC	
Accuflow AMMS	±2%	-	±3%	Compared against Test Separator
Agar	±10%	±10%	±10%	Compared with Single-Phase Measurements, GVF up to 99.99%
ESMER	±10%	±15%	±5%	Field Tests against Test Separator, Accuracy across 1 – 98% GVF
Flowsys	±5%	±20%	±5%	NEL Test Separator, Large deviations for GVF>75% and WC>70%
Multiphase Meters AM mpm	±3%	±8%	-	Tested across full range GVF and WC
Phase Dynamics CCM	±5%	±5%	±5%	Field Tested against conventional Test Separator
Roxar	±10%	±10%	-	Field Tested against Test Separator, GVF 93 – 96%, Significant errors for GVF>96%
Schlumberger Vx	±10%	-	±6%	NEL Test Separator, GVF range 0 – 95%, WC (Absolute)
Current PR Meter	±5%	±5%	±5%	NEL Test Separator, GVF range 0 – 100%

The current meter performances for both liquid and gas velocity predictions were 100% and 98%, within the target accuracy of ±5% respectively, with The water cut performance of 98% was within the specified accuracy. The overall meter performance did not appear to be affected by GVF. The measurement accuracy was at its best when the flow rates encountered were close to the centre of the operating envelope but deteriorated towards the edges.

Unlike most of the conventional meters shown in **Figures 6.1**, the current meter maps the non-linear relationships by pattern recognition / neural net training rather than by theoretical modeling. This ensures that the meter can measure the flow rates of individual phases in oil production lines without the need for separation or a complex sensor. The meter does not require a-priori empirical models or knowledge of slip, does not employ cross-correlation, and does not determine flow rates from the set of equations shown above (so its accuracy is flat across 1-99% GVF).

The meter depends on the naturally occurring multiphase flow patterns in the pipeline which it characterises by neural net analysis of high frequency signals emitted by simple and standard sensors.

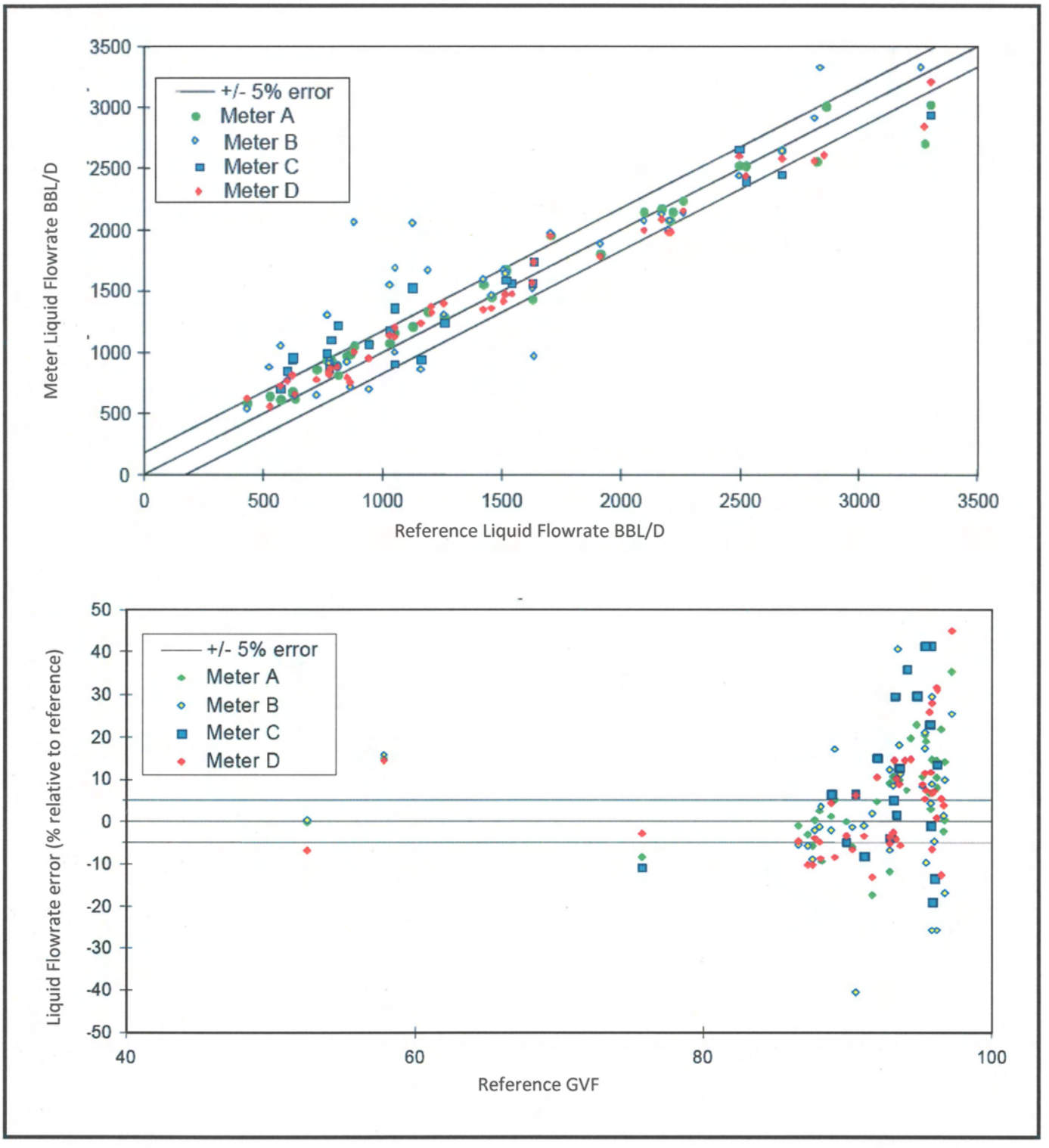

Figures 6.1 (a) and (b) – Liquid Flow rate Measurement Accuracy of four different Multiphase Meters, Mehdizadeh and Williamson, (2004).

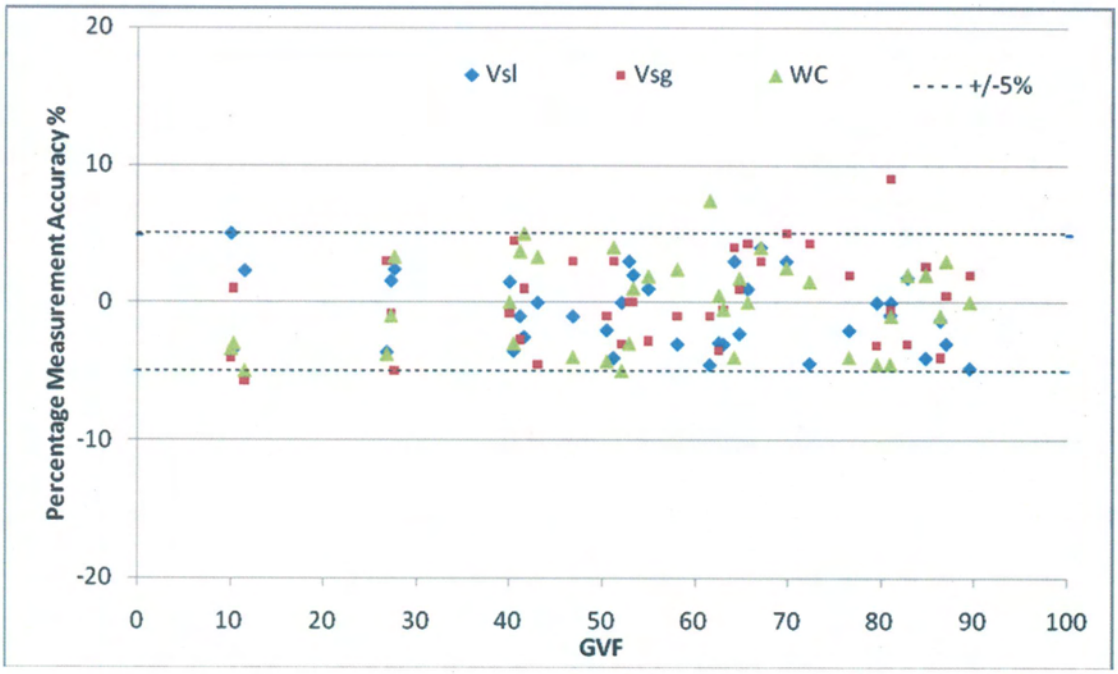

Figure 6.2 PR Meter Multiphase Parameter Measurement Results against GVF

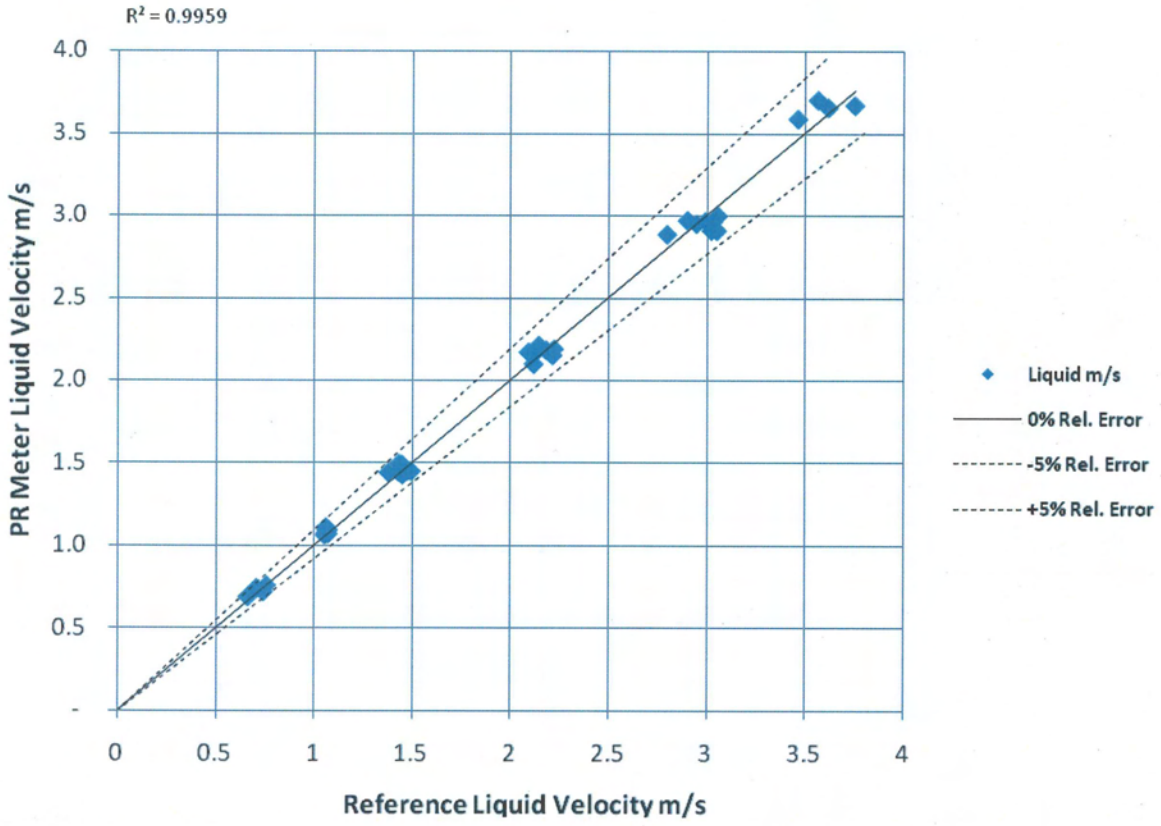

Figure 6.3 PR Meter Liquid Measurement Results against NEL Separator Reference Liquid Velocity (m/s)

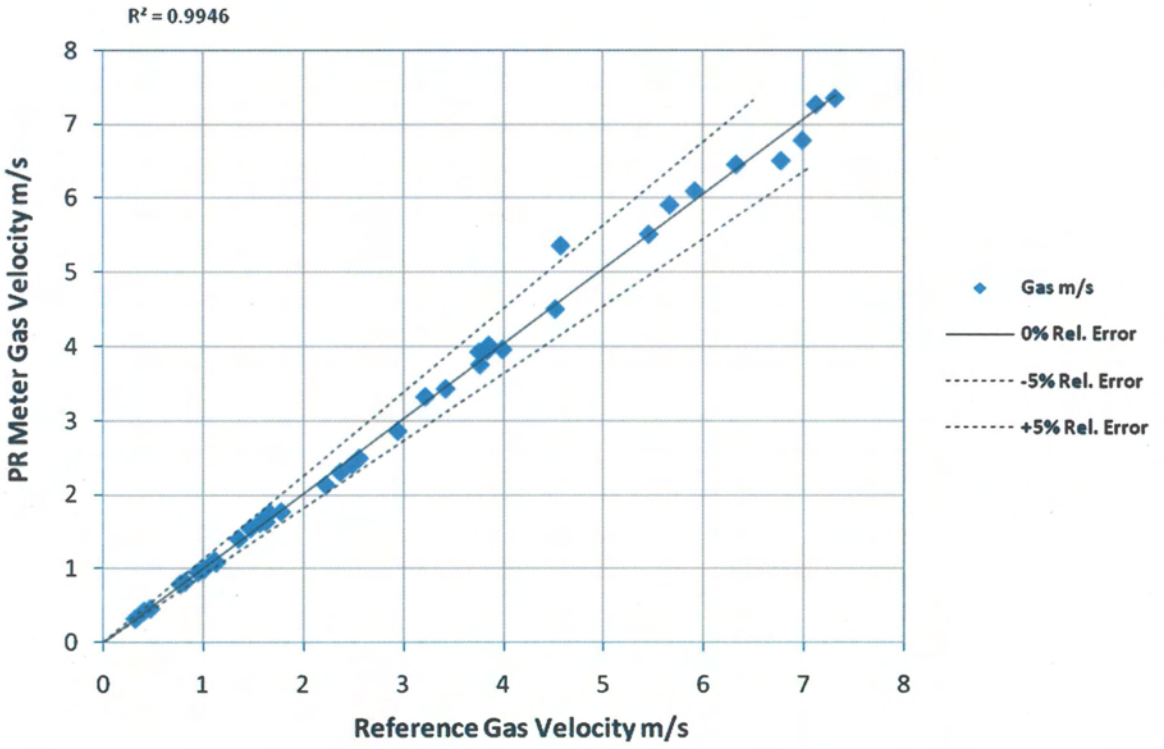

Figure 6.4 PR Meter Gas Measurement Results against NEL Separator Reference Gas Velocity (m/s)

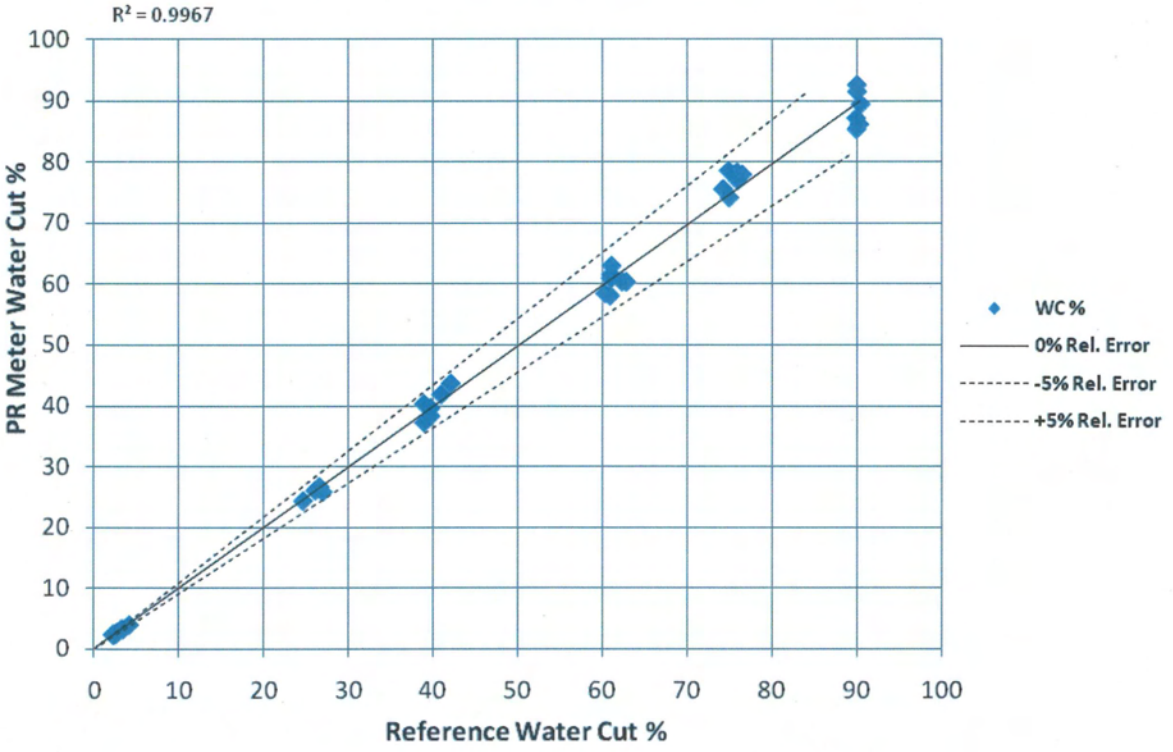

Figure 6.5 PR Meter Water Cut Measurement Results against NEL Separator Reference Water Cut (%)

CHAPTER 7

CONCLUSIONS AND FUTURE WORK

Although Multiphase Flow Measurement is not new, but still relatively nascent in the oil and gas/process industries, the pattern recognition approach for multiphase flow parameter measurements employed in this research work, provides an economical means of non-intrusive multiphase flow measurement. Simple sensors were used to detect shifts in flow conditions, such as flow structure, pressure and salinity changes in combination with a pattern recognition system that measured the flow parameters simultaneously without the need for preconditioning or prior knowledge of either phase. These, coupled with the current levels of oil prices and the global economic meltdown, would reinforce the justification of the industry's goal of high performing and lower cost Multiphase Flow Meters. A summary of the initial project's objectives is presented in this chapter.

7.1 Conclusions

Prior to presentation of the conclusions drawn from this research work, a brief recap of the original project objectives is provided; these are as follows:

- To review the literature describing components of the multiphase metering systems, and the application of pattern recognition techniques in multiphase flow measurements.
- To experimentally collect the response from a range of simple sensors when subjected to three-phase (oil/water/gas) flow conditions, with operating conditions covering a wide range of gas and liquid superficial velocities, in a 4 inch (102mm) horizontal pipe, under two different salinities of 50 and 100 g/l $MgSO_4$, at two different locations on the flow loop.
- To analyse features from the sensor signals' characteristics in relation to key multiphase flow parameters.
- To apply an appropriate pattern recognition model (Neural Network) for the identification of individual phase flow rates and water-cuts.

- To assess the performance of the system, for a range of multiphase flows and the effectiveness of the neural network on the different pipe locations as well as the different salinity levels.

The review of the multiphase flow and its metering reiterated the need for the development of a robust, non-intrusive and low-cost measurement solution to meet the oil and gas industry's requirements.

Employing PR techniques for multiphase flow analysis has been documented by a number of researchers to resolve the multiphase parameter measurements or to identify the prevalent flow regime. The use of sensors in conjunction with PR in multiphase flow measurement has also been reported where two sub-spools that form part of a sensor array installed horizontally have been commercially deployed. However, the flow in these meters involves intrusive measurement components, and reported measurement uncertainty, that do not lend themselves to the current industry requirements for multiphase metering performance standards.

No information has been published in the public domain on the use of non-intrusive, yet simple sensors that detect shifts in flow conditions (flow structure, pressure and salinity), in combination with a pattern recognition system to provide phase composition and velocity information simultaneously without the need for preconditioning or prior knowledge of either phase. However, ongoing work is aimed at achieving these objectives.

This research work has demonstrated that low cost and simple sensors can be exploited, in combination with pattern recognition analysis, to infer the superficial phase velocities and the liquid phase water cut, thus enabling the individual component mass flow rates of the multiphase flow to be determined to a degree of accuracy comparable with several commercially available multiphase flow meters.

The measurement system used for this research consists of temperature and absolute pressure transducers, gamma ray densitometer, a pair each of differential pressure sensors (mounted axially), capacitance, and conductance installed as a single horizontal spool piece, see Figure 3.1 for the location of sensors.

The test matrix covered mainly the three phase (oil, water and gas) slug flow. Data were collected under two different salinities of 50 and 100 g/l $MgSO_4$, and the spool piece was placed at two different locations in the NEL flow loop. A 4" Perspex visualisation section was installed immediately upstream of the sensor spool piece.

For its measurement approach, the pattern recognition system developed in this work relies on the sensors to extract relevant information in the form of features. A Back Propagation Neural Network (BPNN) is then used to relate these features to the liquid and gas superficial velocities, and the liquid phase water cut from which the volumetric flow rates can be calculated for oil, water and gas mixture.

1. Sensor signals features were extracted by means of digital signal processing techniques in three information domains (Amplitude, Linear Prediction Coefficients (LPC), and Line Spectral Frequencies (LSF)). These were found to be most effective based on their discriminatory trend to variations in flow conditions.

2. Feature contour analysis showed that there is a clear relationship between stochastic features and multiphase flow parameters. All features displayed a strong dependency on liquid loading and gas velocity. There was clear evidence from the contour plots that an input-output mapping exists between the above stochastic features and the corresponding multiphase flow parameters. Further dimensionality reduction was not found useful as it resulted in losing some of the discriminatory information present in the data and in reduced classification accuracy.

3. The BPNN used in this study, unlike traditional neural networks, does not require a dedicated validation subset to minimise overfitting; the Bayesian technique controls model complexity (overfitting) automatically using only the training data. Furthermore the Bayesian approach improves generalisation and provides a measure of how many network parameters (weights and biases) are being effectively used by the network. The Neural Network Training optimisation was shown in Figure 4.15 using the Bayesian technique.

4. Absolute Pressure (AP) performance for liquid flow rate indicated that the amplitude and the feature fusion vectors have all successfully predicted a liquid velocity relative measurement error of ± 5%. In particular, the feature fusion vectors

obtained 100% measurement accuracy, while the line spectral frequency (LSF) feature vectors resulted in the best measurement accuracy, with 65% measurement accuracy for the gas superficial velocity.

5. Results from the DP transducers have shown that if only a single differential pressure sensor is available for phase flow measurements on the spool piece, then feature fusion vectors for the single transducer should be used for the liquid and gas volumetric measurements.

6. It can be concluded that if only the AP and DP were to be used for liquid flow rate measurement, then the extraction of fusion features should be considered.

7. The capacitance sensor showed that the amplitude and feature fusion features provided the best discriminatory properties for liquid velocity determination. 78% of all liquid superficial phase velocities (Vsl) were resolved to within ±5% for amplitude features of capacitance 1, and 74% Vsl with feature fusion signal features of capacitance 2. The feature fusion vectors also predicted 71% gas velocity within ±5%. Also amplitude and feature fusion vectors were found to provide the optimal output for the water cut measurements from both capacitance sensors. Hence either of these two feature vectors may be recommended for the simultaneous measurement of gas and liquid flow rates as well as the water cut, with the capacitance signals.

8. LPC and feature fusion of the conductance sensor provided the best discriminatory properties for liquid velocity determination for conductance 1 and conductance 2 respectively. It was also observed that prediction error of the conductance vectors decreased as water cut increased; this confirmed the hypothesis that the conductance sensor performs poorly in oil continuous flow conditions.

9. Gamma sensor features produced the best predictions for superficial gas velocity measurements, with all individual sensors. The water cut measurement performances obtained from the input features of the gamma signal indicated that the amplitude feature input vectors provided the best output accuracies, with 81% of the test data points meeting the specified target within ±5%, while liquid superficial velocity measurement accuracies indicated 71% of the data points were best predicted with the LSF feature vectors.

10. The Gas Void Fraction (GVF) prediction performance was highest, with the feature fusion vectors of the gamma signal having 76% of the data points within the target accuracy of ±5%, followed by the capacitance achieving 60% with feature fusion.

11. It may be concluded that when comparing the eight sensors, the fusion and amplitude feature vectors achieved the best flow rate and water cut prediction accuracies.

12. The individual sensor performance and the improvements in some cases of the feature fusion scenarios have indicated that further flow rate measurement improvements could be achieved with cross-sensor feature fusion.

13. Features chosen for cross-sensor data fusion in this study have shown that a better generalisation can be achieved by selecting the best performing features for the cross-sensor fusion, as against the more traditional fusion of the same domain.

14. The cross-sensor data fusion improved overall performance, whereby the results for both liquid and gas velocity predictions were 100% and 98%, within the target accuracy of ±5% respectively. The water cut performance of 98% and GVF predictions also improved significantly to 95% within the specified accuracy.

15. Studies conducted on location effects showed that when the pattern recognition metering system developed is subjected to a flow condition that was not part of the calibration data, the system will yield significant measurement errors.

16. The results also confirmed that if sufficient calibration data were provided from different locations of the spool piece, the system could be made independent of the test location. In essence, the same pattern recognition model could be used in different test locations, provided the system is adequately calibrated.

17. The Kohonen self-organising feature map (KSOFM), a multilevel hierarchical neural network, classified data points according to the two salinity levels used, while the identification of the phase flow parameters was achieved through the employment of a second layer of the BPNN (one for each for the two salinity levels, i.e. 50 g/l solution is referred to as Salinity 1, the 100 g/l solution as Salinity 2).

18. Salinity specific BPNNs were developed based on results obtained from extensive preliminary repeatability tests; the architecture of the salinity BPNNs were defined to be [n – 8 – 3]. All other parameters were as per original single BPNN model.

19. The multi-level hierarchical neural network model with salinity dependent BPNNs yielded measurement accuracies that matched superficial phase velocity and water cut predictions from the cross data fusion performance discussed earlier.

20. Best liquid flow measurement performance was obtained by Salinity 2 BPNN feature fusion of the three sensors (Capacitance, Conductance and Gamma), with 100% within the specified accuracy of ±5%, while the fusion and amplitude features of the combined sensors in Salinity 1 BPNN yielded 98% each for the gas velocity and water cut predictions respectively.

21. Results from testing the two-salinity multi-level hierarchical networks, reinforced the hypothesis of salinity specificity of the feature correlations in multiphase flow. Good predictions were obtained for test points sharing a common salinity with the BPNN training data, while test points from a differing salinity were poorly predicted.

22. A relationship between the measurement error and water cut has been established, whereby as the test point WC increases, the fluid's bulk conductivity increases and the larger the probability and magnitude of the error in the liquid superficial velocity classification. A significant majority of all liquid and gas velocity measurements at WCs greater than 60% were under-predicted with respect to their target.

23. The results from the study of location and salinity effects show that if substantially alien data are presented to a neural network (as represented by introducing new salinity and flow conditions here) then it will be prone to significant errors; the system must be calibrated with data collected under a sufficiently wide range of conditions (e.g. line pressure, flow regimes, fluid properties, salinity levels, etc).

24. Where the system is expected to experience a sudden change of operating conditions outside the calibration database, a detection system may be considered, which should decide when a feature set does not represent any known measurement parameters; the absolute pressure, conductance, and capacitance sensors should be monitored closely, and if they change significantly from a predefined threshold, the system should be turned into a calibration mode and retrained.

25. The performance of some commercially available multiphase flow meters was reviewed and compared with results of current research findings. Liquid (water and oil) flow rate measurements from the multiphase meters were compared with reference flow rate data, obtained from a gravity based test separator. The plot shows the liquid rate measurements for ±5% accuracy level within the flow range, as shown in Figure 6.1a. Figure 6.1b shows the accuracy of liquid flow rate for the same four multiphase meters presented in Figure 6.1a, showing the impact of GVF on accuracy of the four meters to satisfy the ±5% accuracy requirement for liquid flow rates.

26. In comparison, the current PR meter results have shown that performances for both liquid and gas velocity predictions were 100% and 98%, within the target accuracy of ±5% respectively; the water cut performance of 98% was within the specified accuracy. The overall meter performance did not appear to be affected by GVF. The measurement accuracy was at its best when the flow rates encountered were close to the centre of the operating envelope but it then deteriorated towards the edges.

27. This work has shown that unlike most conventional meters, the current PR meter maps the non-linear relationships by pattern recognition/neural net training rather than by theoretical modeling. The meter learns the details of fluid dynamics behaviour from experience and there is no Newtonian mechanics modeling in the meter, hence its (theoretical) immunity to inaccuracies resulting from incomplete or erroneous flow regime and flow regime transition modeling.

28. The current PR meter is shown to measure flow rates of individual phases in oil production lines without the need for separation or a complex sensor. The meter does not require a-priori empirical models or knowledge of slip, does not employ

cross-correlation, and does not determine flow rates from the set of equations shown above, so its accuracy is flat across the complete range of GVF.

7.2 Future Work

The general consensus is that there is no single multiphase flow meter design capable of providing the required accurate measurements of oil, water, and gas fractions, as well as the phase velocities under all flow conditions. However, this research work has demonstrated that low cost and simple non-intrusive sensors can be used, in combination with a pattern recognition system, to infer the superficial phase velocities and the liquid phase water cut, thus enabling the individual component mass flow rates of the multiphase flow to be determined to a degree of accuracy surpassing several commercially available multiphase flow meters.

It is believed that with further development work on this pattern recognition based system, the ideal multiphase flow meter is in sight, and given below are some recommendations for further enhancements suggested for the current work.

1. In its current form, the measurement model developed will only be valid for the same fluids in identical operating conditions. Application of the technique developed to other installations will require further development work. The present study utilised one type of crude oil (Forties Beryl). No attempt was made to establish the relationship between features' responses and fluid physical properties. This type of study is necessary to generalise the proposed technique. Key parameters that should be considered are oil density, oil viscosity, increased levels of water salinity, from a variety of salts, especially sodium chloride (NaCl), which is the predominantly occurring natural salt encountered in oil and gas exploration. The operating pressure, pipe diameter, and pipe orientation, as well as temperature should also be considered. Perhaps the return of the sensor spool piece to Cranfield from NEL will provide these opportunities for further studies at the Cranfield test facility.

2. A significant source of errors in neural network applications arises from the input of alien data. As was seen in chapters 4 and 5, a network which is trained to discriminate between numbers of classes coming from a set of distributions, will be

confused when confronted with data coming from an entirely new distribution. This was most evidently demonstrated when the current pattern recognition system was trained on data from one location of the test facility, and tested with data from a different location. Results from the study of salinity effects also showed that if substantially alien data are presented to a neural network (as represented by introducing new salinity) then it will be prone to significant errors. The system must be calibrated with data collected under a sufficiently wide range of conditions (e.g. line pressure, flow regimes, fluid properties, salinity levels, etc). Results have shown that in cases where the system is expected to experience sudden and large changes in operating conditions, the absolute pressure, conductance, and capacitance sensors should be monitored closely, and if they change significantly from a predefined threshold, the system should be turned into a calibration mode and retrained. Further studies can enhance this work by developing a novelty detection algorithm into the PR measurement system.

3. Some other feature vectors could be evaluated for their effectiveness on the system performance. These include, but are not limited to, the following: reflection coefficients (RC), log area ratio (LAR), arcsine of reflection coefficients (ASRC), impulse response of LP synthesis filter (IR), etc. Investigations on the evaluation of slug parameters carried out during the earlier stages of this research work, the results from determination of slug lengths, slug translational and film velocities, and other parameters from the test matrix, if included as input features for the neural network model, will no doubt add value to the overall study.

Appendix A. – Review of Commercial Multiphase Flow Meters

A.1 Abbon Flow Master

There are two different versions of the Abbon Flow Master (AFM), both based on the Abbon acoustic detector, electronics and software technology:

- AFM 300C is a clamp-on instrument that uses either existing construction details (such as a choke valve) or a simple flow conditioner as a signal generator with a sensor attached to the surface.

- AFM 300I is an in-line version that incorporates a flow conditioner which increases the acoustic signals, shown in **Figure A.1** It is claimed by the manufacturer that the flow conditioner permits higher accuracy and easier calibration.

Figure A. – AMF In-Line Spool Piece, Abbon (2007).

As the oil well's multiphase flow passes through the measurement section, acoustic energy signals are generated which correlate to the flow rates and composition of the medium (AFM Product Specification Sheet). The AFM employs on-line detection, processing and interpretation using multivariate analysis of the acoustic fingerprint to infer variations in composition and flow rates. However, no information was available in the public domain relating to meter testing or commercial installations of the AFM multiphase meter.

A.2 Accuflow AMMS

The Accuflow Multiphase Metering System (AMMS) is a patented technology comprising a pipe separator design to separate a multiphase flow into a gas-free liquid stream and a liquid-free gas stream, as shown in **Figure A.2**, Accuflow (2007). Conventional single-phase measurement devices are then employed to measure each of the separated streams.

Multiphase fluid from the production flow line enters the vertical pipe tangentially, creating a cyclonic action in the vertical pipe where a majority of the gas is separated and flows upward. The downward inclination of the inlet pipe promotes liquid/gas stratification in the inlet pipe that enhances gas/liquid separation in the vertical separator pipe. The remaining gas, mostly in the form of small bubbles, is carried downward with the liquid stream and enters the horizontal pipe section.

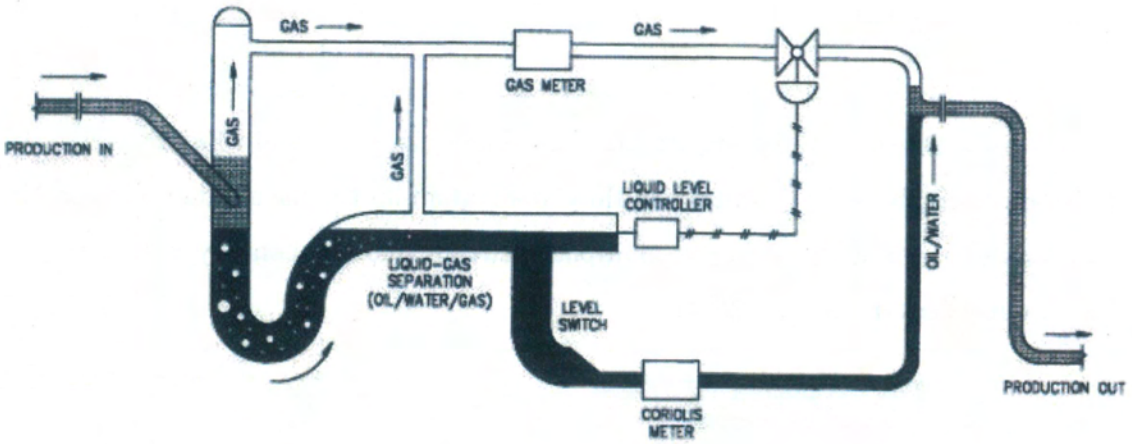

Figure A.2 – Operating Principle of the AMMS, Accuflow (2007).

The liquid level in the horizontal separator pipe section is controlled in the middle of the pipe using a control valve located in the gas flow line. As the liquid stream flows through the horizontal pipe, gas bubbles rise to the gas/liquid interface and are separated as the liquid stream flows towards the outlet end of the horizontal pipe. The large gas/liquid interface area, thin gas-bearing liquid layer, and quiescent flow in the horizontal pipe all contribute to the efficient removal of entrained gas bubbles from the liquid stream.

Accuflow claim that their patented pipe separator design can achieve complete gas-liquid separation and can thus employ conventional proven single-phase measurement devices to measure the separated phase streams (typically vortex or ultrasonic meters for the gas and a Coriolis meter for the liquid).

The AMMS has been employed by Chevron Texaco in the Lost Hills and Cymric Oil Fields in California, USA, since 1996, Shen and Riley, (1998). Chevron Texaco reported AMMS volumetric liquid measurements to within 2% of those of the test separator and agreement to within 3% was obtained for the liquid phase water cut. No gas phase measurements were performed.

Accuflow Inc. claims to have installed units at 65 sites, in six countries, with similar measurement accuracies attained for flow rates of up to 30,000 bpd, and at water cuts and gas fractions up to 99%, Dutton and Daniel (2001).

A.3 Agar MPFM

Agar's MPFM-400 Series is a phase separation type meter comprising a patented Fluidic Flow Diverter (FFD) device and a gas bypass loop shown in **Figure A.3**. The FFD device employs the difference in flow momentum in the gas and liquid phases to divert most of the free gas in the multiphase stream into a secondary measurement loop around the core of the MPFM.

(a) (b)

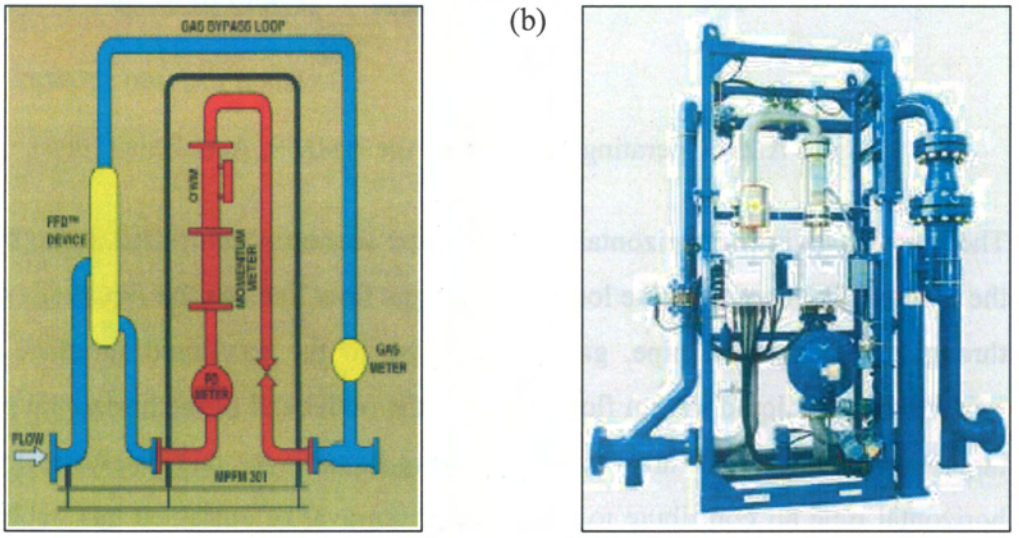

Figure A.3 – Agar MPFM 400-Series (a) Schematic and (b) Skid Mounted (mirrored), Agar and Farchy (2002).

This secondary measurement loop is essentially a wet gas metering system and consists of a Venturi and a vortex shedding flow meter in series. The primary metering loop comprises three components: a positive displacement meter to determine the total volumetric flow of the mainly liquid stream; a momentum meter (dual Venturi) which measures the gas fraction of the flow; and a microwave water-cut meter. After metering, the gas in the secondary bypass loop is recombined with the oil, water and gas measured by the core meter.

The Agar multiphase flow meter is said to have performed to its specifications (±10% of the reading for Gas, Oil and Water) in numerous fields worldwide, up to 99.99% GVF, McNulty and Beg (1997)., Agar and Farchy (2002). Conoco (USA) have tested the Agar MPFM for high GVF under controlled field conditions on its Lafayette (Louisiana, USA) test loop and found it to be accurate to ± 12% compared with reference single-phase measurements, McNulty and Beg (1997). Saudi Aramco have reported trial testing the Agar MPFM at a gas oil separation plant (GOSP), Al-Taweel and Barlow (1999). Here, the plant's separator was used as a reference measurement to evaluate meter accuracy. Approximately 30 comparison tests were made over a wide range of water cuts and GVFs (though the range of GVF was not mentioned). They mentioned that the meter compared well with the test separator and that no significant problems or operational failures occurred. However, the meter tested was said have been undersized for a large portion of the company wells.

A.4 FlowSys TopFlow

The major parts of the FlowSys TopFlow meter are the Venturi insert and the impedance electrodes incorporated inside the throat of the Venturi insert. The differential pressure is measured across the inlet of the Venturi insert while the capacitance or conductance of the mixture flowing through the Venturi insert is measured by the electrodes inside the Venturi throat. Fluid velocity is found from cross-correlation of the high-resolution time signals from pairs of electrodes within the Venturi insert.

The flow rates of the oil, water and gas are then calculated based on the measurements obtained by these sensors as illustrated in **Figure A.4.**

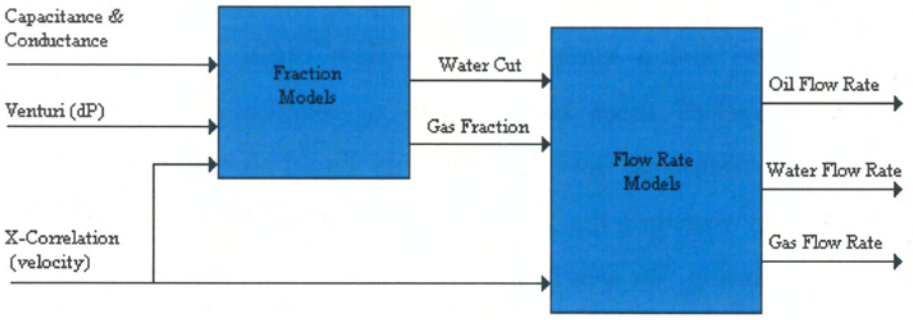

Figure A.4 – Schematic Diagram of the FlowSys TopFlow Meter, Hall (2000).

Laboratory testing of the FlowSys meter was undertaken at the National Engineering Laboratory (NEL), Hall (2000). The test matrix comprised a number of points with liquid and gas flow rates ranging between 0-60 m^3/h and 0-340 m^3/h respectively. Liquid phase and oil flow rate measurements obtained were within a relative uncertainty band of ±5%. However, for test points with a GVF greater than 70%, or water cuts in excess of 75%, large deviations from the reference values were observed. The gas flow rate measurements were found to be within ±20% across a large proportion of the operating envelope.

Further laboratory testing of the TopFlow MPFM was carried out by Christian Michelsen Research (CMR), Klepsvik et al., (2000). The test matrix comprised a number of points with liquid and gas flow rates ranging between 15-40 m^3/h and 20-90 m^3/h respectively. It was reported that 99% of the liquid flow rate measurements were within a relative deviation of ±10% from reference values, 78% of oil flow rate measurements were within ±10% and 84% of the gas flow rate measurements were within ±15%.

In 2001, FlowSys's TopFlow meter was field tested by Eni in Trecate, Italy, Mazzoni, et al., (2001). It was documented that the FlowSys meter gave phase flow rate measurements within ±10% for GVFs up to 92-93% for the gas flow rate and GVFs of up to 86-87% for the liquid flow rates. Liquid and gas flow rates ranged between 6-35 m^3/h and 35-145 m^3/h respectively. However, at GVFs in excess of 92-93%, the liquid flow rate measurement accuracy deteriorated to approximately ±20%. Owing to the limitations imposed by the test wells, the water cut was only examinable between 41-51%. In this range it was reported that the meter was able to classify the majority of the test points to within ±5%.

A.5 Framo / Schlumberger Vx MPFM

The Vx MPFM makes use of two measurement techniques: a Venturi with pressure, temperature and differential pressure sensors for mass flow measurement and dual-gamma densitometry for phase fraction determination. Following a blind tee, the multiphase flows vertically upwards through the metering area. All the measurements are made in the Venturi throat, i.e. absolute pressure, temperature, differential pressure relative to upstream conditions and phase fractions, shown in **Figure A.5**, Theuvent et al (1998).

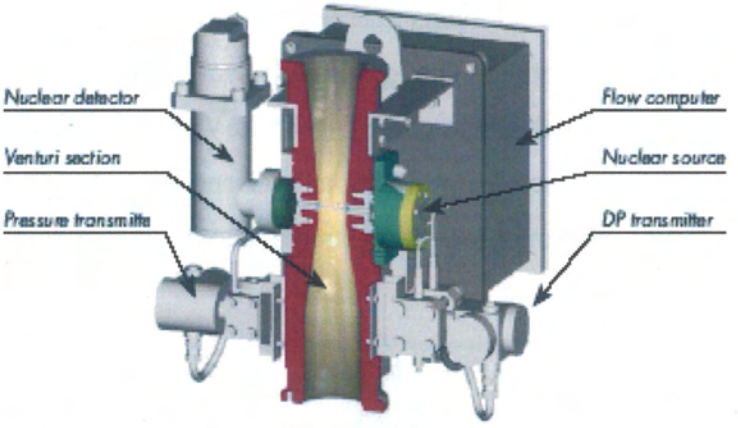

Figure A.5 – PhaseWatcher Vx MPFM , Theuvent et al (1998).

Phase fractions are measured using a dual-energy gamma densitometer employing a barium-133 radionuclide source. The source has energy levels appropriate for measurement of gas fraction and water cut (29 keV and 80 keV). The gamma densitometer is located at the narrowest part of the flow conduit, allowing the low energy levels employed by the gamma meter to be feasibly used with a low strength source.

Laboratory testing of the PhaseWater Vx meter was also undertaken at the National Engineering Laboratory (NEL), Letton et al., (1997). The test matrix comprised a number of points with GVFs ranging from 0 to 95%. Liquid phase and oil flow rate measurements were produced within a relative uncertainty band of ±10% and water cut readings had an associated absolute error of ±6%. No quantification of the gas phase measurement performance was reported.

Al-Khafji Joint Operations installed five PhaseWatcher Vx MPFMs in the offshore-Khafji field for satellite-based monitoring. Well tests were referenced against a test barge comprising a conventional three-phase separator set up. Measurement agreements for the PhaseWatcher Vx meters were reported to exhibit 5-10% relative error for the oil and water flow rates and in excess of 15% for the gas phase flow rate, with respect to the separator measurements, Al-Bourni et al., (2005).

A.6 Haimo MPFM

The Haimo MPFM combines features of inline and partial separation type MPFMs. The phase flow rate measurements and the water cut determination are carried out independently of each other. The gas/liquid two-phase flow meter consists of a Venturi and two identical single-energy (59.5 keV) gamma sensors. The full range three-phase water cut meter comprises a dual-energy (22 and 59.5 keV) gamma sensor and a flow conditioner located upstream, shown in **Figure A.6**, Haimo (2007).

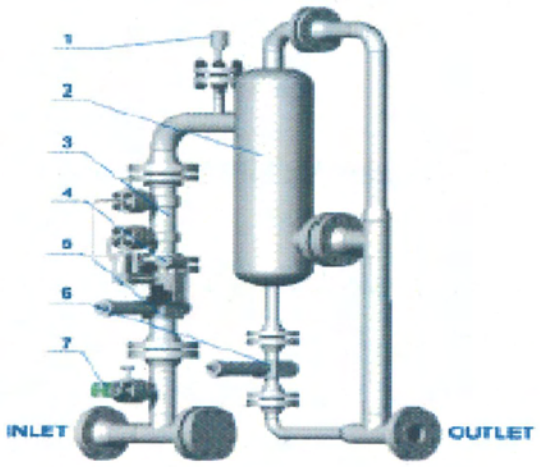

1.Temperature Transmitter 2.Flow Conditioner 3. Venturi Flow Meter
4.Differential Pressure Transmitter 5. Single Gamma Meter
6.Dual Gamma Meter 7.Pressure Transmitter

Figure A.6 – Haimo MPFM, Haimo (2007).

Both the gas and liquid flow rates are measured upstream of the flow conditioner in the two-phase flow meter: the dual-energy gamma densitometer measures the water cut of the conditioned flow mixture.

In March 2005, Haimo claimed to have completed well tests on more than 1500 wells and to have over 100 MFM meters installed in onshore and offshore applications, Haimo Newswire, (2005).

A.7 Jiskoot Mixmeter

Jiskoot's Mixmeter utilises a patented upstream mixer to ensure that a homogenous multiphase flow mixture is present in the meter's measurement section, shown in **Figure A.7.**, Hewitt et al (1997). The mixer attempts to equalise the velocity of the three phases and removes the need for complex slip correction calculations. Phase fractions are determined through the employment of a dual-energy gamma densitometry system; while the phase velocities are determined through the cross-correlation of sensor data. No data were found documenting the Mixmeter's performance in laboratory or field tests.

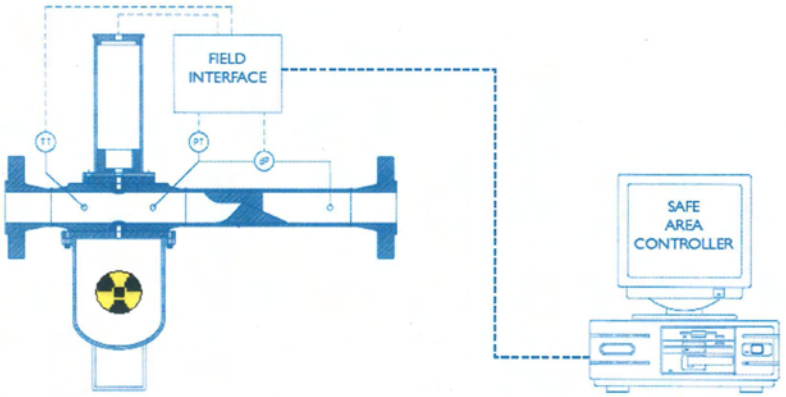

Figure A.7 – Mixmeter MPFM, Hewitt et al (1997).

A.8 PSL ESMER

ESMER exploits advanced signal processing techniques to determine the individual phase flow rates of a multiphase flow mixture. The ESMER system comprises two modular sub-spools: the pressure spool and the impedance spool. The pressure spool contains a differential device (orifice/Venturi/V-cone) equipped with differential pressure and absolute pressure gauges and a temperature sensor. The impedance spool comprises a capacitance sensor for oil external applications, a conductance sensor for water external applications or both for full water cut range applications. The spools are installed in a horizontal orientation.

ESMER is a pattern recognition based meter that establishes the non-linear relationships between an array of sensor measurements and the individual phase flow rates by a combination of pattern recognition and neural network training, illustrated in **Figure A.8.**, Toral et al (1998).

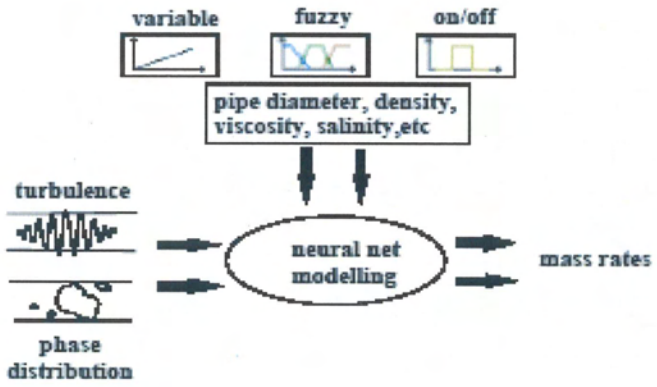

Figure A.8 – ESMER Concept Model, Toral et al (1998).

In 2002, ESMER was field tested by Sarawak Shell Berhad in Malaysia over a 20-month period, Cai et al (2004). In a series of well tests, the meter's measurements were compared against those obtained from a conventional test separator. Good repeatability and trending of the meter against different production rates and flow patterns were reported and it was claimed that ESMER measurements matched the separator measurements to within ±10% for wells which were inside the operating envelope. However, it was noted that the accuracy of the meter deteriorated in well tests located at the boundary of the MPFM's operating envelope and with the passage of time.

A.9 Roxar MPFM 1900VI

The Roxar MPFM 1900VI comprises a capacitance sensor, an inductive sensor, a gamma-ray densitometer, a Venturi meter and a system computer, illustrated in **Figure A.9**, oil, gas and water fractions are determined by electrical impedance and gamma ray density measurements. A cross-correlation algorithm is used to measure individual component flow rates. The Venturi meter measures the mixture flow rate and extends the range of the MPFM 1900VI to cover single-phase liquid where the cross-correlation technique fails to operate, Leggett et al (1996).

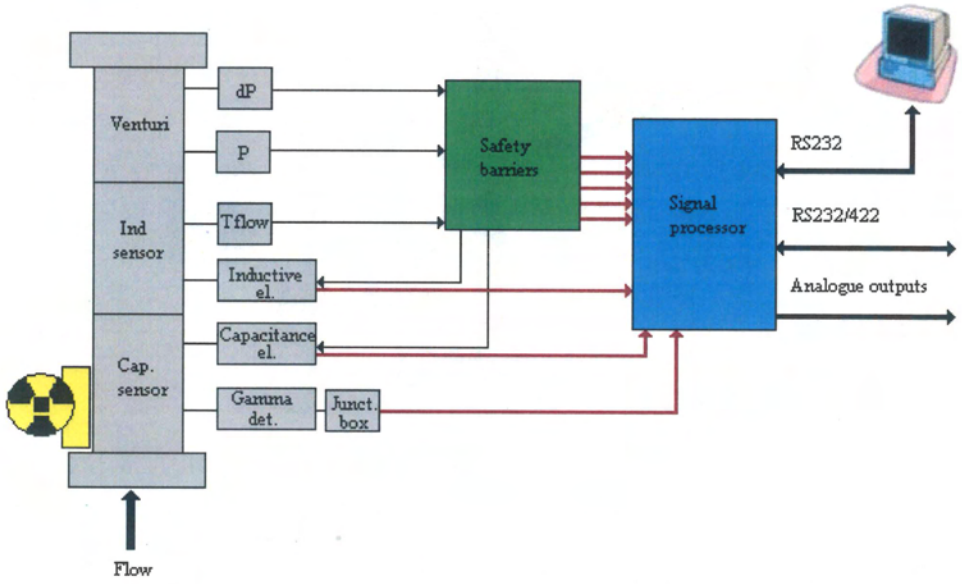

Figure A.9 – Schematic of Roxar MPFM 1900VI Meter, Leggett et al (1996).

Field tests of the MPFM 1900Vi meter were undertaken by the Gulf of Suez Petroleum Company (GUPCO) in Egypt on seven wells, Leggett et al., (1996). During testing, the flow regime observed was noted to range from severe slugging through to annular owing to the dynamics of the gas-lift production system employed (the average GVF ranged from 93 – 98%). It was reported that gas and liquid phase flow rates were measured to within ±10%, relative to the test separator, for GVFs in the range of 93 – 96%. Significant errors were reported for liquid flow rate measurements in tests where the GVF was in excess of 96%.

A.10 eProduction Solutions Inc. REMMS

The Red Eye Multiphase Metering System (REMMS) combines compact separation technology with conventional liquid and gas metering. The multiphase fluid enters the main body through a narrow tangential inlet into the vertical separator body. This forces the liquid and gas to accelerate through the inlet and around the vertical axis of the main body, creating a vortex as shown in **Figure A.10,** eProduction Solutions (2008).

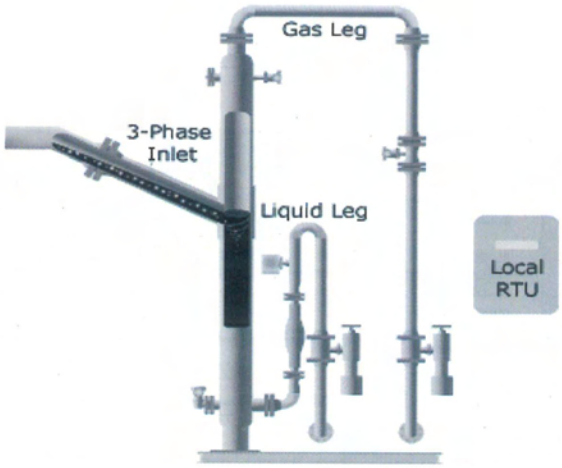

Figure A. 10 REMMS MPFM, eProduction Solutions (2008).

Due to the large density difference between the gas and liquid phases, the gas migrates quickly to the centre while the denser liquid travels to the wall. Once separated, the individual streams are measured with conventional liquid and gas meters, typically Coriolis and vortex meters respectively. The water cut is determined by employing eProduction Solutions proprietary Red Eye 2G Water Cut Meter which exploits infrared absorbance to determine the relative quantities of water and oil in the liquid phase The separated phases are then recombined or transported in separate flow lines. In December 2004, eProduction Solutions completed the installation of 18 REMMS MPFM units in Chad Africa, eProduction Solutions Corporate Website, accesssed (2008). There have been no details of the meters' performance published in the public domain.

A.11 Multi Phase Meters AS mpm

Multi Phase Meters AS's mpm is marketed as a high-performance meter and was developed through a JIP involving Eni, Hydro, Shell, Total, Statoil and ConocoPhillips, Multi Phase Meters Newsletter (2008).. The mpm measurement system is based on patented 3-D Broadband technology which measures the dielectric constant in 3-D to calculate the water density, salinity and conductivity, and the gas concentration in annular flows as shown in **Figure A.11**, Multi Phase Meters Newsletter (2008).

Figure A.11 – mpm Meter, Multi Phase Meters Newsletter (2008).

A Venturi section is employed for flow conditioning and velocity measurement, while a gamma densitometer unit is exploited for phase composition data. A sub-sea version of the meter has also been developed. Field validation tests were undertaken in January 2007 on the Gullfaks A field operated by Statoil and reported gas and oil flow rate measurement accuracies to within ±8% and ±3% respectively across the full range of GVFs and WLRs, Scheers and Wee (2007).

A.12 Multiphase Solutions Inc VMS

Multiphase Solutions Inc. take a software-based approach with their Virtual Metering System (VMS). The VMS uses measurements from existing sensors in and around the well and to infer multiphase flow rates. VMS can use several predictive models to determine flow rate. It approximates the uncertainty of each estimate and then combines these values to achieve the lowest overall uncertainty. Two installations of the Virtual Metering System have been publicised: one installation for Eni in the Gulf of Mexico and another for the Shell Philippines Exploration at Malampaya, Multiphase Solutions Inc., (2008).

A.13 TEA Sistemi Spa LYRA

The TEA LYRA multiphase meter is suitable for multiphase flow measurement when the GVF is less than 90%. A differential pressure section (Venturi, nozzle or orifice, according to the fluids and process specification) is employed to determine the total mass flow rate as shown in **Figure A.13**.

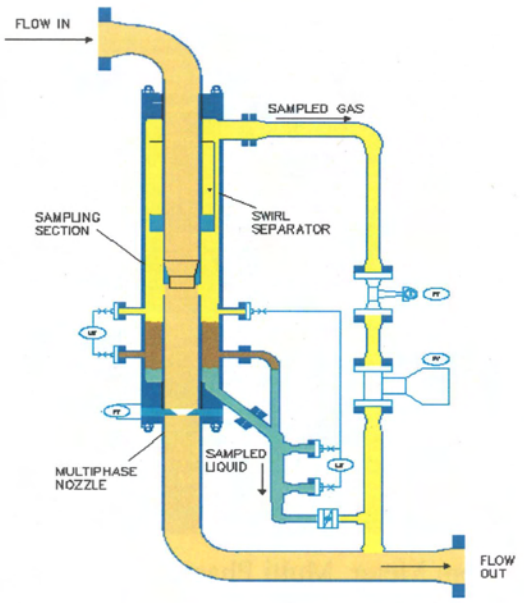

Figure A. 13. – LYRA MPFM, TEA Sistemi Spa (2008).

The water-cut is determined using a patented impedance meter which requires input of the mean density of the gas-liquid mixture. The mean density is measured by a gamma densitometer or, if the liquid fraction is appreciable (~30%), the pressure drop measurement is used to infer the mean density, negating the need for inclusion of a gamma-densitometer in the metering system. Interpretation of the measured data into individual phase flow rates is largely based on proprietary mechanistic models and artificial neural networks trained with well testing data.

LYRA has been marketed in Italy since 1995 and has been installed in three Agip operated oil fields, (Prezioso, Dirillo and Trecate). Although good results have been claimed, no figures pertaining to actual measurement accuracies were available, TEA Sistemi Spa (2008).

A.14 Kvaerner-DUET

This flowmeter uses the attenuation of gamma rays at two different energies to derive the oil, water and gas phase fractions. The mass absorption coefficients of oil and water vary as a function of gamma photon energy, and so the two different absorption rates and continuity relationship allow the phase fractions to be determined. To maximise the transmission of the lower energy gamma rays, the sources and detectors are arranged around a GRP pipe section. Velocity measurement is by cross-correlation

of two gamma densitometer signals, so it responds most accurately to distinct multiphase flow features such as liquid slugs, Roach and Whitaker, (1999).

A.15 Phase Dynamics Inc. CCM

This Compact Cyclone Multiphase Meter (CCM meter) utilises a compact gas-liquid cyclone, to separate the liquid and gas phases prior to measurement, shown in **Figure A.15,** Phase Dynamics Inc. (2008).

Figure A. 15 – CCM Meter, Phase Dynamics Inc. (2008).

Effectively, the system is a modern version of a traditional two phase separator. Coriolis meters are used to measure the separated gas and liquid flow rates. The separated liquid phase is then routed through a Phase Dynamics full range microwave water cut meter, forming an integral part of the CCM multiphase meter. To date, Phase Dynamics have sold and installed 19 CCM meters in Alaska, Wyoming, Siberia, China and Abu Dhabi. The actual dates of these have not been published in the public domain. In 2001, Phase Dynamics reported the field testing of the CCM unit on 1152 wells in the BP operated Milne field in Alaska using a conventional separator for reference measurements. Measurement accuracies of ±5% were claimed for the gas flow rate, liquid flow rate and liquid phase water cut, Phase Dynamics Inc., CCM Sales Presentation (2008).

Appendix B – Review of Slug Flow

B.1 Modeling Multiphase Slug Flow.

Previous work examining experimental and analytical work on slug flow in horizontal and near-horizontal pipes is presented.

- B.1.1 Describes slug flow and the slug flow parameters
- B.1.2 Shows some analysis of the Multiphase flow parameters

An important feature linking the extremes of slug initiation and steady-state slug flow is the way in which slugs develop as they progress along a pipeline. Initially, slugs are formed at high frequency but then a large proportion begins to collapse as they travel downstream and so the frequency reduces. During this process the length of slugs which persist may also increase as they over-run the remnants of the collapsing slugs.

B.1.1 Description of Slug Flow and Slug Flow Parameters

Slug or intermittent flow is the most common occurring flow pattern in hydrocarbon transmission pipelines, Manolis (1995). investigated the advantages and disadvantages when operating in the slug flow regime. Some of the advantages are,

1. Simultaneous transport of large amounts of gas and liquid in small lines.
2. High convective mass and heat transfer coefficients can be achieved due to the high liquid velocities.

Disadvantages are:

1. Significant variations in gas and liquid flow rates can cause mechanical damage to pipeline connections, support and fittings.
2. Dangerous vibration in the pipes due to slugging can cause resonance to occur as the slug frequency approaches the resonant frequency of the pipe system.
3. Erosion-corrosion phenomena in pipelines may be influenced by the intermittency of slug flow.
4. In designing separators, knowledge of the largest slug length that might occur is required.

Slug flow is a very complex phenomenon and inherently unsteady. Complexity arises from particular geometric distribution of the gas-liquid phases, which show variations in space and time.

Figure B1.1 shows an average slug unit cell in fully developed slug. Where the unit cell consists of a slug region of length, l_s and constant holdup a_s followed by a "film" region of length l_f and variable holdup $a_f(x)$. The parameter x indicates axial distance in upstream direction. At point where the preceding slug zone ends and the film zone begins, $x = 0$ and $a_f = a_s$, and at front of the next slug, $x = l_f$ and a_{fe}. Total length of the slug unit is: $(l_u = l_s + l_f)$.

The film region lies between the tail of one slug and the front of the next slug. Liquid leaves the slug tail and drains towards the bottom of the tube to form a stratified layer or "film". This liquid layer is then picked up by the advancing front of the next slug. The gas phase may also be entrained at the slug front and discharged at the end of the slug tail. Each slug unit has several local velocities, which are:

1. Local liquid phase and gas velocity V_{ls} and V_{gs} respectively, in the slug body and usually these velocities are different as the flow regime is changed to annular flow.
2. Variable velocities in the film zone dependent on the local liquid holdup, defined as $V_{ls}(x)$ and $V_{gf}(x)$ respectively. At the end of the film zone and before the arrival of the next slug front, the film zone velocities are denoted by V_{lsf} and V_{gsf}
3. V_t is the translation velocity, and usually it is larger than the local velocities defined above.
4. The superficial velocities J_l and J_g for each phase which is equal to the phase flowrate divided by the total section-area of the pipe.

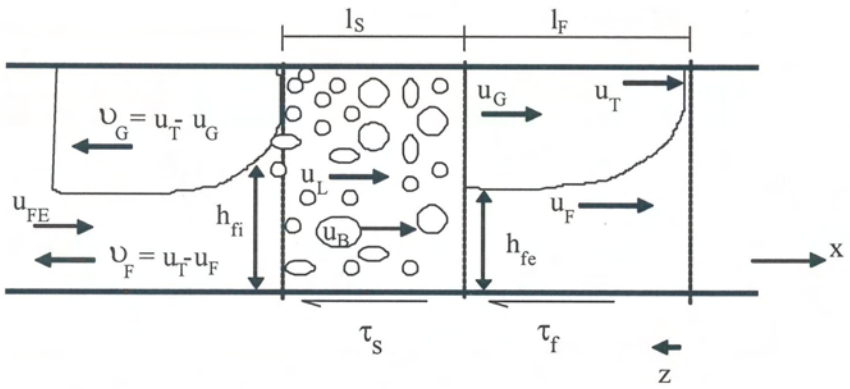

Figure B1.1 - The slug Unit, Manolis (1995).

B.1.1.1 Slug Flow Initiation

The Kelvin-Helmholtz process, shown in **Figure B1.2**, describes the slug flow initiation. There are two main assumptions in the process:
The inlet phase velocities are constant and perfectly stratified flow as initial conditions.

Then a localised disturbance is applied at the interface between phases shown in **Figure B1.2a**, which results in the following points:

- A pressure drop caused by acceleration of the gas phase due to restriction in the area.

- An upward force on the liquid phase, which may cause a wave to be developed if it is comparable with the liquid layer weight as shown in **Figure B1.2b**.

- Any further acceleration in the gas phase and pressure drop might cause a complete blockage in the pipe, see **Figure B1.2c**. However, not every blockage of the pipe can cause a liquid slug. There are specific subsequent processes that cause the slug flow to be built-up. For example, immediate build-up of gas pressure at the rear of the pipe blockage, rapid pickup and assimilation of the liquid layer in the front of the blockage, as a result rapid slug growth.

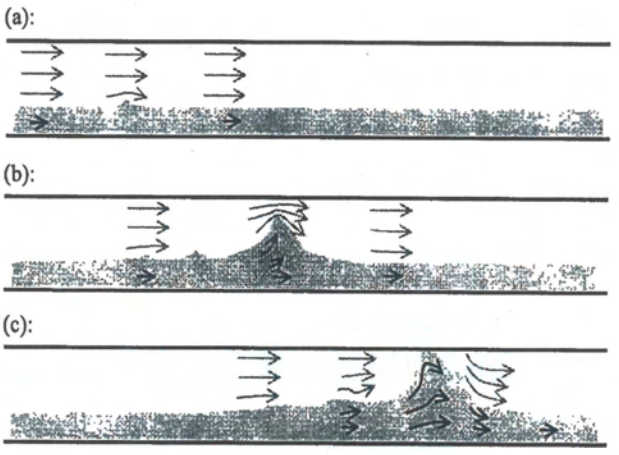

Figure B1.2 Formation of slug flow by Kelvin-Helmholtz instability mechanism: Stewart (2001).
(a) localised disturbance on a perfectly stratified film; (b) pressure drop and wave growth; (c) bridging of the pipe, acceleration of the blockage, and the pickup of fluid

B.1.1.2 Slug Zone Structure

Stewart (2001), visually observed the slug zone to be divided into three regions namely; front region, the body of the slug, and the tail region. Also, the effect of the increase of the gas phase velocity is shown in the same **Figure B1.3**.

Starting from the lowest to the highest gas flowrates, the following flow regimes can be observed;

- The plug flow condition, which occurs at the lowest gas flowrate shown in **Figure B1.3a**.

- Slug flow as shown in **Figure B1.3b**, which occurs by an increase in the gas phase flowrate. In this case, the incoming flow is diverted into a mixing vortex and accelerated to the slug velocity, causing a large irreversible pressure drop in the system.

- And by increasing the gas flowrate the incoming film velocity increased, and there will be more gas and liquid within the mixing zone shown in **Figure B1.3c**.
- Then by reaching the highest gas phase flowrate, the flow will reach the slug-annular condition illustratedby **Figure B1.3d**.

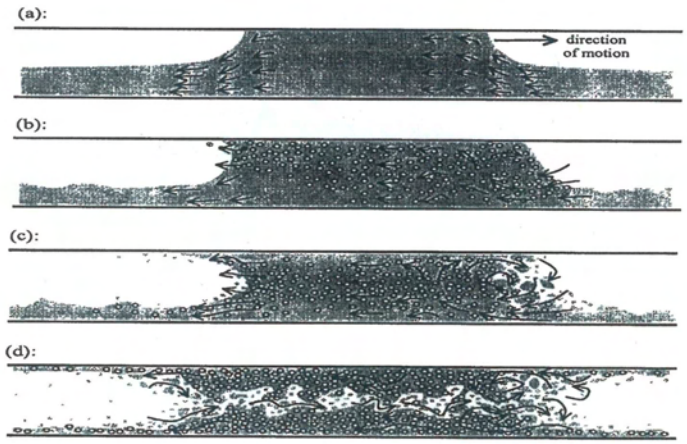

Figure B1.3 The observation of the relative motion of the liquid phase within the slug body, in reference translating with the slug front, Stewart (2001).
(a) Plug flow (low gas velocity); (b) slug flow J_g~3 ms^-1) ;(c) slug flow (3<J_g<7 ms^-1); (d) slug annular flow (J_g>7ms^-1)

B.1.1.3 Film Zone Structure

Stewart (2001), observed that, the length of the film zone far exceeds the slug length within the film zone structure.

Some key factors about the film zone are summarised as follows:

- When the gas and liquid flowrates are very low, there will be a close resemblance to smooth stratified flow. Large waves and precursor waves may appear over the film body.

- By increasing the gas flowrate, gradual gas bubbles from the previous slug zone will be released, and lateral curvature of the film interface occurs. At the end the film geometry creeps round the perimeter to create a liquid annulus

with considerable spray in the gas space, as annular flow conditions are approached.

- By further increasing in the liquid flowrate, towards the bubble flow conditions, a well-defined curved film profile will develop. And obviously, there is a notable reduction in the film zone length, and at the same time the number of developing features between slugs occurs.

B.1.1.4 Slug Frequency

Slug frequency, ν, is defined as the mean number of slug unit which passes a fixed observer in unit time, and increases with increasing liquid flow rate and decreasing pipe diameter. For positive inclination from the horizontal, the slug frequency increases with increasing pipe inclination. Correlations for the slug frequency, ν, have been reported, Gregory and Scott, (1969).

Gregory et al, (1978), Related slug frequency to slug velocity and proposed a correlation based on their data (carbon dioxide-water system in 19 mm diameter horizontal pipe). Slug frequencies were determined from visual observations and pressure pulse recordings. Gregory and Scott, (1969) developed their correlation in term of modified Froude number defined as follows:

$$v = 0.0226\left[\frac{j_l}{gD}\frac{19.75 + j^2}{j}\right]^{1.2} \qquad \text{(B.1)}$$

Where j is the total superficial velocity. However, equation (B.1) is restricted to use in low-pressure applications.

Manolis (1995), took the original correlation of altered Gregory & Scott, 1969) and extended it to high pressure applications, resulting in the similar expression:

$$v = 0.0037\left[\frac{j_l}{gD}\frac{25+j^2}{j}\right]^{1.8} \tag{B.2}$$

B.1.1.5Slug holdup

The average liquid holdup in the slug zone has been found to be dependent on fluid properties, pipe diameter and inclination

Gregory et al (1978), measured the liquid volume fraction using capacitance-type volume fraction sensors in a light oil-air system for 25.8 mm and 51.2 mm diameter horizontal pipes:

$$a_s = \left(1+\left(\frac{j}{8.66}\right)^{1.39}\right)^{-1} \tag{B.3}$$

Andreussi and Bendiksen (1989), studied the inclination effect on the slug holdup, for air-water flow in horizontal condition for a 50mm and 90mm pipe diameter. The models for slug pickup and return at the front implied a strong dependence of a_s upon the relative slug front velocity. This model was used to develop a semi-theoretical correlation of the form:

$$a_s = \frac{V_{ls} - V_{mf}}{\beta V_{ls} + V_{mo}} \tag{B.4}$$

Where expressions for parameters β, V_{mf} and V_{mo} are presented in the original report. The resulting correlation is rather complex; a simple fit to the experimental data are given by the expressions:

$$S = \left\{ \begin{array}{ll} 1 & j \prec 2.5ms^{-1} \\ 1.242 - 0.263\ln j & 2.5 \geq ms^{-1} \end{array} \right\} \tag{B.5}$$

At large gas superficial velocities, the slug holdup takes a minimum value defined by $1/\beta$ which is approximately equal to 0.5.

B.1.1.6Slug Length

Slug frequency and slug length are related parameters, linked to the time of passage of the slug unit. Although a large statistical variation around the mean value of the slug length, l_s exists, the observed experimental mean slug length values are independent of gas and liquid flow rates and range between 12-30 pipe diameters for slug flow, Manolis (1995).

Unlike the slug frequency and the slug holdup correlations, in which described above, the slug length is relatively independent of gas and liquid superficial velocities, Brill et al (1981), developed a correlation to predict liquid slug length for larger diameter pipes, based on their data from 305 mm and 406 mm diameter test lines and on data from 102 mm and 178 mm diameters pipes, and is given by:

$$\ln(3.2808l_s) = -2.663 + 5.441[\ln(39.37D)]^{0.5} + 0.059\ln(3.2808V_m) \qquad \text{(B.6)}$$

In large diameter pipes, Scott et al (1986), proposed the following correlation to calculate slug length:

$$\ln(3.2808l_s) = -25.4134 + 28.4948[\ln(39.37D)]^{0.1} \qquad \text{(B.7)}$$

Nydal et al (1992), used horizontal pipes (53 mm and 90 mm) to measure the length of the slug. The range of the superficial velocities is $j_l = 0.6 - 3.5ms^{-1}; j_g = 0.5 - 20ms^{-1}$. He came up with an equation and that after distinguishing between developing and developed slug, and neglecting the former one,

$$l_s \approx 15D \qquad \text{(B.8)}$$

B 1.2 Multiphase Slug Flow Parameters Analysis

Capacitance and Conductance sensors both offer a wide bandwidth. However, the capacitance sensor allowed the measurement of oil and water continuous mixtures,

compared with conductance sensors which can only operate properly with water continuous mixtures.

Some procedures are proposed to characterize the flow through the analysis of the slug flow by analysing the capacitance sensor signal output, which allows the main slug flow parameter, such as slug velocity, length, frequency, hold-up to be evaluated. The procedure is validated through extensive comparisons with literature data based on two-phase data and flow visualisations by means of video images of the slug flows, which shows a general agreement with present measurement. The operating conditions cover a wide range of gas and liquid superficial velocities, in a 4 inch (102mm) horizontal pipe for both two-phase & three phase flows.

However, correlations used to compare the results cover a wide variety of test fluids, pipe diameters, pipe inclination and phase superficial velocities. The description/characterisation of slug flow with tests and analysis carried out with this experiment is therefore based on available two-phase data, as there are no previous results for three-phase flow.

From the plot of the liquid hold up versus time the number of slugs during the observing period can be obtained and residence time $\Delta\tau_i$ was associated with the ith individual slug, shown in **Figure B1.4**. To this aim, two threshold values have been introduced. These values are the minimum liquid holdup $H_{L,slug}$ (slugs that don't achieve $H_{L,slug}$ are considered travelling waves and discarded from counting) and the cut liquid holdup $H_{L,c}$ according to which the residence times are calculated. In particular the above relationships were introduced, based on a preliminary sensitivity analysis:

$$H_{L,slug} = Max(0.9\, H_{max}, H_S) \tag{B.9}$$

$$H_{L,C} = \begin{Bmatrix} \overline{H} & if & \overline{H} \geq & 0.8 \\ 0.8 & if & \overline{H} < & 0.8 \end{Bmatrix} \tag{B.10}$$

Where $\overline{H}$ = 1- $\overline{\alpha}$ represents the time-average liquid holdup, H_S = *1*- α_S is the average liquid holdup of the liquid slug body, and H_{max} is the maximum liquid holdup recorded value.

The average residence time $\Delta\overline{\tau}$ and the slug frequency υ can be obtained from counting the slug.

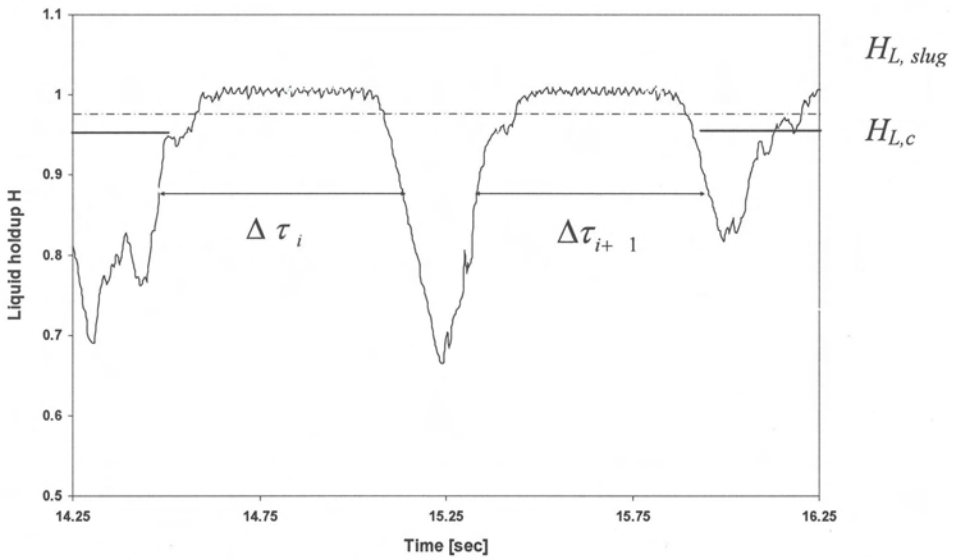

Figure B1.4 Liquid Holdup Vs Time from Capacitance Sensor Signal

The slug translational velocity V_t can also be calculated from the phase continuity equation as a function of the liquid superficial velocity V_{sl}, gas superficial velocity V_{SG} and their sum, the mixture velocity V_M.

$$V_{t1} = \frac{V_{SL}\,\overline{H}_{slug}\,.\quad V_M}{1-\overline{\alpha}-H_{slug}} \tag{B.11}$$

where $\overline{H}_{slug}$ is the average liquid holdup in the slug body as calculated on the basis of counted liquid slugs.

Neglecting the amount of gas present in the liquid slug, the equation becomes:

$$V_{t2} = \frac{V_{SG}}{1-\overline{H}} = \frac{V_{SG}}{\overline{\alpha}} \tag{B.12}$$

Appendix C Additional Information on the Data Acquisition System

1. **A/D & CTR Dig.vi**

This VI controls the data collection process. It configures the A/D and counter cards and also controls the operation of each so that analogue and pulse data are collected synchronously. A configuration case runs during the first iteration of the main programme, allowing the user to check and adjust calibration constants. The MENU allows this configuration case to be run at any time during execution of the main programme.

The order of execution is as follows:

i. The A/D card is configured for triggered operation. Data collection will start when a DIGITAL pulse is received on PFI6. This pulse is generated when analogue output (A/O) channel 0 starts. This is controlled by software.

ii. The Timer/Counter card is configured to collect pulses on the SOURCE pin of counter 0. A signal on the GATE pin determines the frequency at which the pulse count is read. The GATE signal is generated on A/O channel 0 of the A/D card at the same frequency as the data collection rate. In this way the pulse count is updated at the same rate as the analogue signals.

iii. A/O channel 0 is started. This triggers the counter and A/D at the same time, thus synchronising data collection on both devices.

2. **Cals. & ADC.vi**

During the first iteration of the main programme loop this VI displays a list of the calibration constants for the analogue channels. It also configures the A/D card for the required operation (triggered) and sets the sample rate. During subsequent iterations, it reads the sampled data from the input buffer. This is normally done once every second but the frequency may be altered. For example, if the sample rate is 1kHz and the loop time in the main programme is 1 second, this VI will request 1000 data points from the input buffer. If delays have occurred and a scan backlog has built up, the VI will read the outstanding samples available. In order

to keep the A/D and counter scans synchronised, the same number of counts will be requested from the counter buffer.

3. Counter ADC

During the first iteration of the main programme, this VI configures the counter card for buffered data collection. Pulse counts are stored in the buffer every time a pulse is received on the GATE pin. During subsequent iterations, the input buffer is read at the same frequency as the A/D buffer. Thus the two cards produce data at the same rate. If a delay has occurred and a scan backlog has built up, the amount of data to be retrieved from the A/D and counter buffers will be the greater of the two outstanding amounts.

4. Generate Gate.vi

During the first iteration of the main programme, this VI starts generating a square wave signal from A/O channel 0 of the A/D card. The frequency is the same as the A/D sample rate.

5. Meters.vi

This VI displays the values of each of the sampled channels. For the analogue signals, the value shown is averaged over the loop time (typically 1 sec.). The pulse count value is the number of pulses accumulated during one iteration of the main programme.

6. Serial Read.vi

The Multiphase Data Collection computer at N.E.L. has been programmed to transmit a byte string over an RS232 Serial link. This VI reads and parses the byte string. The Serial Link Utility document prepared by Kyle Systems and Consultancy gives details of the string. The VI checks the format of the string and where an error has occurred, requests the N.E.L. computer to retransmit the string.

7. Data File Control.vi

This VI creates a data file for each test point. When the "START" message is received, a data file is created. The filename contains the characters defining the test number and test point number. The date and time values contained in the serial string are written to the data file header. When the "STOP" message is received, the data file is closed. This VI also allows the user to manually save data if the serial link is not available or is not used.

8. Validation

The programme was checked in 3 stages.

i. The sub-VI's have a "simulate" setting that allows test values to be input in order to check correct data flow and the results of calculations. In this mode, it was possible to check for the correct passing of data to the data file.

ii. The programme was tested dynamically using reference inputs from a calibrated voltage source.

iii. Synchronisation of the A/D and counter data streams was done using a function generator. A square wave was connected to the A/D inputs and the counter SOURCE pin. Data was streamed to disk and a step change was made to the frequency of the square wave. The count data and analogue values were compared. With the GATE signal used to trigger both cards, there was no measurable delay between the signals. The test was repeated several times, using different frequencies of square wave and at different sampling rates. Without the GATE signal, there was a noticeable delay between the two signals (up to 0.25s). The delay was not repeatable.

Appendix D Details of accompanying DVD

The companion DVD of this PhD thesis contains the following materials:

1. Experimental Data Folder
    a. Sensor Response Database for Multiphase Flows
        i. <README.txt> a general description of the data structure
        ii. Tests Data NELMU06 01-19 (50g/l MgSO4 Salinity)
        iii. Tests Data NELMU06 21-37 (100g/l MgSO4 Salinity)
        iv. Tests Data NELMU06 38-44 (100g/l MgSO4 Salinity – Location 2)

    b. Template Folder

        v. <INSTRUCTIONS.txt> is a set of a simple to follow instructions to enable the users import data to the template to view the data.

        iv. <NELTEMPLATE.xls> is a spreadsheet in Microsoft Excel format. It contains the summary of all the data files including test conditions and flow regimes.

2. Results Folder Contents
    a. Data Analysis Samples (Feature Extraction) and PR Meter Performance in Microsoft Excel.

    b. Test Matrix (Calculated Superficial Gas and Liquid Velocities)

    c. Sample Matlab Codes

3. The DVD also contains the complete PhD thesis in .PDF format

REFERENCES

Abbon AS, AFM Product Specification Sheet:
http://www.abbon.com/files/AFM3%20Multiphase%20measurements.pdf
(accessed 22nd November 2007).

Abdel-Mohsen, O.M., Maisa, E.G., and Abdulrazag, Y. Z., 'Effect of Salinity and Temperature on Water Cut Determination in Oil Reservoirs', Journal of Petroleum Science and Engineering., Volume 40, 2003, pp. 177 – 188.

Abouelwafa, M. S. A., and Kendall, E. J. M., 'Analysis and Design of Helical Capacitance Sensors for Volume Fraction Determination', J. Phys. E: Rev. Sci. Instrum., Volume 50 (7), 1979, pp. 872 – 878.

Abouelwafa, M. S. A., and Kendall, E. J. M., 'The Measurement of Component Ratios in Multiphase Systems using γ-ray Attenuation', J. Phys. E: Sci. Instrum., Volume 13, 1980, pp. 341 – 345.

Åbro, E., Khoryakov, V. A., Johansen, G. A., and Kocbach, L., 'Determination of Void Fraction and Flow Regime Using a Neural Network Trained on Simulated Data Based on Gamma-Ray Densitometry', Measurement Science and Technology, Volume 10, 1999, pp. 619 – 630.

Accuflow AMMS Product Technology Information:
http://www.accuflow.com/default2.asp?active_page_id=197
(accessed 22nd November 2007).

Acikgoz, M., Franca, F., and Lahey Jr., R. T., 'An Experimental Study of Three-Phase Flow Regimes', International Journal of Multiphase Flow, Volume 18(3), 1992, pp. 327 – 336.

Agar J. and Farchy, D., - 'Wet Gas Metering Using Dissimilar Flow Sensors: Theory and Field Trial Results', Agar Corporation, SPE Annual Technical Conference and Exhibition held in San Antonio, Texas, 2002. SPE – 77349.

Akartuna, S. E., 'Identification of Phase Flowrates in Oil-Gas-Water Flow from Turbulent Capacitance and Pressure Signals', PhD Thesis, Imperial College of Science, Technology and Medicine, London, 1994.

Al-Bourni, H. A., Samizo, N., Bakhteyar, Z., and Alvi, A., 'Application of New Multiphase Flow Measurement Systems with Satellite-Based Monitoring in Offshore Khafji Field', International Petroleum Technology Conference, IPTC 10312, 2005.

Al-Taweel, A.B., and Barlow, S.G. 'Field Testing of Multiphase Meters'. SPE paper 56583, Annual Technical Conference and Exhibition (Houston, Texas, U.S.A), 1999.

American Petroleum Institute (API), 'State of the Art Multiphase Flow Metering', Publication 2566, 1st Edition, Committee on Petroleum Measurements, 2004.

Andreussi, P. and Bendiksen, K. H. 'An Investigation of void fraction in liquid slugs for horizontal and inclined gas-liquid pipe flow'. *International Journal of Multiphase Flow*, 15(6), 937-946, 1989.

Baker, O., 'Simultaneous Flow of Oil and Gas', Oil & Gas Journal, Volume 53,1954, pp.185 – 195.

Baker, R.C. Turbine and Related Flow Meters. Introduction to Flow Measurement – Lecture notes. Cranfield University, School of Mechanical Engineering, Cranfield, U.K. 1998.

Beck, M. S., and Plaskowski, A., 'Cross Correlation Flow Meters: Their Design and Application', Adam Hilgar, Bristol, 1987.

Beg, N.A. 'A Stochastic Method of Multiphase Flow Metering in Pipes' PhD Thesis, *Imperial College of Science, Technology and Medicine*, 1998.

Bishop, C. M. 'Multiphase Flow Monitoring in Oil Pipelines: Application of Neural Networks', pp. 133-155. Kluwer Academic Publishers, Netherlands. 1995b.

Bishop, C.M. 'Neural Networks for Pattern Recognition'. *Oxford University Press,* (Oxford, U.K), 1995a.

Bishop, C. M., and James, G. D., 'Analysis of Multiphase Flows Using Dual-Energy Gamma Densitometry and Neural Networks', Nuclear Instruments and Methods in Physics Research, A327, 1993, pp. 580 – 593.

Blaney, S., 'Gamma Radiation Methods for Clamp-On Multiphase Flow Metering', PhD Thesis, Cranfield University, 2008.

Brill, J. P., and Arirachakan, S. J., 'State of the Art in Multiphase Flow', Journal of Petroleum Technology, Volume 44 (5), 1992, pp. 538 – 541.

Brill, J. P., Schmidt, Z., Coberly, W. A., Herring, J. D. and Moore. D.W. 'Analysis of two-phase tests in large-diameter flow lines' Prudhoe Bay Field. *SPE Journal,* 1981, 363-377, 1981.

Brown, G., 'Evaluation of New Technology for High Accuracy Multiphase Flow Measurment: Part 2 – Neural Networks', NEL Flow Measurement Guidance Note No. 28, June, 2002.

Cai, S., 'An Artificial Neural Network Method for Three-Phase Flow Measurement', PhD Thesis, Imperial College of Science, Technology and Medicine, London, 1995.

Cai, S., Toral, H., Sinta, D., and Tajak, M., 'Experience In Field Tuning And Operation of A Multiphase Meter Based On Neural Net Characterization Of Flow Conditions', FLOMEKO, September 2004.

Chisholm, D., 'Flow of Incompressible Two-Phase Mixtures through Sharp-Edged Orifices', Journal of Mechanical Engineering Science, Vol. 9 (1), 1967, pp. 72 – 78.

Darwich, T., 'A Statistical Method for Two-Phase Flow Metering', PhD Thesis, Imperial College of Science Technology and Medicine, London, 1989.

Darwich, T., Toral, H., and Archer, J.S., 'An Expert System for Multiphase Flow Measurement and Flow Regime Identification', SPG Paper 19136 in SPG Petroleum Computer Conference, Lake Conroe, Texas, 1989.

Deller, J. R., Proakis, J. G., and Hansen, J. H. L., 'Discrete-Time Processing of Speech Signals', MacMillan, 1993.

Department of Trade and Industry (UK), 'Guidance Notes for Petroleum Measurement', Issue 7, December, 2003, pp.8 – 9.

Doan, C. D., and Liong, S. Y., ' Generalization for Multilayer Neural Network Bayesian Regularization or Early Stopping', 2nd Asia Pacific Association of Hydrology and Water Resources Conference, Singapore, 2004.

Dutton, R., and Daniel, P.E., 'Determination of Net Oil for Well Performance Measurement', Class LM2100, Emerson Process Management, 2001.

Dykesteen, E., et al, 'Handbook of Multiphase Metering', Norwegian Society of Oil and Gas Measurement, NFOGM, Revision 2, March, 2005.

eProduction Solutions Corporate Website: http://www.ep-solutions.com
(accessed 8th June 2008).

eProduction Solutions, 'REMMs Product Specification Sheet':
http://www.ep-solutions.com/PDF/Literature/L_REMMS_A4.pdf
(accessed 8th June 2008).

Falcone, G., Hewitt, G.F., Alimonte C., 'Multiphase Flow Metering: Current Trends and Future Developments', SPE Annual Technical Conference and Exhibition held in New Orleans, 2002. SPE – 74689.

Ferschneider, G. (1983). 'Ecoulements Diphasiques Gas-Liquid á Poches et á Bouchon en Conduits'. Cited in: Hale, C. P. (2000). '*Slug Formation, Growth and Decay in Gas-Liquid Flow', chapter 3, p211.*PhD Thesis, Imperial College, London, UK, 2000.

Foresee, F. D., and Hagan, M. T., 'Gauss-Newton Approximation to Bayesian Regularisation', International Joint Conference on Neural Networks, 1997, pp. 1930 – 1935.

Franca, F., Acikgoz,., M Lahey, R. T., and Clausse, A., 'The Use of Fractal Techniques for Flow Regime Identification', International Journal of Multiphase Flow, Volume 17, 1991, pp. 545 – 552.

Golub, G. H and Loan, C.F.V. Matrix Computation. The Johns Hopkins University Press, 2nd Edition, 1989.

Golub, G. H and Loan, C.F.V. 'Matrix Computation', The Johns Hopkins University Press, 2nd Edition (1989).

Goudinakis, G., 'Investigation on the use of Raw Time Series and Artificial Neural Networks for Flow Pattern Identification in Pipelines' , PhD Thesis, Cranfield University, 2004.

Gregory, G.A., Nicholson, M. and Aziz, K. 'Correlation of the liquid volume fraction in the slug for horizontal gas liquid slug flow'. *International Journal of Multiphase Flow*, 4(1), 33–39, 1978.

Gregory, G.A. and Scott, D. S. 'Correlation of liquid slug velocity and frequency in horizontal cocurrent gas-liquid slug flow'. *Journal of AIChE,* 15, 933-935, 1969.

Grossberg, S., 'Grossberg, 'Contour Enhancement, Short-term Memory, and Constancies in Reverberating Neural Networks', Studies in Applied Mathematics, Volume 52, 1973, pp. 213 – 257.

Hagan, M.T., Demuth, H.B and Beale, M. 'Neural Network Design', *PWS Publishing Company,* Boston, U.S.A, 1996.

Haimo MFM Product Brochure:
http://www.haimotech.com/downloads/MFM%20Brochure.pdf
(accessed 22nd November 2007).

Haimo Technology Inc, 'Haimo Newswire', Issue 3, March 2005.

Hall, A.R.W., 'Evaluation of the FlowSys TopFlow Multiphase Flowmeter', NEL, Project No FSY001, Report No 200/2000, October 2000.

Hammer, E. A., and Nordvedt, J. E., 'The Application of a Venturi Meter to Multiphase Flow Meters for Oil Well Production', Proc. 5th Conf. Sensors and Applications, 1991.

Hewitt, G. F., 'Measurement of Two-Phase Parameters', Academic Press, London, 1978

Hewitt, G. F., 'Multiphase Flow Metering', Proc. 2nd Int. Symp. Multiphase Flow and Heat Transfer (Xi'an, China), 1989.

Hewitt, G. F., Shires, G. L., Harrison, P. S., and Parry, S. J., 'The Mixmeter Flowmeter - Another step towards Routine Multiphase Flow Measurement?', 8th International Conference on Multiphase Production Technology '97, Cannes, France: 1997.

Hornik, K., Stinchcombe, M., and White, H., 'Multilayer Feedforward Networks Are Universal Approximators', Neural Networks, Volume 2 (5), 1989. pp. 359 – 366.

Ismail, I., Gamio, J. C., Bukhari, S. F. A., and Yang, W. Q., 'Tomography for Multi-Phase Flow Measurement in the Oil Industry', Flow Measurement and Instrumentation, Volume 16, 2005, pp. 124 – 155.

Jackson, J. E. 'A User's Guide to Principal Components'. John Wiley and Sons Inc. 1991.

Jama, A. A, 'Wet Gas Flow Metering with Pattern Recognition Techniques', PhD Thesis, Cranfield University, 2004.

Jamieson, A.W., 'Multiphase Metering – The Challenge of Implementation', 16th North Sea Flow Measurement Workshop, Gleneagles, Scotland, 1998.

Johansen, G.A., and Jackson, P., 'Salinity Independent Measurement of Gas Volume Fraction in Oil/Gas/Water Pipe Flows, International Journal of Applied Radiation and Isotopes 53, 595-601, 2000.

Kabal, P., and Ramachandran, R. P., 'The Computation of Line Spectral Frequencies using Chebyshev Polynomials', IEEE Trans. Acoustics, Speech Signal Processing, Volume 34, 1986, pp. 1419 – 1426.

Klepsvik, I., Dahl, E., O., Baker, A. C., 'Multiphase Flow Test Report – TopFlow', Christian Michelsen Research, Report CMR-00-F10021, 2000.

Kohonen, T., 'Self-Organized Formation of Topologically Correct Feature Maps', Biological Cybernetics, Volume 43, 1982, pp. 59 – 69.

Kohonen, T., Oja, E., Simula, O., Visa, A., and Kangas, J., 'Engineering Applications of the Self-Organizing Map', Proceedings of the IEEE, Vol. 84 (10), 1996, pp. 1358 – 84.

Leggett, R. B., Borling, D. C., Powers, B. S., and Shehata, K., 'Multiphase Meter Successfully Measures Three-Phase Flow at Extremely High Gas Volume Fraction', SPE Paper 36837, European Petroleum Conference, Milan, Italy, 1996.

Letton, W., Svaeren, J. A., and Conort, G., 'Topside and Subsea Experience with the Multiphase Flow Meter', SPE 38783, October, 1997, pp. 345 –355.

Lippmann, R.P., 'An Introduction to Computing with Neural Nets'. *IEEE ASSP Magazine, Issue 4-12*, 1987.

MacKay, D. J. C., 'Bayesian Interpolation', Neural Computation, Volume 4 (3), 1992, pp. 415 – 447.

Makhoul, J. 'Linear Prediction: A Tutorial Review'. Proc. IEEE, Vol.63, pp.561-580, 1975.

Mallat, S. 'A Theory for Multiresolution Signal Decomposition: the Wavelet Representation', IEEE Pattern Anal. and Machine Intell., Vol. 11, 1989, No. 7, pp. 674-693.

Mandhane, J. M., Gregory, G. A., and Aziz, K., 'A Flow Pattern Map for Gas-Liquid Flow in Horizontal Pipes', International Journal of Multiphase Flow, Volume 1, 1974, pp. 537 – 553.

Manolis, I. G. 'High Pressure Gas-Liquid Slug Flow'. PhD Thesis, Imperial College, London, UK, 1995.

Mazzoni, A., Halvorsen, M., Aspelund, A., 'Field Qualification – FlowSys TopFlow Meter', Agip Test Facility, Trecrate, Italy, April, 2001.

McCoy, D.D., Warner, H.R. Jr, Fisher, T.E. 'Water Salinity Variations in the Ivishak and Sag River Reservoirs, Prudhoe Bay Field' SPE 28577, pp. 117 – 129, 1994.

McCulloch, W., and Pitts, W., 'A Logical Calculus and the Ideas Immanent in the Nervous Activity', Bulletin of Mathematical Biophysics, Volume 5, 1943 pp. 115 – 133.

McNulty, J. G., and Beg, N. A., 'Survey of Multi-Phase Flow Metering Systems', Caltec Report CR 6660, BHR Group, UK, 1997.

Meinhold, T.F. Liquid Flow Meters. Plant Engineering Magazine, Vol. 38, No. 28, pp. 46-60. 1984.

Mehdizadeh, P., and Williamson, J., 'Principles of Multiphase Flow Measurements', Alaska Oil and Gas Commission, 2004.

Merilo, M., Dechene, R. L., and Cichowlas, W. M., 'Void Fraction Measurement with a Rotating Electric Field Conductance Gauge', ASME J. Heat Transfer, Volume 99, 1977, pp. 330 – 332.

Minsky, M., and Papert, S., 'Perceptrons: An introduction to Computational Geometry', MIT Press, 1969.

Mohamed Abdel-Mohsen O., EL Gamal Maisa., Zekri Abdulrazag Y., "Effect of Salinity and Temperature on Water Cut Determination in Oil Reservoirs" Journal of Petroleum Science and Engineering 40, 177 – 188, 2003.

Multi Phase Meters, 'Performance Newsletter':
http://www.mpm.biz/Portals/39/Performance%20Oct%2005.pdf
(accessed 3rd July 2008).

Multiphase Solutions Inc., 'New Project Notification':
http://www.multiphase.com/products/p_vmetering.htm
(accessed 10th July 2008).

Murdoch, J. W., 'Two-Phase Flow Measurements with Orifices', Journal of Basic Engineering, Vol. 84, 1962, pp. 419 – 433.

Nicklin, D. J., Wikes, J. C., and Davidson, J. F., 'Two Phase Flow in Vertical Tubes', Transactions of the Institution of Chemical Engineering, Volume 40, 1962, pp. 61 – 68.

Nydal, O.J., Pintus, S. and Andreussi, P. 'Statistical characterisation of slug flow in horizontal pipes'. *International Journal of Multiphase Flow*, 18(3), 439-453, 1992.

Nyfors, E., and Vainikainen, P., 'Industrial Microwave Sensors', Artech House, 1989.

Oddie, G., et al, 'Experimental Study of Two and Three Phase Flows in Large Diameter Inclined Pipes', Int. Journal of Multiphase Flow, Volume 29, 2003, pp. 527 – 558.

Olsen, A. B., 'Framo Subsea Multiphase Flow Meter System', Proc. Sem. Multiphase Meters and their Subsea Applications, London, 1993.

Olsvik, K., Marshall, M., and Whitaker, T., 'Fluenta Multiphase Flow Meter, Tested and Marinised', 13th North Sea Flow Measurement Workshop, Lillehammer, Norway, 1995.

Ong, K. H., and Beck, M. S., 'Slurry Flow Concentration and Particle Size Measurement using Flow Noise and Correlation Techniques', Meas. Control, Volume 8, 1975, pp. 453 – 460.

Phase Dynamics Inc., 'CCM Product Specification Sheet',
http://www.phasedynamics.com/ccm.html (accessed 10th August 2008).

Phase Dynamics Inc., 'CCM Sales Presentation',
http://www.phasedynamics.com/pdf/ccm_presentation_0206.pdf
(accessed 10th August 2008).

Roach G. J., and Whitaker T. S., 'Long Term Use of A Multi Phase Flow Meter', Kwarner Oilfield Product Ltd. UK, 1999.

Rosenblatt, F., 'The Perceptron: A Probabilistic Model for the Information Storage and Organisation in the Brain', Psychological Review, Volume 5, 1958, pp. 386 – 408.

Sanderson, M.L. Probes, 'Integration Methods and Tracers. Introduction to Flow Measurement' – Lecture Notes. Cranfield University, Sch. of Engineering. Dept. of Process & Systems Engineering, Cranfield, U.K, 1998.

Sanderson, M. L., 'Process Measurement Systems', MSc Module PSE 10, Cranfield University, Bedfordshire, England, 2001.

Scheers A.M. and Slijkerman W.F.J., "Multiphase Flow Measurement Using Multiphase Energy Gamma Ray Absorption (MEGRA) Composition Measurement", Paper SPE 36593 presented at the 1996 Annual Technical Conference and Exhibition. Denver October 1996.

Scheers, L., and Wee, A., 'Challenges at High Accuracy Multi-Phase and Wet-Gas Measurements', Multiphase Measurement Roundtable, April, 2007.

Scheers, L., Busaidi, K., Parper, M., Halvorsen, and Wideroe, T., 'Multiphase Flow Metering Per Well – Can it be Justified? ', 20th North Sea Flow Measurement Workshop, St. Andrews, Scotland, 2002.

Scott, S. L., Shoham, O. and Brill, J. P. 'Prediction of slug length in horizontal large-diameter pipes'. In: *Proceedings of the 56th Regional Meeting on the Society of Petroleum Engineers*, Oakland, CA, April 2-4 (SPE 15103), 1986.

Shen, J. J. S and Riley, R. C., 'Field Evaluation of a Multiphase Meter in Well-Testing Operation', SPE Production & Facilities, 1998, pp. 109 – 117.

Sheppard, C.P., and Russell, D., 'the Application of Artificial Neural Networks to Non-Intrusive Multi-Phase Metering', Control Engineering Practice, Volume 1 (2), 1993, pp. 299 – 304.

Spedding, P. L., and Nguyen, V. T., 'Regime Maps for Air-Water Two-Phase Flow', Chemical Engineering Science, Volume 35, 1980, pp. 779 – 793.

Spedding, P. L., and Spence, D. R., 'A Novel Approach to Flow Regime Prediction in Gas-Liquid Flows', Developments in Chemical Engineering SST, Volume 14 (2), 1994, pp. 407 – 431.

Spedding, P. L., Woods, G. S., Raghunathan, R. S., and Watterson, J. K., 'Flow Pattern, Holdup and Pressure Drop in Vertical and Near Vertical Two- and Three-Phase Upflow', Trans IChemE, Volume 78 (A), April, 2000, pp. 404 – 418.

Stapelberg, H. H., and Mewes, D., 'The Flow of Two Immiscible Liquids and Gas in Horizontal Pipes – Pressure Drop and Flow Regime', European Two-Phase Flow Group Meeting, Varese, 21st-24th May, 1990.

Stewart, D.G. The Evaluation of Dry Gas Meters in Wet Gas Conditions. A Report for the National Measurement System Directorate, Department of Trade and Industry, U.K. 2002.

Stewart, C. 'Instrumentation for the Measurement of Slug Flows'. PhD thesis, University of Strathclyde, UK, 2001.

Taitel, Y., Barnea, D., and Dukler A. E., 'Modelling Flow Pattern Transitions for Steady Upward Gas-Liquid Flow in Vertical Tubes', AIChE Journal 26, no 6, 1980, pp. 345 – 336.

Tarassenko, L. 'A Guide to Neural Computing Applications'. John Wiley and Sons Inc, New York. 1998.

TEA Sistemi Spa Corporate Website, 'LYRA Product Information': http://www.teasistemi.com/html/products_metering_lyra_01.htm (accessed 10th July 2008).

Theuvent, B. C., Segeral, G., Pinguet, B., 'Multiphase Flow Meters in Well Testing Applications', SPE Paper 717475, Annual Technical Conference and Exhibition, New Orleans, USA, 1998.

Thorn, R., G.A., and Hammer, E.A., 'Recent Developments in Three-Phase Flow Measurement', Measurement Science and Technology, Volume 8, 1997, pp. 691 – 701.

Toral, H., Beg, N., and Archer, J. S., 'Multiphase Flow Metering by Software',International Conference on Basic Principles & Industrial Applications of Multiphase Flow, London, 1990.

Toral, H., Cai, S., Akartuna, E., Stothard, K., and Jamieson, A. W., 'Field Trials of the ESMER Multiphase Flow Meter' 16th North Sea Flow Measurement Workshop, Gleneagles, Scotland, 1998.

Tuss, B., Perry, D., and Shoup, G., 'Field Tests of the High Gas Volume Fraction Multiphase Flow Meter', Proc. SPE Annual Technical Conf., Denver, USA, 1996.

Webb, A. 'Statistical Pattern Recognition'. ISBN-0304741643, Oxford University Press, 1999.

Wood, I., 'Multiphase Measurement', 20th North Sea Flow Measurement Workshop, Peebles, Scotland, 2002.

Woods, B. D. and Hanratty, T. J. 'Relation of Slug Stability to Shedding Rate'. *International Journal of Multiphase Flow*, 22(5), 806-828, 1996.

Wu, H., Zhou, F., and Wu, Y., 'Intelligent Identification System of Flow Regime of Oil-Gas-Water Multiphase Flows', International Journal of Multiphase Flow, Volume 27, 2001, pp. 459 – 475.

Wylie, S. R., Shaw, A., and Al-Shamma'a, A. I., 'RF Sensor for Multiphase Flow Measurement through an Oil Pipeline', Measurement Science and Technology, Volume 17, 2006, pp. 2141 – 2149

Yeung, H., Loh, W.L., Ibrahim. A., Collins, S. Creation of a Sensor Response Database in Multiphase Flows. Dept. of Process & Systems Engineering, School of Engineering, Cranfield University, (Cranfield, U.K). 2002.

Yeung, H., Sanderson, M.L., Beg, N.A and McNulty, J.G. Intelligent Systems for Multiphase Flow Measurement and Pattern Recognition Techniques for Multiphase Flow Meters. Report No. 98/HY/FO1598V/189, DFEI, Cranfield University, Cranfield, UK. 1998.